MAXIMUM POWER POINT TRACKING CONTROLLERS FOR TRANSFORMERLESS GRID-CONNECTED PV SYSTEMS

BY

MUHAMMAD USMAN MUKHTIAR

A Thesis Presented to the
DEANSHIP OF GRADUATE STUDIES

KING FAHD UNIVERSITY OF PETROLEUM & MINERALS

DHAHRAN, SAUDI ARABIA

In Partial Fulfillment of the
Requirements for the Degree of

MASTER OF SCIENCE

In

ELECTRICAL ENGINEERING

December 2015

KING FAHD UNIVERSITY OF PETROLEUM & MINERALS

DHAHRAN- 31261, SAUDI ARABIA

DEANSHIP OF GRADUATE STUDIES

This thesis, written by **MUHAMMAD USMAN MUKHTIAR** under the direction his thesis advisor and approved by his thesis committee, has been presented and accepted by the Dean of Graduate Studies, in partial fulfillment of the requirements for the degree of **MASTER OF SCIENCE IN ELECTRICAL ENGINEERING.**

Dr. Mohammad Ali Abido
(Advisor)

Dr. Ali Ahmad Al-Shaikhi
Department Chairman

Dr. Ibrahim El-Amin
(Member)

Dr. Salam A. Zummo
Dean of Graduate Studies

Dr. Ibrahim Omar Habiballah
(Member)

17/2/16
Date

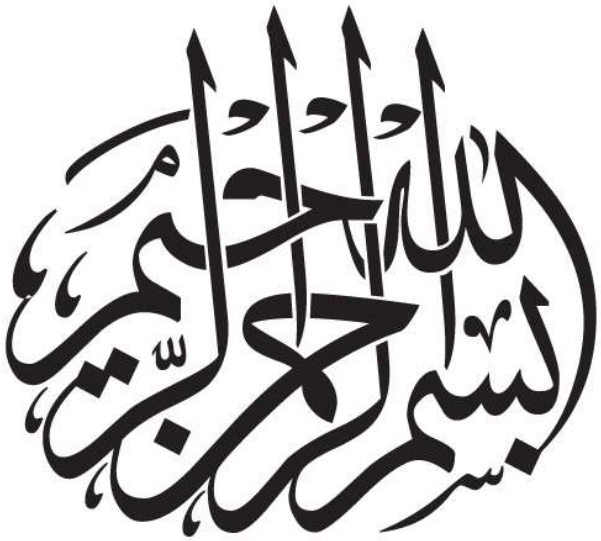

This Thesis is dedicated to

My Beloved Parents

My Brothers and Sisters

And

My Teachers

Every Bit of me is a little bit of you

ACKNOWLEDGMENTS

In the name of Allah, the most Merciful, the most Gracious

"All praise is to Allah, the Lord Of The Creation (1). The Most Gracious, the Most Merciful (2). Owner of the Day of Recompense (3). You alone we worship and from You alone we seek help (and may we always) (4). Guide us on the Straight Path (5). The path of those whom You have favored (6). Not the path of those who earned Your anger - nor of those who are astray (7)."
Ameen

Surah Al-Fatihah

All praise is due to ALLAH and peace be upon the Prophet Muhammad ﷺ and his family, his companions (may ALLAH be pleased with them) and his followers.

With immense respect, I would like to extend my deepest gratitude to my family because without their prayers, love, positive reception and affection I would not have been able to achieve my desired goal in life. I will always be thankful to them for their continuous moral and emotional support and ever-needed prayers.

It has been my honor to be able to work with Dr. Muhammad A. Abido. I would like to admire his supervision, suggestions and guidance right from the beginning till the end of this research. His constant motivation helps me to produce quality work. I would like to thank my committee members: Dr. Ibrahim El-Amin and Dr. Ibrahim Omar Habiballah for their useful response, advice and the time they spent reviewing this thesis.

I am very obliged to King Fahd University of Petroleum & Minerals for providing me an opportunity to pursue my graduate degree. I would also like to appreciate all the support that I received from the Electrical Engineering Department in carrying out this research.

I would like to thank all my friends Ijaz, Bilal, Abdul Mateen, Emad Areed, Fazal, Umar, Omar, Asim, Faraz, Irfan and all the seniors at KFUPM for providing the moral support, pleasant atmosphere and never forgettable moments.

TABLE OF CONTENTS

LIST OF TABLES

LIST OF FIGURES

LIST OF ABBREVIATIONS

ANFIS	:	Adaptive Neuro-fuzzy Inference Systems
ANN	:	Artificial Neural Network
CT	:	Clark Transformation
CMBC	:	Constant maximum boost control
CMI	:	Cascaded Multi-level inverters
DE	:	Differential Evolution
ESB	:	Energy Storage Batteries
FIR	:	Finite Impulse Response
FS	:	Fourier Series
FT	:	Fourier Transform
IEC	:	International Electrotechnical Commission
IEEE	:	Institute of Electrical and Electronics Engineers
MBC	:	Maximum Boost Control
NI	:	National Instrument
PCC	:	Point of Common Coupling
PLL	:	Phase Lock Loop

PWM	:	Pulse Width Modulation
PV	:	PhotoVoltaic
RES	:	Renewable Energy Resources
RMS	:	Root Mean Square
RTDS	:	Real Time Digital Simulator
SBC	:	Simple Boost Control
THD	:	Total Harmonic Distortion
TDD	:	Total Demand Distortion
VI	:	Virtual Instruments

ABSTRACT

Full Name : Muhammad Usman Mukhtiar

Thesis Title : Maximum Power Point Tracking Controller for Transformerless Grid-Connected PV System

Major Field : [Electrical Engineering]

Date of Degree : [December 2015]

Use of PV systems is increasing due to the depletion of fossil fuels. Two stage converters commonly used with PV systems reduces the efficiency, increases the cost and device count. Single stage Z-source inverter has been proposed and implemented in this research work to overcome the problem of two stage converters. Laboratory prototype and real time implementation of Z-source inverter have been done for stand-alone and grid-connected PV systems in this research work to explore and improve the performance of the converter. PV array has been modelled and used with Z-source converter and various feedback controllers have been proposed and implemented for stand-alone and grid-connected mode for improved, reliable and robust control for power conversion systems. Simulations have been carried in Simulink/Matlab environment and real time performance of the power conversion system has been evaluated using Real Time Digital Simulator (RTDS) and dSPACE1103. A laboratory prototype of Z-source inverter has been used for maximum power point tracking of Chroma PV Simulator with feedback control.

ملخص الرسالة

الاسم الكامل: محمد عثمان مختيار

عنوان الرسالة: المتحكمات للتتبع نقطة الطاقة القصوى المتصلة بالشبكة الكهروضوئية بدون محول كهربائي.

التخصص: [هندسة كهربائية]

تاريخ الدرجة العلمية:[ديسمبر 2015]

أدى نضوب الوقود الحفرى إلى زيادة استخدام الطاقة الكهروضوئية.يعاب على المحولات ثنائية المرحلة التى تستخدم غالبا مع هذه الأنظمة أنها تقلل الكفاءة و تزيد التكلفة وعدد الأجهزة المستخدمة. العمل البحثى فى هذه الأطروحة يقدم و يطبق استخدام Z- source Inverter للتغلب العيوب السابقة. تم تنفيذ و تطبيق نموذج معملى ل Z- source Inverter لكل من الأنظمة الكهروضوئية المستقلة و المتصلة بالشبكة الكهربية بهدف استكشاف و تحسين أداء المحول. كذلك تم نمذجة نظم الطاقة الكهروضوئية مع Z- source Inverter مع استخدام طرق متعددة للتغذية الخلفية فى كلا الحالتين المستقلة و المرتبطة بالشبكة الكهربية بهدف تحسين و زيادة اعتمادية نظم تحويل الطاقة. تمت محاكاة النظام باستخدام برنامج Simulink/Matlab و تم تقييم التطبيق العملى باستخدام Time Digital Simulator (RTDS) and dSPACE1103. بالإضافة إلى ذلك تم استخدام نموذج معملى ل Z-source inverter للتتبع نقطة التشغيل ذات القدرة القصوى باستخدام Chroma PV Simulator مع تحكم بتغذية خلفية.

CHAPTER 1

INTRODUCTION

1.1 Background

Energy crisis and environmental concerns have increased the interest of researchers in renewable energy sources. The kingdom of Saudi Arabia receives a high direct normal irradiation of 2200 kwh/m^2/y which makes PV to be the most suitable renewable energy for the kingdom. The country is ambitious to diversify energy supply with increasing focus on renewable energies so that dependence on fossil fuels is reduced. Consumption of electricity is likely to increase from 51 GW in 2011 to 120 GW in 2030. Renewable energy contribution is expected to be 54 GW by 2032 with PV adding 16GW to the mix [1].

With annual population growth of 3.2%, economic growth of 6.8% and industrial production growth of around 6%, the demand for optimum new energy mix is increasing. Increased industrialization over the last two decades has increased focus on reliability and stability of the supply [1]. With a large number of consumers connected to transmission systems and the number still increasing it's, therefore, very important to study ways and means to enhance power system performance in the many countries.

This thesis work is focused on the development of electrical model of PV modules and its use in grid connected PV system. quasi-Z-source inverter has been used in this work for

power conversion from PV arrays to the grid and control scheme would be developed that would ensure reliable and effective integration of PV with the grid. The grid connected PV system would be developed on Real Time Digital Simulator (RTDS) and the proposed controller will be implemented using the dSPACE DS 1103 controller.

1.2 Thesis Motivation

The motivation of this thesis work is inspired by some non-resolved issues in the field of grid-connected inverters for efficient and effective transfer of power to the grid. The efficiency of the inverter depends upon the number of stages of power conversion and robustness of its controller. To remove multiple stages of power conversion, single stage quasi-Z-source inverter has been introduced by researchers and some feedback controllers have been developed by researchers to work with PV systems in grid-connected mode but the performance and control of quasi-Z-source inverter depend upon its new PWM techniques. The single stage quasi-Z-source inverter in transformerless grid-connected mode has driven the attention of researchers for reliable and effective control strategies and PWM techniques and its performance with power systems.

The literature survey has shown that novel reliable PWM controllers and MPPT controllers for quasi-Z-source based PV is required in power systems. Based on the work done on quasi-Z-source inverter and the ever growing application of quasi-Z-source network in renewable energy systems, reliable PWM techniques and improved feedback controllers have been developed in this research work and their performance has been evaluated using experimental prototype of the systems in laboratory.

1.3 Thesis Objectives

The research objective of this work is focused on development of grid connected PV systems. The objectives can be described as below:

1. Developing a generalized PV array simulator using PV model that can work under different conditions.
2. Developing transformerless grid connected PV system with quasi-Z-source inverter using the developed PV array simulator.
3. Developing a Maximum Power Point Tracking controller that can work for changing conditions.
4. Building a laboratory prototype of the PV system with quasi-Z-source inverter.

1.4 Thesis Methodology

The research work was performed as following:

A detailed literature survey was done to assess technological advances in grid-connected inverters and use of quasi-Z-source networks in grid-connected modes. A thorough study of control system for quasi-Z-source inverter has been done.

A design procedure for the quasi-Z-source inverter was developed. Then, the software and hardware prototypes of quasi-Z-source inverter were developed using the design procedures. Various PWM controllers for control of quasi-Z-source inverters were developed and implemented. These PWM techniques for quasi-Z-source were implemented in RSCAD and their performance were checked in Real Time Digital Simulator (RTDS).

The developed quasi-Z-source inverter was used with PV systems. Stand-alone and grid-connected PV systems with quasi-Z-source were developed in Simulink. Experimental setup was developed for the implementation of quasi-Z-source inverter and its control. PWM controller and feedback controller for laboratory prototype of quasi-Z-source inverter were employed in dSPACE1103 for various environmental conditions. So, the experimental investigation of the PWM control of quasi-Z-source inverter was done. Also, the performance of feedback control strategy for the prototype was evaluated.

Real time setup was established for performance evaluation of new power controllers using RTDS and dSPACE1103. The grid-connected PV system with quasi-Z-source inverter was implemented in RSCAD and its feedback ANFIS power controller was employed in dSPACE.

1.5 Thesis Contribution

The main contribution of this work is proposing new efficient PWM techniques and effective control of grid-connected PV system with Z-source inverter. Furthermore, prototype has been built for Z-source inverter in laboratory.

The specific thesis contributions are:

- Improved Maximum Power Point Tracking controllers based on PWM techniques for quasi-Z-source inverter.
- A prototype for quasi-Z-source inverter to evaluate its performance and control in power system has been developed to improve the voltage and efficiency of various power system networks.

- Three improved PWM Techniques have been implemented to enhance the performance of quasi-Z-source inverter.
- Two improved control strategies for feedback control quasi-Z-source based grid-connected PV system have been developed for effective power, voltage and current control of the system.
- A laboratory scale prototype has been developed for quasi-Z-source connected PV system for transformerless mode of operation that can be connected to power system for smart-grid operation.

1.6 Thesis Breakdown

Elaboration on research problem, research objectives and research methodology has been done in chapter one. The second chapter will briefly cast light on the fundamental concepts of the photovoltaic systems, PV modules, and maximum power point tracking techniques, literature survey on the use of Z-source inverter, various power and current controllers used for Z-source inverters. Chapter 3 will discuss PV module modelling, optimization of PV module parameters and the design and implementation of Z-source inverter. Chapter 4 presents various efficient PWM techniques for Z-source inverter and its implementation. The Simulink results for these techniques are also discussed. Chapter 5 gives details of feedback controllers implemented for PV connected Z-source inverter and their performance have been evaluated. Implementation of PI controllers and ANFIS controllers in Simulink/MATLAB environment is elaborated. Implementation of these controllers in real environment has also been presented. Chapter 6 discusses experimental setup and prototype implementation of Z-source inverter and its test for MPPT with

Chroma PV simulator. Finally, chapter 7 will conclude the findings and suggest the future work.

CHAPTER 2

LITERATURE REVIEW

All of the hazardous consequences coming from fossil fuels can be eliminated using Renewable Energy Resources (RES). Also, the deregulation in electricity markets and the development of the distributed generation (PV SYSTEMS) technologies are promoting the use of RES in power generation [3]. Among the renewable energy sources (RES), solar energy is the promising and photovoltaic (PV) system provides the most direct method to convert solar energy into electrical energy without environmental contamination. As PV cells are semiconductor devices, they are quiet, static, and require less maintenance and have low operational cost as compared to other RES like wind energy[2]. Electricity production using PV systems is expected to reach 200 GW during 2020 and 800 GW during 2030 (European Photovoltaic Industry Association (EPIA) report) [3]. This increase in the deployment of PV generation has led researchers to work on the different issues of photovoltaic like PV cells material, modelling of the PV panel, maximum power point tracking algorithms, power electronics converter used to integrate PV array with grid and its impact on power system etc.

2.1 PV Modules

To carry out a simulation study on PV systems, an efficient and robust electrical model is required which can produce various electrical characteristics, i.e., I-V and P-V of photovoltaic panel with different conditions like varying radiation, temperature, partial shadowing techniques etc. [4][5]. These characteristics of PV systems are highly non-

linear, so it is not suitable to model it using DC or controllable sources[6]. In [7], modelling of PV module has been done using ideal diode and four parameter models. Researchers have proposed and worked out various models for PV panels which includes those models which utilizes empirical correlation factors, those models which have been proposed to use analytical details of PV Cell and those models which combines both of these techniques[4][8][9] [10][11]. PV models presented so far in the literature are either very low detailed or very complex and sophisticated to be used for studies of simple energy systems. One of the model is the one that scales maximum power point based on temperature and irradiation, so the coefficients relative to irradiance and temperature for maximum power point is required to evaluate the behaviour of PV module. A way of changing I-V curve from given conditions of environment to second conditions is used[12].

Bilinear interpolation technique has been proposed and used in that uses 4 different I-V curves such that two of them at changed temperature and two of them at changed irradiance. In this case, the characteristics of PV module or panel are determined by interpolation of four curves with open-circuit voltage and short-circuit current to find solar irradiance and temperature, respectively for ambient or normal conditions. These complex and sophisticated models need a lot of data usually very difficult to obtain[13].

Sandia Lab model is the most reliable, effective, pragmatic and efficient model for PV systems given in which uses 3 inputs namely wind velocity, temperature and irradiance and it calculates current and the voltage at five different points on the curve. The data required for this model is comprised of 30 constants obtained from experiments to check the characteristic behaviour of any PV module or panel. The data can be obtained for

many PV modules or panels available commercially. Energy system studies like load flow and other studies when done with these models give good results but would be complex and would take large amount of time[11][14].

Some other models have been proposed using Artificial intelligence techniques which give reliable and fast parameter estimation for four and five parameter models[15],[16]. Differential evolution technique has been used in [16] to estimate the parameters that works fine under certain conditions but under low irradiance the performance is low. A genetic Algorithm technique has been employed in [17] to model PV modules which also shows satisfactory results but at low temperatures and irradiance the performance is not good. PV module modelling has been attempted by some researchers under partial shading conditions which under some restricted conditions give good results but improvement is still required[18][19][20].

To improve the performance of PV systems, improved models have been tried using seven parameter models of PV modules[4][21]. The two diode model gives better performance under low irradiance and temperatures but the methods developed so far can work under restricted conditions.

2.2 Models of PV Module

PV modules can be modelled using an equivalent electrical models which can also be connected in any electrical circuit and thus can easily be used for the overall transient and dynamic studies of a power system especially when connected to the grid. Different types of PV models have been given as shown below, namely double diode model, R_{SH} model, R_S and ideal diode model. Figure 2.1 shows the ideal diode model which consists of a current source in parallel with a diode.

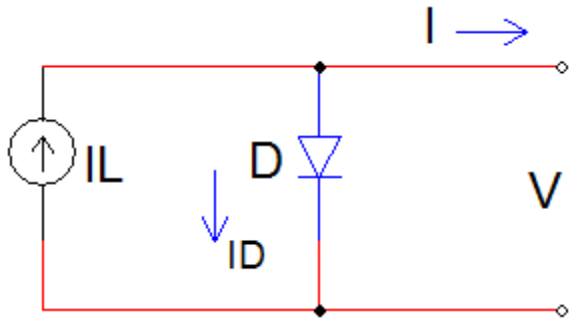

Figure 2.1 Ideal diode model

Figure 2.2 shows the four parameter model of PV module also known as R_S model which consists of a series resistor in the output current path in addition to the ideal diode model.

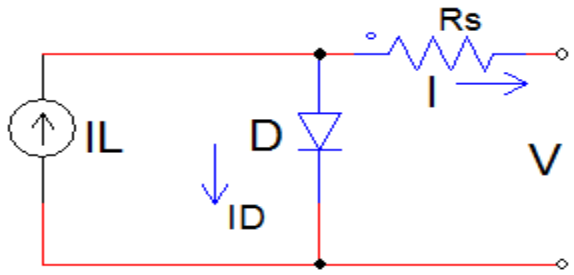

Figure 2.2 Four parameters model

Figure 2.3 shows the five parameters model (R_{SH} model) with a shunt resistor and series resistor to give more accurate results.

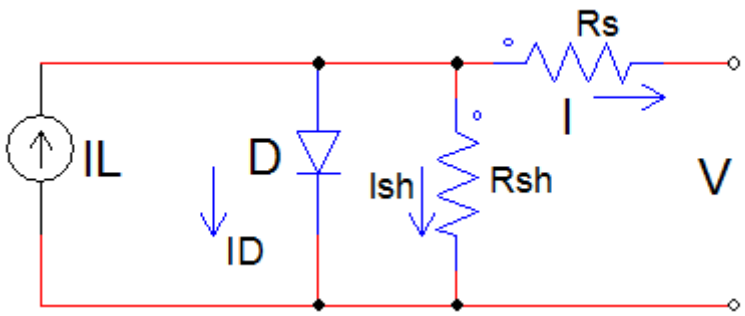

Figure 2.3 Five parameters model

Figure 2.4. Shows the seven parameters model (double diode model) to count for junction recombination loss. It consists of 2 diodes in parallel to the current source, a shunt resistance and a series resistance. The seven parameters are I_L, I_{d1}, I_{d2}, a_1, a_2, R_{sh} and R_s where I_L is the inner PV current, I_{d1} and I_{d2} are currents through the two diodes,a_1 and a_2 are the diode ideality factors, R_{sh} is the shunt resistance and R_s is the series resistance.

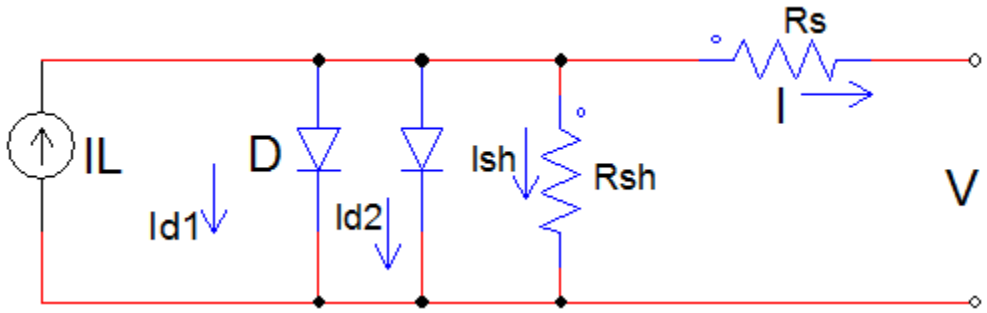

Figure 2.4 Seven Parameters PV model

The important part of the implementation is the estimation and calculation of the parameters of the model. The efficiency, performance and effectiveness of these models depend on the values of the parameters which in turn depend on the algorithm used for identification and calculation.

Various manufacturer provides the PV modules.

2.3 Maximum Power Point Tracking

PV module produces voltage and current that are dependent upon temperature and irradiance. With constant irradiance (G), the power-voltage characteristics of a typical PV module are shown in Figure 2.5. With constant temperature (T), the power-voltage characteristics of a typical PV module are shown in Figure 2.6.

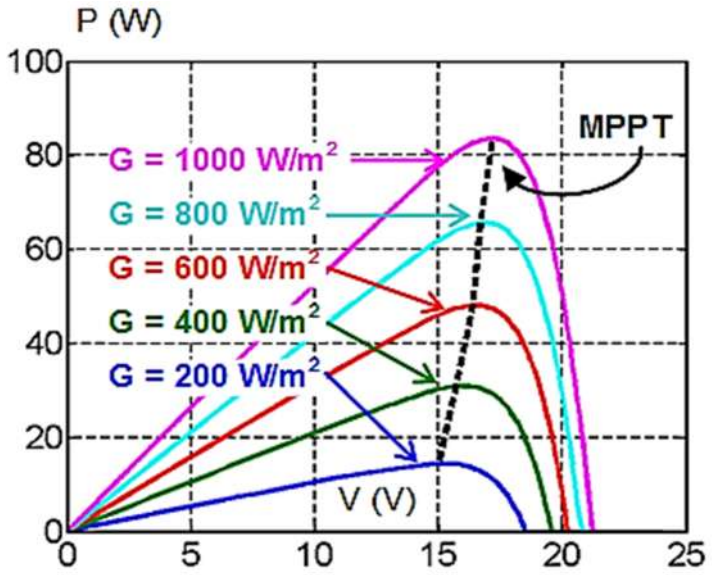

Figure 2.5 Power vs voltage characteristic for Constant temperature [10]

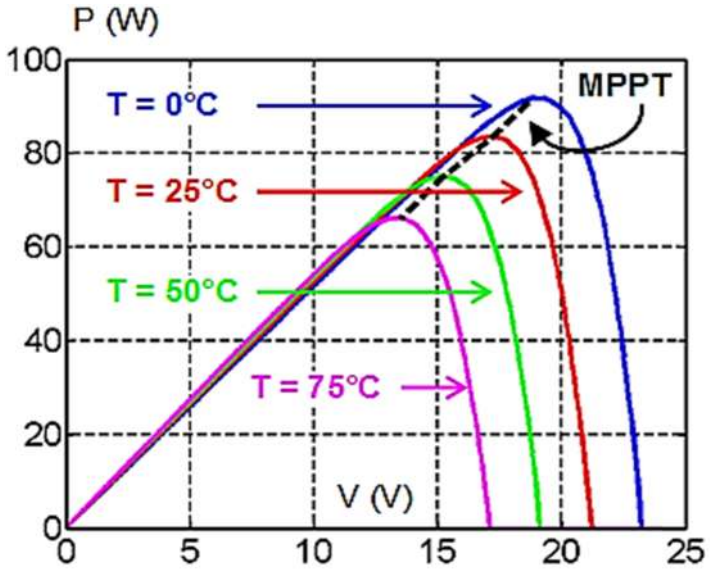

Figure 2.6 Power Vs Voltage Characteristic for PV module for constant irradiation [10]

The open circuit voltage (V_{oc}) is the maximum voltage from a PV module. At V_{oc}, the PV module open circuit current (I_{oc}) is zero. The short circuit current is the maximum current from a PV module. At short circuit current (I_{sc}), the output PV module voltage (V_{sc}) is zero. The maximum power from PV module is obtained at a voltage less than open circuit voltage and at current less than short circuit current. These values of voltage and current are maximum power voltage (V_{MMPT}) and maximum power current (I_{MMPT}). This is the maximum power point (MPPT) at given irradiation and temperature as shown in Figure 5 and Figure 6. If the current is increased or decreased due to the load seen by PV module, the operating point is changed from the maximum power point and power less than maximum power is drawn from the PV module. For constant irradiation and temperature, the maximum power point is constant.

The purpose of Maximum power tracking controller is to apply proper resistance after sampling the output from PV to track the maximum power point, thus extracting maximum power from the PV under the given conditions of irradiation and temperature.

For constant condition there is only operating point at which the corresponding voltage and current would result in maximum power.

The IV characteristic is generally linear but behaves like inverse exponential function at the knee as shown. Maximum power will be extracted from the device when the slope of the curve is equal and opposite to I/V ratio. This point is also called maximum power point. A resistance value of V/I will extract the maximum power from the device. If the resistance is different from this value, maximum power will not be extracted and maximum power point tracking controller is required to search for this point[26].

2.4 Perturb & Observe methods (P&O)

In this method, the controller changes the voltage by a small amount and checks the change in power, if the power is increasing it further increases the voltage until it reaches the maximum power point after which the power starts to decrease with increase in voltage. This is widely used method. It gives fluctuations in output power. The algorithm for Perturb and Observe method is shown in Figure 2.7.

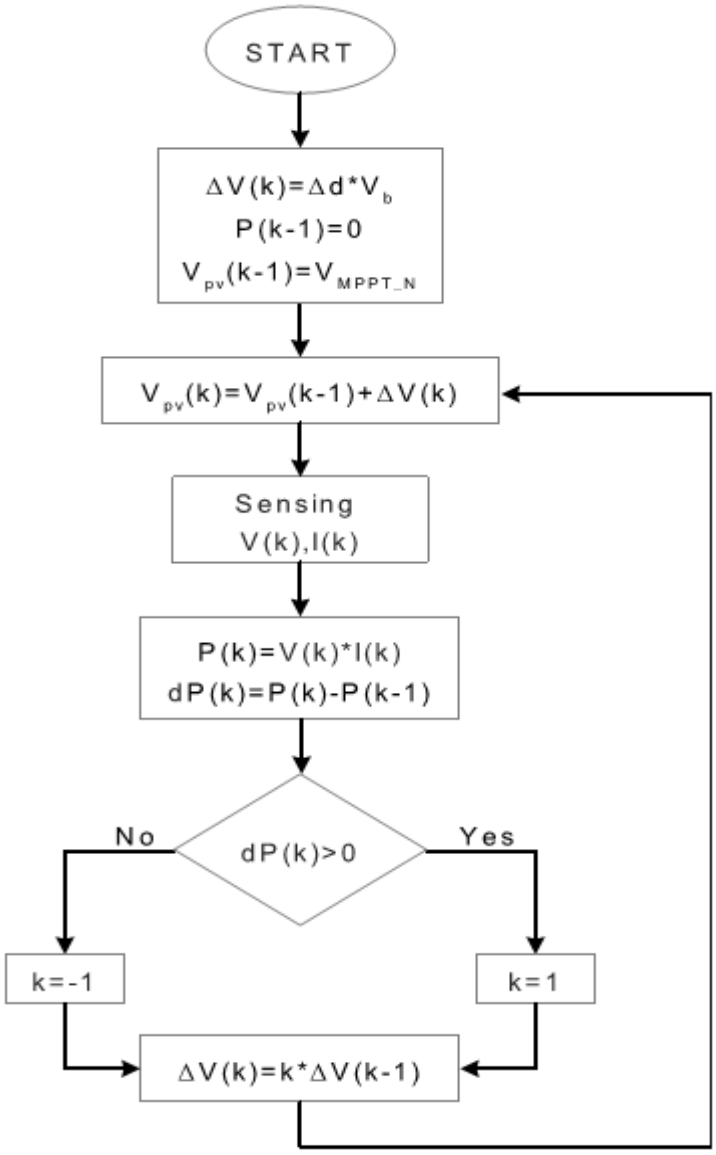

Figure 2.7 P&O algorithm [114]

Where V(k) is the present sampled voltage, V(k-1) is the previous sampled value of voltage, I(k) is the present sampled current value and P(k) is the present calculated maximum power value for PV module.

A schematic diagram for MPPT control of PV systems using Perturb and Observe method is shown in Figure 2.8.

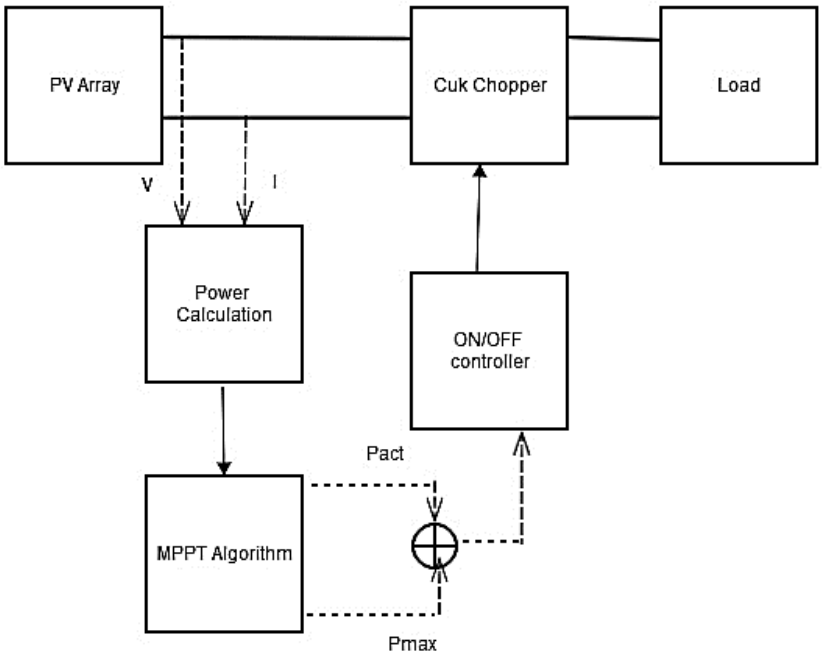

Figure 2.8 Schematic diagram for MPPT control of PV systems

Various simple P&O based MPPT controller has been attempted in literature [1]. Chee Wei Tan did the analysis of this method for MPPT[2].

2.5 Incremental conductance method

In this method, the controller uses the incremental changes in voltage and current to check the effect of voltage variation. It uses the dI/dV to find the sign of dP/dV, when the incremental conductance and array conductance is same then that is the maximum power point. A graph showing Incremental Conductance is shown in Figure 2.9.

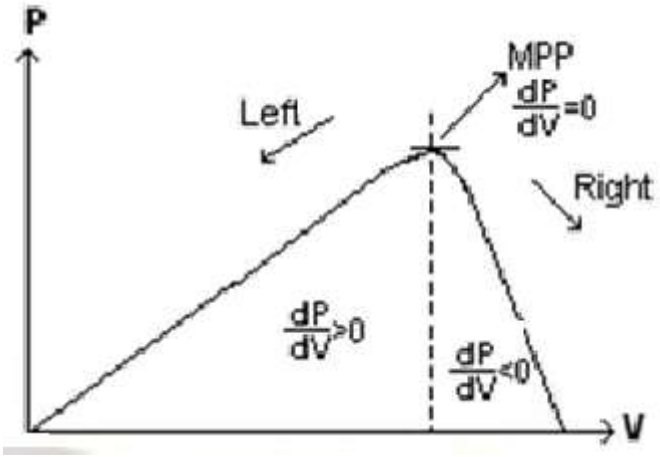

Figure 2.9 Flow chart for Incremental conductance method [26]

If dI/dV = -1/V, then it represents the maximum power point. If dI/dV >-1/V, then the maximum power point is to the right. If the dI/dV < -1/V, then the maximum power point is to the left. Where I and V are PV array output current and voltage respectively. The left hand side of equations represents incremental conductance of PV module and the right hand side represents the instantaneous conductance. When the ratio of change in output conductance is equal to the negative output conductance, the solar array will operate at the maximum power point.

Some researchers have developed Incremental conductance based MPPT controllers that control the DC-DC converters. Simulation and Hardware Implementation of Incremental Conductance MPPT with Direct Control Method Using Cuk Converter has been done.

Classical MPPT techniques uses irradiations and temperature to find maximum power point. Fast tracking of the maximum power point, robustness under changing conditions and reliability are required in MPPT controllers. In this work, fast tracking MPPT controllers have been proposed which are robust and reliable under various conditions.

2.6 Artificial Intelligence based methods

Artificial techniques like Adaptive Neurofuzzy Inference System and Neural networks have been used to design versatile MPPT controller. A schematic diagram for ANFIS based MPPT control of PV systems has been shown in Figure 2.10.

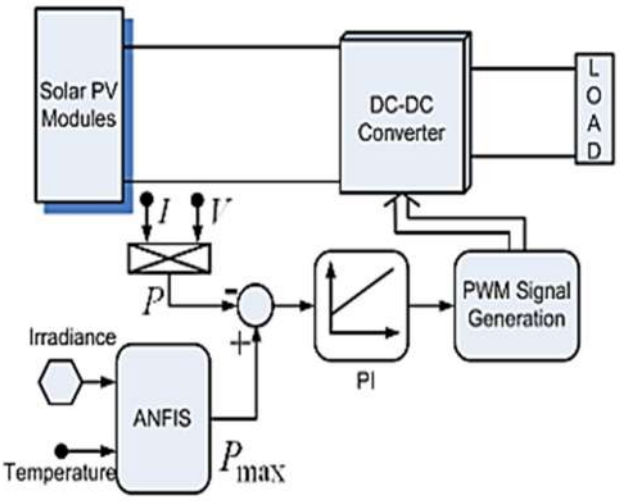

Figure 2.10 Diagram for ANFIS based MPPT [28]

Different artificial intelligence based MPPT controllers have been designed by researchers to control the switching of DC-DC converters.

2.7 Z-source inverter and its application in PV systems

In conventional voltage source converter, a DC voltage source is connected in parallel to a capacitor and then feeding a three phase bridge. The bridge consists of six switches which in turn comprise of transistor or IGBT's and anti-parallel diode. Some limitations of conventional V source inverter are:

1. Voltage source inverter is a buck inverter, i.e , the output ac voltage is always less than the input dc voltage.
2. The switches in upper and lower leg cannot be turned on simultaneously otherwise shoot through would occur which can damage the device, so dead time is required between switching which induces distortion in waveforms.
3. An ac filter is also required which causes losses and increases control requirements.

In conventional current source Inverter, a DC current source is connected to the three phase bridge inverter through an inductor. It has following limitations:

1. Current source inverter is a boost inverter, i.e, the output voltage is always greater than the input dc.
2. Only one of upper switch and one lower switch have to be ON but opening of one them can cause open circuit of inductor which can damage the device. So overlap time is needed which causes waveform distortion.
3. Series diodes are required with switches like IGBTs and transistors to prevent reverse voltage, this prevents the use of low cost switching modules.

2.8 Types of Z-source inverters (ZSI)

Various Topologies for Z-source inverters have been presented in the literature [119]. Z-source inverters are mainly voltage fed and current fed inverters. These two types of conventional Z-source inverters are shown in Figure 2.11 and Figure 2.12.

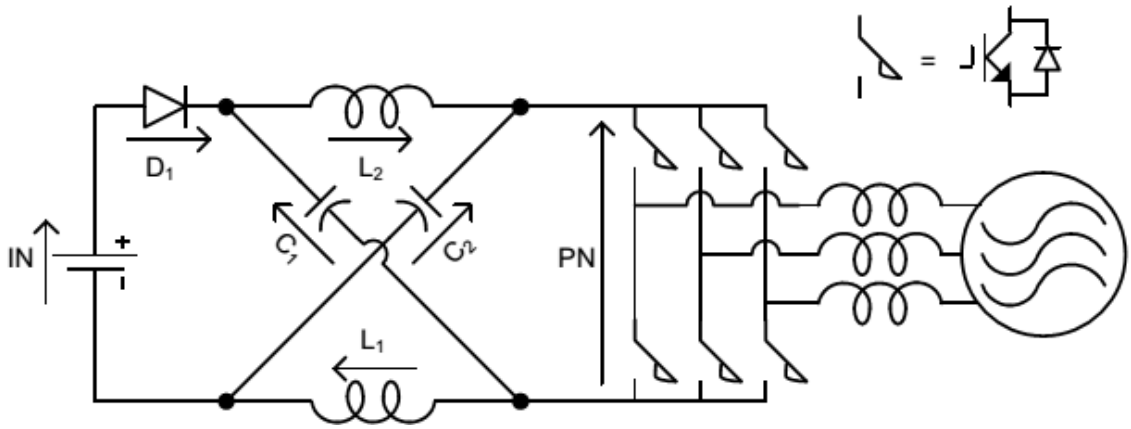

Figure 2.11 Voltage Fed ZSI with Discontinuous Input Current [113]

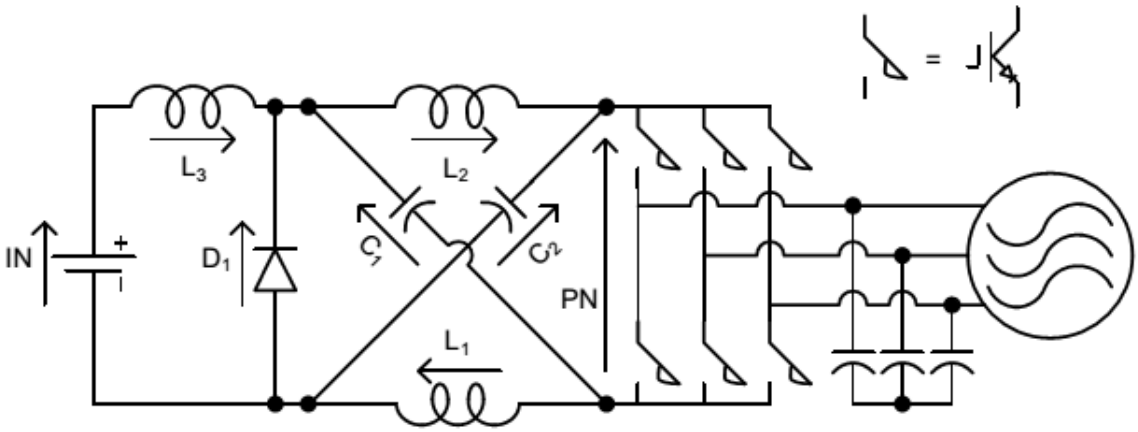

Figure 2.12 Current Fed ZSI with Continuous Input Current [113]

The voltage fed ZSI has some significant drawbacks; namely that the input current is discontinuous in the boost mode and that the capacitors must sustain a high voltage. The main drawback of the current fed ZSI is that the inductors must sustain high currents. Also, control complexity is an issue when the ZSI is used in a back-to-back configuration due to the coupling of the inverter switching functions.

To overcome these drawbacks, four new types of Z-source inverters have been proposed in the literature [113].

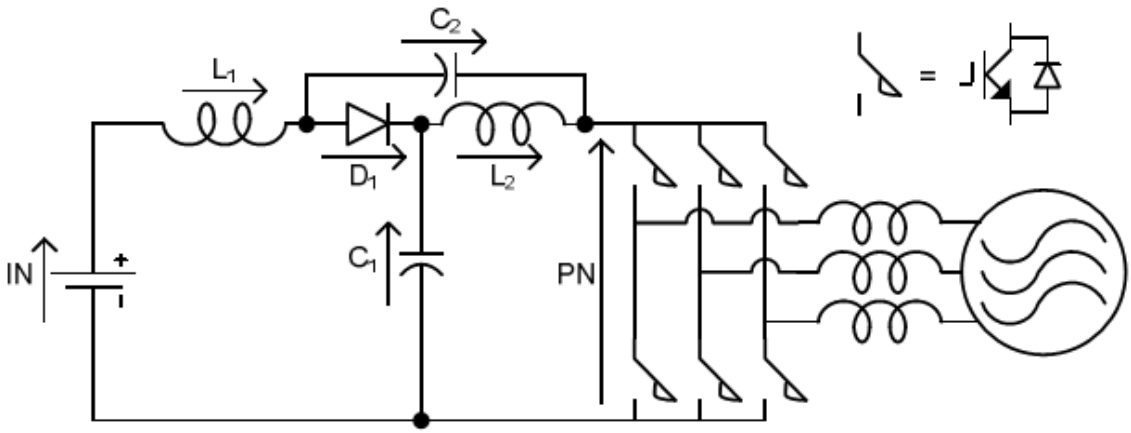

Figure 2.13 Voltage Fed qZSI with Continuous Input Current [113]

Two of these inverters are voltage fed quasi-Z-source inverter (qZSI) as shown in Figure 2.13 and Figure 2.16 and the other two are current fed qZSI as shown in Figure 2.14 and Figure 2.15.

The novel qZSI topologies shown in Figure 2.13 and Figure 2.16 , in a manner consistent with the voltage fed ZSI, can be made bidirectional by replacing the diode, D1, with a bidirectionally conducting, unidirectionally blocking switch. The qZSI, shown in Figure 2.13, when compared to the ZSI shown in Figure 2.11, features lower dc voltage on capacitor C2 as well as continuous input current, while the qZSI topology, shown in Figure 2.16, features lower dc voltage on capacitors C1 and C2, however, the input current is discontinuous. Also, due to the input inductor, L1, the qZSI shown in Figure 2.13 does not require input capacitance, unlike the ZSI and the qZSI shown in Figure 2.16.

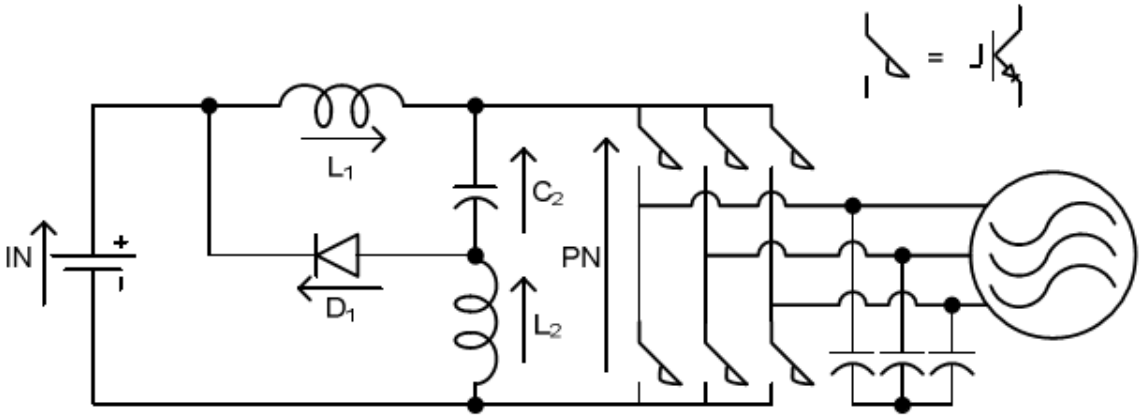

Figure 2.14 Current Fed qZSI with Discontinuous Input Current [113]

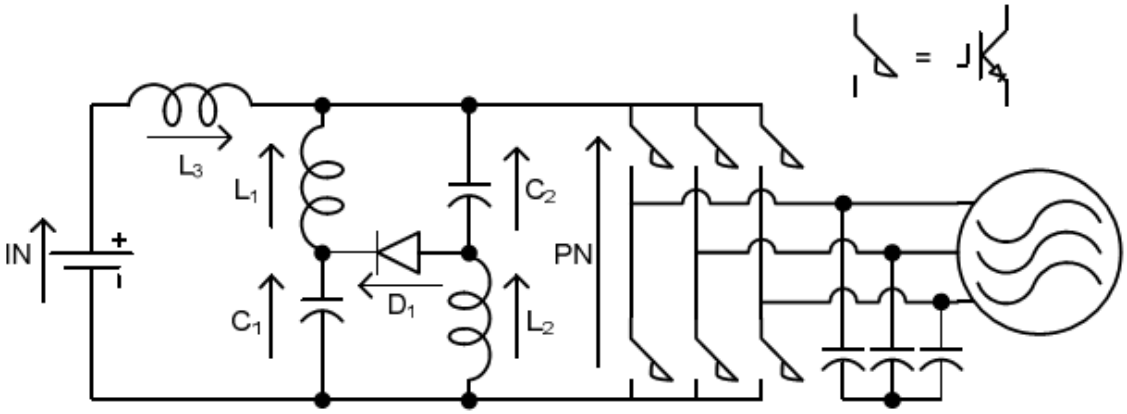

Figure 2.15 Current Fed qZSI with Continuous Input Current [113]

The current fed qZSI topologies shown in Figure 2.14 and Figure 2.15, in a manner consistent with the current fed ZSI, are bidirectional with the diode, D1. The qZSI shown in Figure 2.14, when compared to the ZSI shown in Figure 2.12, features reduced current in inductor L2, as well as reduced passive component count, while the qZSI shown in Figure 2.15 features lower current in inductors L1 and L2. Again, due to the input inductor, L3, the ZSI and qZSI in Figure 2.12 do not require input capacitance.

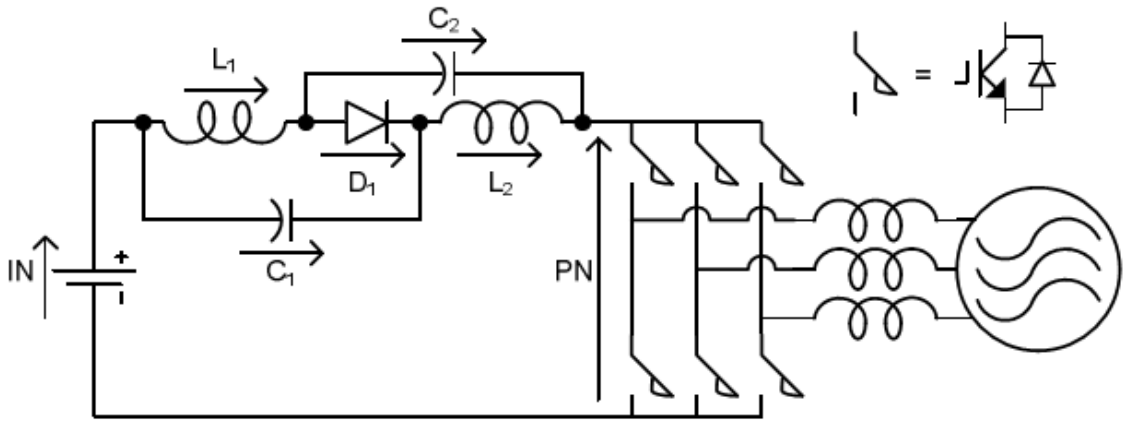

Figure 2.16 Voltage Fed qZSI with Discontinuous Input Current [113]

All four qZSI topologies also feature a common dc rail between the source and inverter, unlike the traditional ZSI circuits. Furthermore, these qZSI circuits have no disadvantages when compared to the traditional ZSI topologies. These qZSI topologies therefore can be used in any application in which the ZSI would traditionally be used

Table 2.1 shows the governing equations of the various forms of voltage fed ZSIs discussed earlier [113]. These equations are derived using Kirchhoff's current and voltage laws and state-space averages of inductors and capacitors for each circuit. These equations are derived by applying aforementioned laws in different modes of operation for voltage fed inverters.

Table 2.1 Voltage Fed ZSI and qZSI Governing Equations

	Voltage Fed ZSI	Voltage Fed qZSI w/ Continuous Input Current	Voltage Fed qZSI w/ Discontinuous Input Current
$\frac{V_{C1}}{V_{IN}}$	$\frac{1-D}{1-2D}$	$\frac{1-D}{1-2D}$	$\frac{D}{1-2D}$
$\frac{V_{C2}}{V_{IN}}$	$\frac{1-D}{1-2D}$	$\frac{D}{1-2D}$	$\frac{D}{1-2D}$
$I_{L1} = I_{L2}$	$\frac{P}{V_{IN}}$	$\frac{P}{V_{IN}}$	$\frac{P}{V_{IN}}$
I_{C1}	$-I_{PN} - I_{L1}$	$-I_{PN} - I_{L1}$	$-I_{PN} - I_{L1}$
I_{C2}	$-I_{PN} - I_{L2}$	$-I_{PN} - I_{L2}$	$-I_{PN} - I_{L2}$
$\frac{V_{L1}}{V_{IN}} = \frac{V_{L2}}{V_{IN}}$	$\frac{D}{1-2D} - S_D * \frac{1}{1-2D}$	$\frac{D}{1-2D} - S_D * \frac{1}{1-2D}$	$\frac{D}{1-2D} - S_D * \frac{1}{1-2D}$
$\frac{V_{PN}}{V_{IN}}$	$\overline{S_D} * \frac{1}{1-2D} \geq 0$	$\overline{S_D} * \frac{1}{1-2D} \geq 0$	$\overline{S_D} * \frac{1}{1-2D} \geq 0$
$\frac{V_D}{V_{IN}}$	$S_D * \frac{1}{1-2D} \geq 0$	$S_D * \frac{1}{1-2D} \geq 0$	$S_D * \frac{1}{1-2D} \geq 0$
I_D	$I_{L1} + I_{L2} + I_{PN}$	$I_{L1} + I_{L2} + I_{PN}$	$I_{L1} + I_{L2} + I_{PN}$
I_{IN}	I_D	I_{L1}	$-I_{PN}$

Table 2.2 shows the equations that govern the operation of various forms of current fed ZSI and qZSIs. In these equations, D is the shoot-through duty cycle and S_D is the shoot-through function. S_D is defined to be 1 when the inverter is in shoot-through mode and 0 when inverter is in active mode.

Table 2.2 Current Fed ZSI and qZSI Governing Equations

	Current Fed ZSI	Current Fed qZSI w/ Discontinuous Input Current	Current Fed qZSI w/ Continuous Input Current
$\frac{I_{L1}}{P/V_{IN}}$	$\frac{1-D}{1-2D}$	$\frac{1-D}{1-2D}$	$\frac{D}{1-2D}$
$\frac{I_{L2}}{P/V_{IN}}$	$\frac{1-D}{1-2D}$	$\frac{D}{1-2D}$	$\frac{D}{1-2D}$
$\frac{I_{L3}}{P/V_{IN}}$	1	Not Applicable	1
V_{C1}	V_{IN}	Not Applicable	V_{IN}
V_{C2}	V_{IN}	V_{IN}	V_{IN}
V_{L1}	$V_{PN} - V_{C2}$	$V_{PN} - V_{IN}$	$V_{PN} - V_{C1}$
V_{L2}	$V_{PN} - V_{C1}$	$V_{PN} - V_{C2}$	$V_{PN} - V_{C2}$
V_{L3}	$V_{C1} + V_{C2} - V_{PN} - V_{IN}$	Not Applicable	$V_{PN} - V_{IN}$
$\frac{I_{C1}}{P/V_{IN}}$	$\frac{D}{1-2D} - S_D * \frac{1}{1-2D}$	Not Applicable	$\frac{D}{1-2D} - S_D * \frac{1}{1-2D}$
$\frac{I_{C2}}{P/V_{IN}}$	$\frac{D}{1-2D} - S_D * \frac{1}{1-2D}$	$\frac{D}{1-2D} - S_D * \frac{1}{1-2D}$	$\frac{D}{1-2D} - S_D * \frac{1}{1-2D}$
$\frac{I_{PN}}{P/V_{IN}}$	$\overline{S_D} * \frac{1}{1-2D} \geq 0$	$\overline{S_D} * \frac{1}{1-2D} \geq 0$	$\overline{S_D} * \frac{1}{1-2D} \geq 0$
$\frac{I_D}{P/V_{IN}}$	$S_D * \frac{1}{1-2D} \geq 0$	$S_D * \frac{1}{1-2D} \geq 0$	$S_D * \frac{1}{1-2D} \geq 0$
V_D	$V_{C1} + V_{C2} - V_{PN} \geq 0$	$V_{IN} + V_{C2} - V_{PN} \geq 0$	$V_{C1} + V_{C2} - V_{PN} \geq 0$
I_{IN}	I_{L3}	$I_{L1} - I_D$	I_{L3}

From Table 2.1, it can be seen that the only parameters which change for the different voltage fed topologies are the capacitor voltages, and the input current. The maximum shoot through duty cycle, D, is 0.5 for these topologies with a positive input voltage, V_{IN}. Therefore, by the gain equations for the capacitor voltages, it can be seen that with the qZSI circuits, the capacitor voltages are reduced when compared with the traditional ZSI. If the input voltage is negative, it is also possible to operate the voltage fed topologies with a shoot through duty cycle, D, greater than 0.5. In this case, the ZSI has lower capacitor voltage than the qZSIs. Similarly, from Table 2.2, it can be seen that when the

shoot through duty cycle, D, is less than 0.5, the current through the inductors is decreased for the current fed qZSI topologies when compared to the traditional current fed ZSI.

When the shoot through duty cycle, D, is greater than 0.5 for the current fed ZSI or the qZSIs, the power flow is negative, and the current through the inductors is lower for the ZSI than the qZSIs. If the diode D1 is replaced with a bidirectionally blocking, unidirectionally conducting switch in any of the current fed topologies, it is possible to feed the system with a positive or negative voltage, and several new operating regions are allowed.

2.9 Z-source Inverter Structure

Z source Inverter has been used by researchers in place of conventional current source and voltage source inverter to improve the efficiency of the PV systems. Conventional current source inverter or voltage source inverter can only boost or buck the voltage and also electromagnetic interference and other restrictions lowers their efficiency while Z source inverter is buck-boost inverter which eliminates various problems with conventional inverters and also the need for boost converter is removed by the use of z source converter. Z-source inverter and its improved performance with PV systems will be explored in this thesis work and a novel Maximum Power Point Tracking controller will be designed for Z-source inverter in this research work.

To overcome these limitations, Z source inverter is suggested which is given in Figure 2.17. It consists of two capacitors and two inductors connected[22] as shown in Figure

and then feeding the three phase bridge. The switches used can have series diodes or anti parallel diodes as shown in Figure 2.17 and Figure 2.18.

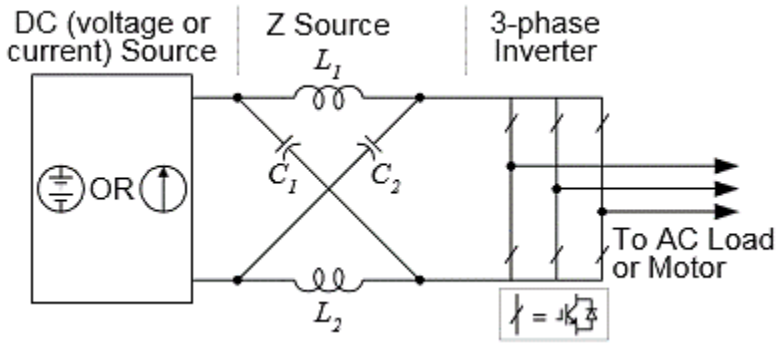

Figure 2.17 Z source inverter with switches with anti-parallel diodes [22]

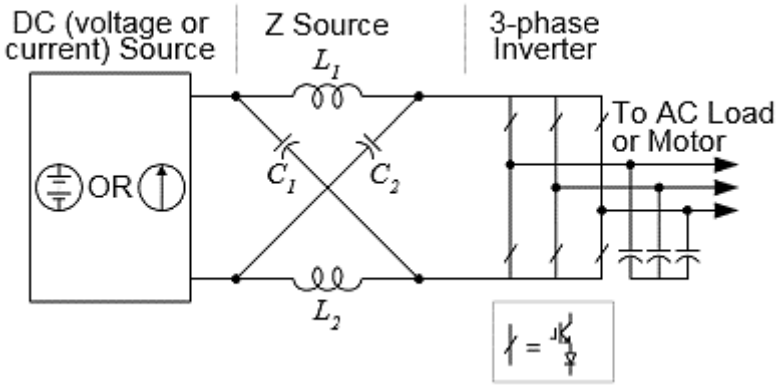

Figure 2.18 Z source inverter with switches series diodes [22]

The unique characteristic of Z-source inverter is that it is a buck boost inverter and the output ac voltage can have any value between zero and infinity theoretically. This characteristic is obtained by the permissibility of shoot through state in Z-source inverter which is forbidden in other inverters. This shoot through state is obtained by seven ways; either by turning ON simultaneously the two switches in any one of the three legs, or by combination of the two legs with all the four switches ON or by turning ON all the six switches simultaneously. This shoot through state makes it a buck boost inverter. This

state is also known as shoot-through zero states. This shoot-through zero states is shown in Figure 2.19.

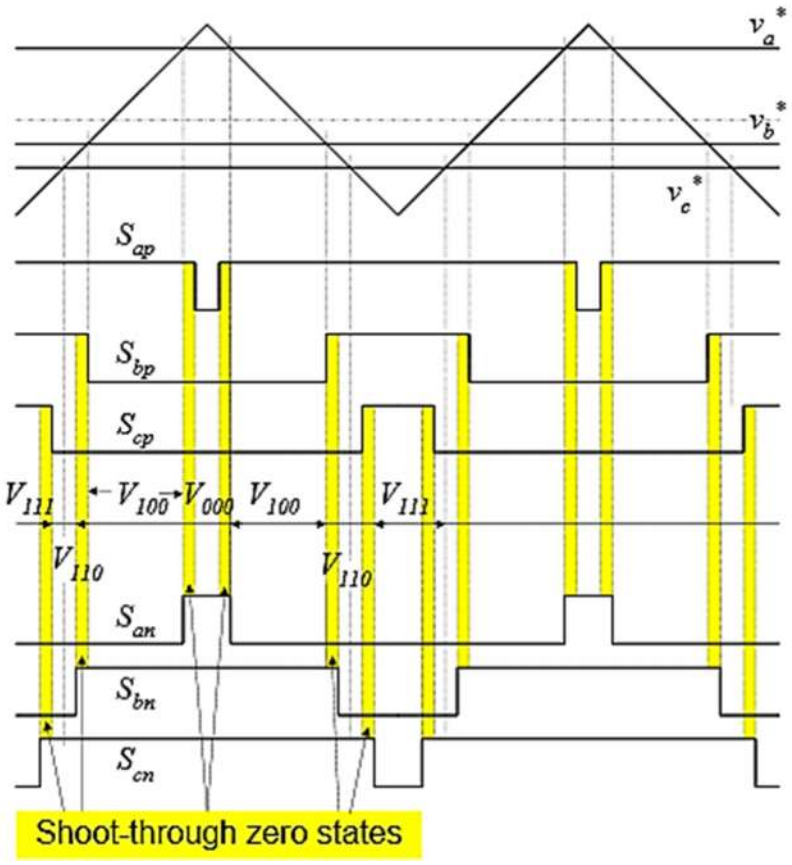

Figure 2.19 Switching states for Z source inverter [22]

Z-source inverter has been analyzed below:

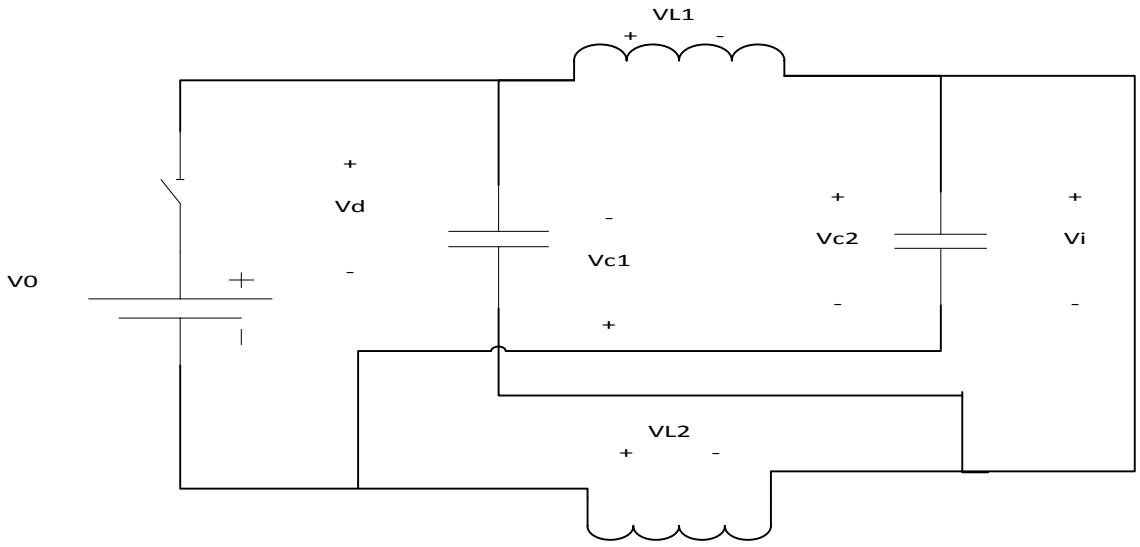

Figure 2.20 Z source inverter equivalent diagram during zero state

If the switching period is T and the shoot through time is To as shown in Figure 2.20, then

$$\boldsymbol{v_L = V_C} \quad , \quad \boldsymbol{v_{d=}\, 2V_C} \quad \text{and} \quad \boldsymbol{v_i = 0} \qquad \text{.....(2.9)}$$

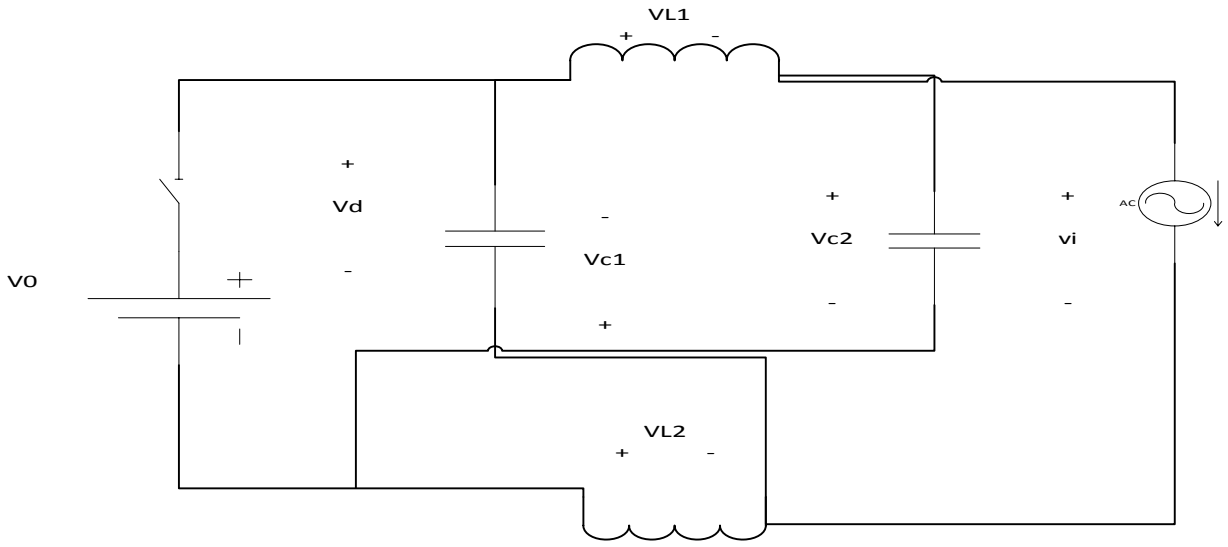

Figure 2.21 Z-source inverter equivalent diagram during non-zero states

During any non-zero state as shown in Figure 2.21, the equations are as follow:

$$\boldsymbol{v_{L=}V_o - V_C} \quad , \quad \boldsymbol{v_d = V_o} \quad , \quad \boldsymbol{v_i = V_C - v_L = 2V_C - V_o}$$

…….(2.10)

The peak voltage across the DC link is given by:

$$\boldsymbol{v_i = V_C - v_L = \frac{T}{T_1 - T_o} V_o = B.V_o} \qquad \text{…….(2.11)}$$

Where B is the boost factor obtained from zero state and is given by:

$$\boldsymbol{B = \frac{T}{T_1 - T_o} = \frac{1}{1 - 2\frac{T_o}{T}} \geq 1} \qquad \text{…….(2.12)}$$

The output ac voltage from the inverter is given by:

$$\boldsymbol{v_{ac} = M.B.\frac{V_o}{2}} \qquad \text{…….(2.13)}$$

Where M is the modulation index. The output voltage can be stepped up or stepped down by choosing a factor Bb such that

$$\boldsymbol{B_b = M.B = (0 \sim \infty)} \qquad \text{..……..(2.14)}$$

Many control strategies have been designed for use of Z-source inverter in PV systems. In [27], fuzzy logic has been used to design a controller for Z-source inverter for PV systems. In [28], ANFIS controller has been designed to control Z-source inverter for PV systems. In [23], another control strategy has been applied for Z-source inverter to track the maximum power point for four parameter model. In [28], a modified form of Z-source inverter known as quasi Z-source inverter has been used to track maximum power point to improve the performance and reduce losses. In [24], some simple modifications

for control techniques were used for slight improvement in performance. In [29],[30], study of control techniques for Z source inverter with quasi modifications were done and some comparisons were done. In [31] and [32], switch inductor and unified maximum power point tracking techniques were analyzed for Z-source inverter.

2.10 Quasi-Z-Source Inverter

Quasi-Z-source inverter (qZSI) is a new topology derived from the traditional Z-source inverter (ZSI). The qZSI inherits all the advantages of the ZSI, which can realize buck/boost, inversion and power conditioning in a single stage with improved reliability. In addition, the proposed qZSI has the unique advantages of lower component ratings and constant dc current from the source. All of the boost control methods that have been developed for the ZSI can be used by the qZSI. The qZSI features a wide range of voltage gain which is suitable for applications in photovoltaic (PV) systems, due to the fact that the PV cell's output varies widely with temperature and solar irradiation.

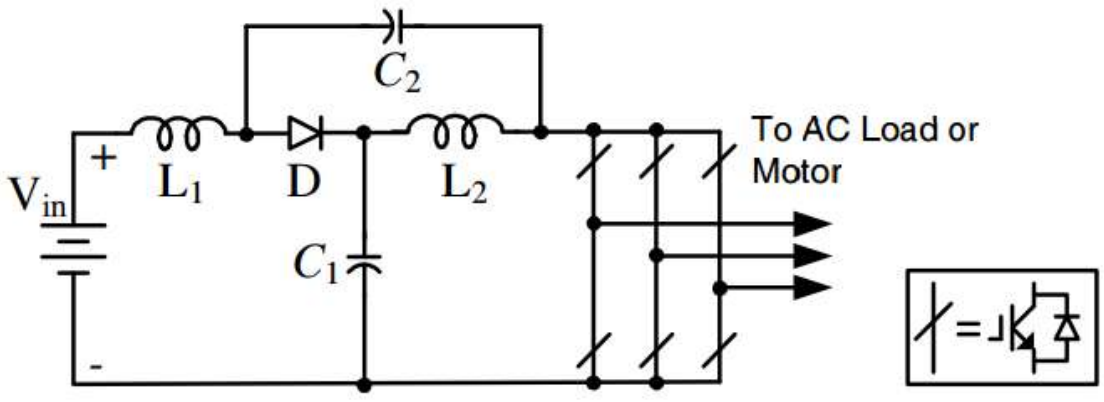

Figure 2.22 Quasi-Z-Source Inverter

If the switching period is T and the shoot through time is T_o, V_{C1} is the voltage across capacitor C_1, V_{C2} is the voltage across capacitor C_2, v_{L1} and v_{L2} are the voltage across inductor L_1 and L_2, V_{pv} is output voltage of PV module, v_i is the input voltage of inverter.

$$V_{C1} = v_{L1}\,, \quad V_{C2} + V_{pv} = v_{L2}\,, \qquad v_i = 0 \qquad \text{.....} \quad (2.15)$$

During any non-zero state as shown in Figure 2.15, the equations are as follow:

$$v_{L1=} V_{C1} - v_i = -V_{C2}, \quad v_{L2} = V_{pv} - V_{C1} \quad , v_i = V_{C1} + V_{C2} \qquad \text{.....} \quad (2.16)$$

The average voltage across the DC link is given by:

$$v_i = \frac{T_1(V_{C1}+V_{C2})}{\mathrm{T}} = \frac{T_1}{T_1 - T_o} V_{pv} = B.V_{pv} \qquad \text{.....(2.17)}$$

Where B is the boost factor obtained from zero state and is given by:

$$B = \frac{T_1}{T_1 - T_o} = \frac{1}{1 - \frac{T_o}{T_1}} \geq 1 \qquad \text{.....(2.18)}$$

The output ac voltage from the inverter is given by:

$$v_{ac} = M.B.\frac{V_i}{2} \qquad \text{.....(2.19)}$$

2.11 Applications and Control of Z-source Inverter

The control system for a power conversion system must have a fast and reliable dynamic response to minimize the effects of users and grids. More recently, various studies of voltage-fed ZSIs/qZSI have been done and their derived topologies are studied to improve the voltage gain of the basic ZSI/qZSI [6]–[12]. Investigation for feedback control and parameter design by state space averaging or dynamic modeling has been done in [36]–[46]. Many applications of Z-source have been explored by researchers such

as traction drive [47]–[50], wind [51]–[53], and PV power conversions [54]–[56]. Use of Z-source in combinations with traditional power conversion techniques, e.g., integrating with energy storage batteries (ESBs) has been investigated in [57]–[63]. Some advance applications such as coupling into the conventional matrix converter [64]–[76], neutral-point-clamped inverter [67]–[69], and cascade multilevel inverter (CMI) [70]–[77], etc. Studies also carried out current-fed ZSI/qZSI [78]–[80] and ZS/qZSI dc–dc converters [81]–[86]. Here, voltage-fed ZSI/qZSI are taken into account in view of their widespread investigations

Single-loop feedback control with PI controller has been investigated for Z-source using input dc voltage in [36], using capacitor voltage of Z-source network in [38], [48] and using dc-link voltage in [39], [42]. In [40], a sampling circuit is used to sample pulsating dc-link voltage to be used as a feedback variable which makes the hardware very complex. Feedback control is usually based on Z-source capacitor voltage which is used as control variable. The relationships between Z-source capacitor voltage and dc link peak voltage, i.e., $V_{dc}=V_c/(1-D)$ and $V_c^*=(V_{in}^* + V_{dc}^*)/2$ have been used in [48].In [37], a proportional control has been implemented for inner current loop to regulate dc-link peak voltage and fast response and it has been improved in [41] with a PI control.

Non-linear control for Z-source with a dc source has been implemented using model predictive control (MPC) in [44], [45]. In [42] and [61], sliding mode control has been employed for simple Z-source network to regulate dc –link voltage. Fuzzy control for simple Z-source network with a dc source has been used to regulate dc voltage in [60]. Neural network is another non-linear control that has been used to regulate dc-link voltage for Z-source connected with dc source in [43]. Neural network controller needs

training by using training data. All of these non-linear techniques have been used for simple dc-source connected to Z-source but for complex system connected to Z-source, these controllers have not been used. In these non-linear control methods, quantities like input dc voltage, capacitor voltage of Z-source network, load current, and dc-link voltage are sampled and used as controller input variables to calculate to the control signals for switching devices.

Performance, speed and reliability of these non-linear control methods are high as compared to conventional PI controllers. But in complex application like grid connected mode, wind energy system and PV systems, the use of these controllers is limited and needs improvement and robust design. MPC controller was used to adjust output waveform, response and robustness with minimum cost function but it limits the switching states which makes it unsuitable under complex applications [44], [45].

Reduction in fossil fuels and climatic changes have resulted in search for alternative energy resources of which PV has emerged as the biggest contributor to global energy markets [87], [88]. PV panel production rate is increasing and has reached 52 GW in 2012 and global installed PV capacity has reached more than 100 GW [89]. PV is dependent upon environmental conditions like irradiation and temperature, so the output of PV panel is changing, intermittent and not constant [90]. Therefore, an effective, robust and reliable control system are required to operate PV connected systems effectively and efficiently. Inverters are the major component used with PV and different topologies have been used and discussed in [91].Conventional two-stage inverters are replaced by single stage Z-source inverter to increase the efficiency and reduce the cost [60]-[62].The concept of Z-source can be used for all power conversion networks and

different conversion circuits can be derived for example Z-source/quasi Z-source converters [64]-[66], Z-source with neural point being clamped [67]-[69]. QZ-source network coupled with cascaded multi-level inverters (CMI) [71]-[77] and battery-storage (ESB) [57]-[63].

Many new semi-conductor devices are built using WBG semiconductor materials to improve conversion systems. The present energy conversion systems are used for small-level and some medium level PV systems but for large-level PV plants/system the use of converters and controllers is a challenge [90],[103],[105].

2.12 Transformerless grid connected PV system

A diagram of grid-connected PV system is shown below in Figure 2.22.:

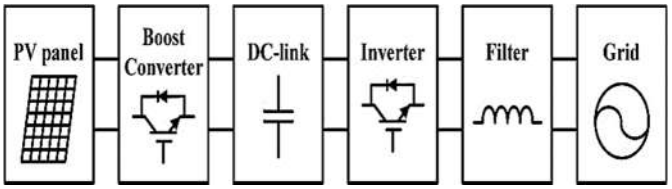

Figure 2.23 Grid connected PV system[33]

In grid connected PV system, the output voltage from a PV array system is converted to AC voltage using either current source inverter or voltage inverter both having some advantages and disadvantages. One can only boost and other can only step down the input voltage. The output AC voltage of the inverter is filtered out using filters and then synchronized with a grid. A maximum power point tracking (MPPT) control is required to track the maximum power, voltage and current from the PV with changing irradiation and temperature. The MPPT control is connected to a DC-DC boost converter to check for maximum voltage and current available from PV array system and adjust the duty

cycle of boost converter to keep the output DC voltage of the boost converter at a constant value that is used by the DC-AC inverter. The inverter is controlled by a PWM technique in which a carrier signal is compared with a reference signal and pulses are generated based on this comparison. These pulses are then sent to the switches of the inverter to convert the input DC voltage to an output AC voltage of desired frequency and magnitude. The harmonics from this output AC voltage is filtered out by using filters and then through a grid transformers, the PV system is connected to a local grid. In [33], the grid connected transformer has been eliminated to improve the efficiency and power transfer of the PV systems. In [34], a single phase multi-level inverter has been used for power conversion for PV systems connected to a grid but the transformer reduces the efficiency and also the inverter is not able to do buck-boost operations. To improve the performance of PV systems transformerless grid connected topologies have been adopted which increases the efficiency and reduces the losses by removing grid-transformer [22][23][24].

CHAPTER 3

DESIGN OF PV MODULE AND Z-SOURCE INVERTER

Z-source inverter is a single stage topology and it includes two capacitors, two inductors and a diode. The capacitors and inductors are called impedance network. It is used to boost up the voltage to the required DC link voltage level. The design of a Z-source network requires selecting capacitors, inductors and diodes of specific rating that can work efficiently and effectively under nominal conditions. In this chapter, the design procedure of electrical components is presented.

3.1 Modelling of PV Module

Five parameter model of a PV module is shown in Figure 3.1.

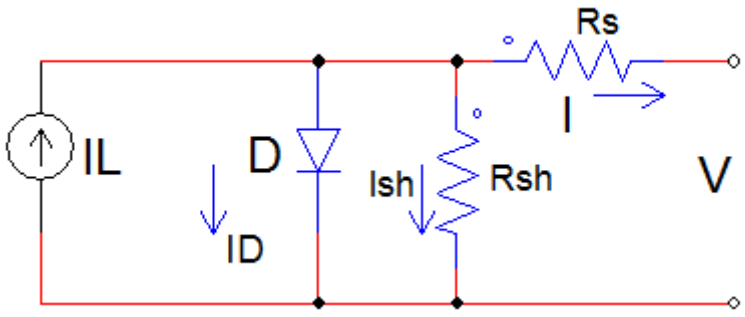

Figure 3.1 Five Parameter Model of PV Module

Five parameter model is analyzed below:

The equations governing the five parameter model are given below:

The five parameters are R_{sh}, R_s, a, I_d and I_L. R_{sh} represents shunt resistance, R_s stands for series resistance, a is the modified ideality factor, I_d is the diode current and I_L is the PV current.

Applying Kirchhoff's current law:

$$I = I_L - I_d - I_{SH}$$

…….(3.1)

The current through the diode is given by:

$$I_d = I_o \{\exp\left[\frac{(V+IR_S)}{a}\right] - 1\}$$

…….(3.2)

And current through the series resistance is given by:

$$I_{SH} = \frac{V+IR_S}{R_{SH}}$$

...……(3.3)

Putting these values in eqn (1) to obtain the following equation:

$$I = I_L - I_o \left\{\exp\left[\frac{(V+IR_S)}{a}\right] - 1\right\} - \frac{V+IR_S}{R_{SH}}$$

…….(3.4)

Where a is the modified diode ideality factor and is given by:

$$a = \frac{N_S\, n\, kT}{q}$$

……..(3.5)

The IV-characteristic at some key points is obtained as below:

(1) At short circuit condition, V =0, and

I = $I_{SC,ref}$.

$$I_{SC,ref} = I_{L,ref} - I_{o,ref}\left\{\exp\left[\frac{I_{SC,ref}R_{S,ref}}{a_{ref}}\right] - 1\right\} - \frac{I_{SC,ref}\,R_{S,ref}}{R_{SH,ref}}$$

…..(3.6)

(2) At open circuit, I =0 and V = $V_{OC,ref}$,

$$I_{L,ref} = I_{o,ref}\{\exp\left[\frac{V_{OC,ref}}{a_{ref}}\right] - 1\} + \frac{V_{OC,ref}}{R_{SH,ref}}$$

……..(3.7)

(3) At maximum power point, I= $I_{MP,ref}$ and V= $V_{MP,ref}$

$$I_{MP,ref} = I_{L,ref} - I_{o,ref}\left\{\exp\left[\frac{V_{MP,ref} + I_{MP,ref}R_{S,ref}}{a_{ref}}\right] - 1\right\} - \frac{V_{MP,ref} + I_{MP,ref}\,R_{S,ref}}{R_{SH,ref}} \quad ...(3.8)$$

These parameters were optimized using differential evolution and the developed model was used in the research work.

3.2 Parameter Optimization for PV module

Different techniques can be applied to optimize the parameters for the PV modules. Differential evolution is one of the effective methods for this purpose [16]. In differential evolution, mutation is applied first to generate a trial vector, which is then used within the crossover operator to produce one offspring. Mutation step sizes are not sampled from a prior known probability distribution function. Mutation step sizes are influenced by differences between individuals of the current population.

General Differential Evolution algorithm is described as below:

Set the generation counter, $t = 0$;

Initialize the control parameters, β and pr;

Create and initialize the population, C(0), of n_s individuals;

While** stopping conditions (s) not true **do

For** each individual, $\mathbf{x}_i(t) \in C(t)$ **do

Evaluate the fitness $f(\mathbf{x}_i(t))$;

Create the trial vector, $u_i(t)$ by applying the mutation

Create an offspring, $\mathbf{x}_i'(t)$, by applying the crossover op

If** $f(\mathbf{x}_i'(t))$ is better than $f(x_i(t))$ **then

Add $x'_i(t)$ to C(t+1);

end

else

Add $\mathbf{x}_i(t)$ to C(t+1);

end

end

end

Return the individual with the best fitness as the solution;

This optimization process is carried out with three basic operations:

- Mutation
- Cross over
- Selection

First, the mutation operation creates mutant vectors by perturbing each target vector with the weighted difference of the two other individuals selected randomly. Then, the cross over operation generates trail vectors by mixing the parameters of the mutant vectors with the target vectors, according to a selected probability distribution. Finally, the selection operator forms the next generation population by selecting between the trial vector and the corresponding target vectors those that fit better the objective function [25]. In [17], optimization has been done for four parameters using genetic algorithm.

3.3 Design of Z-Source Inverter

This chapter presents detailed process for design of Z-source inverter. The schematics of the Z-source is given in Figure 3.2.

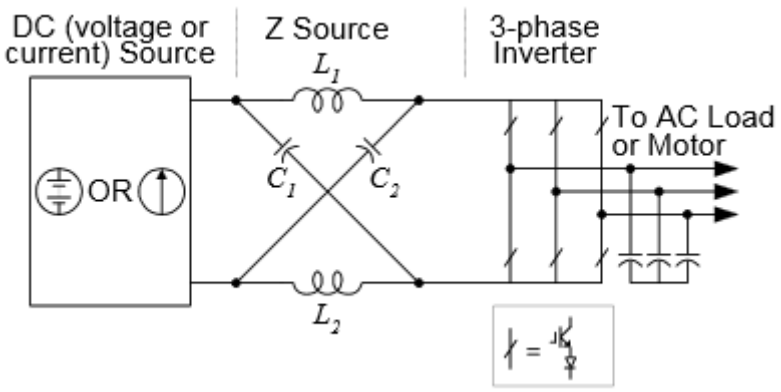

Figure 3.2 Z source inverter with switches series diodes [22]

The electrical components that need to be selected or designed are the two inductors and two capacitors of Z-source network, one capacitor for input stage, and diode [36], [37], [40]. The shoot-through states and non-shoot-through states gives unique features to Z-source inverter. Shoot-through states are those in which both the IGBTs in one leg or two legs or three legs are turned on simultaneously causing a short circuit resulting in a shoot up. These states are allowed only in Z-source for a specific time known as shoot-though time per cycle. All other states which are allowed in voltage source inverters or current source inverters in which only one IGBT in one leg is turned on at any time are non-shoot-through states. These states are responsible for chopping of input dc voltage signal in positive and negative direction, thus giving rise to ac signal with many harmonics and these harmonics can be removed by using low pass filters. Using voltage and current equations for various electrical components in these two states, the Z-source components are designed.

3.4 Inductor Design

When the Z-source inverter is operating in normal states, no shoot through results and voltage is across capacitor is always equal to input dc voltage resulting in zero voltage

across inductor and pure dc current through it. Inductor is needed in Z-source to limit the current ripples that would result from boost process by using shoot through states. When the shoot through state is turned ON, the current in inductor linearly rises and voltage across it becomes equal to the voltage across capacitor. When non-shoot-through states are turned ON, current in the inductor decreases and thus voltage across it will be the difference between capacitor voltage and input dc voltage.

The average current through the inductor is given by:

$$I_{L=}\frac{P}{V_{in}} \qquad \text{.....(3.9)}$$

Where V_{in} is the input dc voltage and P is the power delivered.

The shoot-through duty ratio can be calculated from the voltage gain equation for Z-source inverter derived in previous chapter:

$$\frac{1}{1-2D_o} = \frac{V_o}{V_{in}} \qquad \text{.....(3.10)}$$

The average voltage across Z-source capacitor is given by:

$$V_c = \frac{Vpv+Vdc1max}{2}$$

.....(3.11)

A certain level of ripple current allowed is chosen, then the value of inductor can be calculated by using inductor current for impedance network.

$$L = \frac{DTs*Vc}{Iripple}$$

.....(3.12)

So, any value above this inductance value will be enough to transmit the required power under required values of output voltage and current.

3.5 Capacitor Design

The required DC capacitors value can be obtained by using the capacitor ripple voltage formula:

$$\Delta Vc = \frac{Iave*To}{C} \quad \text{.....(3.13)}$$

Where ΔVc is the voltage ripple across the capacitor, $Iave$ is the average current through the capacitor, To is the shoot-through time and C is the capacitance of the Z-source capacitor.

The average current is given by the formula:

$$Iave = \frac{Po}{Vi} \quad \text{.....(3.14)}$$

The shoot-through time is given by:

$$To = 1 - \frac{\sqrt{3}}{2} M\, Ts \quad \text{.....(3.15)}$$

From equation (3.13), capacitance can be calculated as below:

$$C = \frac{Iave*To}{\Delta Vc} \quad \text{.....(3.16)}$$

Any value of capacitance higher than this will be enough for the nominal conditions.

3.6 Inverter IGBT Module

SEMITEACH – IGBT inverter is used for prototype implementation of Z-source inverter as shown in Figure 3.3. This IGBT module can perform three different function; it has

inverter IGBT module for converting DC voltage to AC voltage, it has a rectifier bridge to convert AC voltage into DC voltage and it can be used as a buck converter to step down the input DC voltage. An isolated uncontrolled rectifier is also a part of this embedded system. A couple of 2200μF DC capacitor is provided in the DC link rail of the module for storing energy. The inverter module can work for maximum input DC voltage up to 600V and it can provide maximum output rms 400V with maximum current of 30 A.

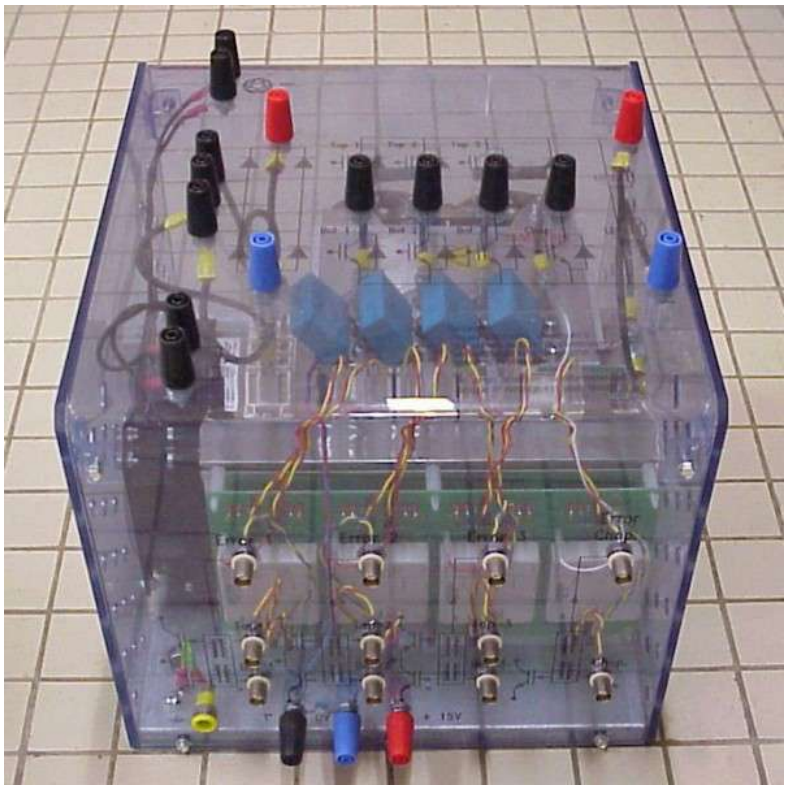

Figure 3.3 Real Time Inverter and Rectifier Module

3.7 Low Pass Filter Design

A three phase LC low pass filter is implemented and used in this work to obtain. The cutoff frequency is 60 Hz. The filter is a Y-connected LC filter. The cutoff frequency for an LC filter is given:

$$f = \frac{1}{2\pi\sqrt{LC}} \qquad \text{……..(3.17)}$$

Where L and C are the values of inductor per phase and ac capacitor per phase. The values of L and C are chose such that sinusoidal waveform of required frequency is obtained. If the switching frequency of IGBT's is higher, the lower harmonics can be eliminated and even high cutoff frequency can give pure sinusoidal waveform due to absence of lowers harmonics. If the switching frequency is as high as 7 kHz, a cutoff frequency of 200 Hz will give us sinusoidal waveform of 60 Hz due to absence of lower harmonics.

3.8 Implementation of Z-source Inverter and LC Filter

The input voltage level has been chosen to be 170 V and 1000 watts of power was delivered. The output voltage level has been chosen to be 110 V rms for nominal conditions..

If the nominal delivered power is taken to be 1000 watt, then the inductor current is calculated using (3.9),

$$I_L = \frac{1000}{170}$$

$$I_L = 6\ A$$

For safety, 10 A is selected.

The minimum duty cycle ratio is chosen to be 0.5 for boost operation, so

$D_o = 0.5$

The average voltage is given by (3.11):

$$V_c = \frac{500 + 170}{2}$$

$V_c = 300$ V

If frequency is 10 kHz then,

Ts = 1/f = 0.0001 sec.

Product of duty cycle ratio and time period is:

DTs = 0.0001 * 0.5

DTs = 50 u sec

The ripple current allowed is taken to be 6 A, then the value of inductor can be calculated by using (3.4) for impedance network.

I ripple = 6 A

$$L = \frac{50 * 160}{6}$$

L = 1300 uH = 1.3 mH

So, any value above 1mH will be enough to transmit the required power under required values of output voltage and current. If I_{ave} is 10 A, shoot-through time per cycle, T_o is 50 u sec and the capacitor voltage ripple is limited to 3% at peak power, then the capacitance value is calculated using (3.17),

$$C = \frac{10 * 50 * 10^{-6}}{400 * 0.03}$$

C = 50 micro Farad

The voltage across capacitance is chosen to be 400 V. The second capacitor in upper leg of Z-source network experiences a voltage stress half than that of the DC link capacitor, so the upper leg capacitor voltage rating should higher than 200V in this case. The maximum rms current ratings of Inductor wire is chosen to be 12 A. The diode in Z-Source network is chosen to be Power Diode IN1190 which can withstand maximum inverse voltage upto 650 volts.

The capacitor values were selected to be 200 uF which gives the inductor values for LC filter to be 10 mH. The switching frequency of inverter is 10 kHz, so that there will be harmonics above 150 Hz. A wire of gauge 0.01 cm(diameter) was used for winding of the inductors of LC filter.

3.9 Discussion

In this chapter, a design procedure was explained to calculate and design various components of Z-source inverter and LC filter. The procedure was derived in a systematic way so that all the components were analyzed during various states.

A prototype of Z-source inverter was built up in laboratory using the above calculated values of various components and this developed model was used to assess the performance of feedback controller with dc source and maximum power point tracking under normal and shadowing conditions with Chroma PV Simulator.

CHAPTER 4

PWM CONTROLLERS FOR Z-SOURCE INVERTER

Z-source inverters are used for both DC-DC conversion and DC-AC conversion with the help of Z network and inverter. The Maximum power point of the input photovoltaic source is controlled by the switching of Z-source inverter. Pulse Width Modulation (PWM) techniques are employed to provide switching signals for the inverter. The switching signals to the inverter are in the form of pulses and the width of the pulse and their ON-OFF period determines the output of an inverter. Different algorithms and techniques are employed to provide certain switching pulses to IGBTs of the inverter for desired outputs. In this study, a comparison of a carrier signal with certain reference signals forms the basis for generation of pulses.

4.1 Pulse Width Modulation Techniques

Pulse Width Modulation (PWM) techniques are used for proper switching of inverter IGBTS for a desired output. PWM techniques are based on comparison of reference

signals with a carrier signal. For Z-source inverter the PWM techniques are based on comparison of 5 signals with a carrier signal.

For Z-source inverter, the 3 reference signals are generated using power controllers, current controllers and voltage controllers. Three basic methods for quasi Z-source inverter are simple Boost control [40], maximum boost control [41] and constant maximum boost control [42].

4.2 Simple Boost Method (SBC)

In this method the upper and lower envelops (Vp and Vn) are straight lines with constant values equal to or greater than the top envelop of three reference modulating signals Va, Vb and Vc as shown in Figure 4.1. When the carrier signal is greater than both the upper envelop Vp and the envelop of three modulating reference signals, all the three legs are switched ON to trigger shoot-through state. Similarly, when the carrier signal is smaller than both the lower envelop Vn and the envelop of the modulating reference signals, shoot-through states are triggered. In between, the switches will be in traditional Pulse Width Modulation (SPWM) mode. These shoot through states are added with the SPWM states to generate pulses for the quasi z-source inverter IGBTs. Shoot through states result in various boost capabilities, different voltage gains and different stresses on the switches.

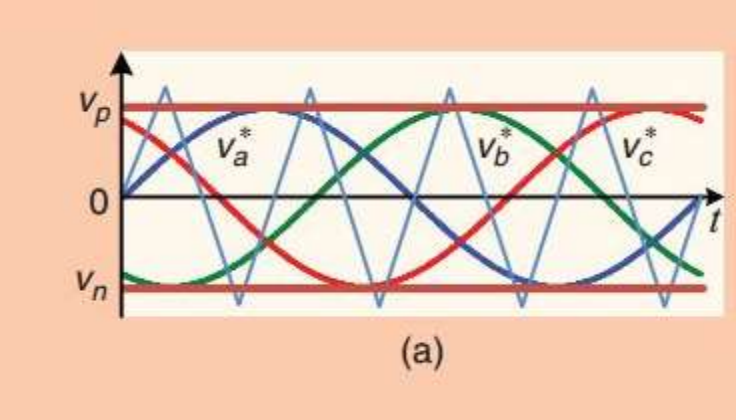

Figure 4.1 Simple Boost Control Method [55]

The maximum duty cycle ratio for SBC is given by:

$$D_{max} = 1 - M \quad \text{.....(4.1)}$$

The maximum shoot-through duty ratio for SBC is given by:

$$G_{max} = \frac{M}{2M-1} \quad \text{.....(4.2)}$$

The maximum gain for SBC is given by:

$$\frac{V_s}{V_{in}} = 2G - 1 \quad \text{.....(4.3)}$$

4.3 Simulation Results for SBC

Open loop PWM for SBC method is implemented for system specifications given in table 4.1.

Table 4.1 System Specification for SBC

Open Loop System Specification	
Input DC Voltage	100 V
Z-source Inductor	160 uH
Frequency	60 Hz

Z-source Capacitor	1000 uF
Low Pass Filter Capacitor	400 uF
Low Pass Filter Inductor	10 mH
Carrier frequency	333Hz
Three Phase Load	100 ohm per phase
Output voltage	1000 V

The open loop system consists of a DC voltage source connected to a Z-source network and inverter. The output of inverter passes through a low pass filter tuned at 60 Hz to feed a three phase output load as shown in Figure 4.2.

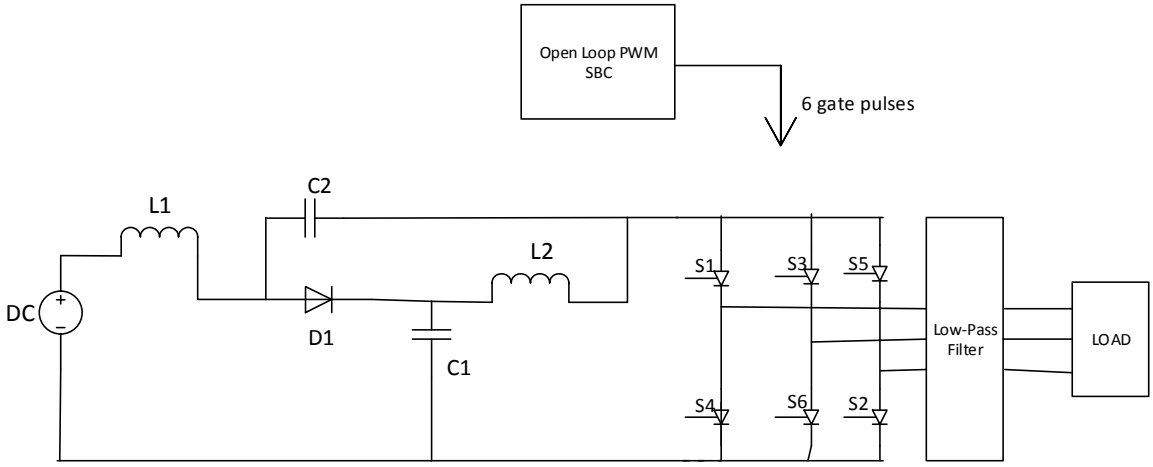

Figure 4.2 System diagram with DC input

The system was implemented in Simulink/Matlab environment. SBC carrier frequency was chosen to be 333Hz. The input voltage was 100V DC and the output ac voltage at the

output of LC filter was 1000V rms. The simulations results are shown in Figure 4.3-Figure 4.8.

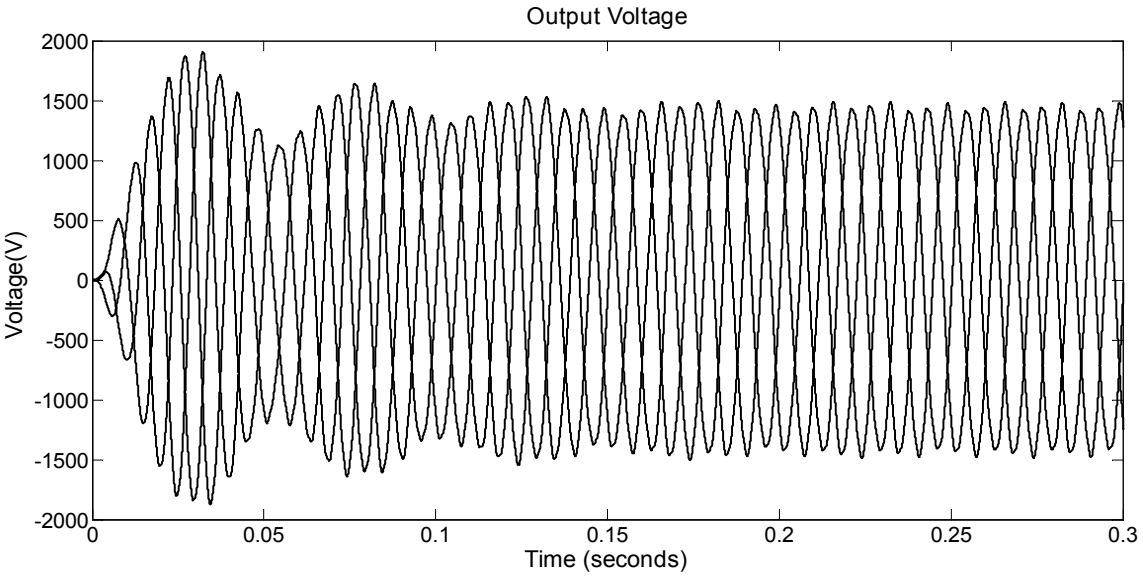

Figure 4.3 Output Voltage for SBC

Figure 4.3 shows that the output voltage peak value is 1300 V. After some initial transients, the voltage attains a steady-state value. As the DC link capacitor voltage reaches saturation, the output voltage also stabilizes with a frequency of 60 through a low pass LC filter tuned at 200 Hz.

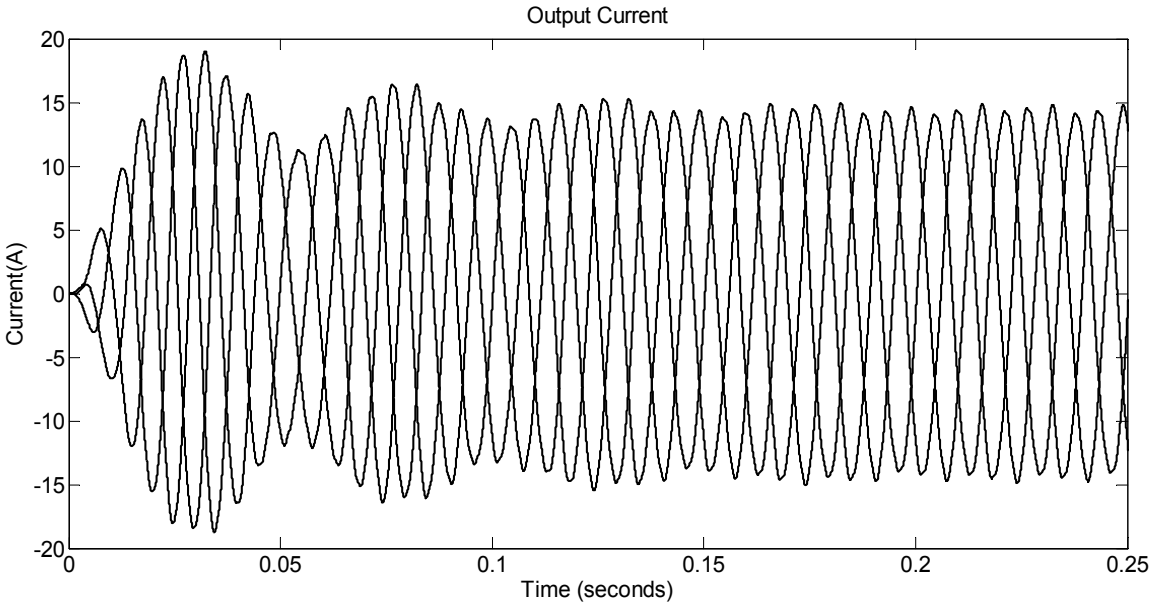

Figure 4.4 Output current for SBC

Figure 4.4 shows that the output current for SBC reaches a maximum value of 13A and stabilizes at 0.15 seconds. The output current is drawn by the load, as the load is increased, the output current increases. The output ac current has a frequency of 60 Hz.

Fig 4.5 shows the inverter output voltage which changes between -1500V and 1500V. The switching of IGBTs is controlled by PWM. The input DC voltage is chopped by the switching of the IGBTs so that the output is ac with higher order harmonics which are filtered by 60Hz low pass filter.

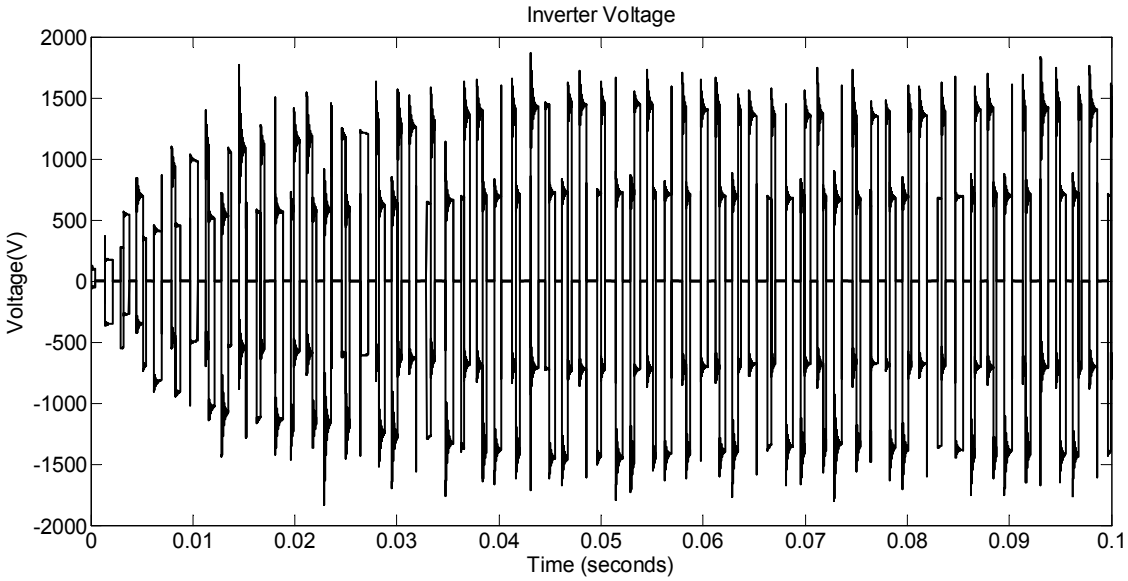

Figure 4.5 Inverter Voltage for SBC 4.6

The inverter current is shown in Figure 4.6 which is ac in nature as a result of PWM. It has many higher order harmonics which will be filtered by low pass 60Hz LC filter.

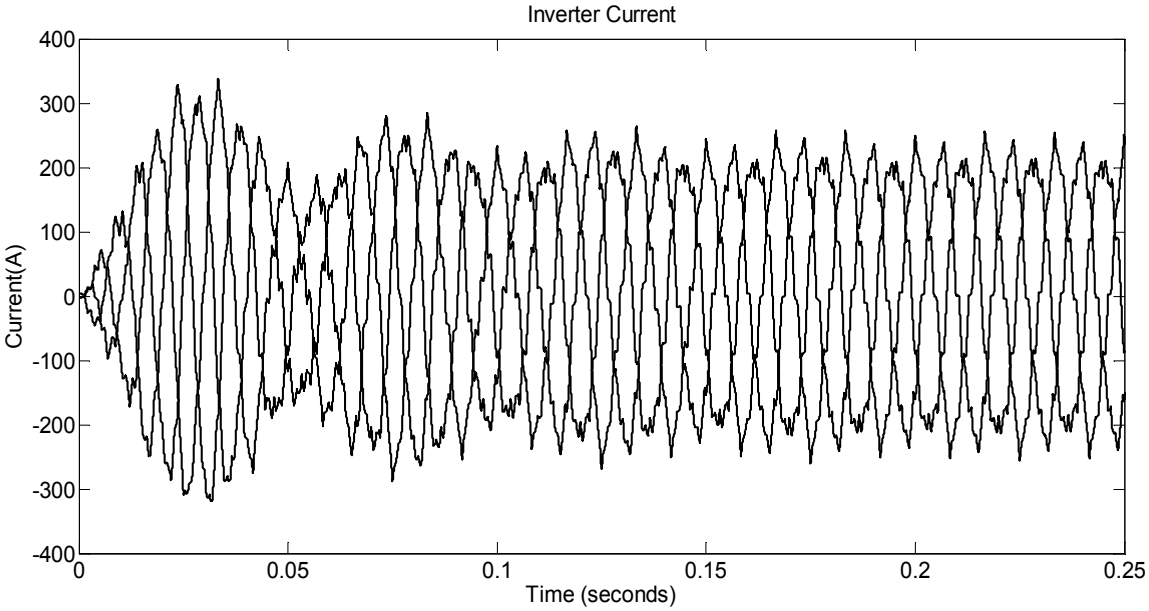

Figure 4.6 Inverter current for SBC

Carrier signal and modulating signals are shown in Figure 4.7. The carrier signal is triangular in nature with peak value of 1 V. Modulating signals are three ac signals and two shoot-through envelops. The two envelops are constant with values of 0.8 and -0.8 in this case. When the carrier signal is greater than upper envelop, all the switches are turned on to trigger shoot-through states. Similarly, when the carrier signal is less than the lower envelop, the shoot-through states are again triggered. The three modulating signals are for normal PWM action.

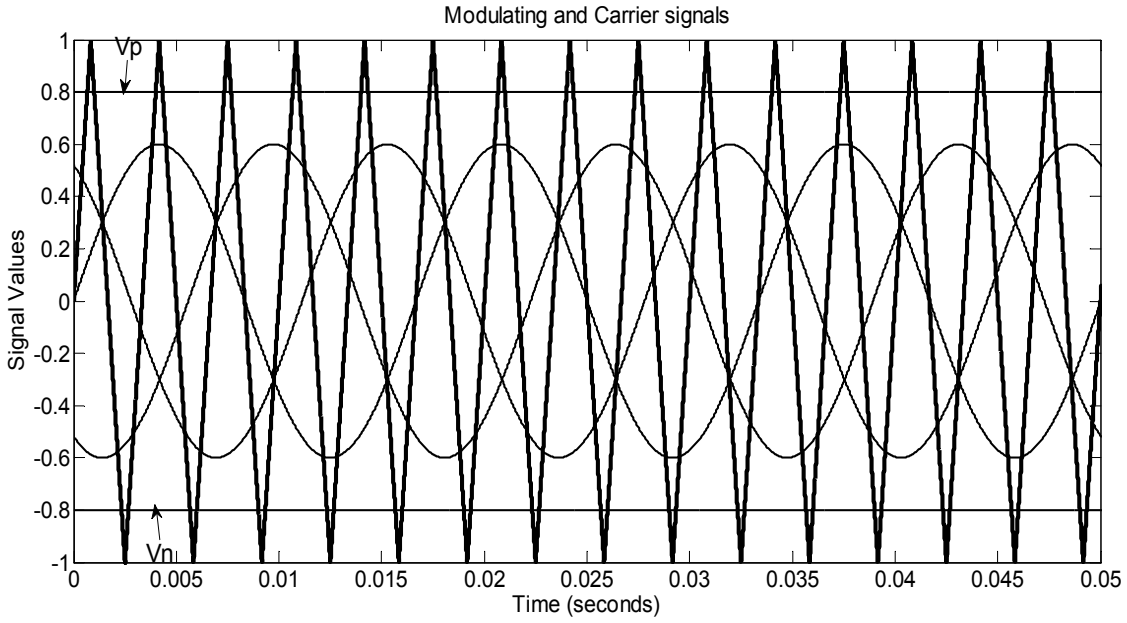

Figure 4.7 SBC Reference signals generated

The Z-source capacitor voltage is shown in Figure 4.8 which reaches a constant value of 1700V after initial transients. As the dc link voltage changes in Z-source inverter case, so the capacitor of Z-source network is chosen for dc reference.

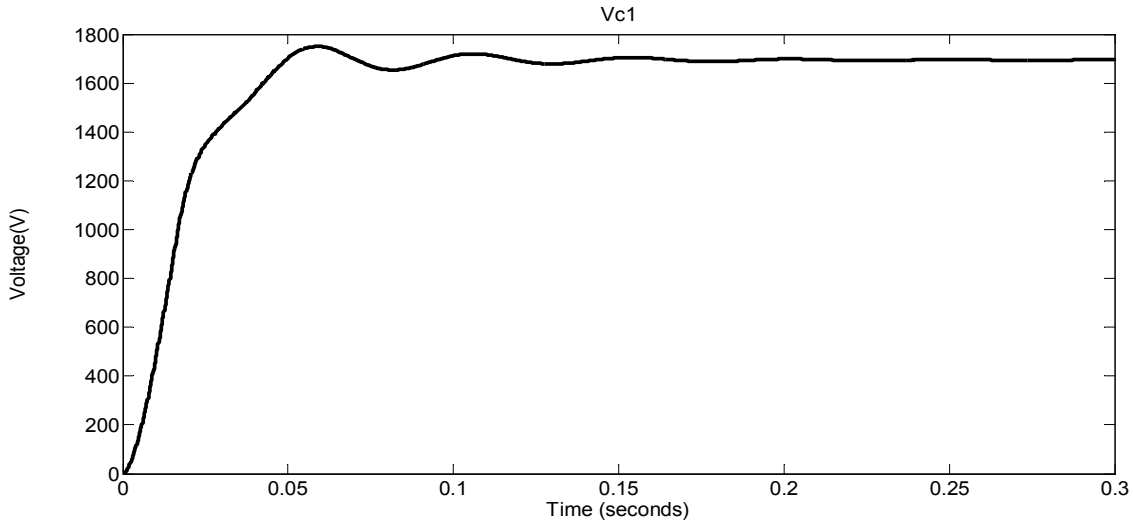

Figure 4.8 Z-source capacitor DC link voltage

4.4 Maximum Boost Method and Maximum Constant Boost Method

In this maximum boost control (MBC) method, the shoot-through reference is equal to the upper or lower envelops and it utilizes all the zero states as shoot-through states as shown in Figure 4.9. The shoot-through ratio of maximum boost control technique changes at a frequency equal to six times the nominal frequency of the system resulting in low frequency harmonics in the capacitor voltage and inductor current outputs of z-source. This implies higher values of components, so the MBC method is suitable for high frequency output or fixed frequency output.

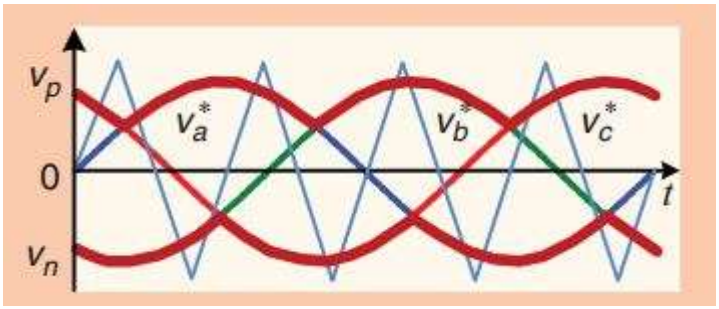

Figure 4.9 Maximum Boost Control Method [55]

The maximum duty cycle ratio for MBC is given by:

$$D_{max} = 1 - \frac{3\sqrt{3}M}{2\pi} \quad \text{……..(4.4)}$$

The maximum shoot-through duty ratio for MBC is given by:

$$G_{max} = \frac{\pi M}{3\sqrt{3}M - \pi} \quad \text{…….(4.5)}$$

The maximum gain for MCBC is given by:

$$\frac{V_s}{V_{in}} = \frac{3\sqrt{3}G}{\pi} - 1 \quad \text{…….(4.6)}$$

In maximum constant boost control (MCBC) method, the shoot-through reference is obtained by slightly changing the shoot-through reference of MBC so that shoot-through duty ratio remains same for every cycle as shown in Figure 4.10. In this method the gain is higher than that of SBC and the low frequency harmonics resulting from MBC method are reduced.

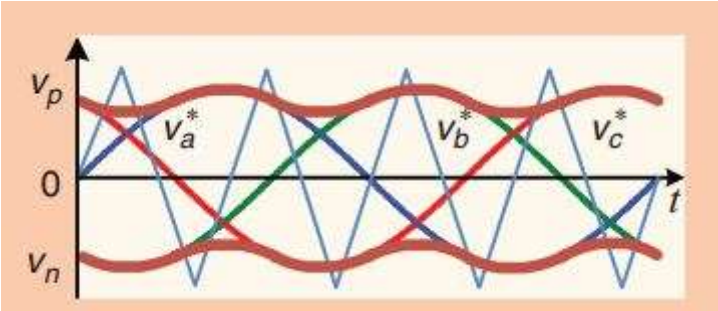

Figure 4.10 Maximum Constant Boost Control Method [55]

The maximum duty cycle ratio for MCBC is given by:

$$D_{max} = 1 - \frac{\sqrt{3}M}{2} \quad \text{.....(4.7)}$$

The maximum shoot-through duty ratio for MCBC is given by:

$$G_{max} = \frac{M}{\sqrt{3}M-1} \quad \text{.....(4.8)}$$

The maximum gain for MCBC is given by:

$$\frac{V_s}{V_{in}} = \sqrt{3}G - 1 \quad \text{.....(4.9)}$$

4.5 Simulation Results for MBC

MBC was implemented in Simulink/Matlab environment for the DC source connected Z-source inverter with system specifications as shown in table 4.2.

Table 4.2 System for MBC

Open Loop System Specification	
Input DC Voltage	100 V
Z-source Inductor	160 uH
Frequency	60 Hz
Z-source Capacitor	1000 uF
Low Pass Filter Capacitor	400 uF
Low Pass Filter Inductor	10 mH
Carrier frequency	333Hz
Three Phase Load	100 ohm per phase
Output voltage	1000 V

The open loop system consists of a DC voltage source connected to a Z-source network and inverter. The output of inverter passes through a low pass filter tuned at 60 Hz to feed a three phase output load as shown in Figure 4.10.

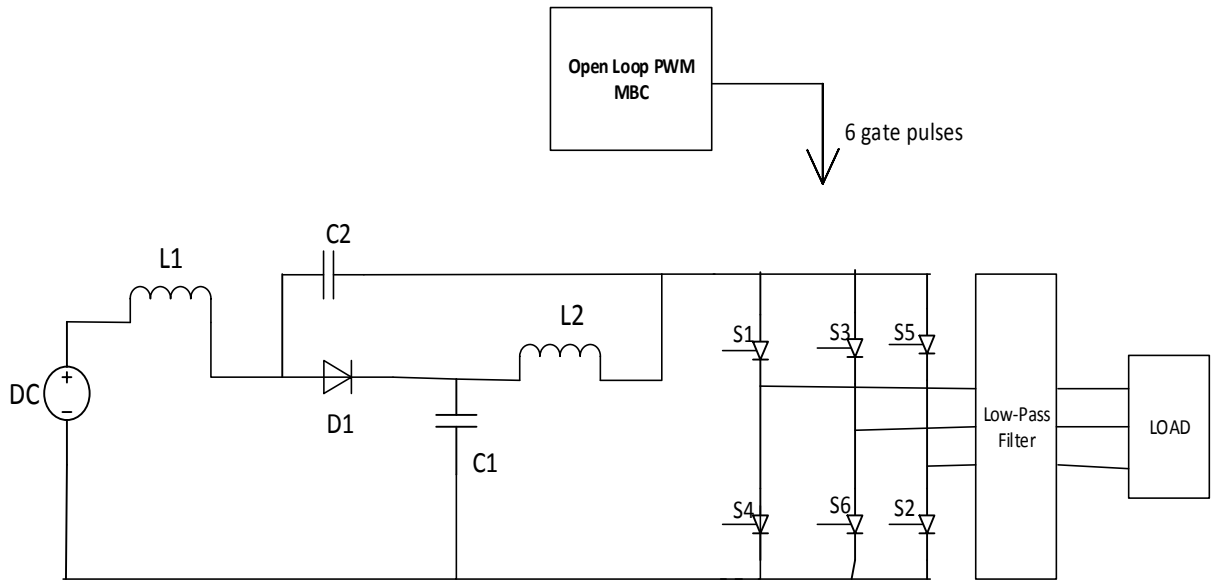

Figure 4.11 DC source connected Z-source system with MBC

The carrier frequency was 333Hz and the output voltage obtained in this case was 1400 V rms with some lower harmonics. The results of the simulation for maximum boost control are shown in Figure 4.11 - Figure 4.16.

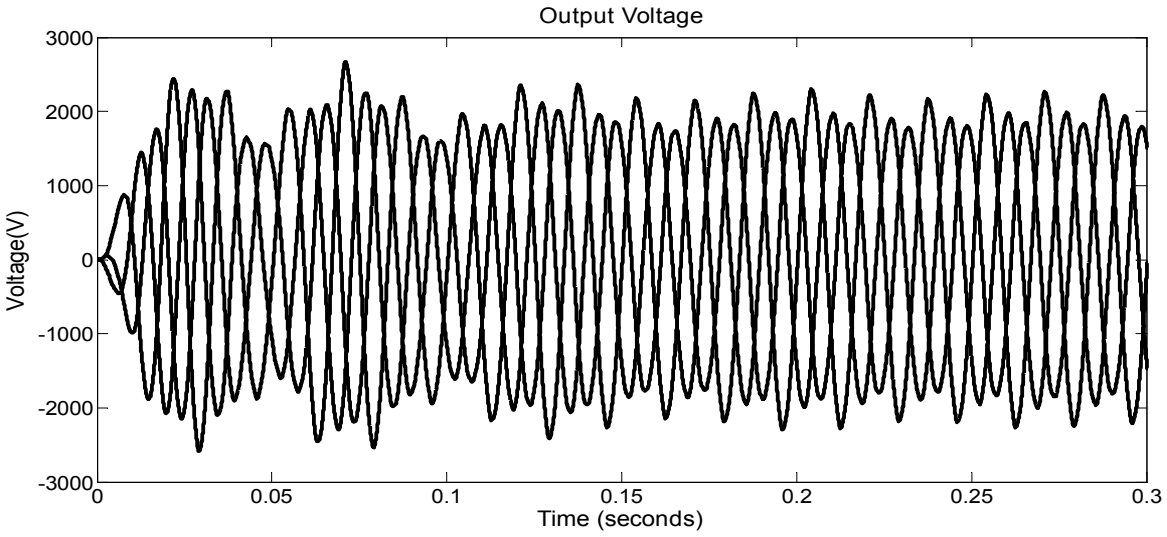

Figure 4.12 Output voltage for MBC

The output voltage for MBC is shown in Figure 4.12. The output voltage in this case has more harmonics in output voltage as compared to SBC. The peak voltage is 1700 V. Output current is shown in figure 4.13. The peak value of output current is 17A. The output current has also some higher order harmonics in this case.

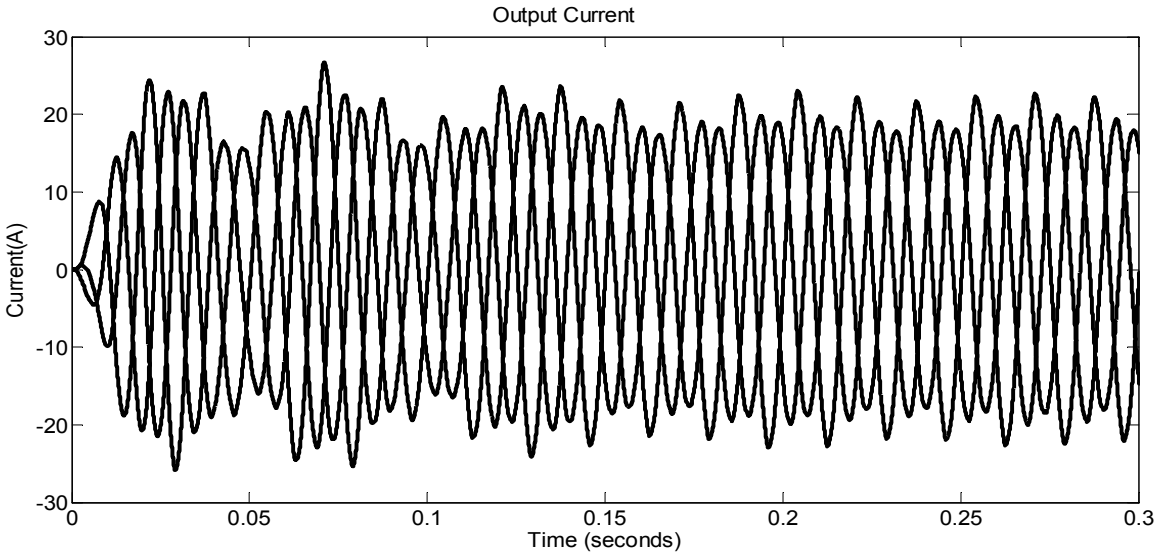

Figure 4.13 Output current for MBC

Figure 4.14 shows the inverter output voltage as a result of MBC. The peak value is 2000V and it has more harmonics as compared to SBC. As the modulating signals used in this case have higher frequency components, so it results in increased number of harmonics in output signals. Also, the inverter voltage value is higher in this case as compared to SBC case.

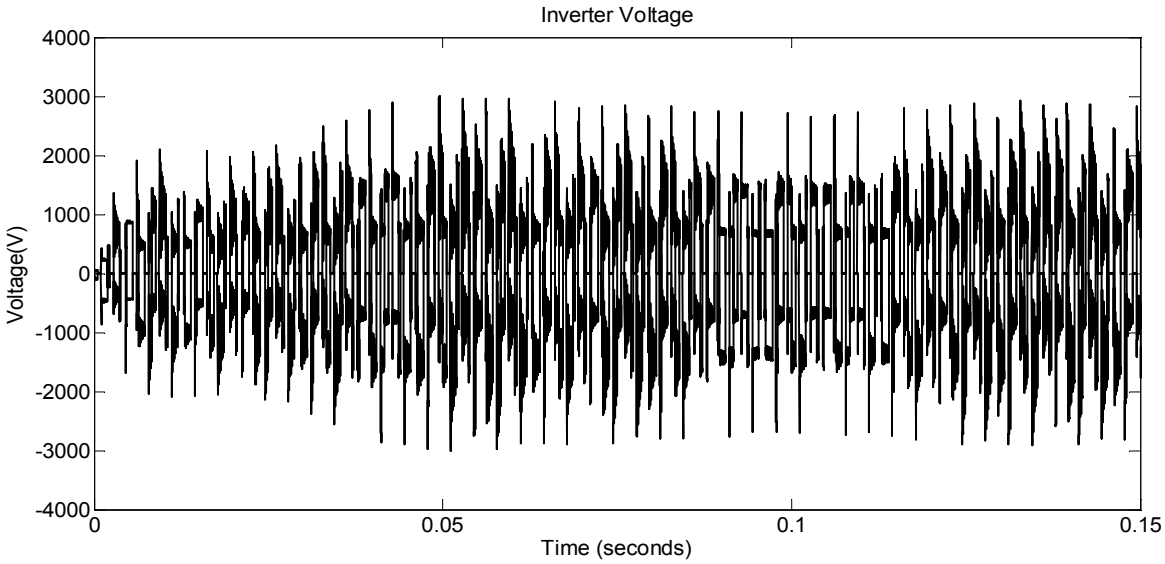

Figure 4.14 Inverter voltage

The inverter current has peak value of 200A as shown in Figure 4.15. The inverter current is ac in nature but not pure sinusoidal. An LC filter of 60Hz is used to make it pure sinusoidal.

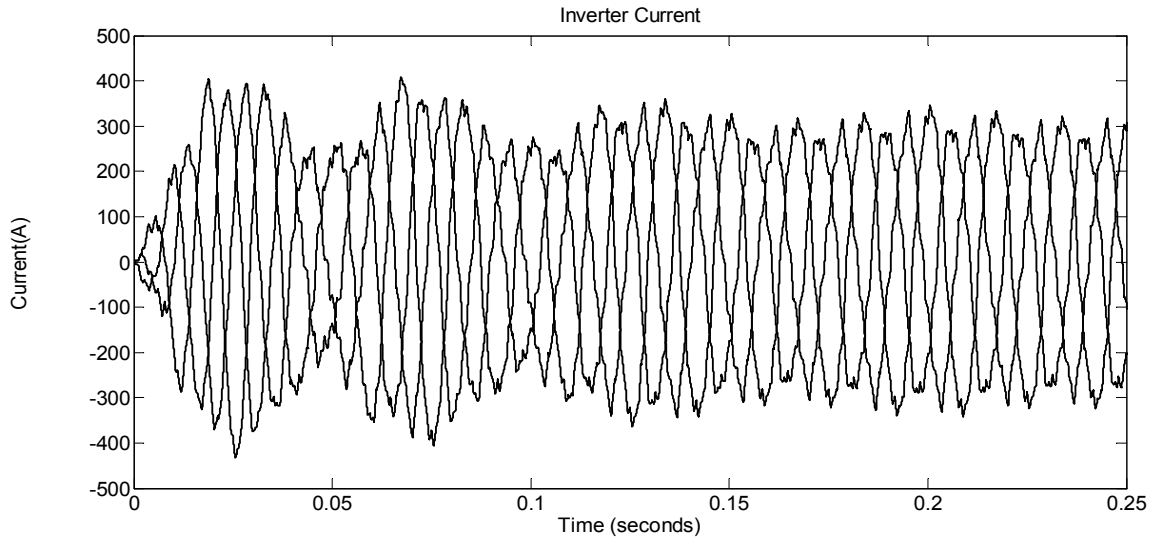

Figure 4.15 Inverter current

The Z-source capacitor dc voltage in this case is 1500V as shown in Figure 4.16 and as the dc voltage reaches steady state, the output signals also reaches steady state values.

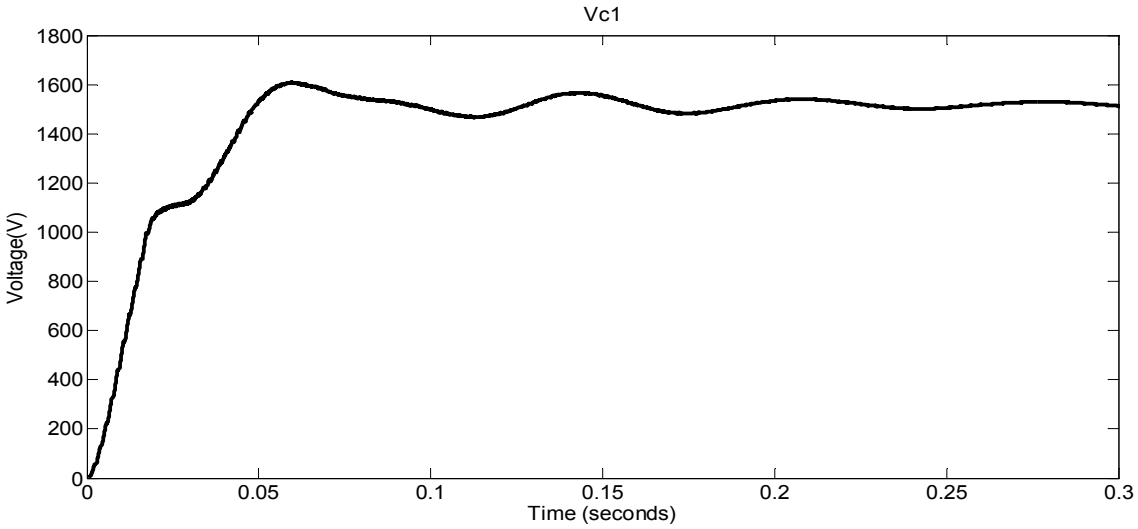

Figure 4.16 Vc1

The carrier signal and five modulating signals for MBC are shown in Figure 4.17. The three ac modulating signals have higher order harmonics in this case which boost up the system output quantities but results in presence of higher order harmonics. The envelopes are constant at 0.8 and -0.8 to trigger shoot-through states.

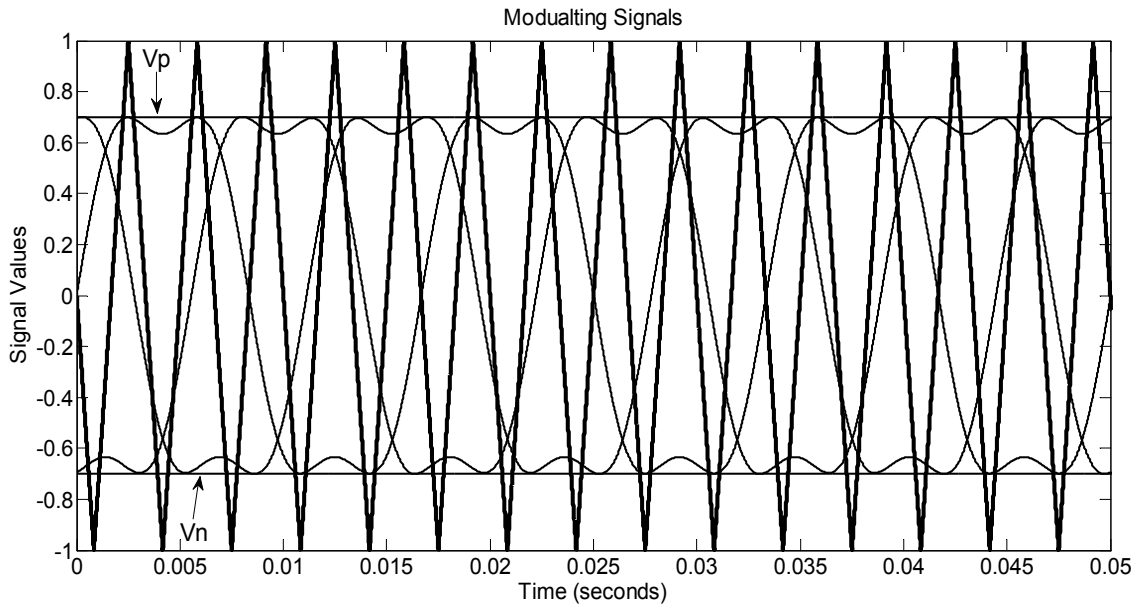

Figure 4.17 Reference signals generated for MBC

4.6 Simulation Results for MCBC

Maximum Constant Boost Control (MCBC) method was implemented in Simulink/Matlab environment for the DC source connected Z-source inverter with system specifications as shown in TABLE 4.3.

Table 4.3 System Specification for MCBC

Open Loop System Specification	
Input DC Voltage	100 V
Z-source Inductor	160 uH
Frequency	60 Hz
Z-source Capacitor	1000 uF
Low Pass Filter Capacitor	400 uF
Low Pass Filter Inductor	10 mH
Carrier frequency	333Hz

Three Phase Load	100 ohm per phase
Output voltage	1000 V

The open loop system consists of a DC voltage source connected to a Z-Source network and inverter. The output of inverter passes through a low pass filter tuned at 60 Hz to feed a three phase output load as shown in Figure 4.18.

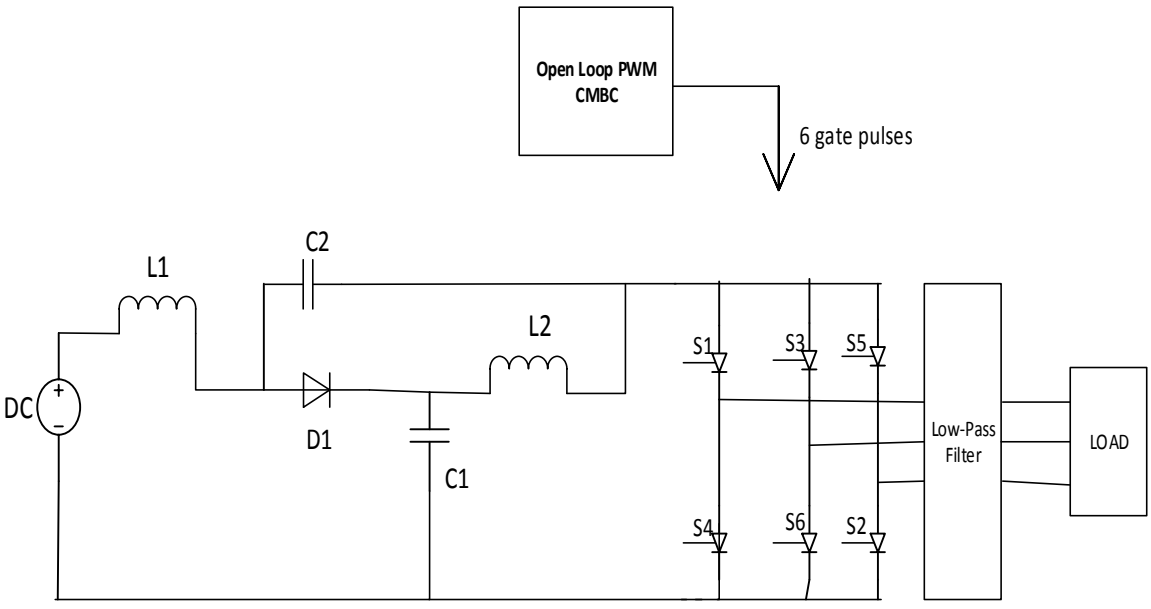

Figure 4.18 DC source connected Z-source system

In MCBC method, the output voltage obtained was 2000 V rms which was high as compared to previous two methods with low harmonic components. Thus making it a

reliable and effective PWM technique as compared to previous two. The Simulation results are shown in Figure 4.19-Figure 4.24.

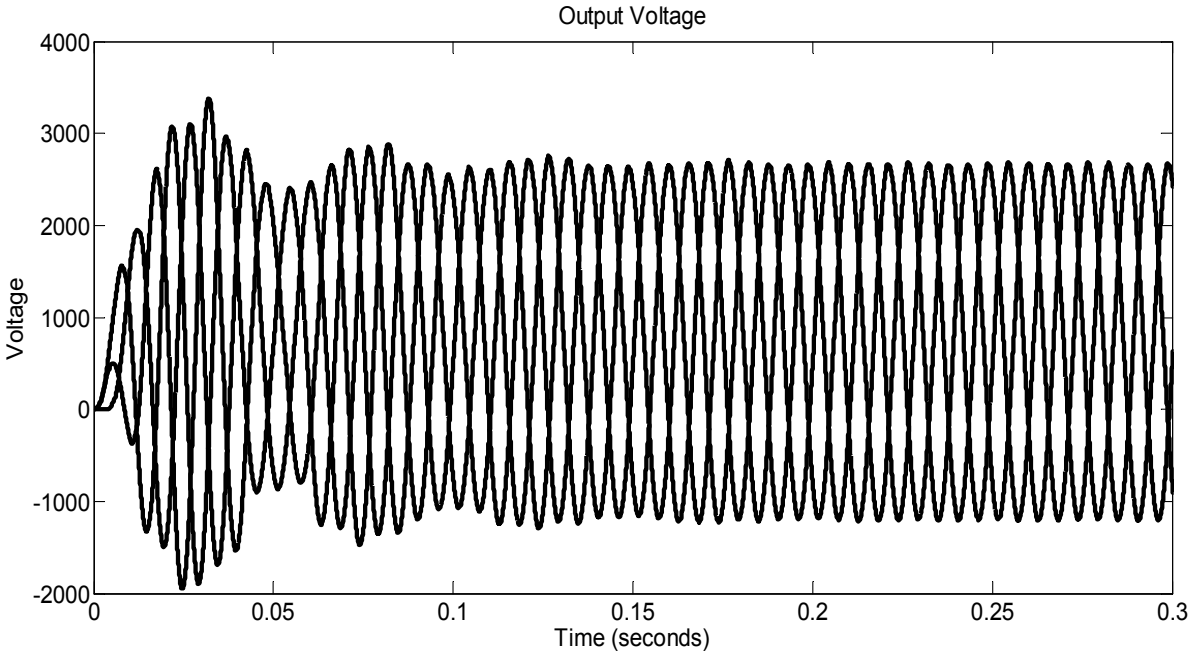

Figure 4.19 Output voltage for MCBC method

The output voltage for MCBC is shown in Figure 4.19 which reaches a maximum value of 2100V. The output current is shown in Figure 4.20. The harmonics content increase but the boost factor increases. Harmonics increases as the modulating signal and envelops have higher order harmonics.

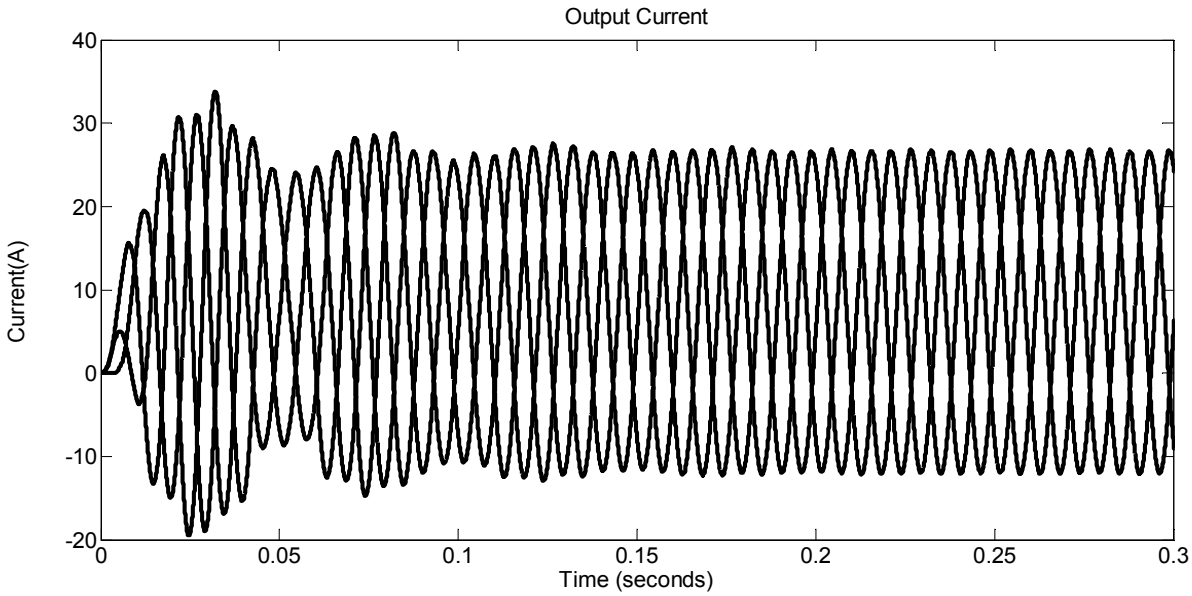

Figure 4.20 Output current for MCBC method

The inverter output voltage attains a peak value of 2000V as the input Dc voltage pulsates between 0 and 2000V. The chopping of input dc voltage results in output ac signal with higher order harmonics. The carrier frequency and frequency of modulating signal determines the number of higher order harmonics.

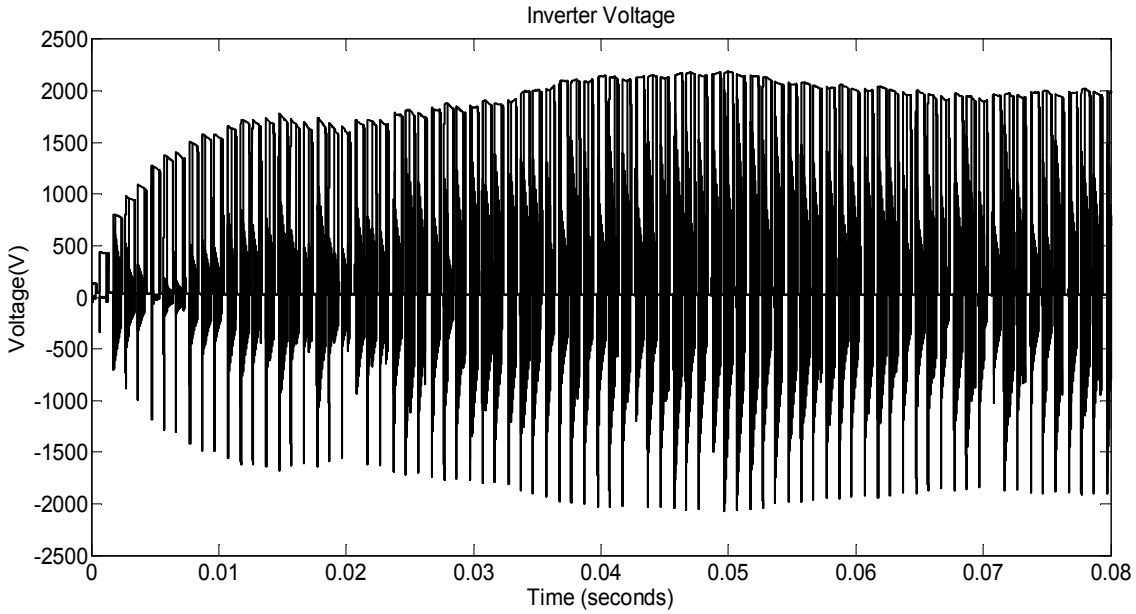

Figure 4.21 Inverter voltage

The inverter current has reached a higher value than previous two methods as shown in Figure 4.22. The harmonic content also increases, so an LC filter with sharp cut-off frequency is needed in this case.

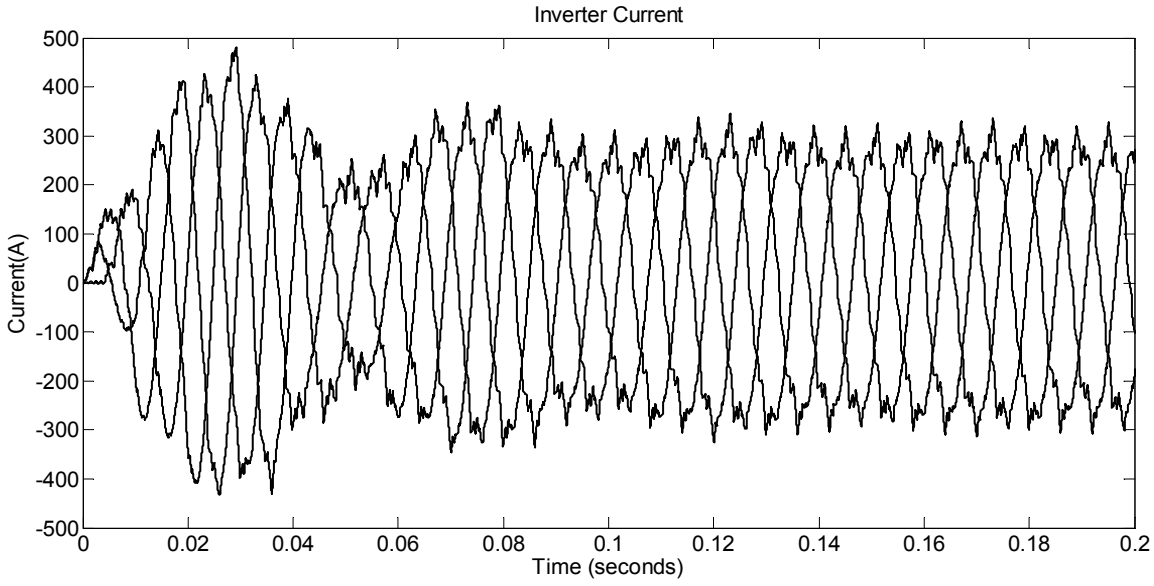

Figure 4.22 Inverter current

The Z-source capacitor voltage is lower in this case and reaches a maximum voltage of 1450V as shown in Figure 4.23. It has some ripples as compared to previous two methods resulting in increased number of harmonics in output quantities.

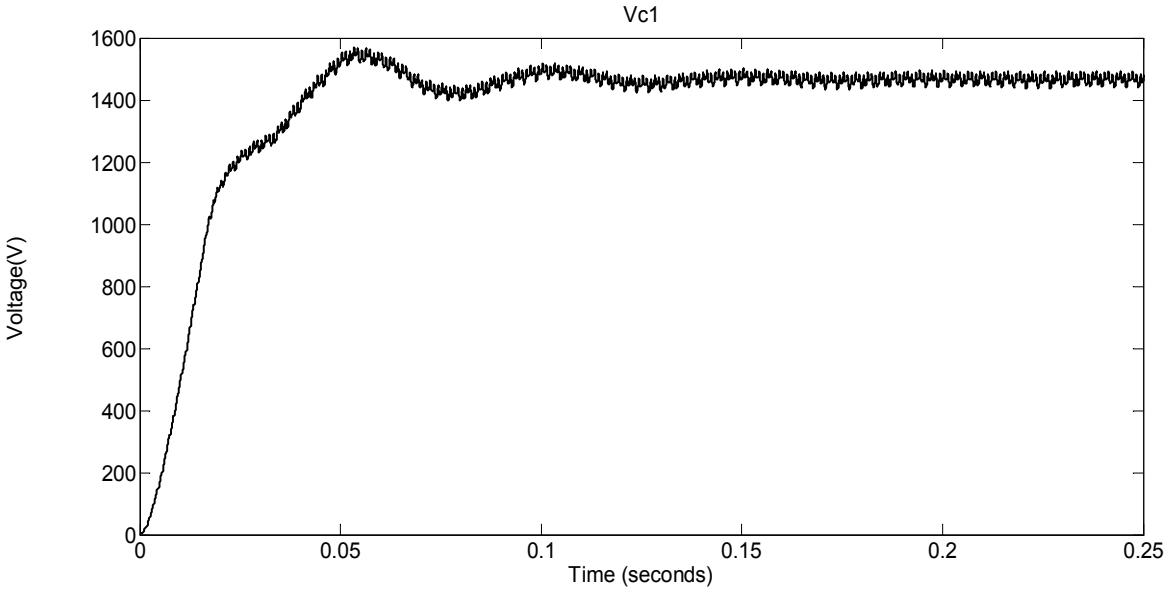

Figure 4.23 DC link voltage

The carrier signal and modulating signals for MCBC are in Figure 4.24. The envelopes in this case are also alternating signals with dc offsets of 0.6 and -0.6. This method results in boosting the output voltage and current. The results in this case are improved as compared to previous two cases in terms of harmonic contents and gain compromise.

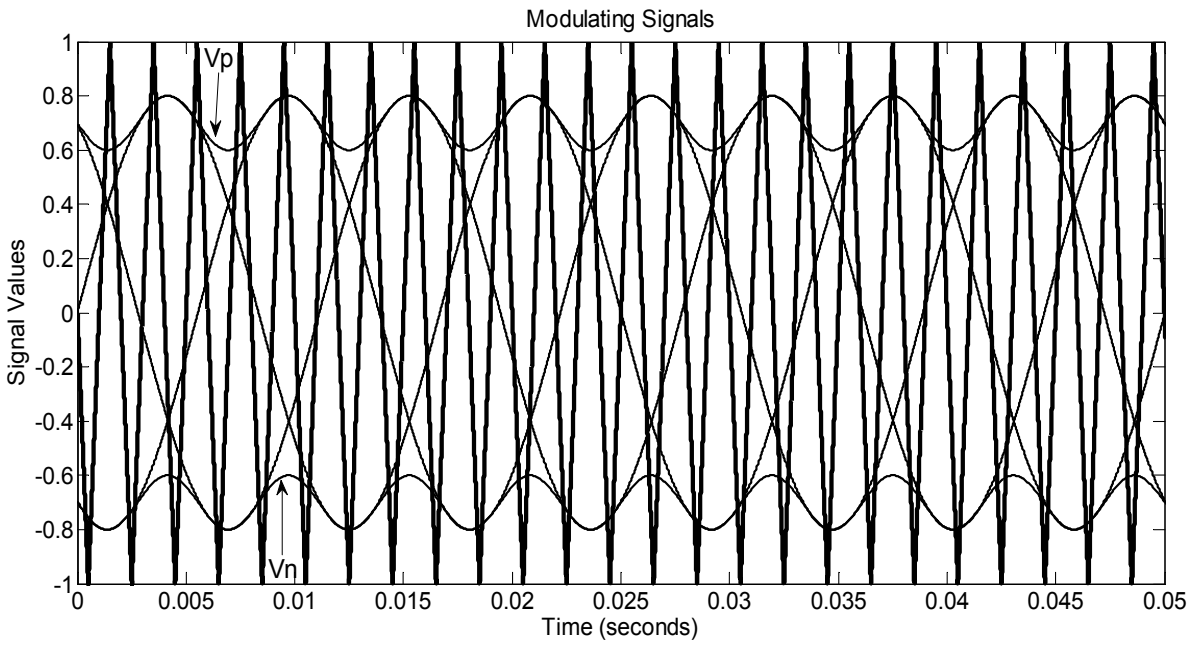

Figure 4.24 Reference signals generated for MCBC

4.7 Discussions

Different PWM control methods like Simple boost control, Maximum boost control and constant maximum boost control techniques have been employed and their performance have been evaluated for Z-source converters which paves the way for future formulation and research of more efficient space-vector PWM techniques for complex power conversion systems. The performance of Maximum constant boost controller was higher than other two PWM techniques. These PWM techniques use 5 control signals and a carrier signal to generate switching signals for IGBTs. Out of these 5 signals, three of these signals were generated by feedback controller and two signals by MPPT tracking algorithm. The shoot-through duty ratio was used in these controllers to control the shoot-through of dc-link voltage.

These PWM techniques will help researchers to propose and formulate new PWM techniques and these 3 techniques can be used with different feedback controllers to enhance the performance of power conversion system, thus adjusting the output voltage, reducing harmonic contents, providing more robust, effective and desired results in multi-level inner connected systems with CMI and ESB.

CHAPTER 5

FEEDBACK CONTROL FOR GRID-CONNECTED PV SYSTEM WITH QUASI-Z-SOURCE INVERTER

In the grid-connected mode, the feedback controller control the power flow from the PV system to the grid. Voltage and current controllers are also needed to control the voltage output and current output of the system. The feedback controllers samples the three phase output voltage, output currents, dc link voltage, PV current and PV voltage. Feedback controllers compare the reference powers with the sampled quantities to generate reference signals for PWM control methods. The feedback controller also generate the shoot-through references from the duty cycle calculation from maximum power point tracking algorithm. These reference modulating signals and shoot-through reference signals are used to generate required pulses for the IGBTs.

5.1 dq-Controller

A controller has been designed for stand-alone PV system to check the performance of the controller. PI controllers are then extended to grid-connected PV system. dq-controllers are implemented to convert from rotating frame to stationary reference frame of direct and quadrature axis along with phase angle which makes the control simple for the system given in Figure 5.1.

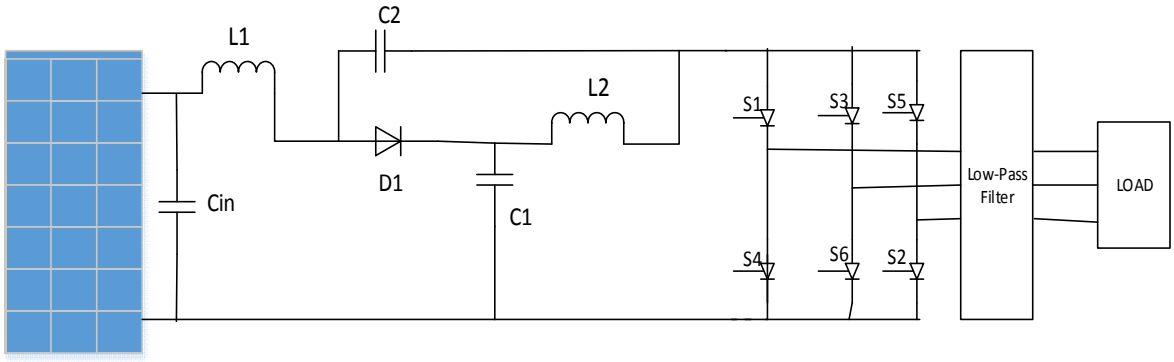

Figure 5.1 Z-source connected PV System

The output voltage to the load is sampled and passed through Phase-Locked Loop (PLL) which gives the phase angle that is used to keep track of the reference. The shoot-through reference is calculated using the required duty-cycle value obtained MPPT block. The shoot-through reference is calculated using the formulae for simple boost control, maximum boost control or constant maximum boost control as shown in Figure 5.2. The direct and quadrature component of voltage and current are used to calculate reference current signals and required reference signals for modulation for PWM as shown in Figure 5.3.

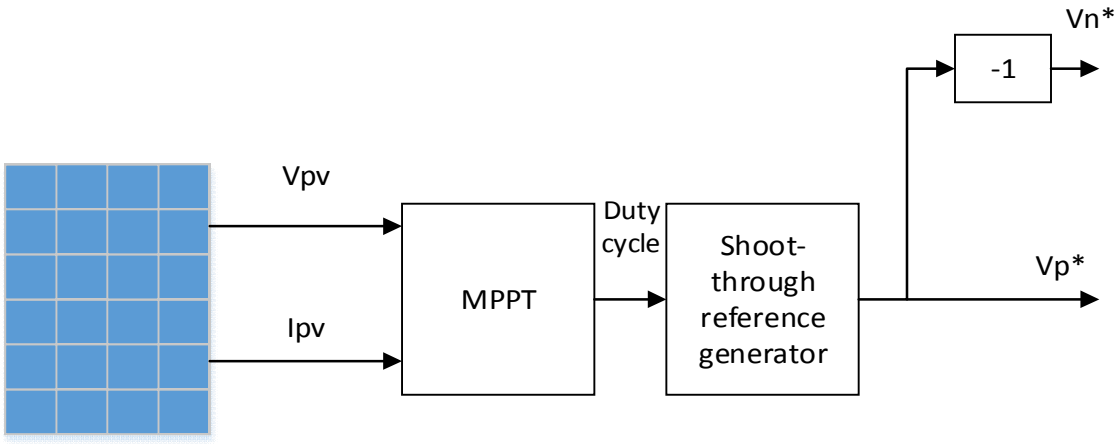

Figure 5.2 Shoot through Reference Generator

The detail diagram of dq-controller is shown in Figure 5.3. The output current and output voltages are sampled and then normalized. The phase angle is determined by PLL and dq-conversion is done to take the control to stationary reference frame. The maximum power calculation with zero reactive power is done by reference current generator block and finally based on dc reference tracking and maximum power calculation, modulating signals are generated for PWM. The shoot-through reference is determined by MPPT block and then through-through reference generator block as shown in Figure 5.2.

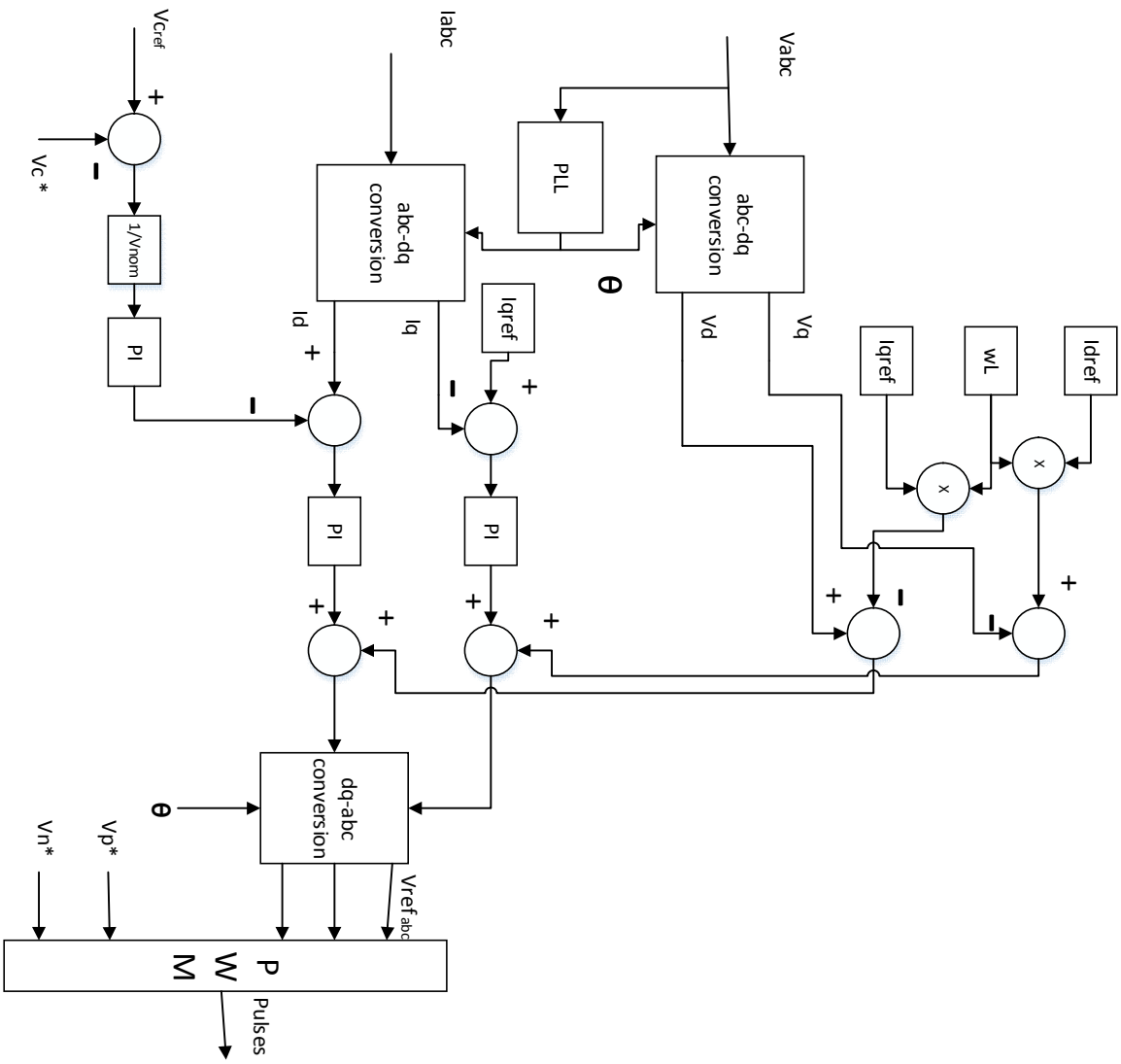

Figure 5.3 dq-based PI Feedback Controller

5.2 Simulation Results for PI-based dq-controller

The system specifications are given in Table 5.1. The dq-controller was implemented as a test case and simulation was run to obtain the required output voltage, current and power values as shown in Figure 5.4 – Figure 5.9. The results show that performance of dq-controller is reliable and fast in terms of fast tracking, efficiency and robustness. The voltage value reaches 110 volts rms phase to ground and almost 1000 watts are delivered

to the load. The settling time for Z-source capacitor voltage is fairly good but not ultra-high.

Table 5.1 Closed Loop System Specification

Closed Loop System Specification	
PV Maximum Voltage	170 V
PV Maximum Current	6.05 A
PV Maximum Power	1000 watt
Z-source Inductor	160 uH
Frequency	60 Hz
Z-source Capacitor	1000 uF
Low Pass Filter Capacitor	200 uF
Low Pass Filter Inductor	12 mH
Carrier frequency	333Hz
Three Phase Load	100 ohm per phase
Output voltage	110 V

The PI controller values were K_I= 800, K_P = 1800. With these values, the controller was able to track the reference dc voltage efficiently. The output current and voltage are shown in Figure 5.4. The output frequency is 60Hz. Initially there are some transients but after some time, as the dc capacitor voltage reaches its reference value, the output voltage and current attain steady-state value. The frequency of 60Hz is tracked by PLL and the modulating signals also have the same frequency. The output current is dictated by load and maximum power point tracking. The output signals have some harmonic contents. As

the cut-off frequency becomes sharper, the harmonic content decreases. Also, increase of carrier frequency increases frequency contents. Initially, when the dc voltage rose to its reference value the output voltage has harmonics, but when it reached its reference value, the output voltage and current attained steady state values.

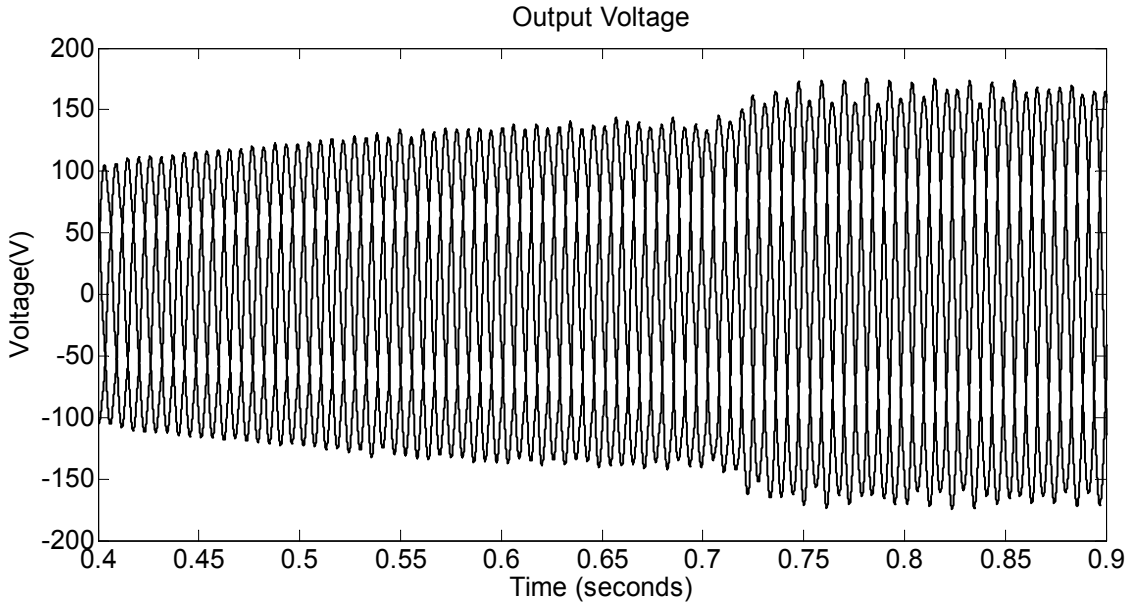

Figure 5.4 Output Voltage for DQ Controller

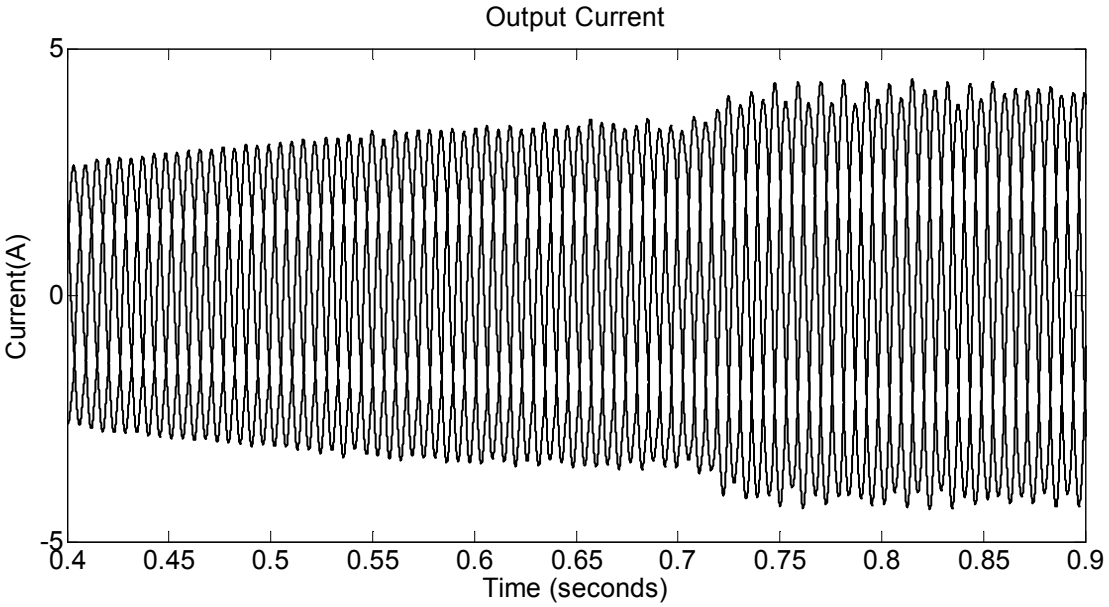

Figure 5.5 Output Current for DQ Controller

The maximum current value is 6.05A which is attained efficiently by MPPT as shown in Figure 5.6. Initially, the current value of PV is at open circuit condition but after some time the PV current reaches its maximum value which shows the effective tracking of MPPT and control of feedback control.

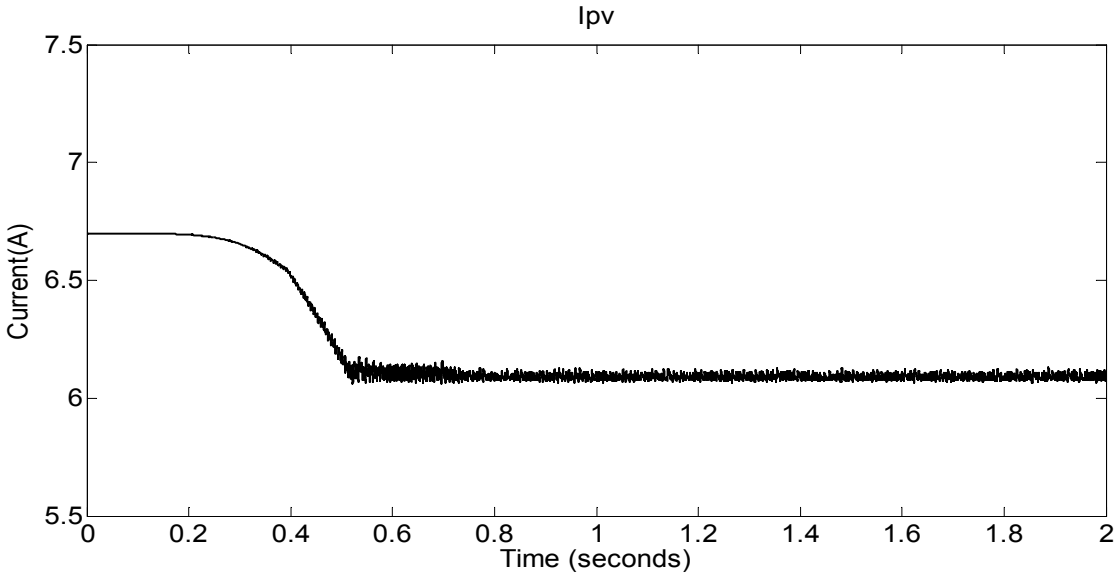

Figure 5.6 PV current for DQ Controller

PV maximum voltage is 170V in this case and is tracked reliably by MPPT as shown in Figure 5.9. Initially, the PV module is in open circuit case but after some time the feedback controller and MPPT successfully tracks the maximum power point with high speed and then stabilizes it.

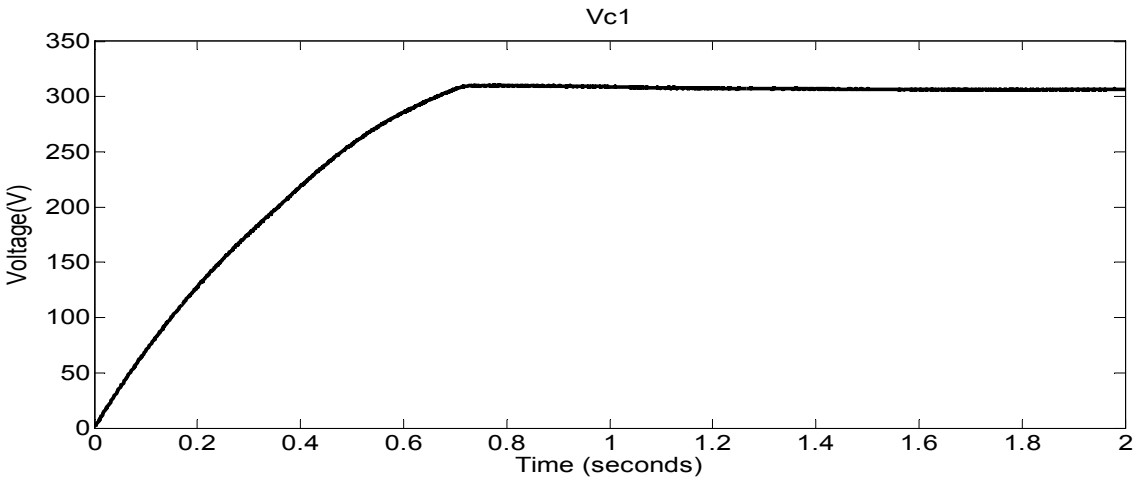

Figure 5.7 Vc1 for DQ Controller

The dc capacitor tracking is shown in Figure 5.7. The dc capacitor charges and the dc reference PI controller has K_p = 800 and K_I = 1800. Before reaching steady state reference value, the output voltages and currents have transients also but once it reaches the reference constant value, all other quantities also attains steady state value.

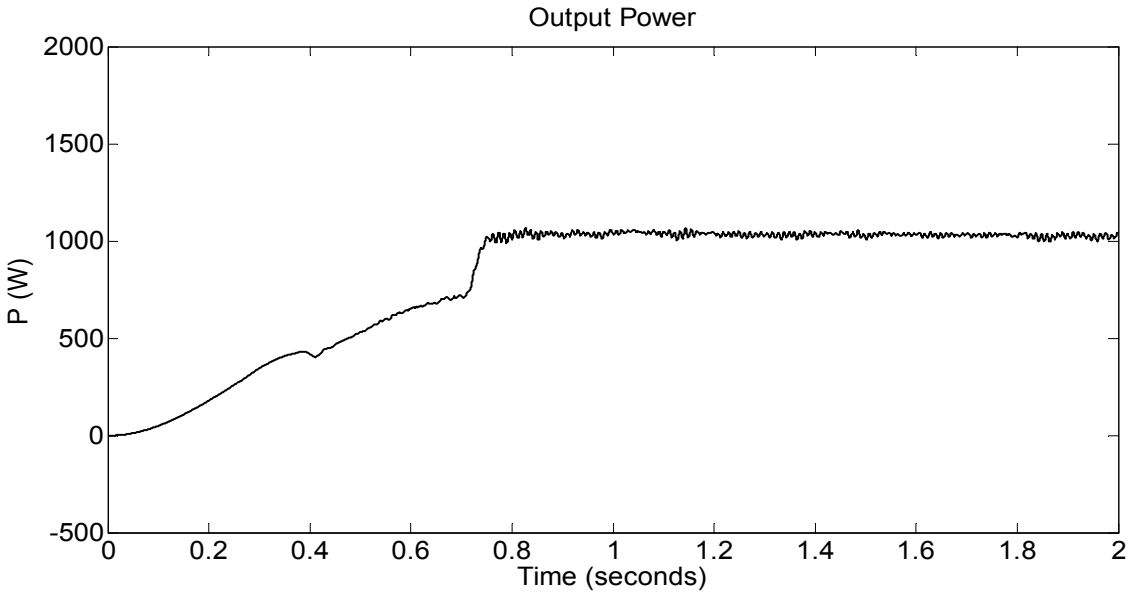

Figure 5.8 Output Power for DQ Controller

The output maximum real power tracking is also shown in Figure 5.8. The output power increases until it reaches the maximum power of 1000 watts and then attains a steady state value which shows the effective control of dq-controller. The efficiency and effectiveness of dq-controller is evident from these results and the maximum voltage, current and power tracking for stand-alone PV power conversion system with Z-source inverter.

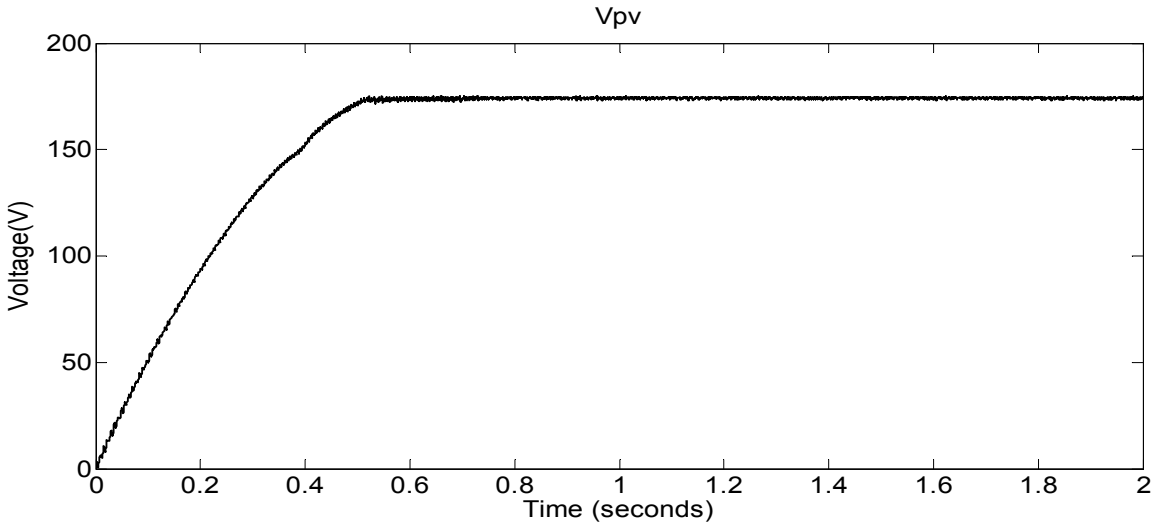

Figure 5.9 PV Voltage for DQ Controller

5.3 Alpha-Beta Controllers

Alpha-beta controllers based on alpha-beta conversions without phase angle consideration by PLL, thus allowing simplifying the feedback control using stationary reference frame domain. Alpha-beta based PI controllers are implemented for the system shown in Figure 5.10.

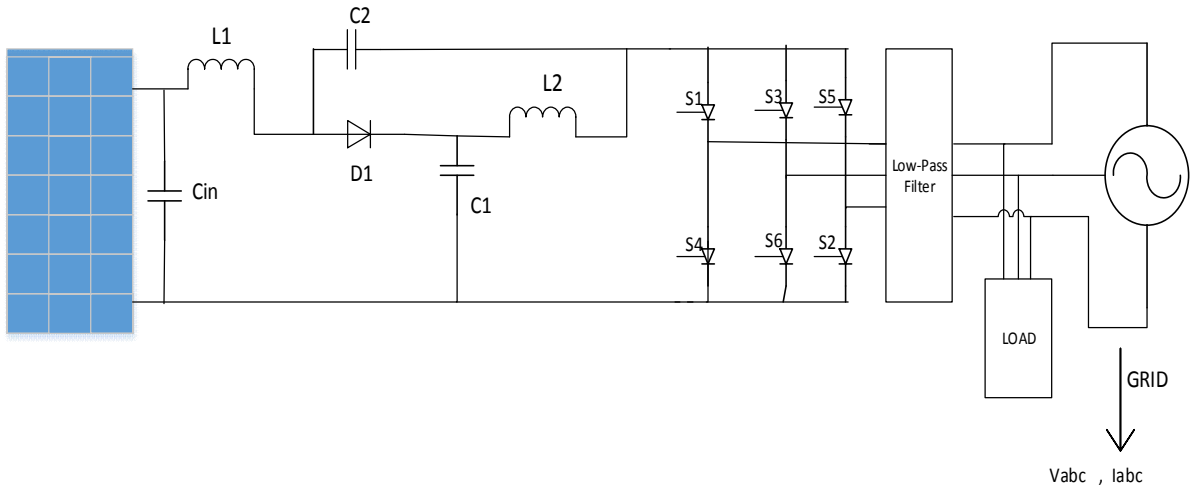

Figure 5.10 System diagram for PI controller

The voltages and currents are sampled from the grid side and converted to alpha-beta domain using transformations and reference I_α and I_β are calculated using equation 5.1. Three PI Controllers are used to calculate reference real power P*, reference Vα* and vβ*. The gains for first PI controller that tracks the DC voltage reference for Z-source capacitor C1 comes out to be K_p = 800 and KI = 1800. The gains for second and third PI controllers were same and come out to be K_p = 50 and KI = 10 for both. The block

diagram of Alpha-beta based PI controllers is shown in Figure 5.11. The three reference modulating signals and two shoot-through references are calculated and these five signals are compared with triangular carrier signal to generate required pulses for the IGBTs.

If recative power reference Q is zero, reference Iα and Iβ are given by:

$$I_\alpha = \frac{V_\alpha * P}{V_\alpha^2 + V_\beta^2} \quad \text{.....(5.1)}$$

$$I_\beta = \frac{V_\beta * P}{V_\alpha^2 + V_\beta^2} \quad \text{.....(5.2)}$$

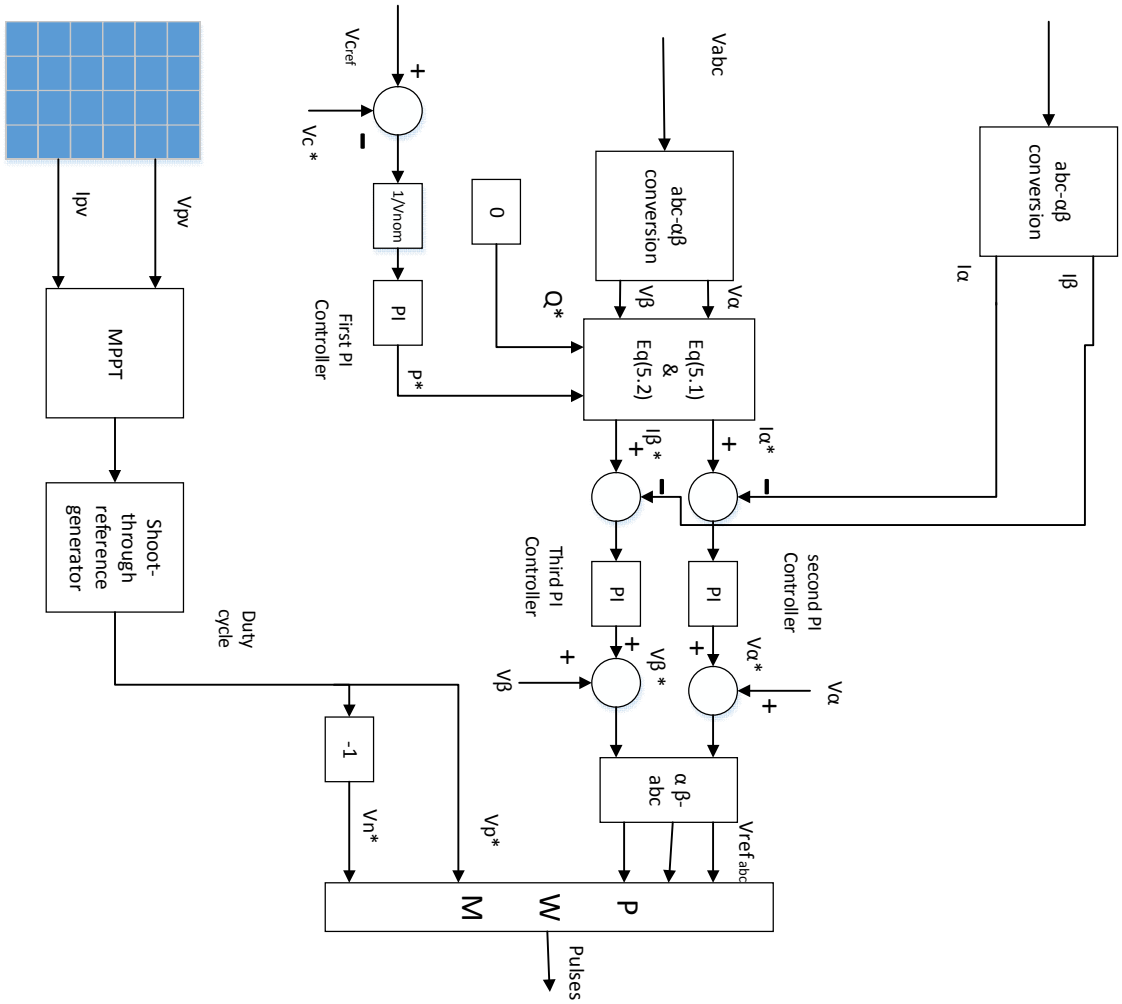

Figure 5.11 Alpha-Beta Feedback Controller

5.4 Simulation Results for PI-based Alpha-beta controller

The System Specifications are given in Table 5.2.

Table 5.2 System Specification for Alpha-beta controller

Closed Loop System Specification	
PV MaximumVoltage	170 V
PV Maximum Current	6.05 A
PV Maximum Power	1000 watt
Z-source Inductor	160 uH
Frequency	60 Hz
Z-source Capacitor	1000 uF
Low Pass Filter Capacitor	200 uF
Low Pass Filter Inductor	12 mH
Carrier frequency	333Hz
Three Phase Load	100 ohm per phase
Grid Voltage	190 V

5.4.1 Case I : Constant Irradiance

The simulations results shows the values of output current and voltages, inverter current and voltages, V_{pv} and I_{pv} tracking, V_{c1} tracking, output power and reference signals generated by controller for fixed irradiance of 1000 w/m^2 are shown in Figure 5.12 –

Figure 5.20. The output voltage is synchronized with the grid voltage and maximum power point is efficiently tracked.

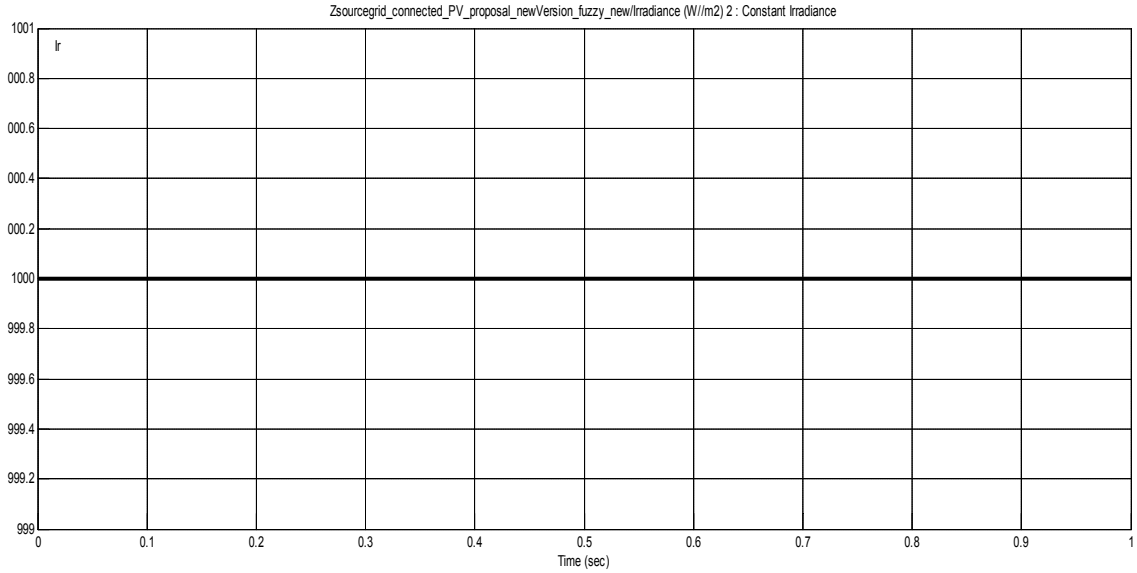

Figure 5.12 Irradiation for PV Module

The irradiation and temperature are constant for PV module. The temperature has been constant at 25ºC and irradiation was constant at 1000 w/m^2. With these constant condition, the output voltage for grid-connected PV system is shown in Figure 5.13. The output voltage has initially some transients but as the input dc capacitor voltage reaches reference value of 400V, the output voltage stabilizes with a frequency of 60Hz and synchronized with the grid.

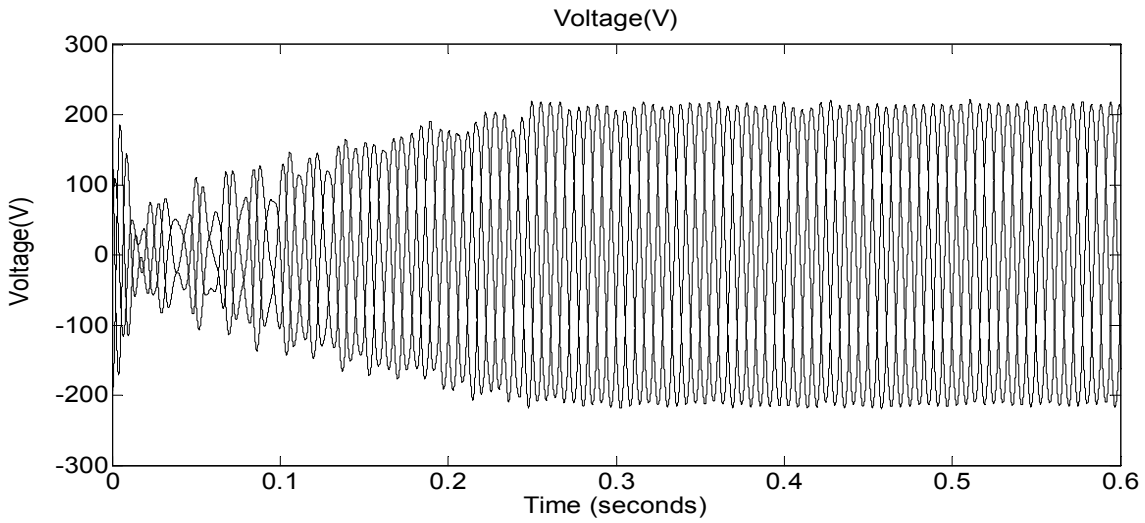

Figure 5.13 Output Voltage for Alpha-Beta Controller

The output current reaches a peak value of 5A as drawn by the load and determined by maximum power point tracking controller. The output current is obtained through LC filter with cutoff frequency of 60 hz. As the sharpness of the cutoff frequency increases, harmonics in output current decreases.

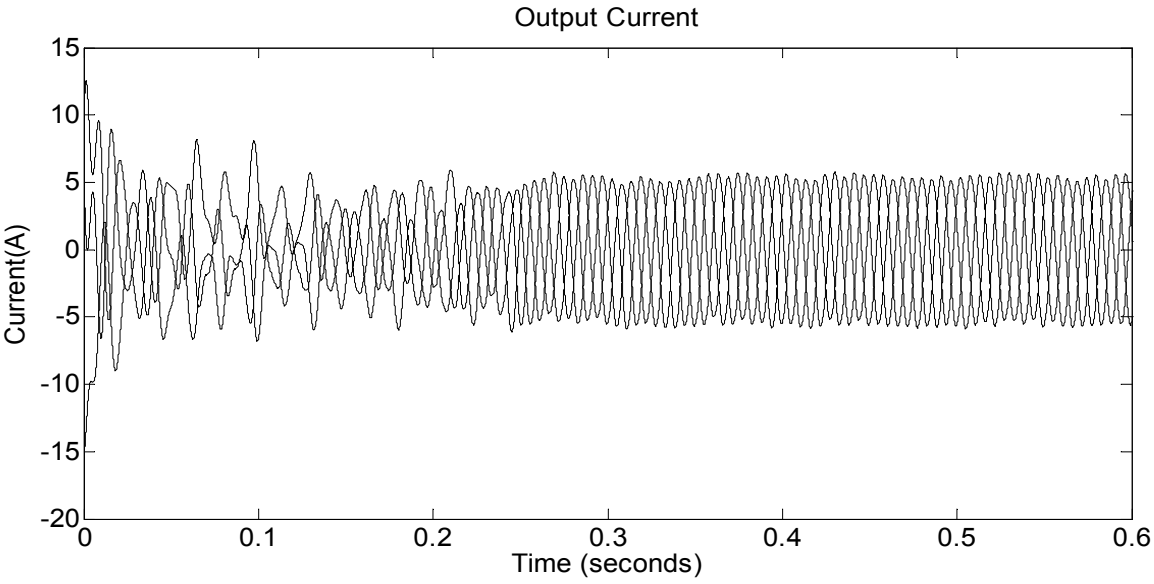

Figure 5.14 Output Current for Alpha-Beta Controller

The inverter voltage and current are shown in Figure 5.15 and Figure 5.16. The output voltage of inverter is ac signal with peak value of 450V and the chopping of input dc voltage is done at frequency determined by carrier frequency. The output current of inverter is ac with harmonics which is filtered by LC low pass filter.

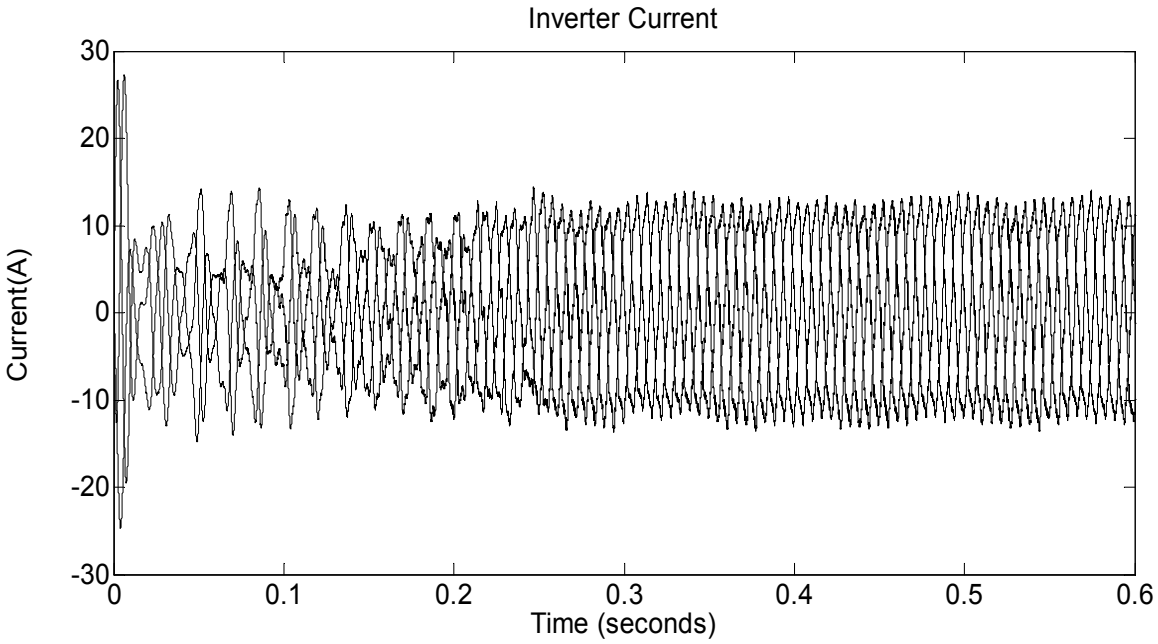

Figure 5.15 Inverter Current for Alpha-beta Controller

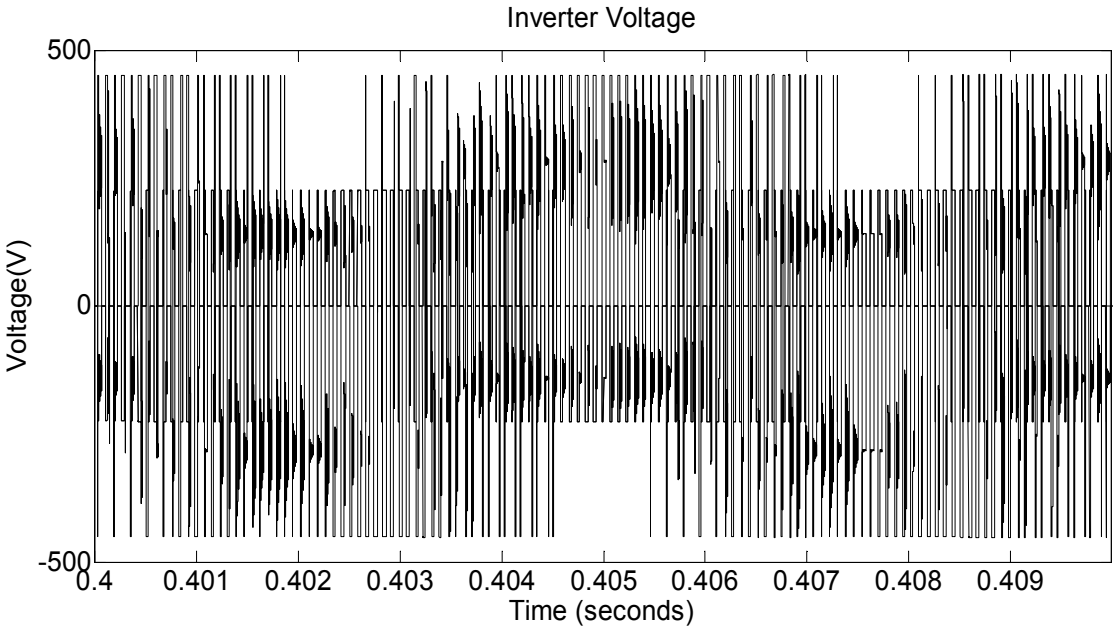

Figure 5.16 Inverter Voltage for Alpha-beta

The maximum power and maximum current tracking for grid-connected feedback system is shown in Figure 5.17 and Figure 5.18. The output power is successfully tracked and becomes constant after reaching 1000 watts and PV current reaches the maximum value of 6.05 at 0.3 seconds and becomes constant. This shows that the MPPT and feedback controller is providing an effective control.

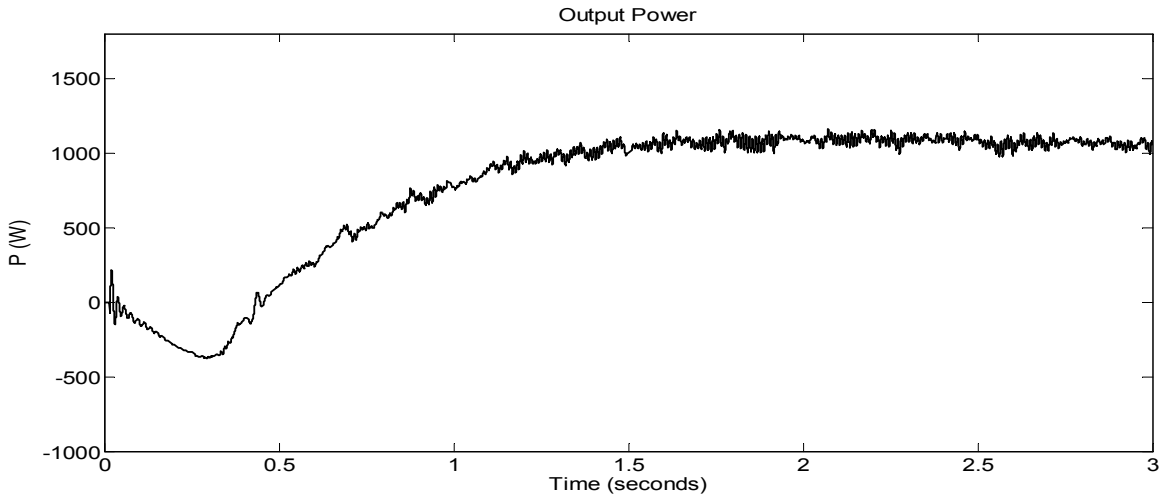

Figure 5.17 Output Power for Alpha-Beta Controller

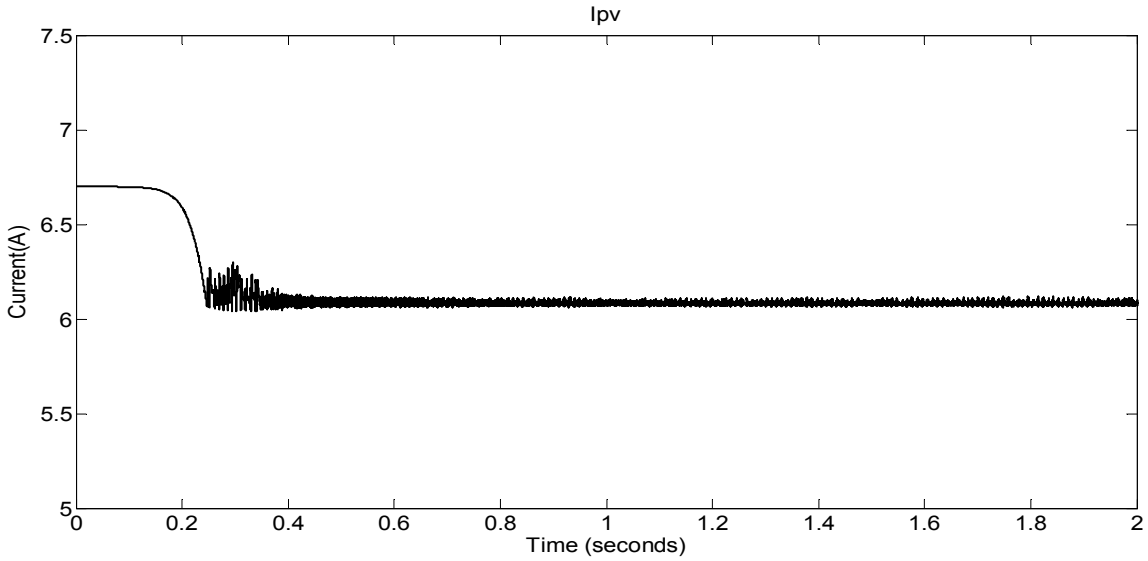

Figure 5.18 PV Current for Alpha-beta Controller

The maximum PV voltage tracking is shown in Figure 5.19. It reaches its maximum value of 170V and becomes constant at 0.3 seconds which shows the fast and efficient tracking of controller.

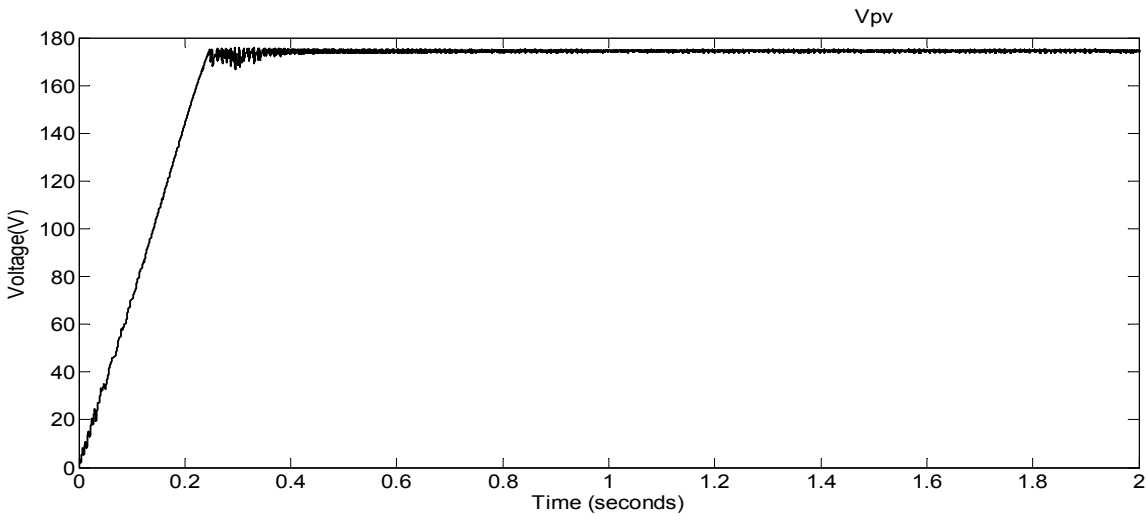

Figure 5.19 PV Voltage for Alpha-beta Controller

The dc voltage tracking is shown in Figure 5.20 and it attaints its maximum value after some time. The dc reference tracking depends upon the proportional and integral gains of dc reference PI controller. As the dc voltage reaches reference value and stabilizes, all the output quantities also stabilizes and reaches their steady state values. The output of dc voltage reference tracking controller provides the signal for maximum real power tracking and deliverance to the load.

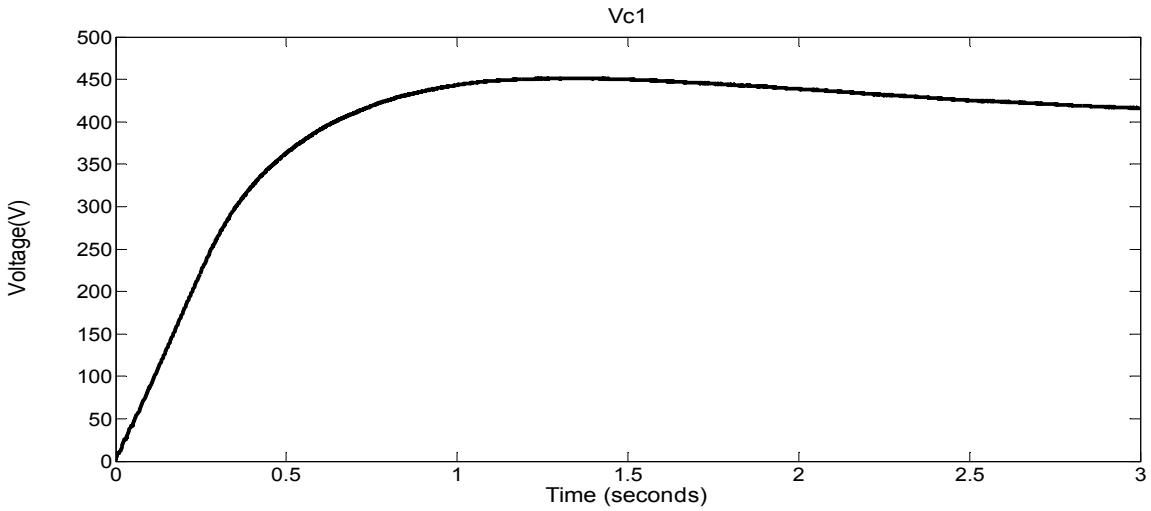

Figure 5.20 Z-source Capacitor for Alpha-beta Controller

5.4.2 Case II: Changing Irradiations

In case II, the irradiance value for PV module was initially constant at 1000 w/m2 but at time = 0.7 sec, the irradiance decreased to 700 w/ m2 and remained there till time =1.51 sec. At time = 1.51 sec, the irradiance ramped up to 1000 w/m2 as shown in Figure 5.21. The reference voltage tracking and maximum power point tracking along with output voltage, current and power are shown in Figure 5.22 – Figure 5.27.

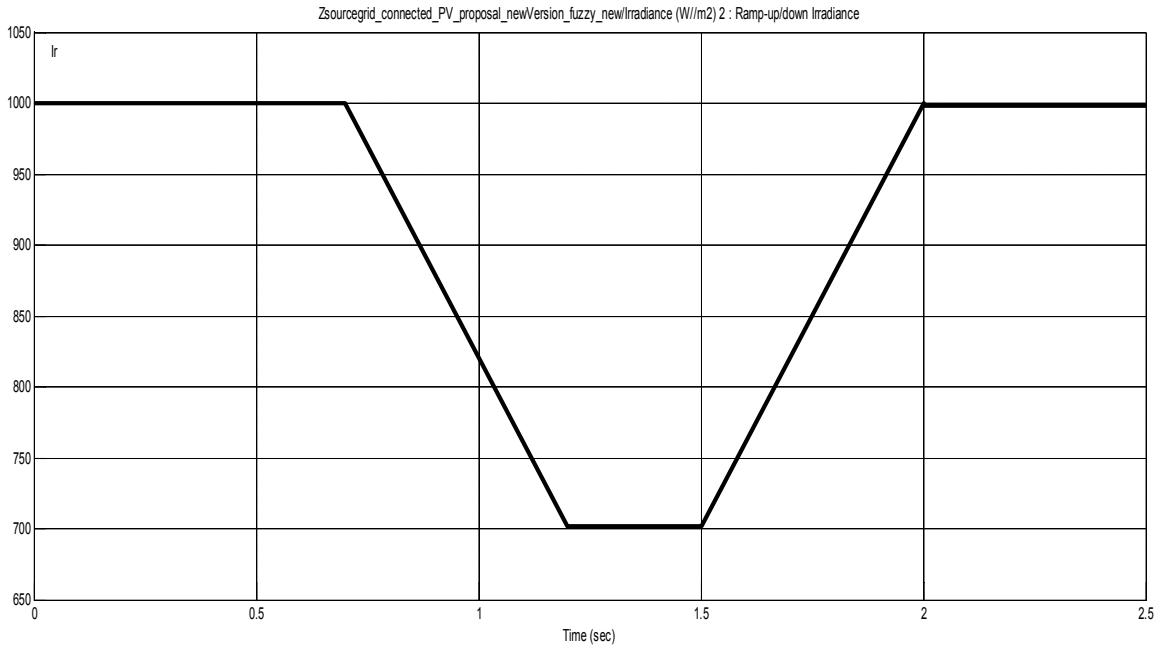

Figure 5.21 Changing Irradiation for PV Module

The maximum PV voltage tracking during changing condition is shown in Figure 5.22. Initially the PV voltage reaches a maximum value of 170 V at irradiation equal to 1000 w/m^2. After 0.7 seconds, the irradiation decreases to 700 w/m^2 and PV voltage is tracked to new maximum 163V. After 1.5 seconds, the irradiation increases back to 1000 w/m^2 and PV voltage reaches 170 V. So the maximum voltage is tracked effectively and successfully.

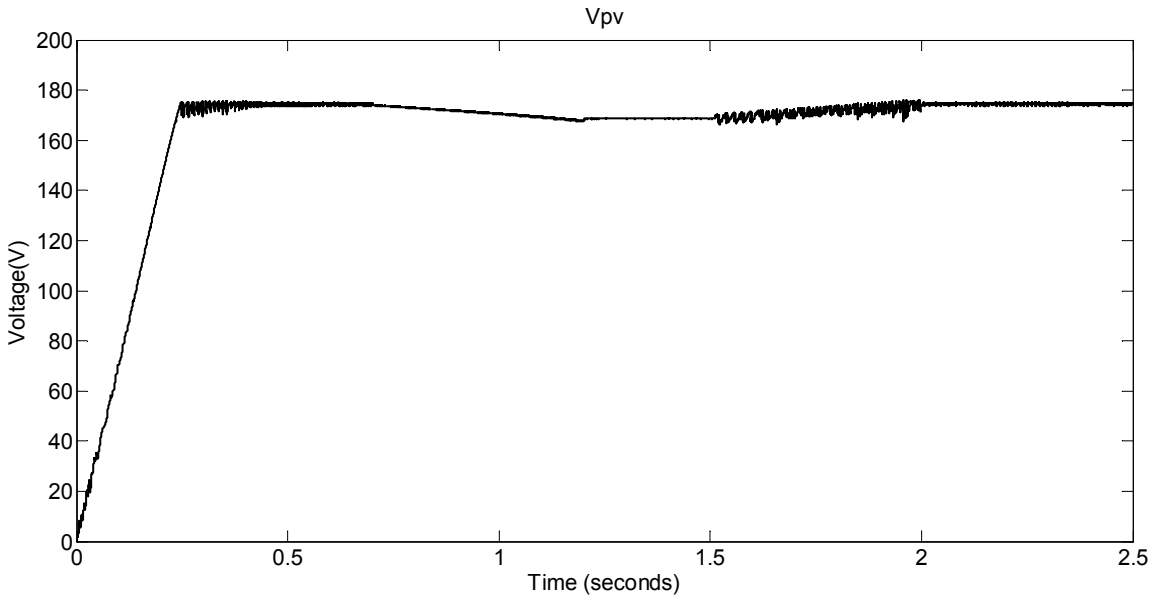

Figure 5.22 PV Voltage for Alpha-Beta Controller under changing conditions

The PV current tracking is shown in Figure 5.23. Initially, the PV module is in open circuit condition with current equal to 6.7A and after some time, the PV current is tracked to maximum power point value of 6.05A. With the decrease in irradiations, the PV current decreases and new PV current corresponding to maximum power point is achieved which is 4.25A. With irradiation coming back to 1000 w/m^2, current is tracked to 6.05A.

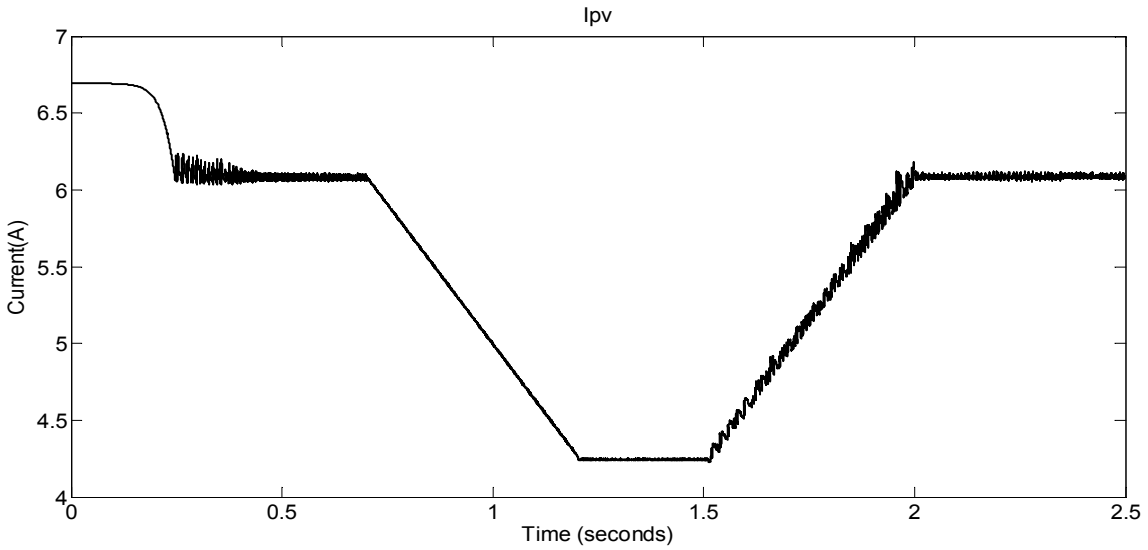

Figure 5.23 PV Current for Alpha-Beta Controller under changing conditions

The Z-source capacitor dc voltage tracking done by dc referencing PI controller is shown in Figure 5.24. As the irradiation changes, controller tries to keep the voltage near to reference value and as the irradiation increases and reaches 1000 w/m^2, the dc voltage is brought close to reference value.

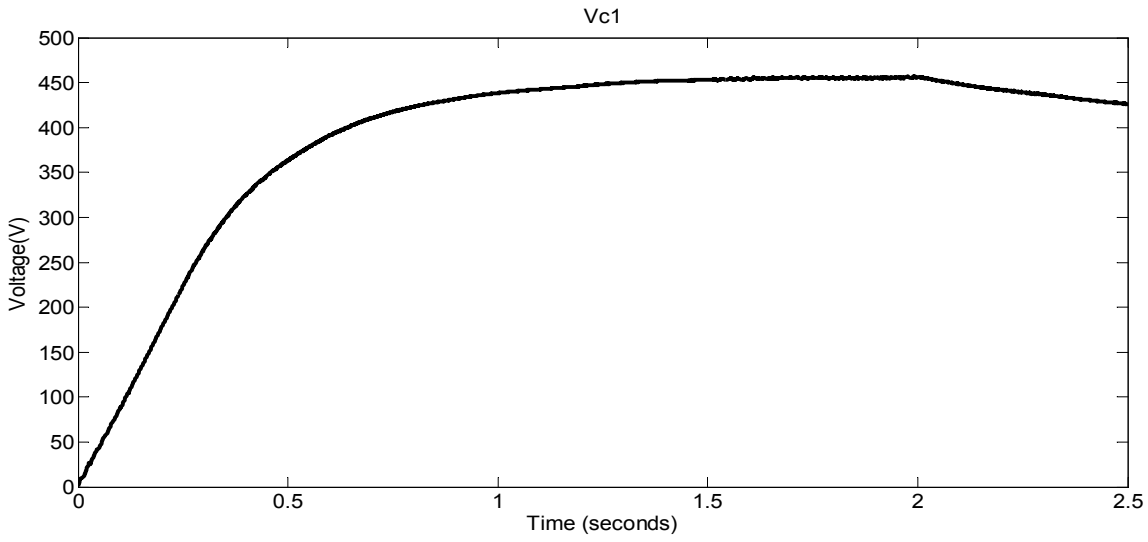

Figure 5.24 Z-source capacitor for Alpha-Beta Controller under changing conditions

The tracking of maximum power and its deliverance to load has been shown in figure 5.25. Initially the maximum power of 1000 watt is delivered, then 700 watts and power reaches back to 1000 watts.

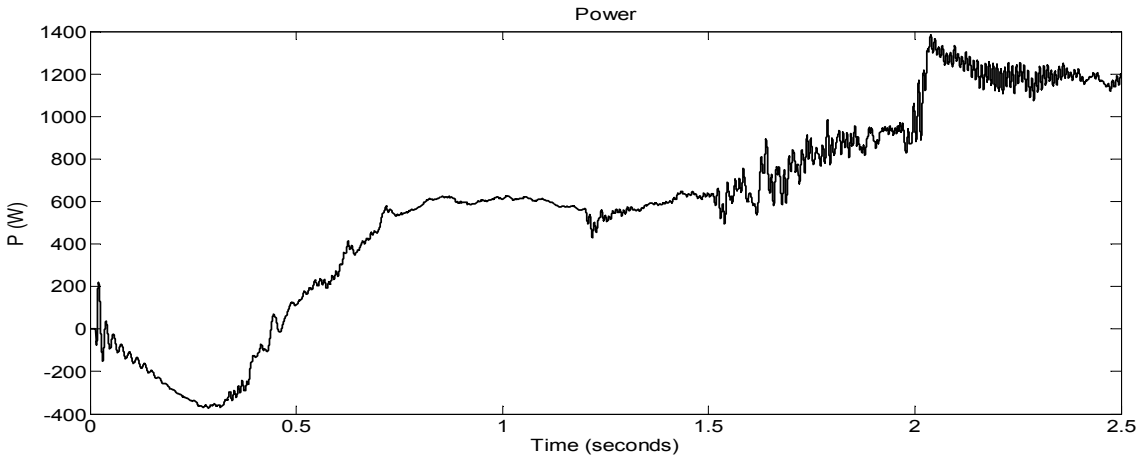

Figure 5.25 Output power for Alpha-Beta Controller under changing conditions

Three phase output voltages and currents are shown in Figure 5.26 and figure 5.27. Voltages and currents have steady-state values during constant irradiation and temperature. During the change of irradiation, there are some transients in the output current and it is damped quickly by current controllers.

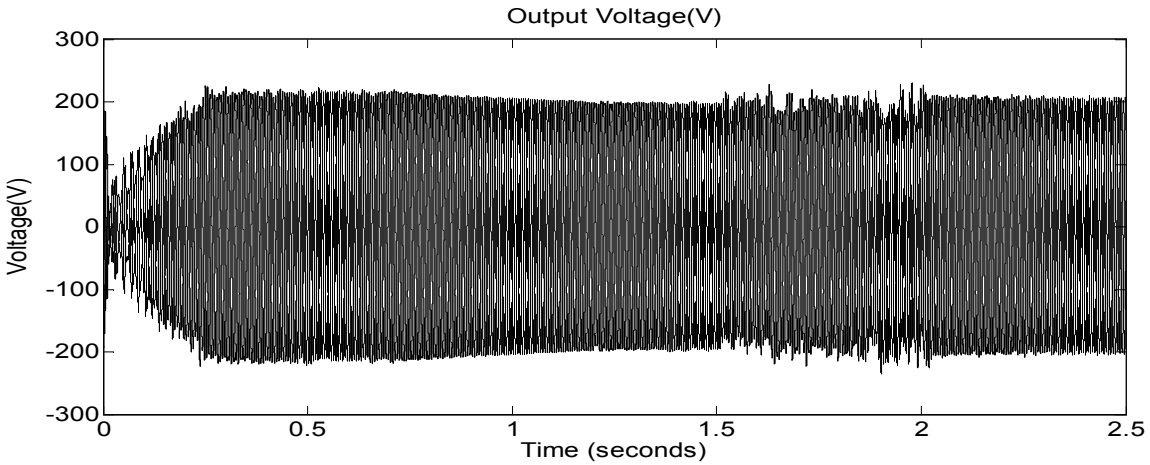

Figure 5.26 Output Voltage for Alpha-Beta Controller under changing conditions

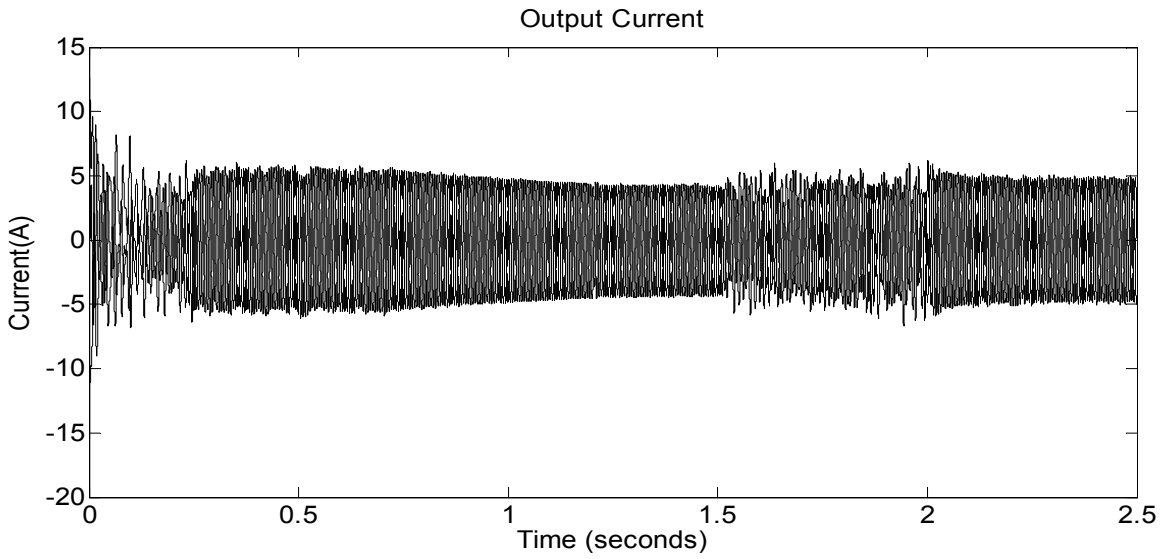

Figure 5.27 Output Current for Alpha-Beta Controller under changing conditions

5.5 ANFIS Feedback Controllers

Adaptive neuro-fuzzy inference systems are used to train systems according to input-output data. The ANFIS system uses either Takagi-Sugeno models or Mamdani models to build up trained system. Takagi-Sugeno system allows membership functions for output as well while Mamdani models allow only linear outputs. In ANFIS models, inputs are assigned membership functions and the inputs will attain values from these membership functions and Takagi-Sugeno models are used to fuzzify the inputs and then defuzzifications are done using one of the four available methods to obtain outputs. For training of ANFIS, there are two methods; assign the rules manually or using training data to train ANFIS which assign the rules itself.

For the first controller to track the dc reference, rules are developed according to table 5.3 where different states are assigned to the two inputs. The two inputs for the first ANFIS controller are error or difference between reference value of Vc1 and its measured value and the change in error. Five states are assigned to each input namely

negative small (NS), Negative large (NL), positive small(PS), positive large(PL) and zero(Z).

Table 5.3 Rules for PI Controller 1

dError \ Error	NL	NS	Z	PS	PL
NL	NL	NL	NS	Z	PS
NS	NL	NS	NS	NL	PS
Z	NS	NS	Z	PS	PS
PS	Z	NL	PS	PS	PL
PL	PS	PS	PS	PL	PL

The rule base for ANFIS Controller1 that tracks the dc reference is shown is Figure 5.28 and rule surface is shown in Figure 5.29.

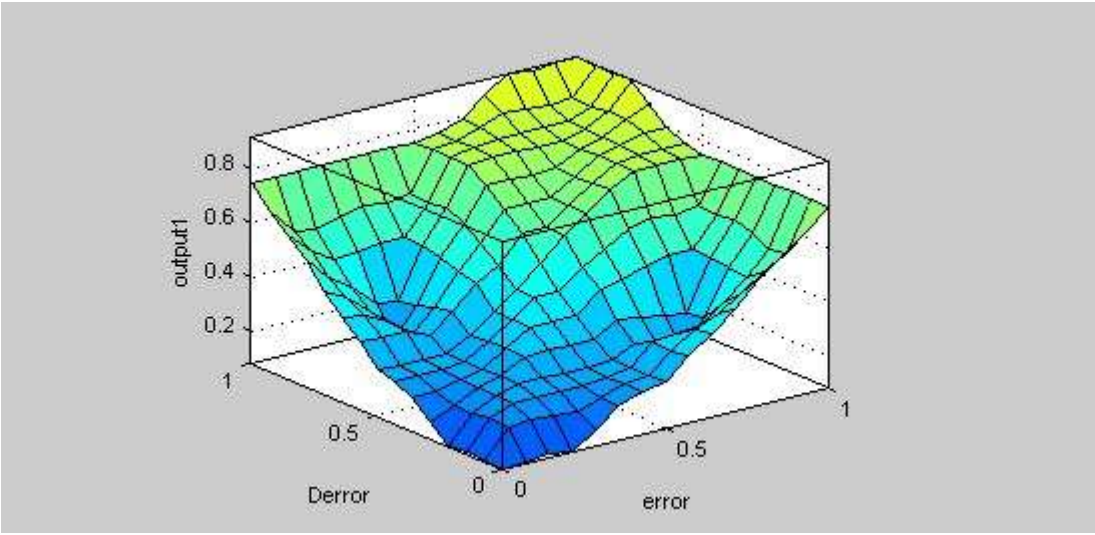

Figure 5.28 Rule Surface for ANFIS DC Reference Controller

For current Controller 1 and 2, training was done using cyclic and linear data. For training ANFIS, 7 gussian membership functions were assigned to each input training of controller 1 and 7 membership functions were assigned to each input of controller 2 and training was done using back propagation algorithm. After training ANFIS controllers were obtained. Different parameters for controller 2 and 3 are shown in Figure 5.30 – Figure 5.35.

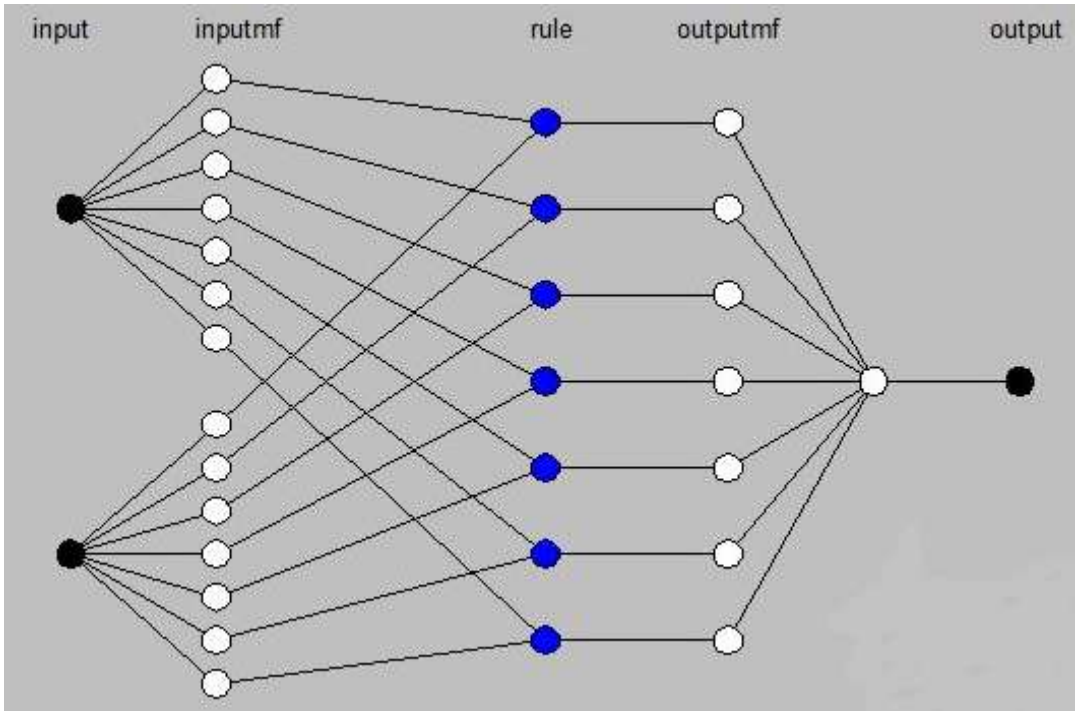

Figure 5.29 Structure for ANFIS Current Controller 1

The membership functions corresponding to rules for current ANFIS controller after training are shown in Figure 5.30 and Figure 5.31. Gaussian membership function attain different mean values, stand deviations and shifts as a result of training. The output achieves linear function value as a result of training.

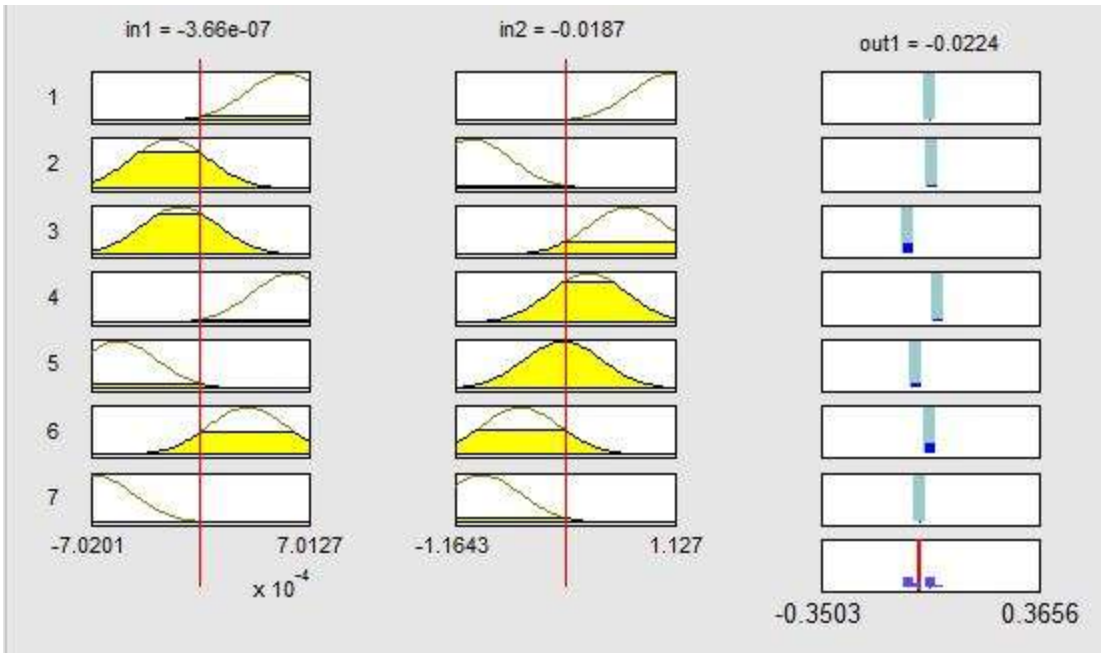

Figure 5.30 Rules for ANFIS Current Controller 1

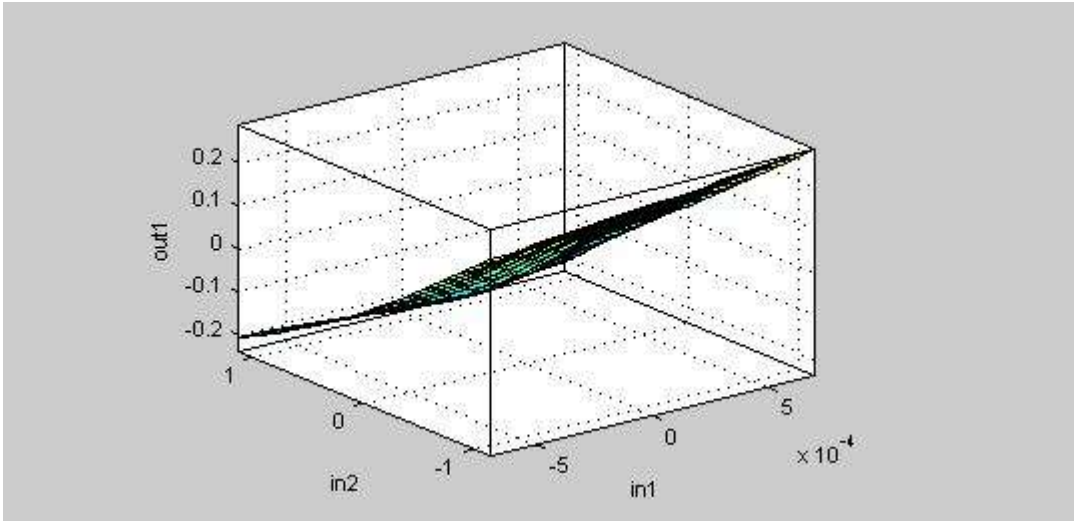

Figure 5.31 Rule Surface for ANFIS Current Controller 1

Figure 5.32 shows the structure of ANFIS current controller 2. The two inputs are assigned 6 Gaussian membership functions and they are trained using six rules. The output is defuzzified using weighting method by training to get the output values.

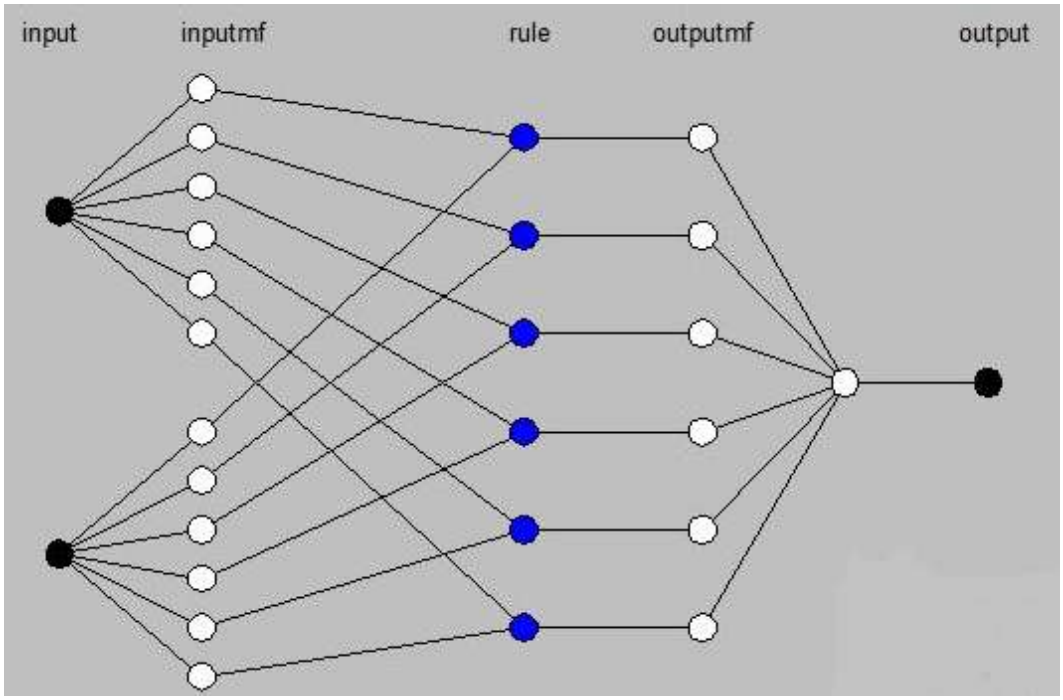

Figure 5.32 Structure for ANFIS Current Controller 2

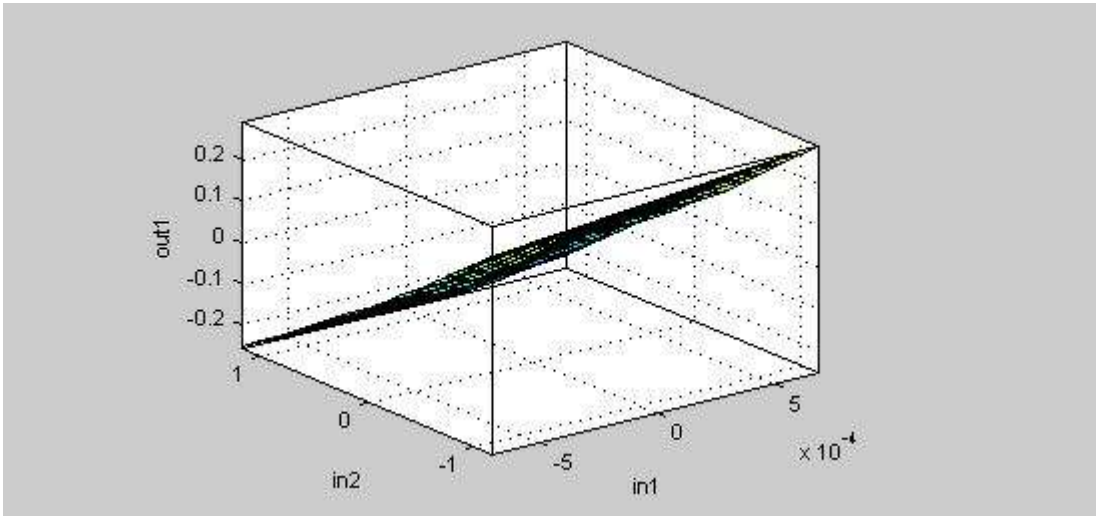

Figure 5.33 Rule Surface for ANFIS Current Controller 2

The grid connected PV system for which the ANFIS controller is designed is shown in Figure 5.34.

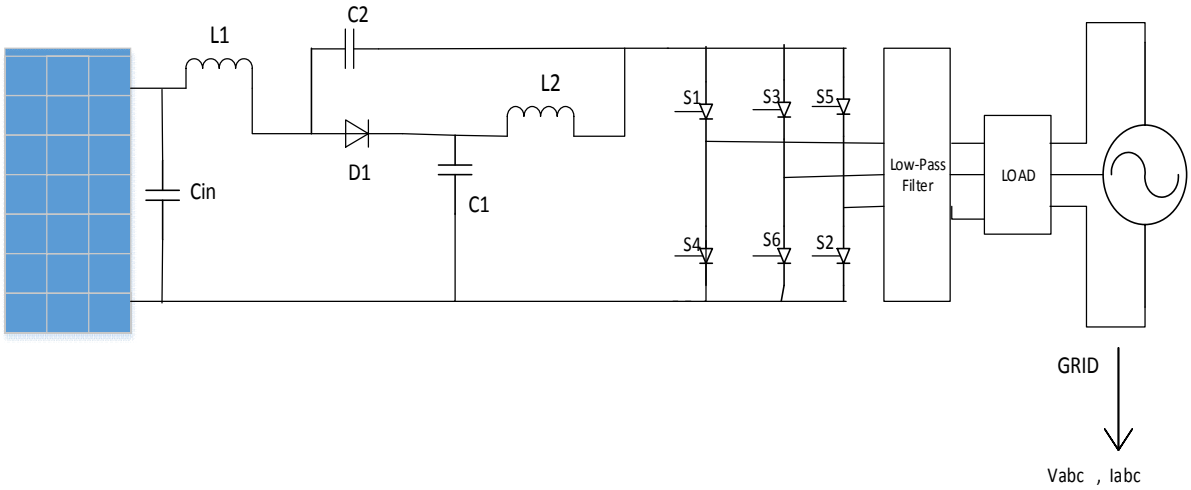

Figure 5.34 Grid Connected PV system

The complete control diagram based on ANFIS controllers is shown in Figure 5.36. The dc reference is tracked by dc reference ANFIS designed through rules in table 5.3. The different values of error and change in error determines the output of the ANFIS controller. The two reference current controllers to track maximum power from PV to grid are obtained through training. These ANFIS controller take reference current for maximum real power and measured output currents in alpha beta domain and calculates the required signals for PWM to achieve maximum power deliverance to grid and control output quantities.

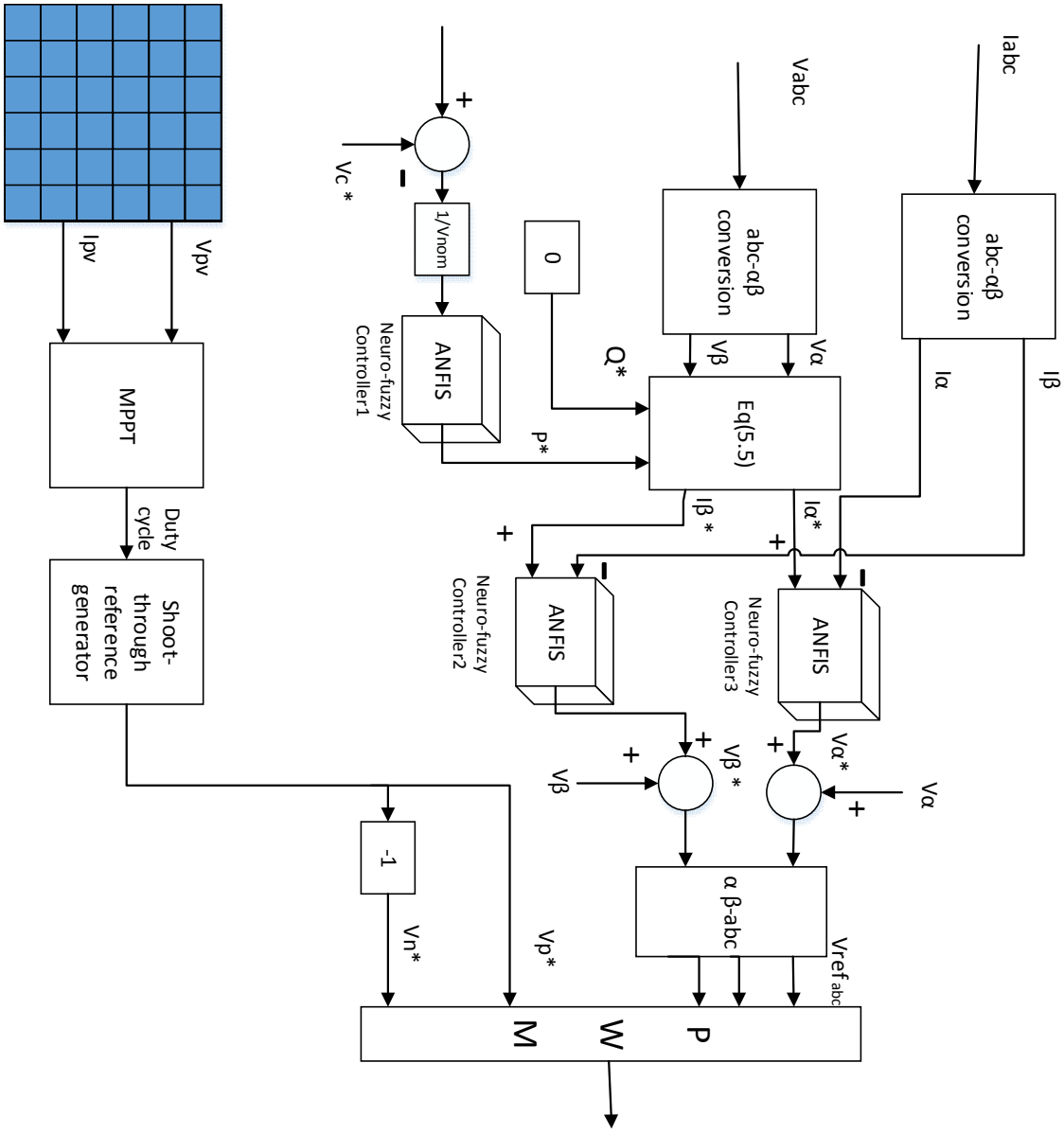

Figure 5.35 ANFIS Based feedback Controller

5.6 Simulation Results for ANFIS-based controller

5.6.1 Case I: Constant Irradiation

In case I, irradiation for PV module is constant at 1000 w/m2. The ANFIS controllers are fast in tracking the dc reference and maximum power point to deliver maximum power to the load as shown in Figure 5.37 - Figure 5.43 .

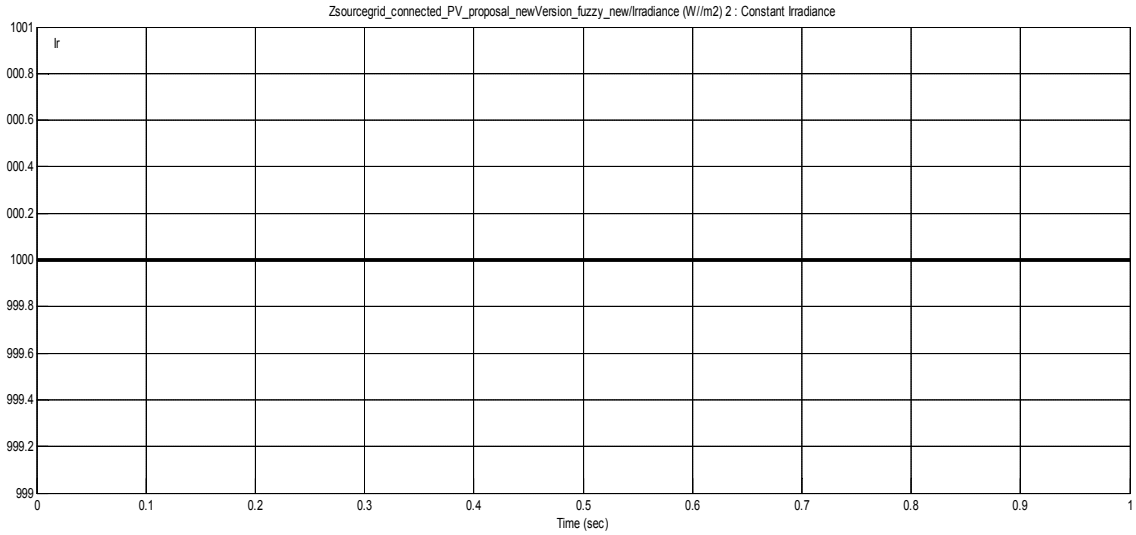

Figure 5.36 Irradiation for PV Module

The maximum current tracking corresponding to maximum power point under constant irradiation and temperature conditions of STC by ANFIS based controller is shown in Figure 5.37. The tracking of current is smoother and it reaches the maximum current value at 0.1 sec and becomes constant at 6.05 A.

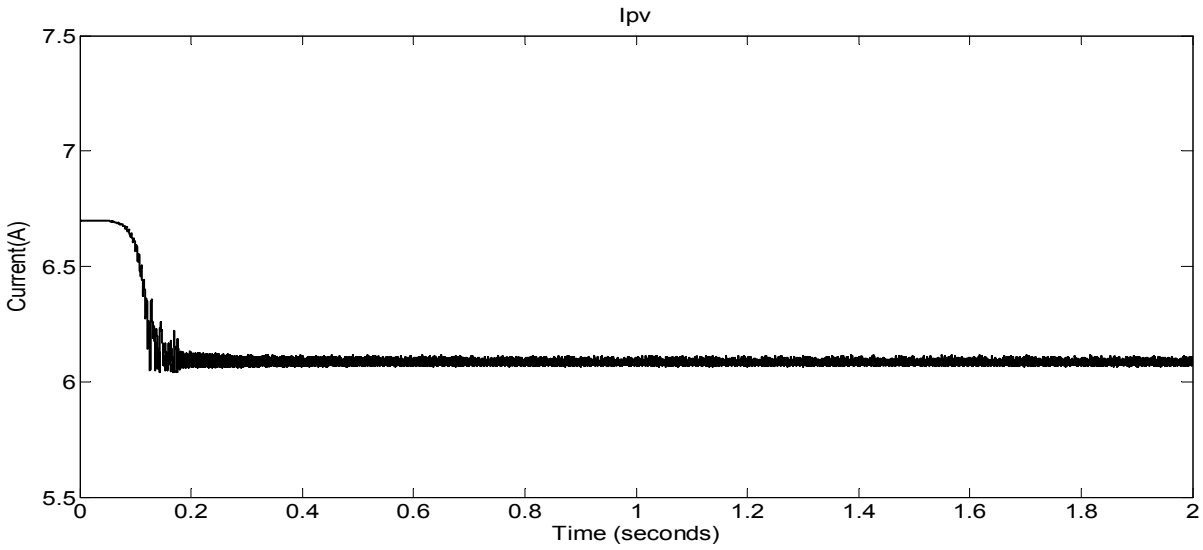

Figure 5.37 PV Voltage for ANFIS Feedback Controller

PV maximum voltage tracking under constant conditions by ANFIS based controller is shown in Figure 5.38. The maximum value of voltage corresponding to maximum power point is achieved at 0.1 seconds and becomes constant at 170 V.

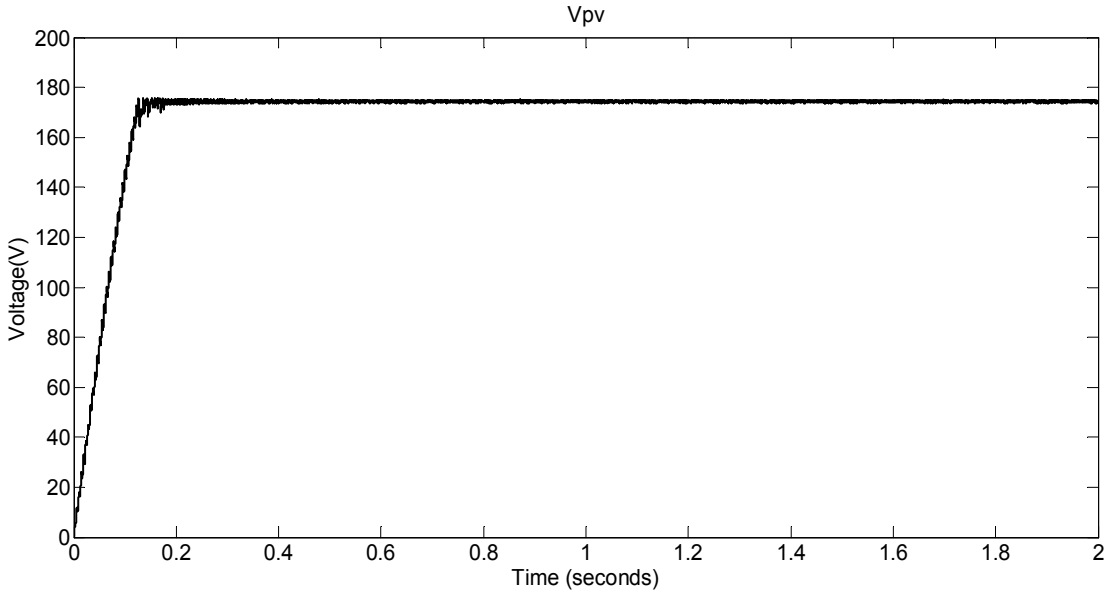

Figure 5.38 PV Current for ANFIS Feedback Controller

Z-source capacitor dc voltages reaches the reference of 400V at 0.2 seconds and becomes constant as shown in Figure 5.39. It shows the accuracy and fast tracking of dc reference ANFIS controller.

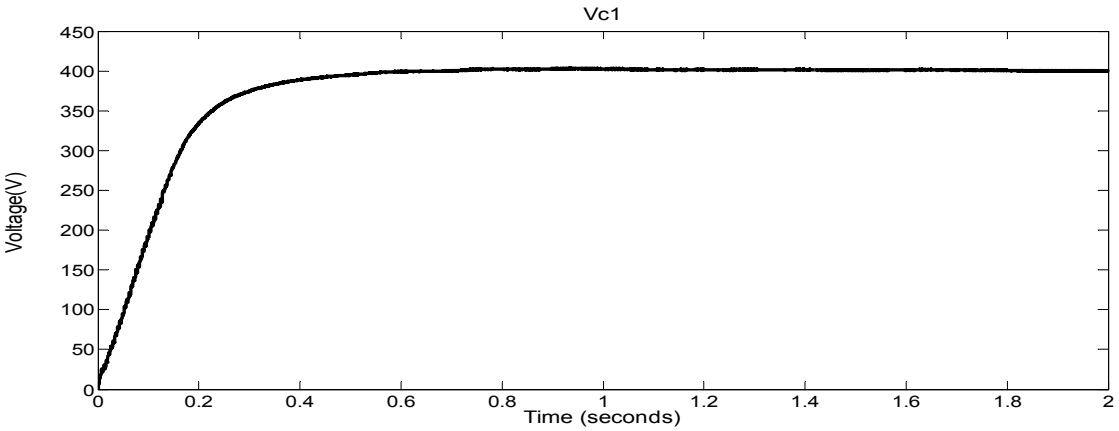

Figure 5.39 Z-source Capacitor Voltage for ANFIS Feedback Controller

Maximum power of 1000 watts is extracted from PV and delivered to grid efficiently as shown in Figure 5.40. The output current and voltages are sampled and used in calculation by current ANFIS controller to extract maximum power.

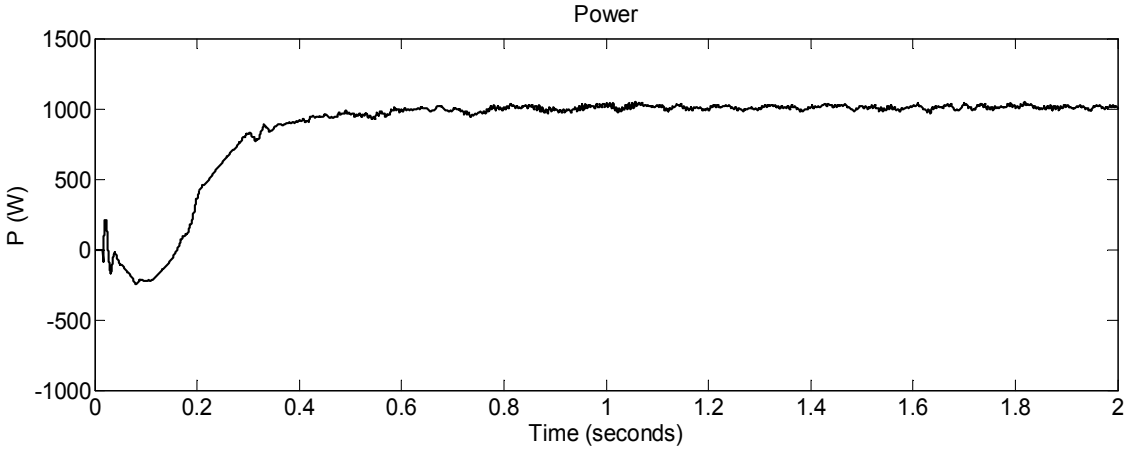

Figure 5.40 Output Power for ANFIS Feedback Controller

Three phase output voltages and currents for ANFIS based controller have been shown in figure 5.41 and Figure 5.42. After some initial transients, the output current and voltage reach their steady state values. These current and voltages are synchronized with grid and required voltage and current for load is provided. The initial disturbance is due to the fact that the dc link capacitor voltage has not reached the reference value, so that output of the inverter is not yet equal to the magnitude of the grid voltage. After sometime, the capacitor voltage reaches reference value and the output of the inverter reaches a value which enables the LC filter to give 60 Hz sinusoidal wave synchronized with grid.

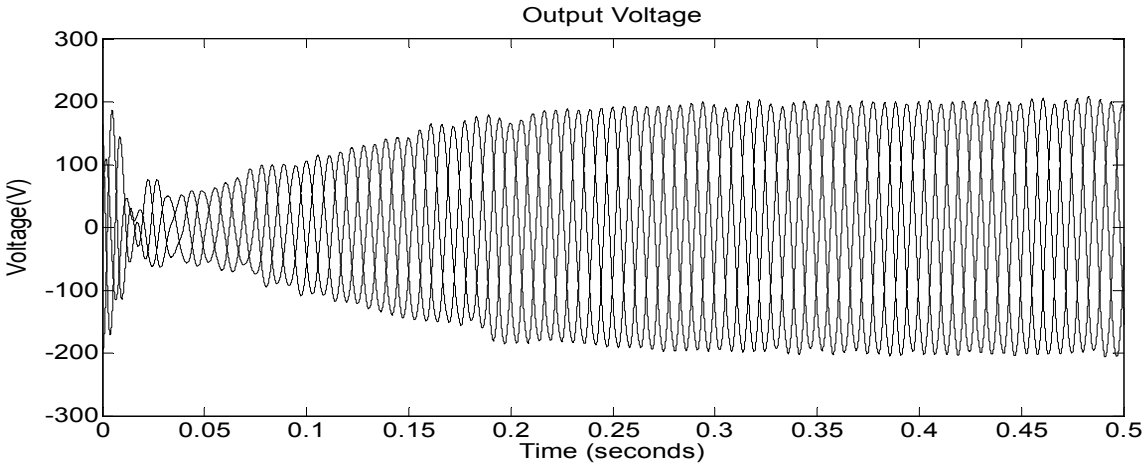

Figure 5.41 Output Voltage for ANFIS Feedback Controller

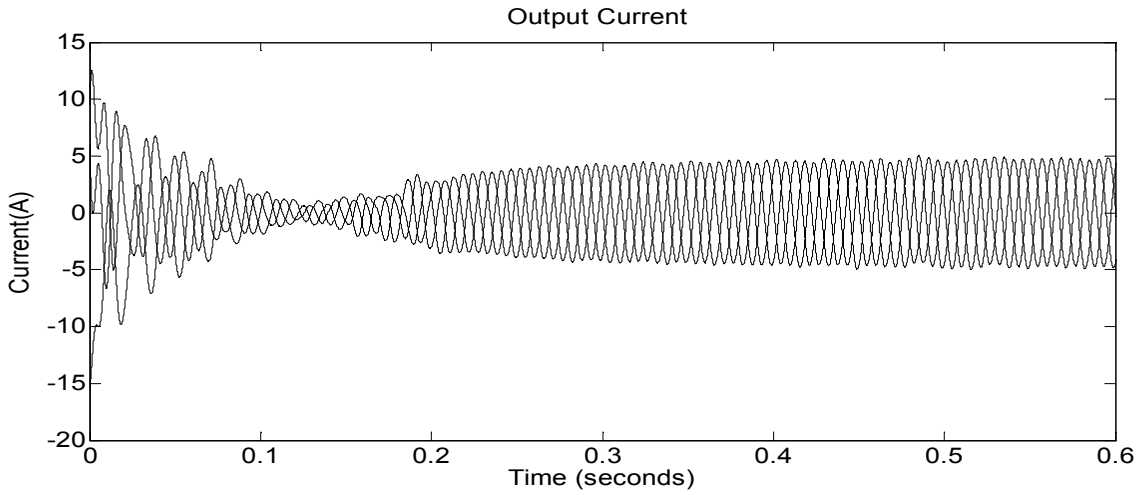

Figure 5.42 Output Current for ANFIS Feedback Controller

5.6.2 Case II: Changing Irradiation

In this case, the irradiance is changing as it ramps down to 700 w/m2 at time = 0.7 sec and ramps up to 1000 w/m2 at 1.51 sec. The performance of ANFIS controller for this changing condition is shown in Figure 5.44 – Figure 5.50.

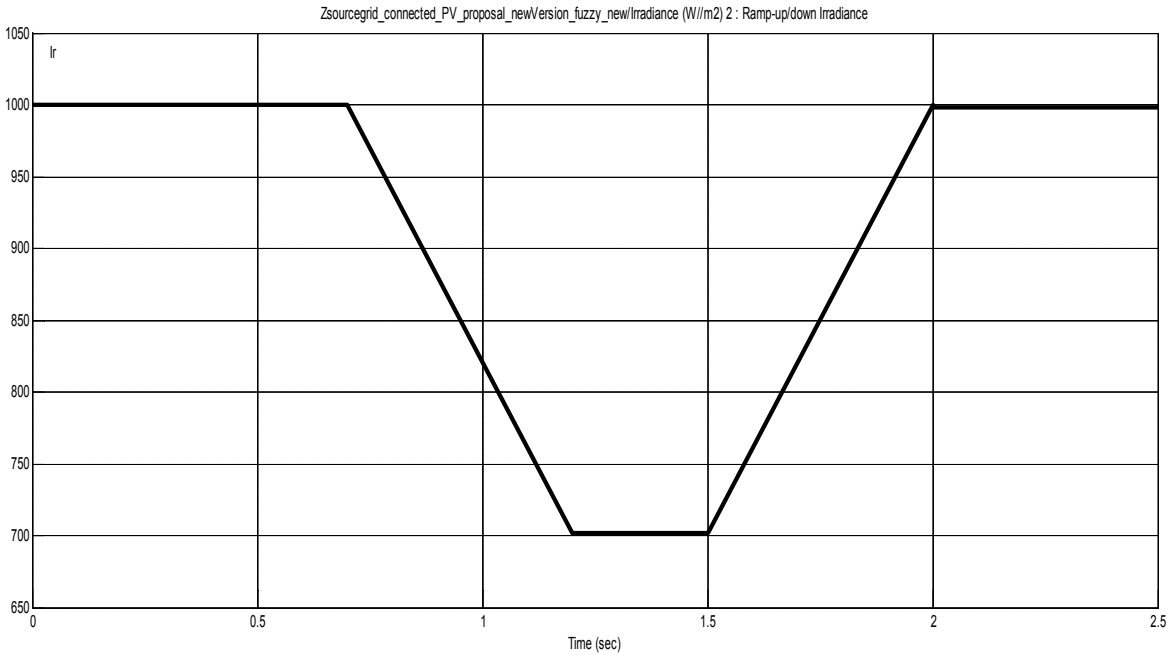

Figure 5.43 Changing Irradiations for PV Module

The output currents and voltages under changing conditions are shown in Figure 5.44 and Figure 5.45. These output signals are perfectly sinusoidal at 60Hz and they have slight harmonic contents during the change in irradiation but due to control action of controllers, they are stabilized.

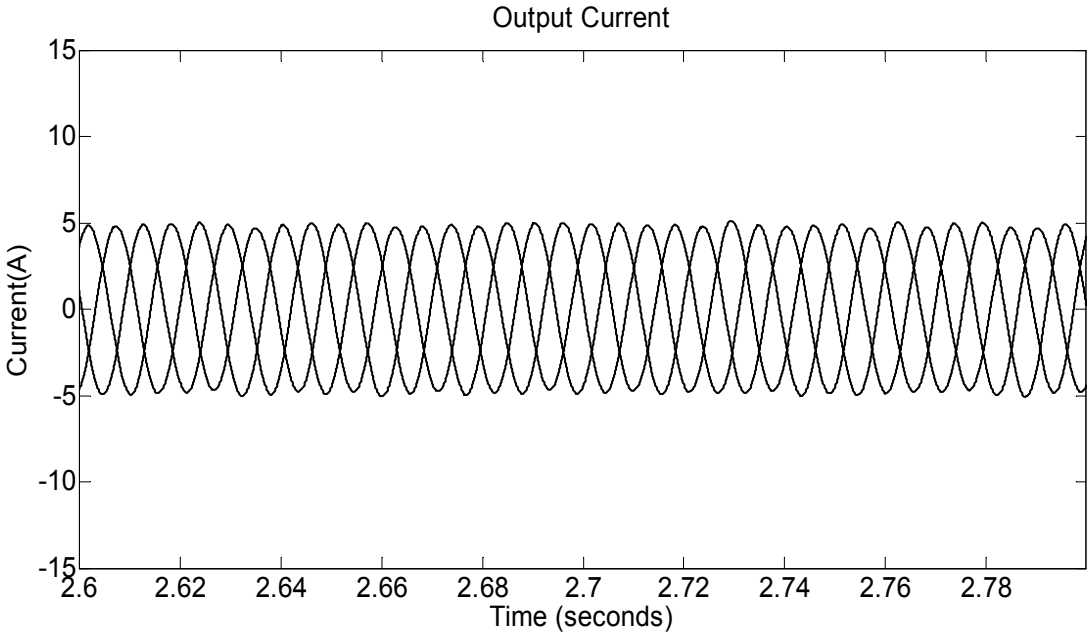

Figure 5.44 Output Current for ANFIS Feedback Controller under Changing conditions

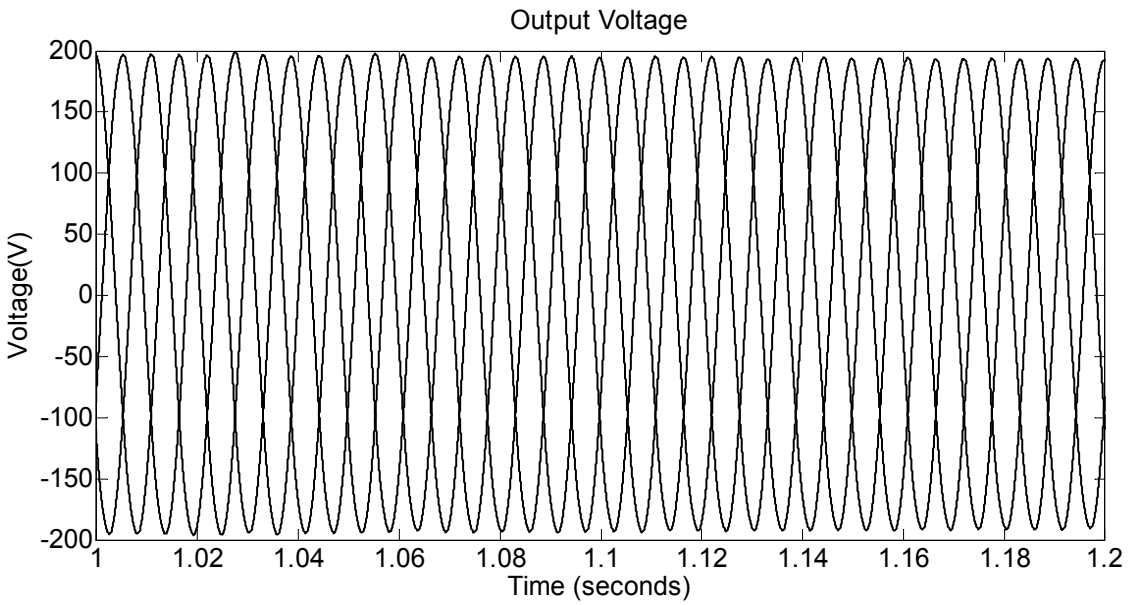

Figure 5.45 Output Voltage for ANFIS Feedback Controller under changing conditions

Output power tracking during changing conditions is shown in Figure 5.46. The output power initially reaches the maximum value of 100 under STC conditions. During the decrease in irradiation, the output power is quickly tracked to new maximum value of 700 watts. As the irradiation increases back to 1000 w/m^2, the output power is effectively tacked to 1000 watts.

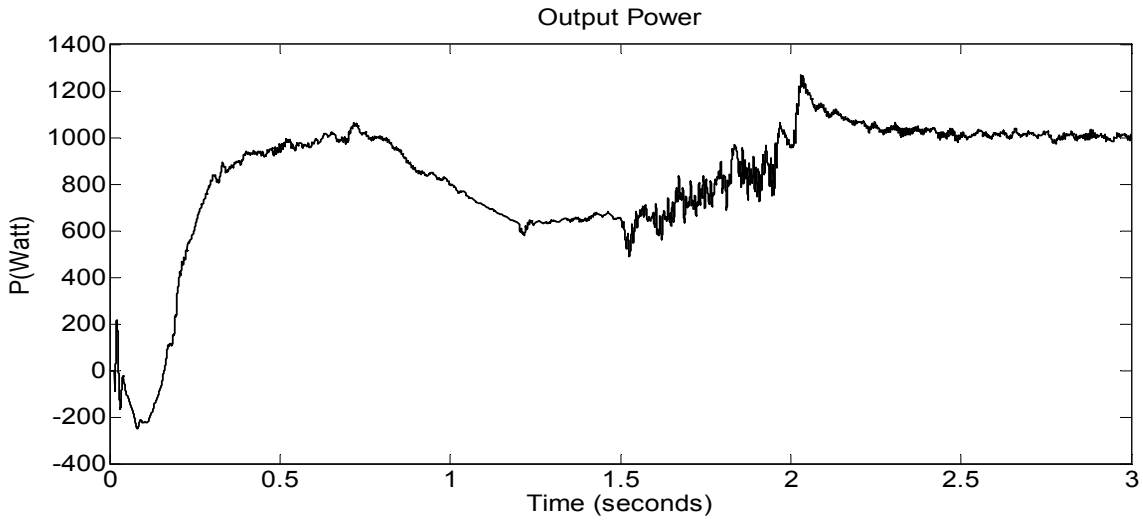

Figure 5.46 Output Power for ANFIS Feedback Controller under changing conditions

DC voltage tracking is shown in Figure 5.47. The voltage is tracked to reference value of 400 V quickly initial constant environmental conditions. As the condition changes, their is slight change in capacitor voltage value but it is quickly restored back to 400 V and during changing conditions, it is kept near to reference value of 400V thus keeping the output quantities of currents and voltages at their steady-state values.

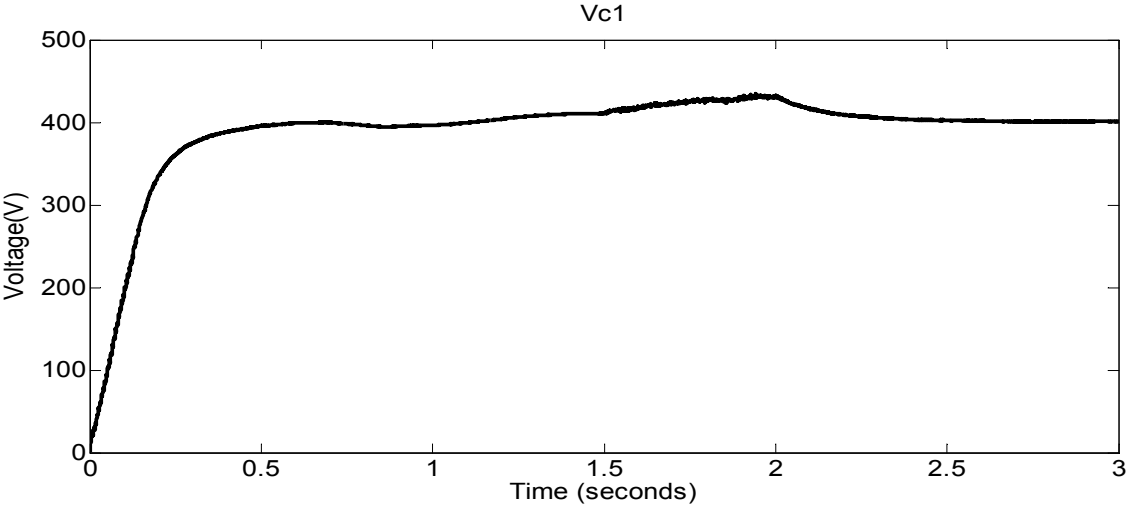

Figure 5.47 Vc1 for ANFIS Feedback Controller under changing conditions

PV voltage and current tracking are shown in Figure 5.48 and Figure 5.49. The current attains the maximum value of 6.05 at 1000 w/m^2 and 4.25A at 700 w/m^2. PV volatge attains maximum value of 170 V volts at 1000 w/m^2 and 163 V at 700 w/m^2. The tracking is fast and smooth.

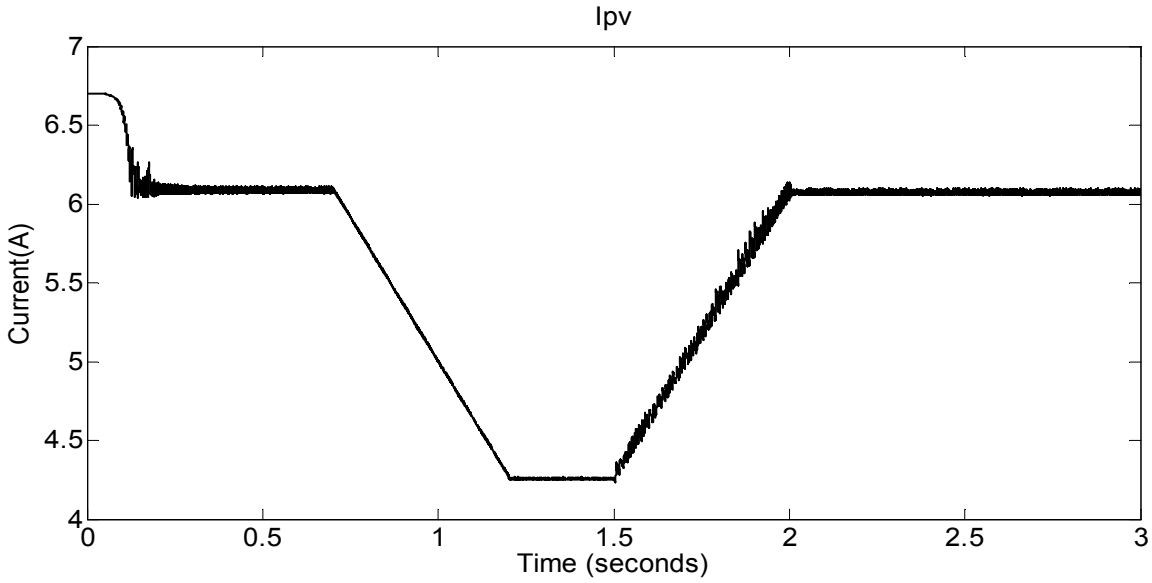

Figure 5.48 Ipv for ANFIS Feedback Controller under changing conditions

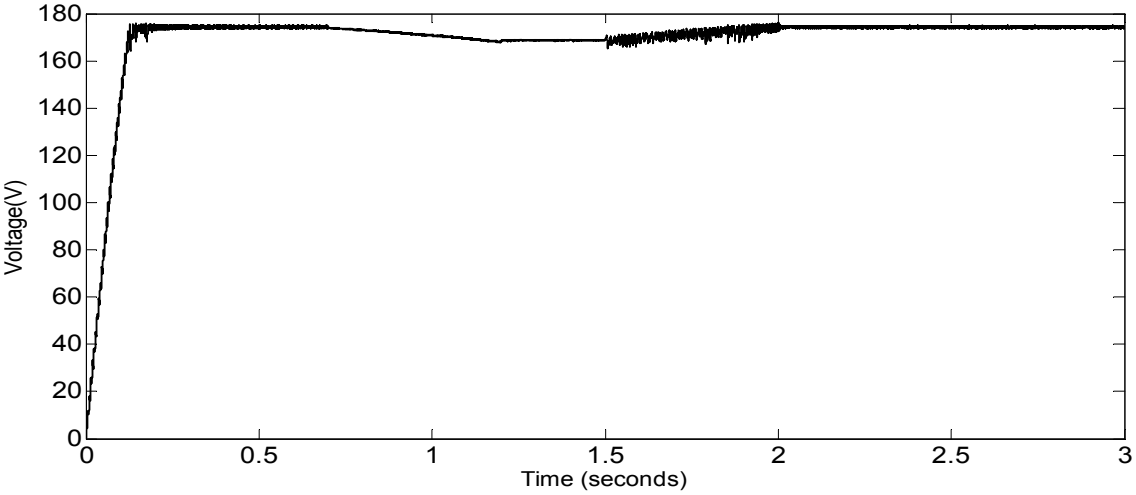

Figure 5.49 Vpv for ANFIS Feedback Controller under changing conditions

5.7 Comparison Between Literature and New PI Controller:

The developed PI controller has been compared with literature work. In [115], a PI based feedback power controller has been developed and simulations have been done in PSIM software. The performance of developed PI controller has been evaluated for tracking the MPPT and dc reference.

The PV open circuit voltage in [115] is 425 V, short-circuit current is 7.9 ampere. The maximum power point voltage and current are 355V and 7.3 A respectively at 1000 w/m^2 and 25^o C. The irradiation is changed to 1300 w/m^2 at 0.4 seconds. At 0.7 seconds, irradiation is returned to 1000 w/m^2.

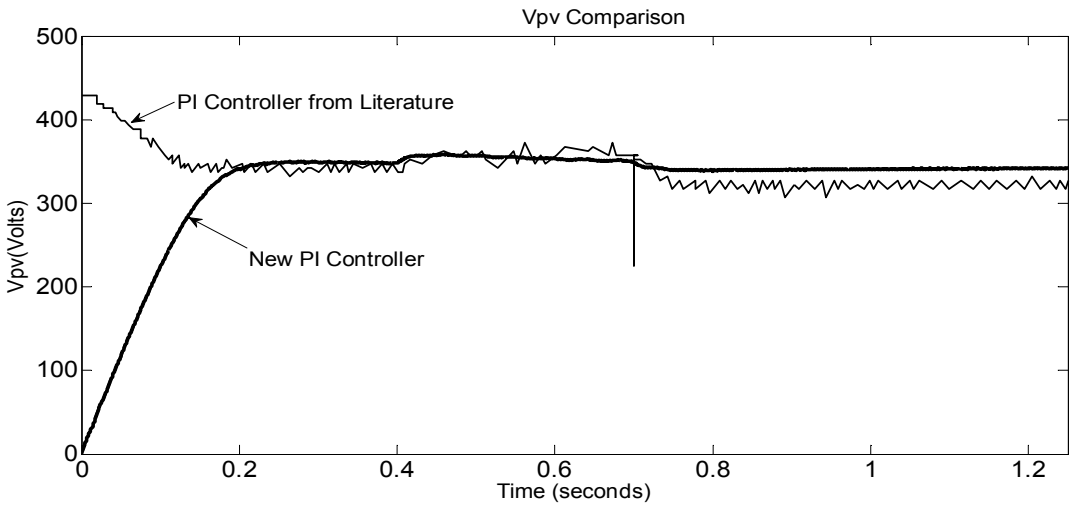

Figure 5.50 Vpv Comparison

The maximum power point voltage is tracked quickly by the proposed PI controller as compared to the controller in literature as shown in Figure 5.50. The maximum voltage is 355 V under normal conditions and it increases to 365V as the irradiation increases and returns back to this value at 0.7 seconds. The maximum power point current is tracked

smoothly and quickly by the proposed PI controller as shown in Figure 5.51. The maximum current value is 7.3 A and increases to 9.5 A as the irradiation increases to 1300 w/m^2 as reduces to 7.3 A as the irradiation decreases to 1000 w/m^2 at 0.7 seconds.

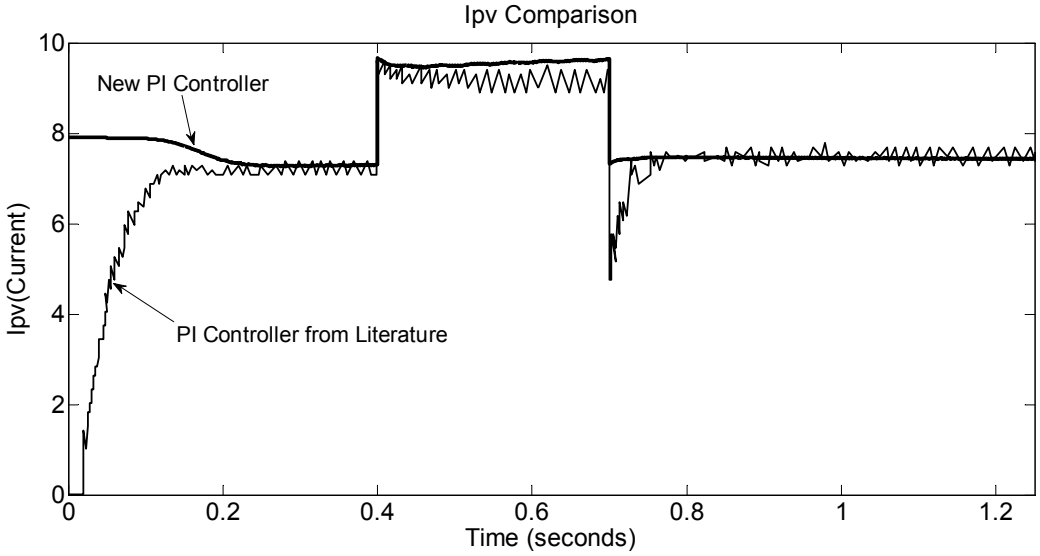

Figure 5.51 Ipv Comparison

Figure 5.52 shows the comparison for dc reference tracking by the two controllers. Proposed PI controller accurately and smoothly tracks the dc reference of 400 V. As the irradiation increases, the dc reference is regulated to 400V under the changing conditions. The proposed controller is more robust as compared to the controller in literature under changing conditions. The output power comparison for two controllers is shown in Figure 5.53. The maximum power is 2500 watts under standard conditions and increases to 3200 watts under increased irradiation situation. The proposed controller shows fast and robust tracking of maximum power under changing conditions as compared to the controller in literature.

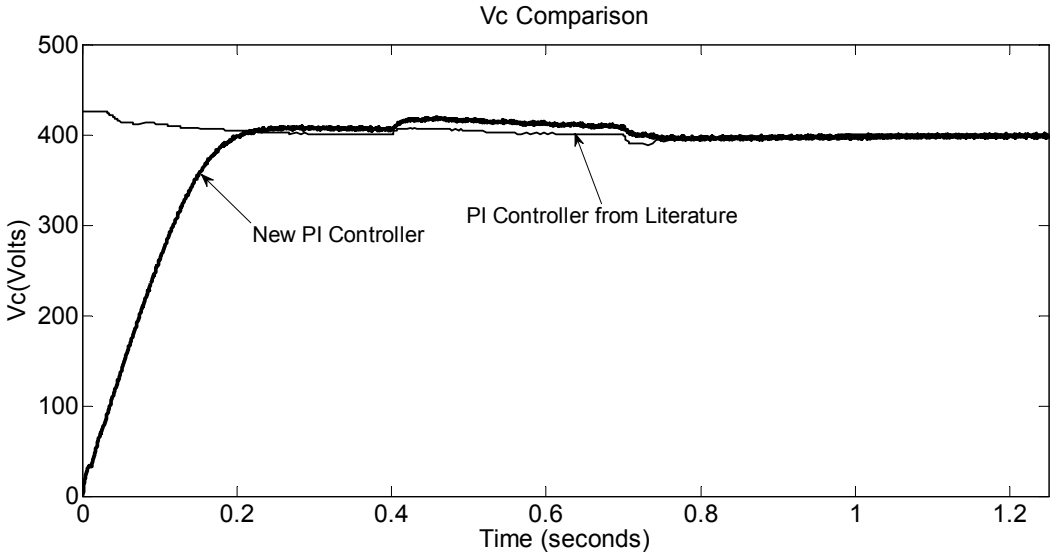

Figure 5.52 Vc Comparison

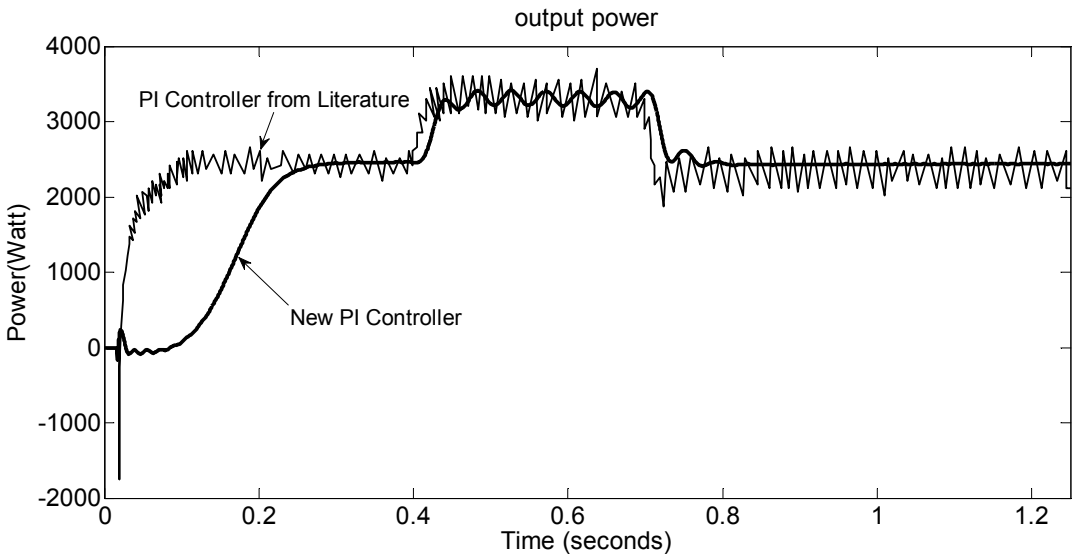

Figure 5.53 Output power Comparison

So, the overall performance of the proposed controller is better than the controller in literature in terms of fast tracking, accuracy and robustness. Under changing environmental conditions, the proposed controller shows efficient and reliable response.

5.8 Comparison Between ANFIS and PI Controllers:

5.8.1 Case I: Comparison for Constant Irradiations:

For constant irradiance and temperature case, the ANFIS Controller is fast and accurate in tracking the dc reference. Also, ANFIS controllers are fast in tracking the maximum power point with accuracy. The comparison of the two types of controllers is shown in Figure 5.51- Figure 5.54

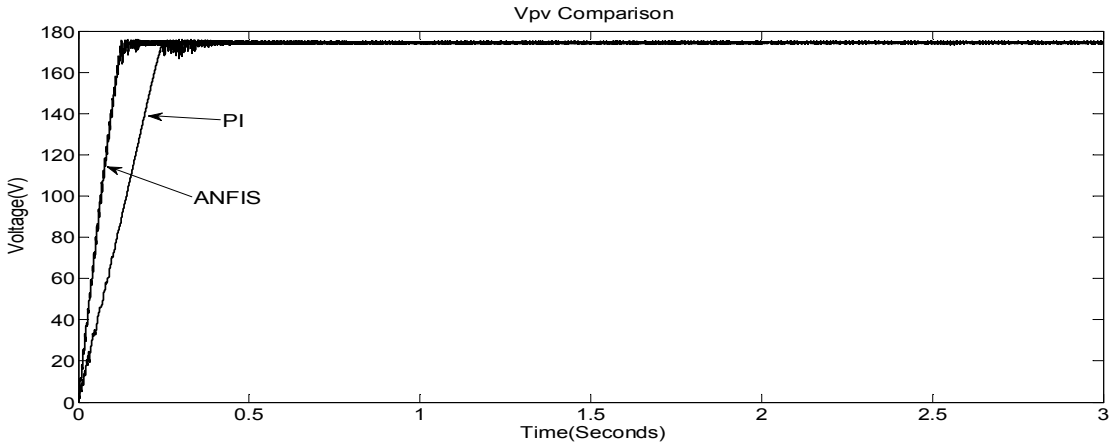

Figure 5.54 Comparison of Vpv for ANFIS and PI-based Alpha-beta controllers

Comparison between the two controllers for PV voltage tracking under constant conditions is shown in Figure 5.50. The voltage value corresponding to maximum power point is 170 volts. In case of alpha-beta controllers, it is reached in 0.3 seconds while in case of ANFIS controller, it is reached in 0.1 seconds with less ripples in a reliable way.

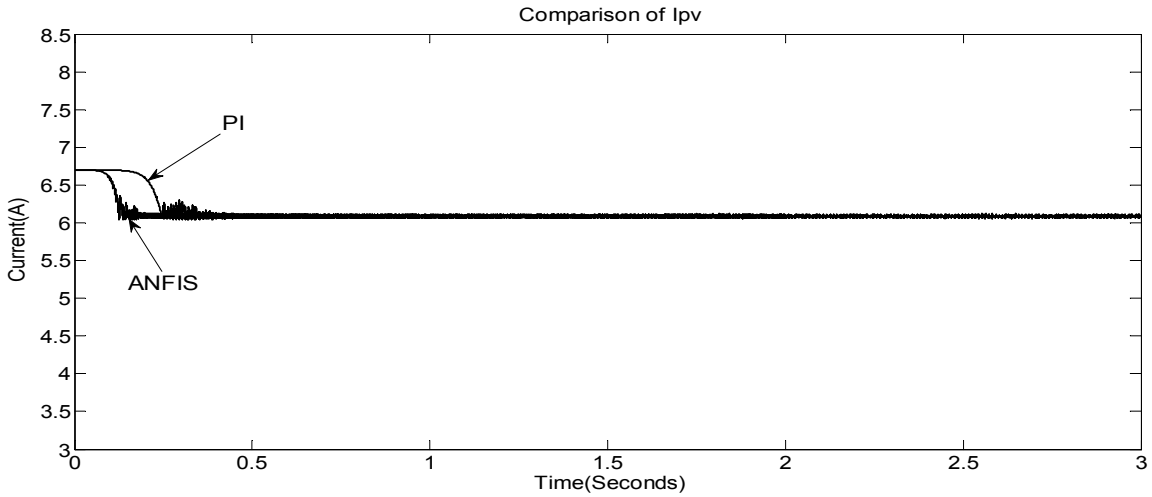

Figure 5.55 Comparison of Ipv for ANFIS and PI-based Alpha-beta controllers

The PV current tracking comparison by the two types of controllers under constant ambient conditions is shown in Figure 5.51. In case of alpha-beta controller, the current value of 6.05A is reached at 0.3 seconds while in case of ANFIS based controller, the current value is attained in 0.1 seconds. This shows the speed and robustness of the ANFIS based controller.

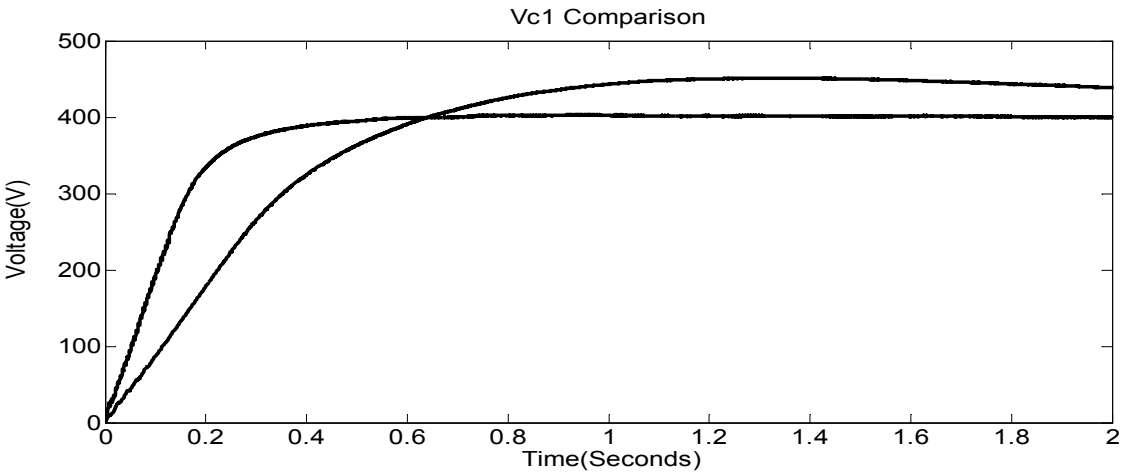

Figure 5.56 Comparison of Vc1 for ANFIS and PI-based Alpha-beta controllers

The PV power tracking comparison by the two types of controllers under constant ambient conditions is shown in Figure 5.51. In case of alpha-beta controller, the power value of 1000 watts is reached at 1.2 seconds while in case of ANFIS based controller, the power value is attained in 0.22 seconds. This shows the speed and robustness of the ANFIS based controller.

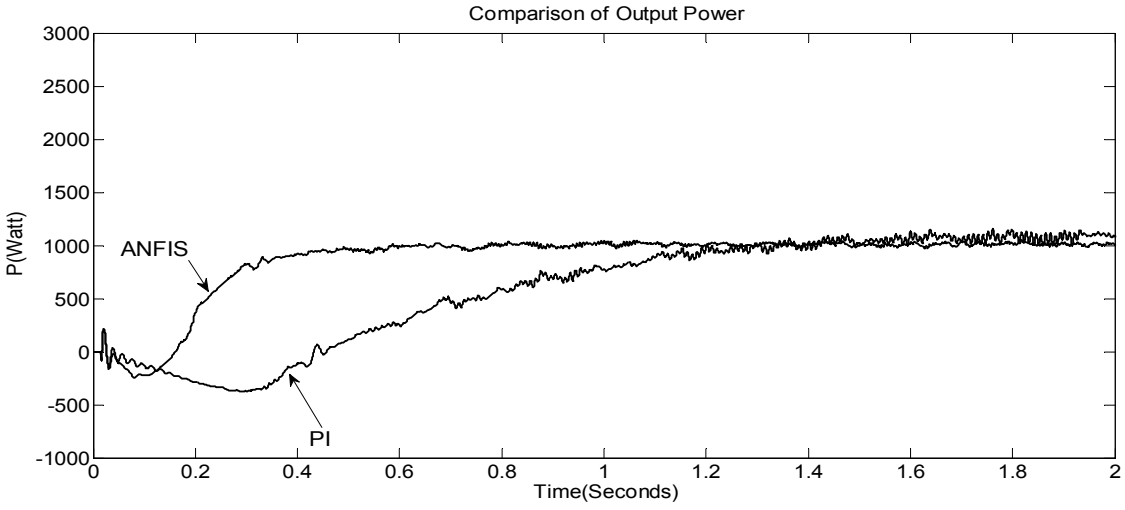

Figure 5.57 Comparison of Output Power for ANFIS and PI-based Alpha-beta controllers

5.8.2 Case II: Comparison for Changing Conditions

For changing conditions, the comparison of ANFIS-based controllers with PI controllers is shown in Figure 5.55 – Figure 5.58. The ANFIS-based controllers are reliable and robust as compared to conventional PI controllers and provides a fast and effective control under various changing conditions. The feasibility and superiority of ANFIS-based controllers is evident form the comparison results.

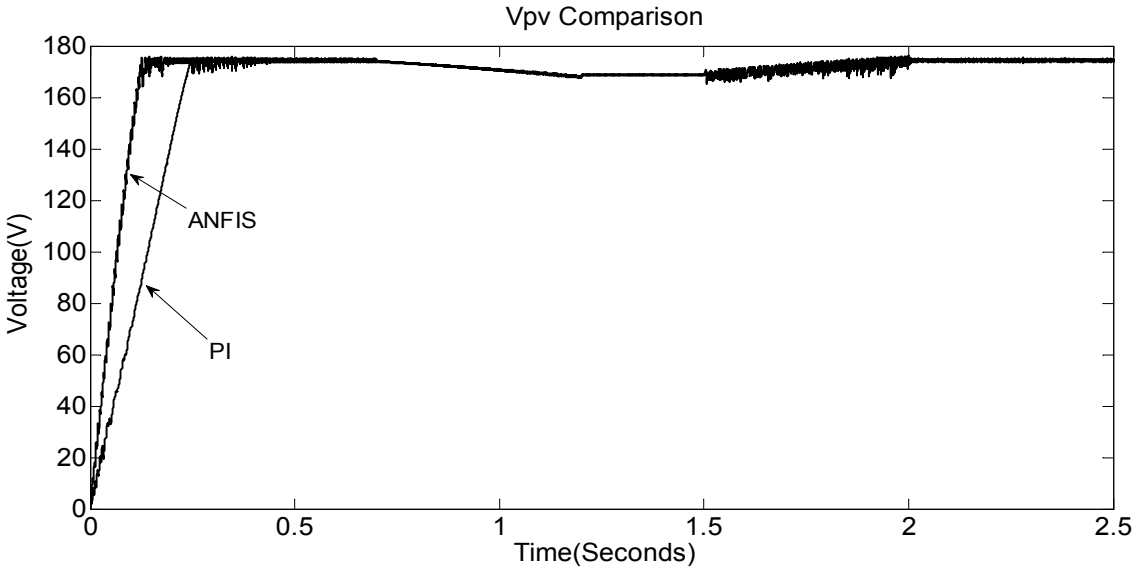

Figure 5.58 Comparison of V_{pv} under changing Conditions

Figure 5.54 shows the comparison of PV voltage tracking under changing conditions. When the irradiation is 100 watts initially, alpha beta controller tracks the PV voltage value corresponding to maximum power point in 0.3 seconds while ANFIS based controller tracks it in 0.1 seconds. During the decrease in irradiation to 700 w/m^2, the ANFIS based controller tracks new PV voltage corresponding to new maximum power point very fast which is 163 V. during changing conditions ANFIS based controller shows more robustness and reliability as compared to alpha beta controllers.

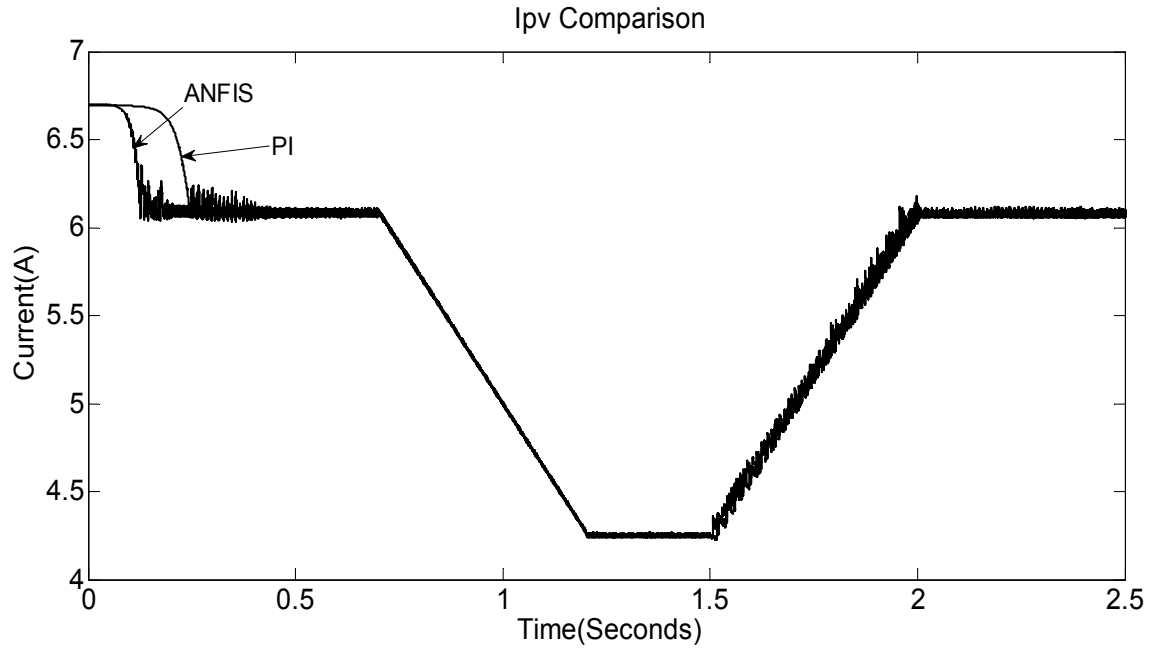

Figure 5.59 Comparison of Ipv under changing conditions

PV current tracking corresponding to changing irraditions is hown in Figure 5.55. the PI controllers track the maximum current in 0.3 seconds and ANFIS based controller tracks it in 0.1 seconds. During decrease of irradiations, ANFIS based controller tracks new maximum point very swiftly as compared to PI controllers which shows the superiority of ANFIS controller in changing ambient conditions.

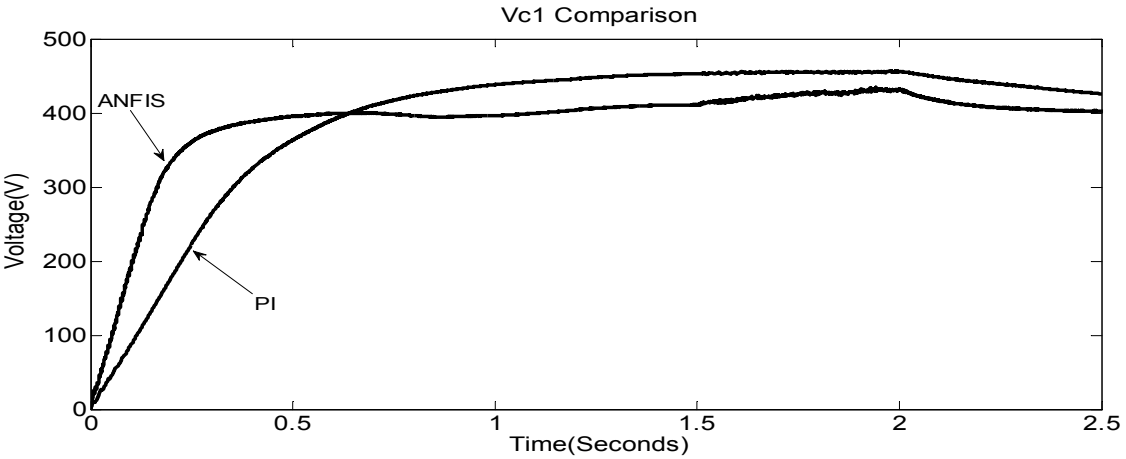

Figure 5.60 Comparison of Vc1 under changing conditions

During changing conditions, the Z-source capacitor voltage is tracked to its reference value and is stabilized at its reference value by the two controllers. But ANFIS controller is more robust and accurate in tracking and stabilizing the dc voltage to its reference.

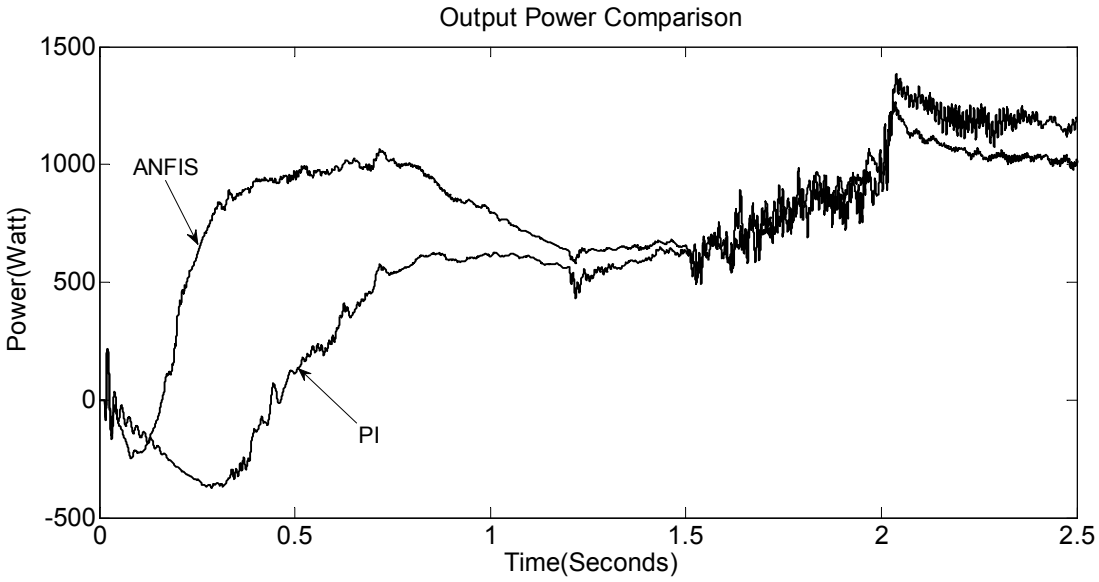

Figure 5.61 Comparison of Pout under changing conditions

Output Power tracked during changing condition by the two types of controllers is shown in Figure 5.57. ANFIS controller tracks the power quickly to 1000 watts when irradiation was 1000 w/m^2. When irradiation decreased to 700 w/m^2, the output power is swiftly tracked to its maximum value of 700 watts. At 2 seconds, the irradiation value reaches 1000 w/m^2 and the output power is successfully taken to the level of 1000 watts and efficiently delivered to the load. The alpha-beta controllers on other hand have slow tracking and less accuracy as compared to the ANFIS based controller.

5.9 Comparison Between RSCAD and Simulink Results

The results from RSCAD/dSPACE real time simulation were compared with the results from Matlab/Simulink environment. Figure 5.62 shows the comparison for I_{pv} for the two setups. The maximum value of current is 6.1 A. The maximum current value is tracked quickly and reliably by the controller in dSPACE1103. The ANFIS controller in Matlab/Simulink environment also tracks the maximum value of current and attains steady-state values. The real time results are in accordance with Simulink results.

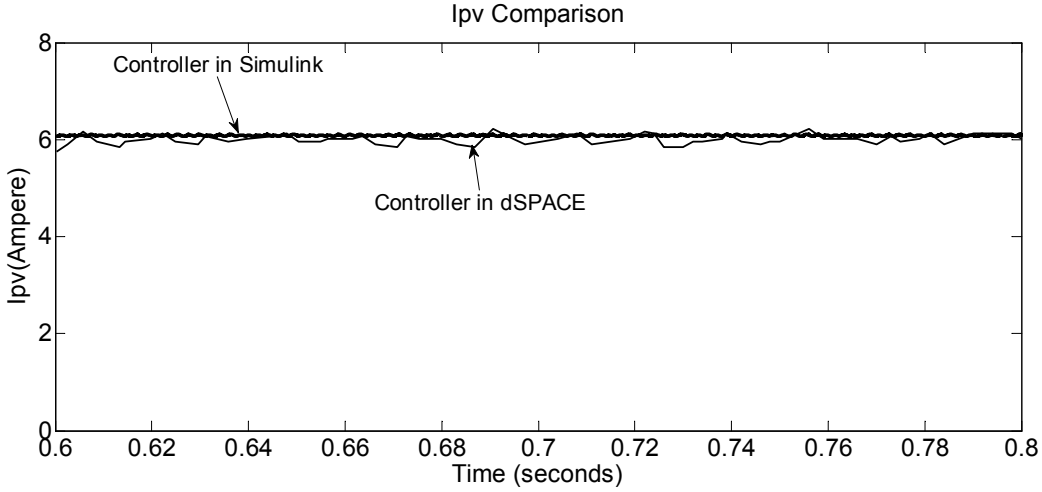

Figure 5.62 Ipv Comparison Between RSCAD and Simulink results

Figure 5.63 shows the comparison for V_{pv} for the two setups. The maximum value of the PV voltage is 174 V. The maximum value of voltage is tracked by the controller in dSPACE1103 efficiently and quickly. The controller in Simulink tracks the maximum PV voltage of 174 V accurately. The real time results matches the Simulink results.

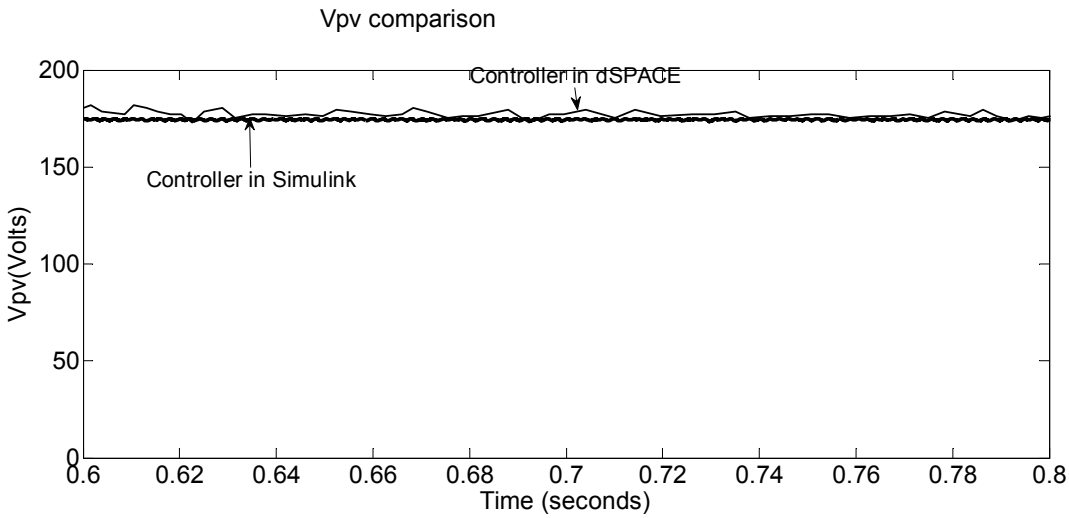

Figure 5.63 Vpv Comparison Between RSCAD and Simulink Results

The maximum power value is 1000 watts. The controller in dSPACE1103 tracks the maximum power reliably corresponding to maximum power point. The maximum power value tracked by the controller in Simulink is slightly lower than that of real time result but it is still in accordance with the real time results as shown in Figure 5.64.

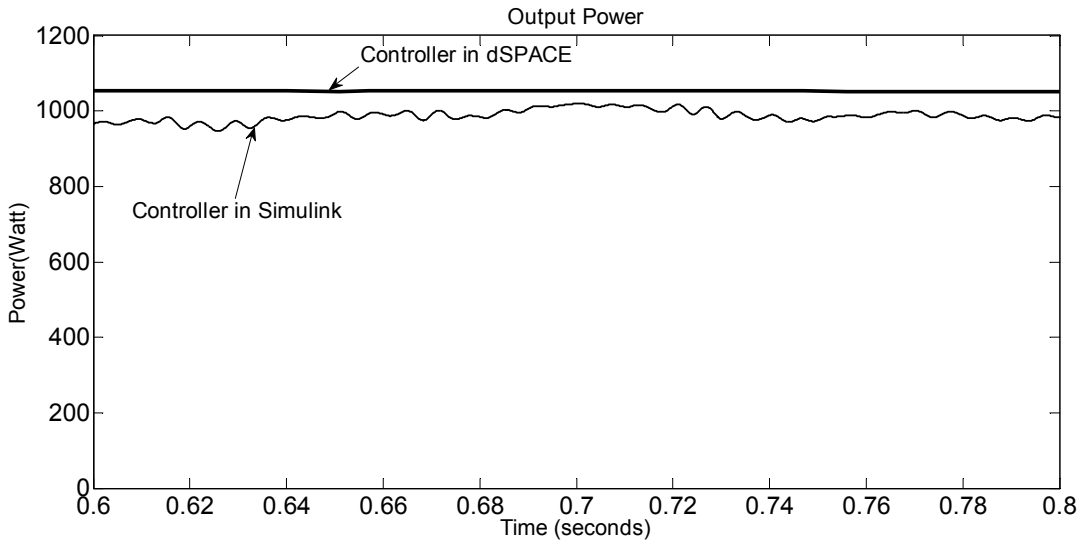

Figure 5.64 Output Power Comparison

The real results are very useful in validating the working of controller in real time conditions. The comparison of the two setups shows the effectiveness, reliability and robustness of the ANFIS controller developed in this research work.

5.10 Discussions

Different feedback Controllers have been implemented for Z-source connected to PV systems in this chapter and their performance under different conditions have been implemented. Finally the performance, speed, reliability and robustness of alpha-beta conversion based PI controllers and ANFIS controllers have been compared under constant and varying conditions which shows that ANFIS controllers are very robust, fast and reliable as compared to PI controllers with design given in this research work. Thus, ANFIS controllers have been successfully used for complex power conversion system like PV system connected to the grid. The use of ANFIS controllers can be extended to complex power conversion systems and cascaded

multi-level converter systems where high level of robustness, reliability and efficiency is required, thus making ANFIS controllers presented in this study as future controllers

CHAPTER 6

EXPERIMENTAL IMPLEMENTATION OF Z-SOURCE INVERTER

In this chapter grid connected Z-source inverter has been implemented in Real Time Digital Simulator (RTDS) and its controller has been employed in dSPACE1103 in real-time loop-in control. Performance of ANFIS controller has been evaluated using this real time environment. A prototype of Z-source inverter, LC filter, connected to chromo solar simulator has also been developed separately for testing with a dc source, a PV simulator for dynamic MPPT test and partial shadow test.

6.1 Experimental Implementation in RTDS and dSPACE 1103

The system diagram implemented in RSCAD software for RTDS is shown in Figure 6.1-Figure 6.3. Controller in dSPACE 1103 has also been shown in Figure 6.4 and Figure 6.5. the input PV maximum voltage is 215 volts and it is boost upto 320 volts. The ANFIS controllers were implemented in dSPACE 1103. This controller takes output current, out voltage, Z-source capacitor voltage, V_{pv}, I_{pv} as control variables and generate five control signals for PWM modulation, i.e., three modulation signals and 2 shoot-through envelops. The results show the robustness and reliability of ANFIS controllers in real-time environment. The output voltage level are 190 volts rms and output current for load is 10 A rms. Carrier frequency was set at 6500 Hz.

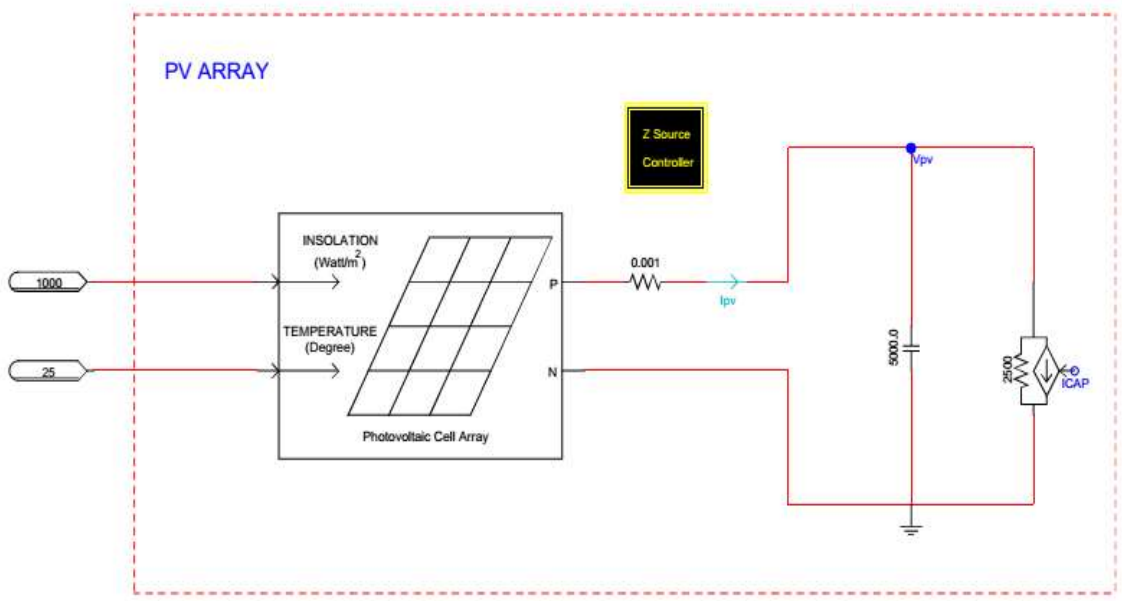

Figure 6.1 Grid-connected PV system in RSCAD

The PV module in RSCAD is shown in Figure 6.1. A Norton equivalent of small step component is used to inter connect small and large time step components. The temperature and irradiation are 25^{o}C and 1000 w/m^{2}. The PV maximum power voltage and current values can be set to desired value by changing the number of modules or arrays.

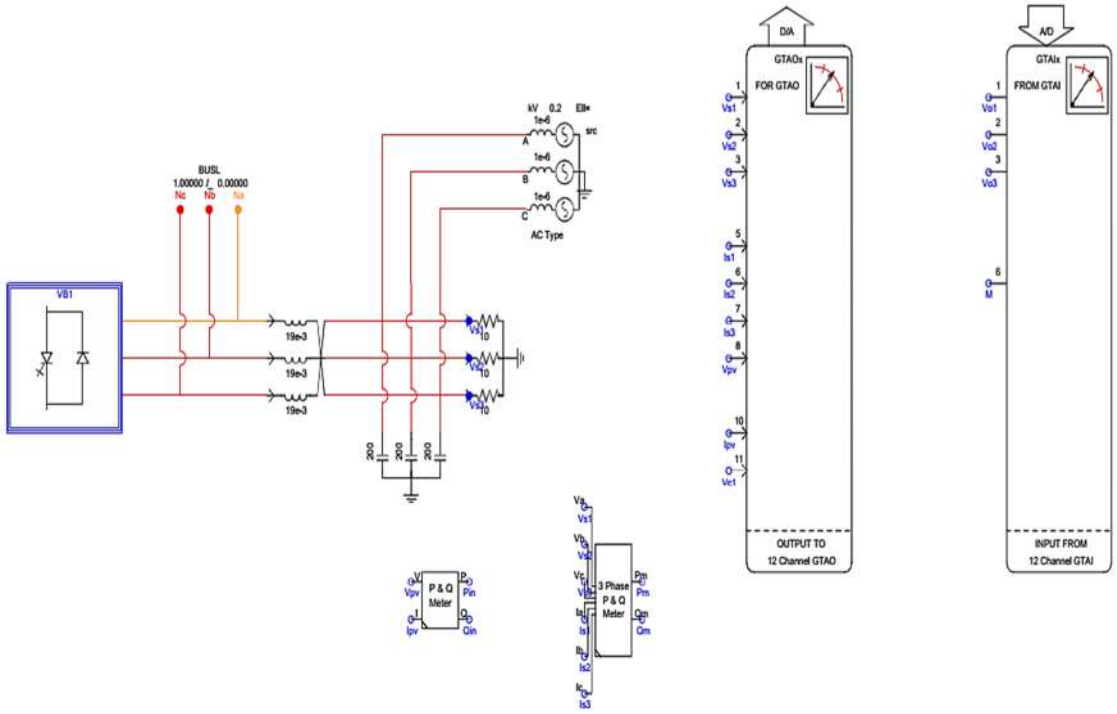

Figure 6.2 Inverter with Z-source network

The Z-source inverter along with grid connected load is shown in Figure 6.2. The input and output cards are also shown. The output current and voltages, PV voltage and current and dc capacitor voltage is sent to dSPACE1103 for controller action through output card. Three modulation control signal and shoot-through duty cycle is received through input card from dSPACE1103.

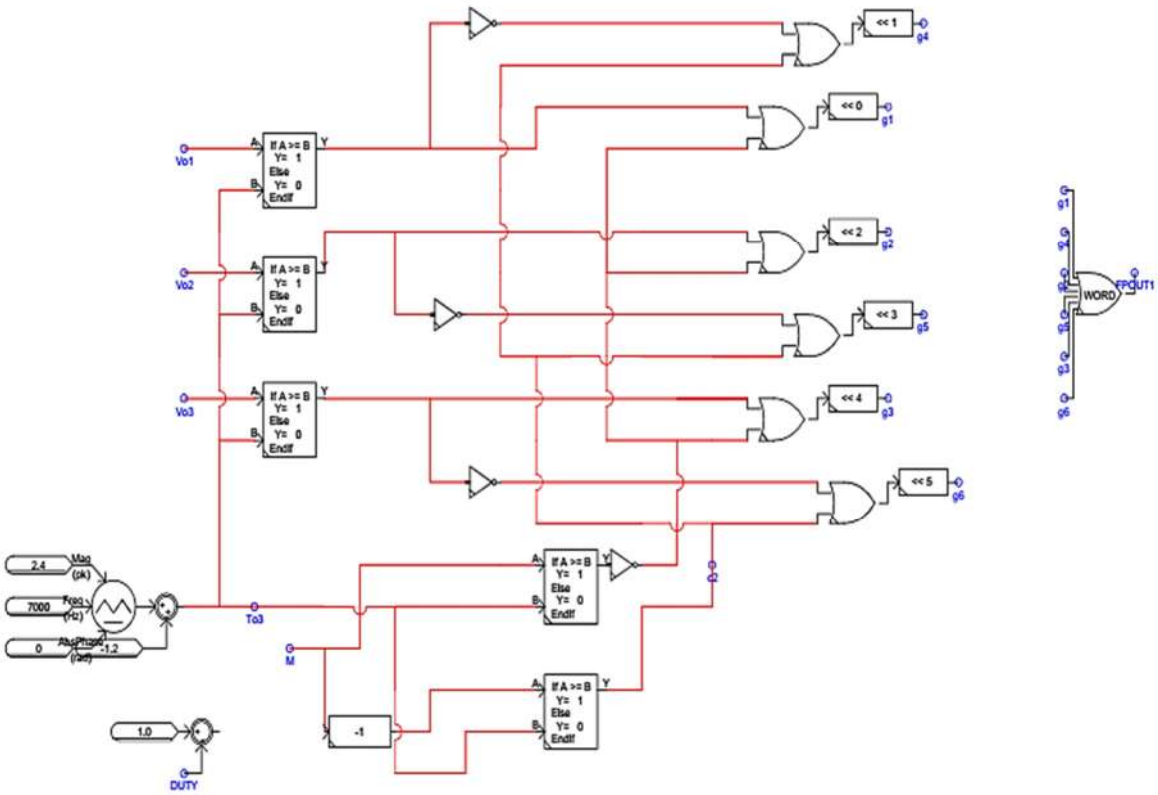

Figure 6.3 Pulse generator for Z-source

The switching pulse generator for z-source inverter is shown in Figure 6.3. The carrier frequency is 7000 Hz. The carrier signal is compared with three modulating signals and shoot-through duty cycle generated by dSPACE1103 to generate switching signals for IGBTs. The output pulses are multiplexed into a Boolean word and sent to the inverter for switching action.

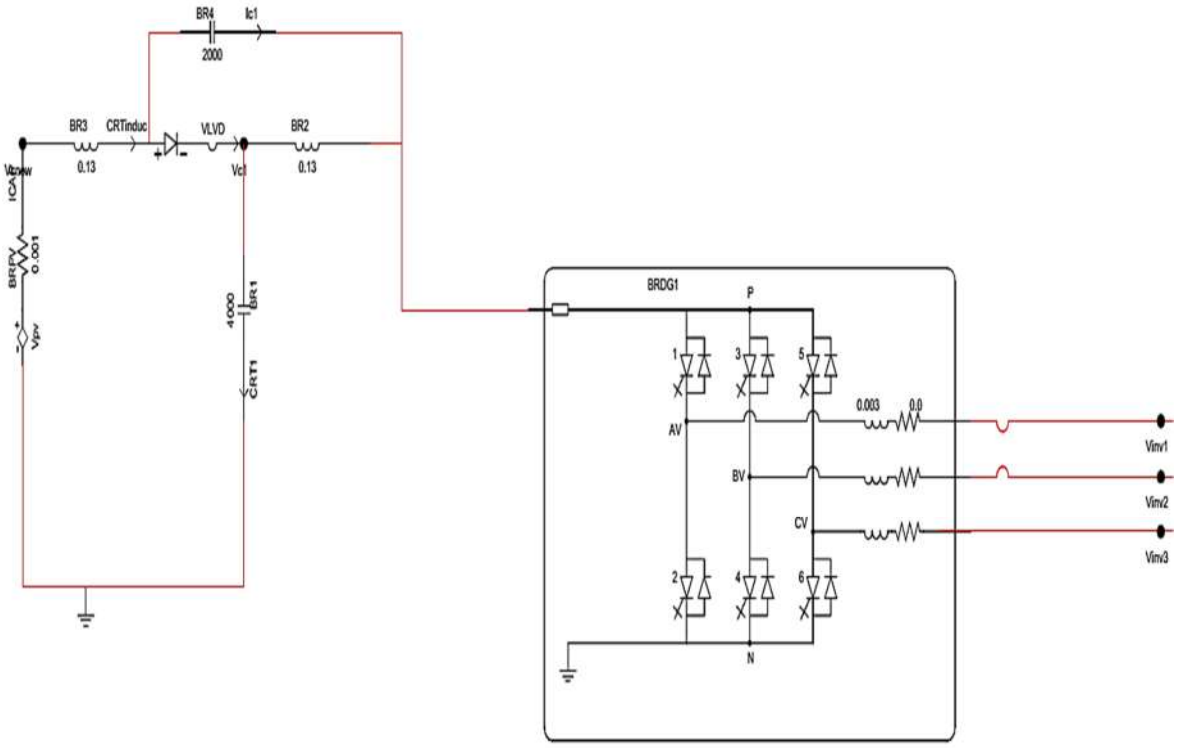

Figure 6.4 Z-source Inverter in dSPACE 1103

Z-source inverter built in small time step component is shown in Figure 6.4. The current and voltage obtained from Norton equivalent is fed to the input of Z-source inverter and output of Z-source inverter is fed to low pass LC filter interconnected through unity ratio interconnection transformer between small time and large time step components in RSCAD. The output of inverter is ac signal with many harmonics that requires LC low pass filter to obtain 60 Hz pure signal. A detailed diagram of ANFIS controller in dSPACE1103 is shown in Figure 6.5. Three ANFIS controllers are shown in the diagram. The dc reference ANFIS controller is designed using rule table and other two are trained using training data.

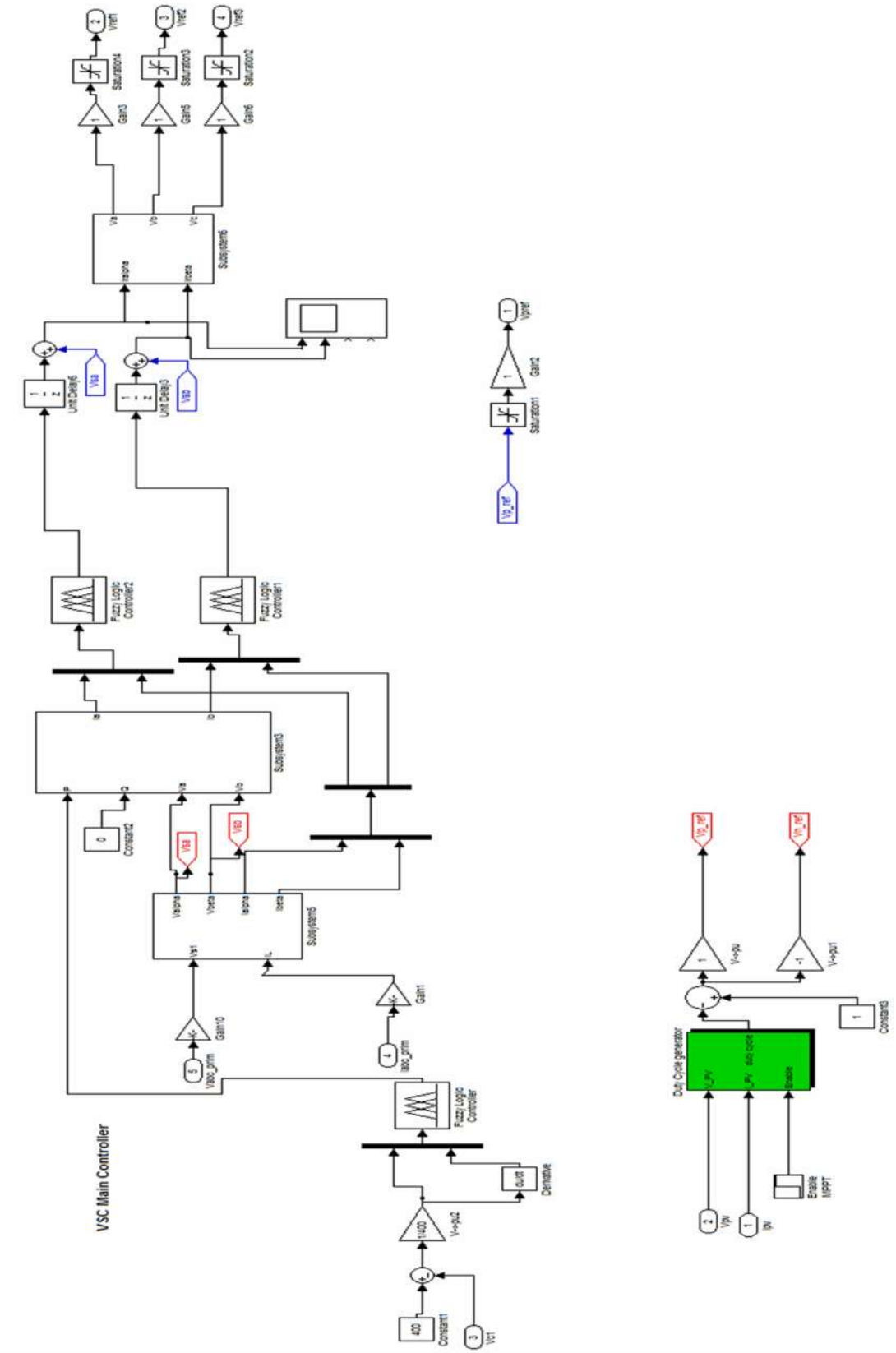

Figure 6.5 Detail view of ANFIS Feedback Controller

The results obtained from RSCAD are shown below:

Figure 6.6 shows the maximum value of voltage obtained is 215 V and it is stabilized and controlled by ANFIS controller. The PV voltage is boosted by PWM action for Z-source inverter to raise it to 320 Volts to reach the dc reference voltage as shown in figure 6.7. The dc reference voltage is held constant by the NAFIS controller which shows the effectiveness and reliability of the ANFIS controller in dc level tracking.

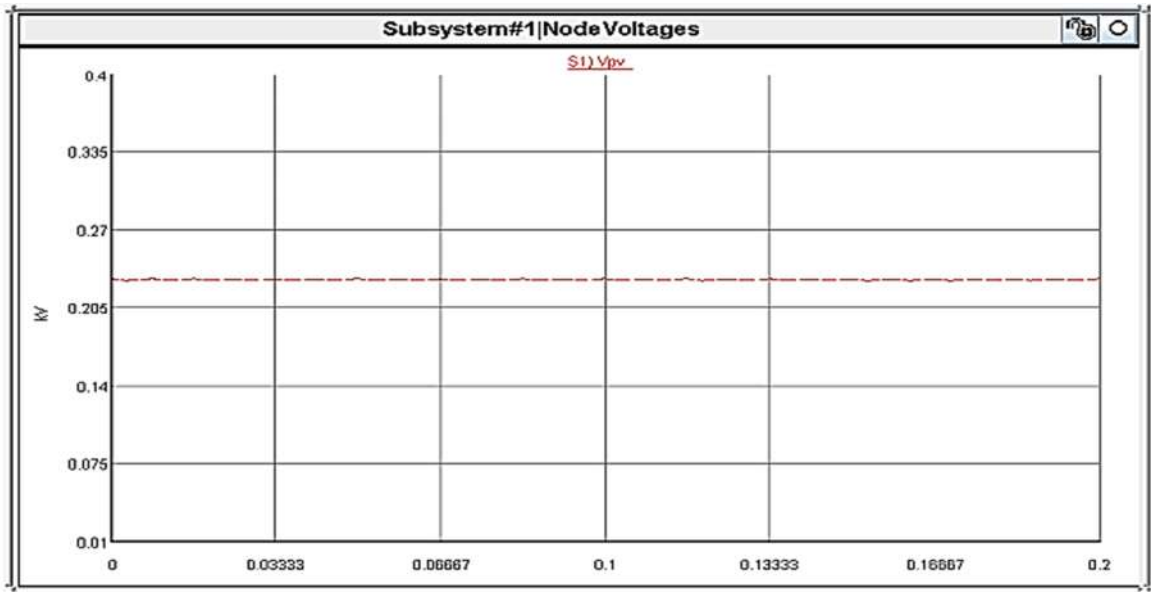

Figure 6.6 V_{pv} from RSCAD

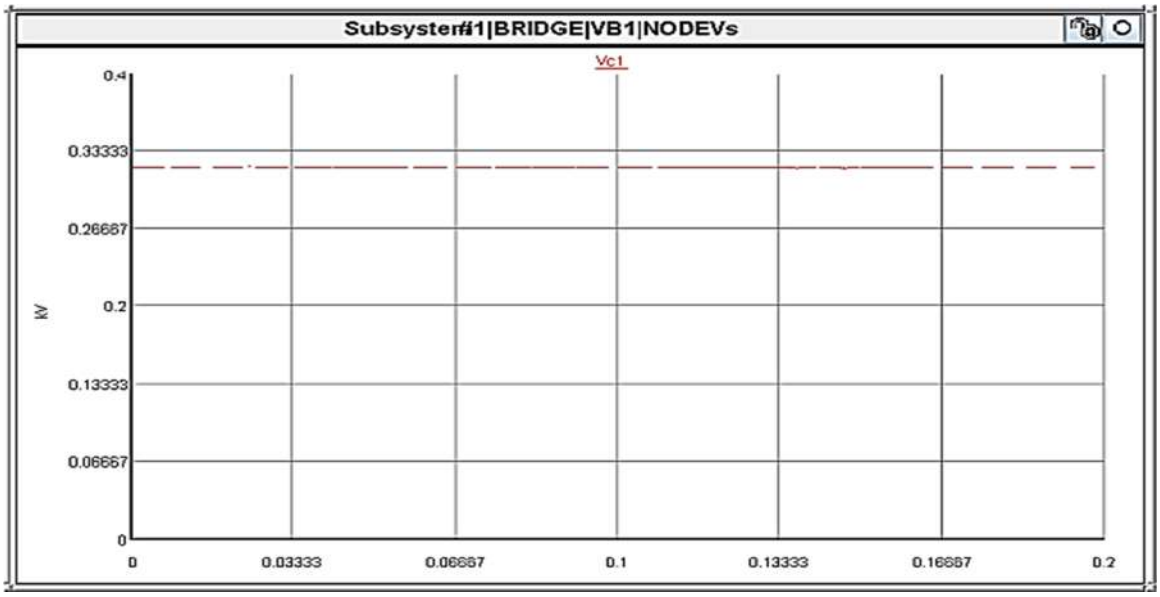

Figure 6.7 V_{c1} from RSCAD

The output voltage of inverter is shown in Figure 6.8. The PWM results in proper switching of IGBTS resulting in ac signal with many harmonics. The inverter changes the input dc voltage to output ac signal by switching at the frequency of carrier signal.

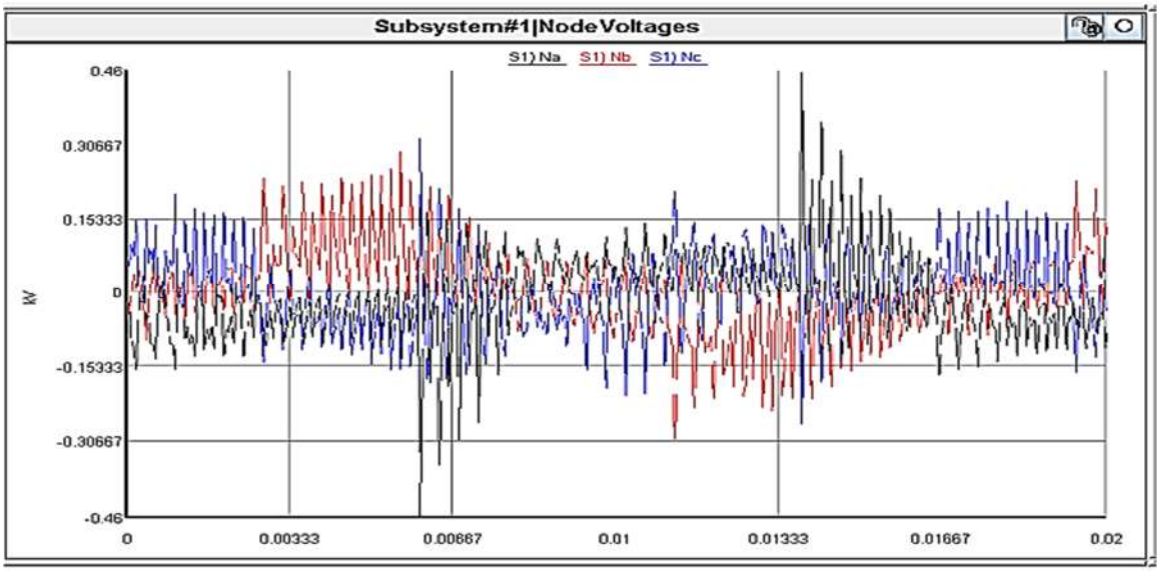

Figure 6.8 Inverter voltage from RSCAD

The output current of inverter is shown in Figure 6.9 which contains higher order harmonics which is filtered by low pass LC filter to obtain perfect sinusoidal wave at 60 Hz. The peak value of inverter current reaches 20A.

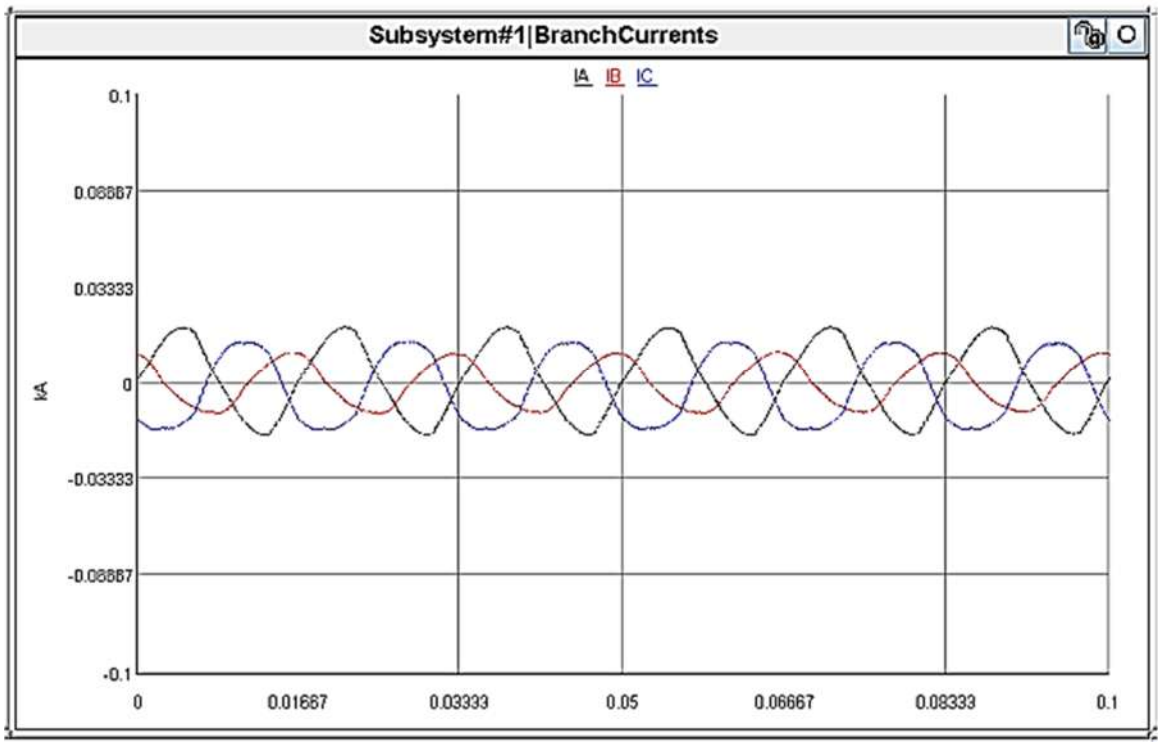

Figure 6.9 Inverter current from RSCAD

Figure 6.10 shows the output voltage after filter which is perfectly sinusoidal and is delivered to the grid connected load. The output voltage shows that the performance of NAFIS current controllers is reliable and efficient for grid-connected PV systems and proper training results in robust ANFIS controllers that can control the outputs of complex power conversion systems.

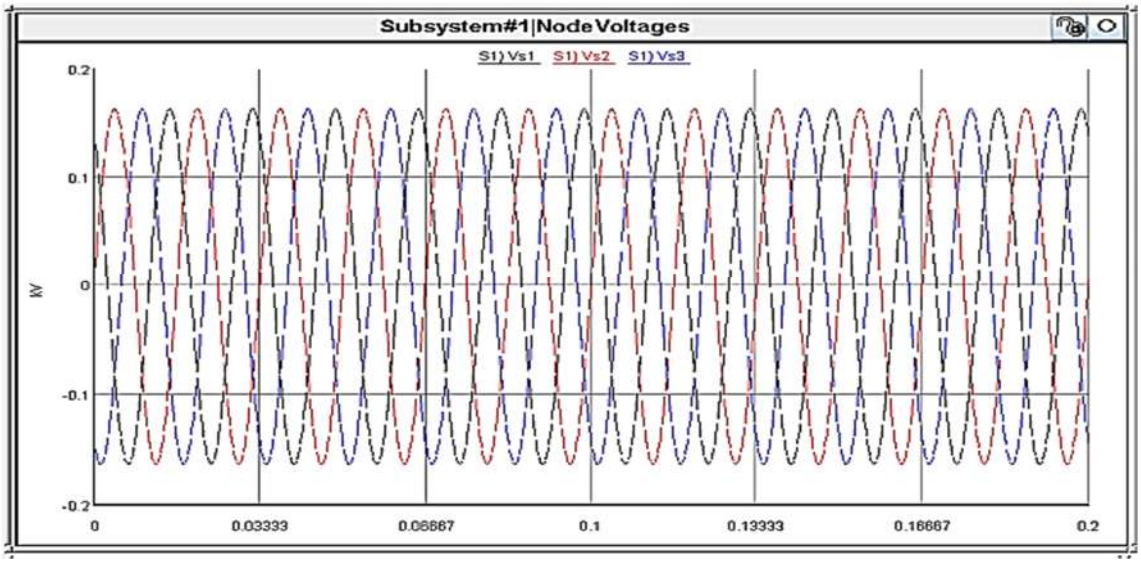

Figure 6.10 output voltage from RSCAD

The output current with a peak value of 15 A is shown in Figure 6.11. The output current is obtained after filtered sharply at 60 Hz cutoff frequency. The output current is drawn by the load. The output current shows that the ANFIS controller is robust in controlling the output quantities and keeping them in steady state values.

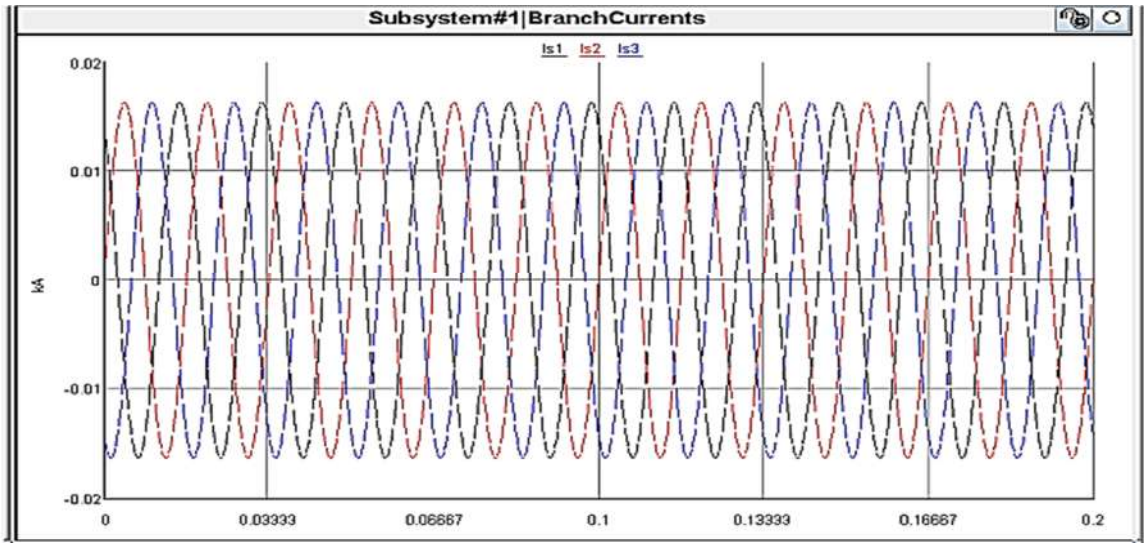

Figure 6.11 Output current from RSCAD

Figure 6.12 shows the control modulating signals generated by ANFIS controller and sent to RTDS for switching of Z-source inverter. The three modulating signals are sinusoidal in nature with peak value of 0.4. These three signals are compared with a triangular carrier signal of 7000 Hz frequency to generate pulses for IGBTs. These modulating signals are responsible for voltage source switching actions of inverter to convert dc signal to ac.

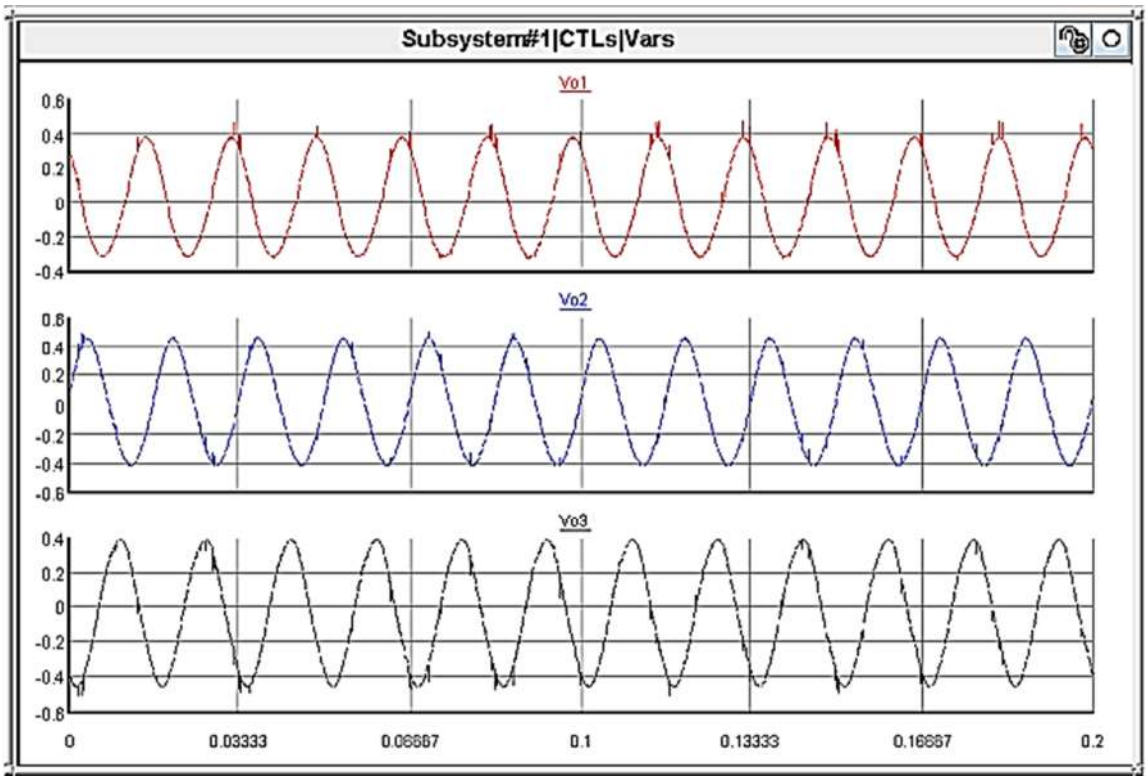

Figure 6.12 Control signals from dSPACE 1103

Figure 6.13 shows the shoot-through duty cycle generated by controller in dSPACE1103 and is sent to RTDS. This shoot-through reference is responsible for boost action of Z-source inverter to take the dc capacitor voltage value up to the required dc reference value. These shoot-through reference acts as envelops in positive and negative direction

to be compared with the carrier signal and generate shoot-through states for Z-source inverter.

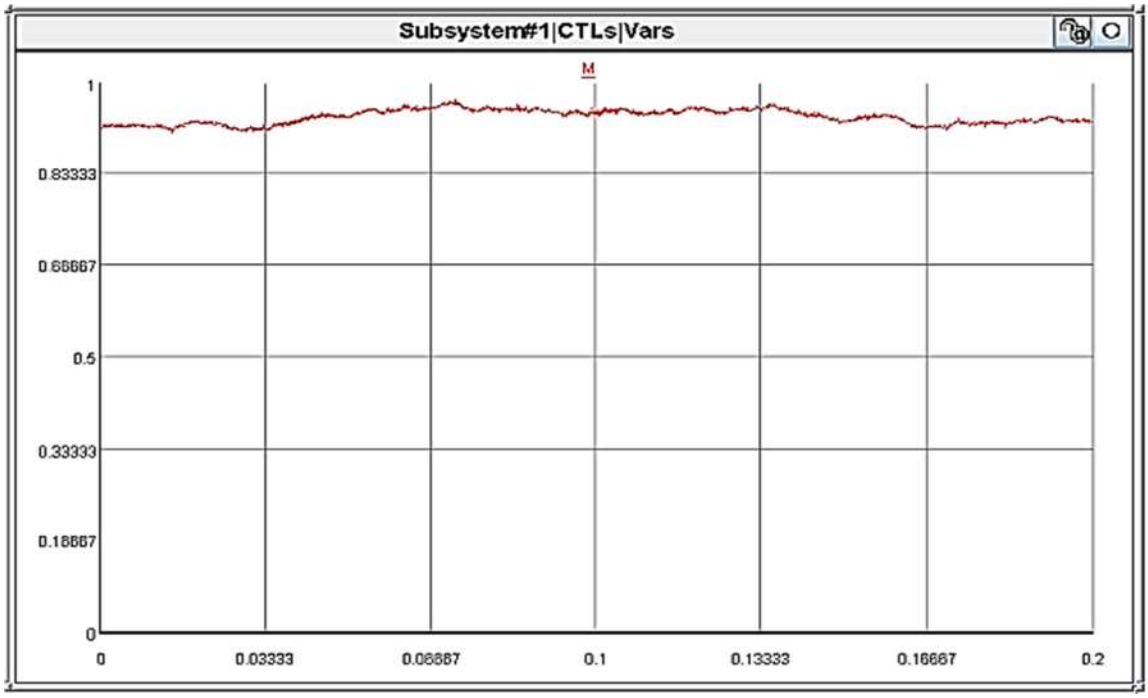

Figure 6.13 Shoot-through duty ratio from dSPACE 1103

The pulses generated by the PWM for Z-source inverter have been shown in Figure 6.14. The pulses shows the shoot-through and non-shoot-through states. During the time when all the switches in one leg or two legs or three legs are turned on, it results in shoot-through states for Z-source inverter. When only one switch is turned on in one leg, it results in non-shoot-through states. At 0.0002 seconds, the IGBTS are in shoot-through states while at 0.00033 the IGBTs are in non-shoot-through states.

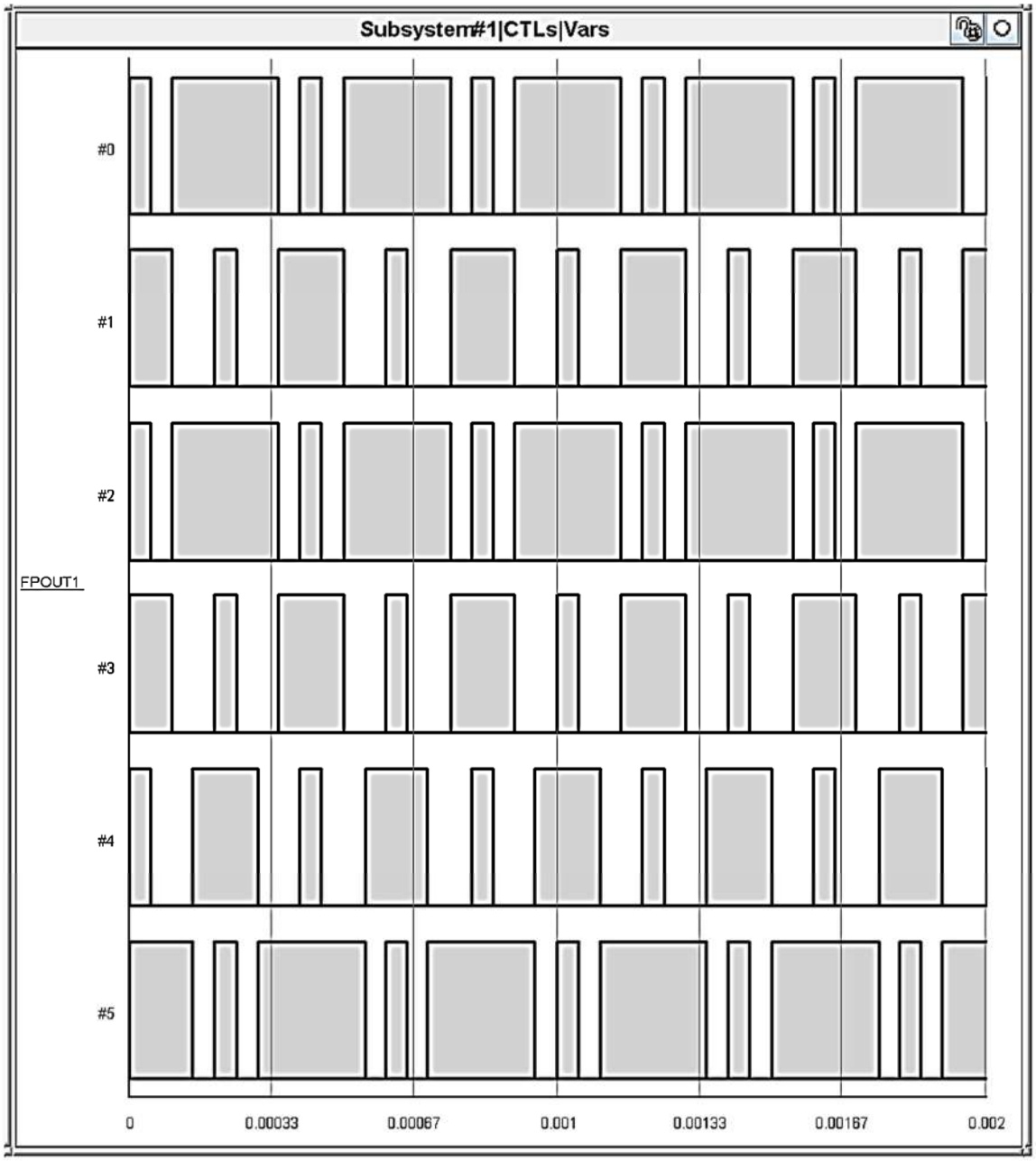

Figure 6.14 Pulses generated by PWM

6.2 Prototype of Z-source Inverter

A prototype of Z-source Inverter was built in laboratory with Z-source inductors equal to 1.3 mH and Z-source capacitors equal to 1000 uF. PV capacitor was selected to be 2200 uF and SEMITEACH – IGBT inverter was used in the prototype. For LC filter , inductor was 10mH per phase and capacitor was 200 uF AC per phase. Resistive load was used. The following test cases were carried out using the Z-source prototype with Pi controller running in dSPACE 1103 interfaced with Simulink environment.

6.2.1 Zsource with dc source

The simulation results of Z-source inverter with a dc-source in stand-alone mode is shown in Figure 6. 15 – 6.18. The carrier frequency was set at 6000Hz and PI controller based on dq conversion was used. The input dc voltage was 100 V and output rms voltage was 75 volts.

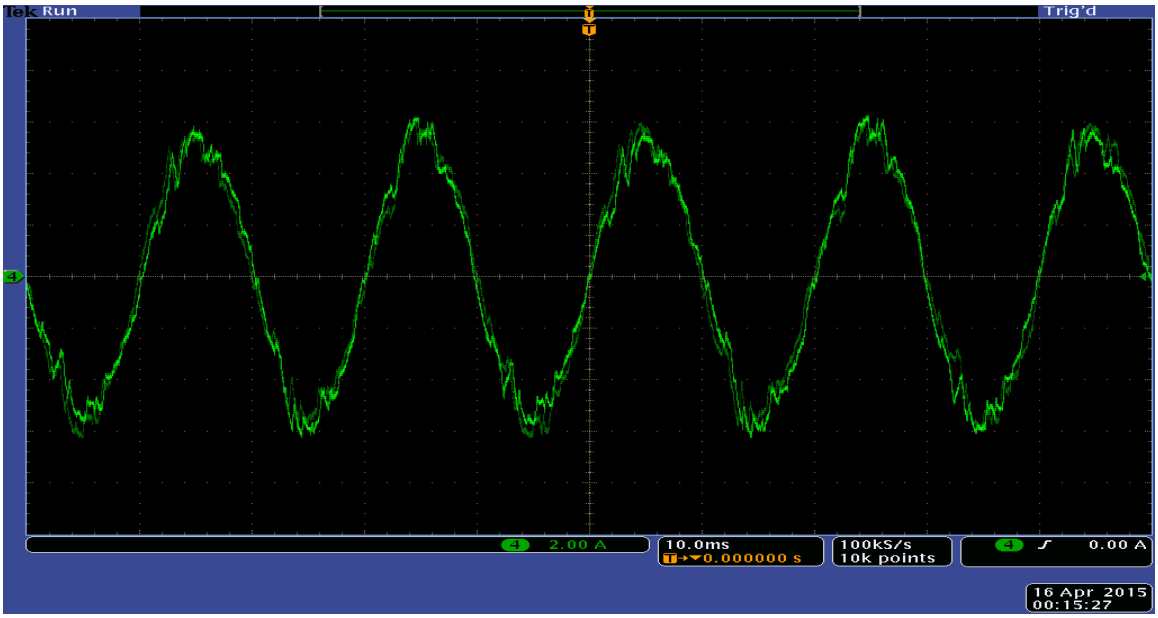

Figure 6.15 Inverter output current

The output current of Z-source inverter is shown in Figure 6.15 which is sinusoidal in nature and has many harmonics. These harmonics are removed by the LC filter prototype and gives a perfectly sinusoidal waveform as shown in Figure 6.15.

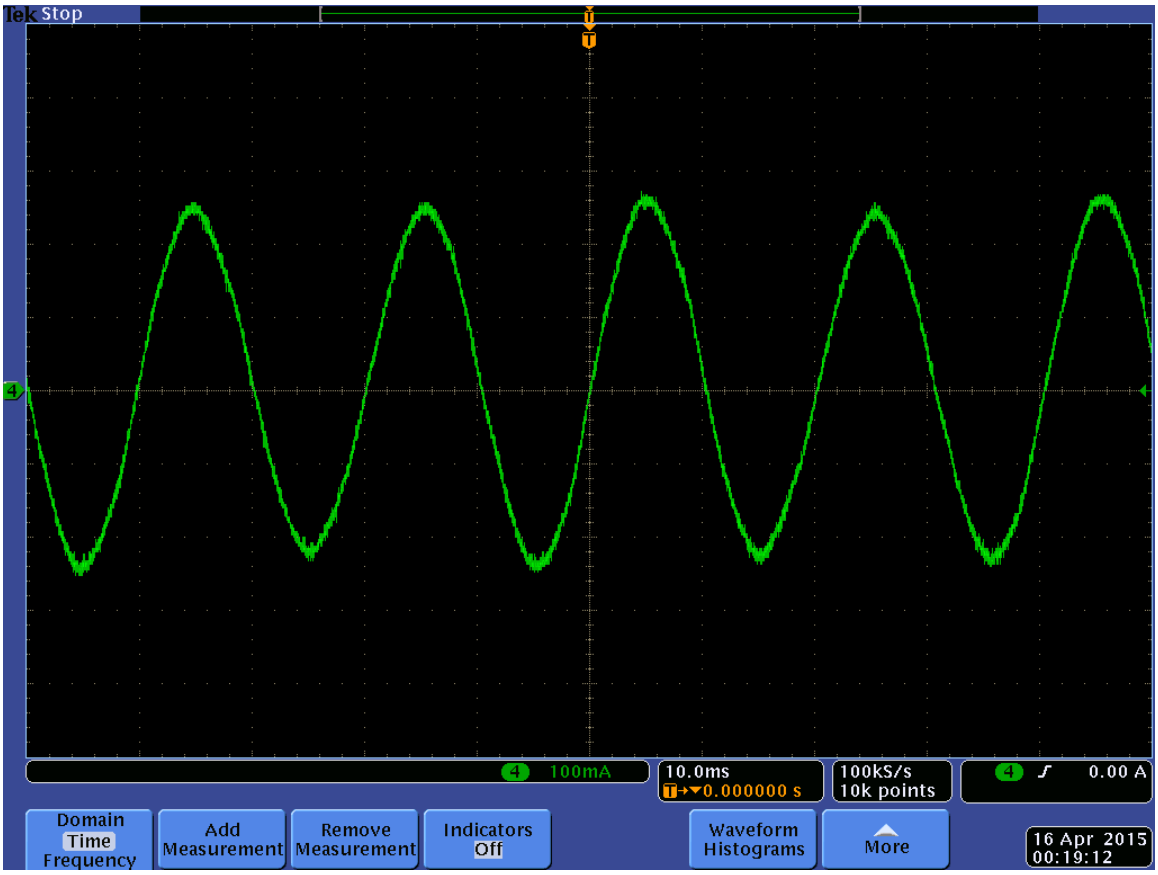

Figure 6.16 LC filter output current to load

The output voltage obtained through LC filter and fed to the load is shown in Figure 6.17 and 6.18. The peak value is 75 and it has a frequency of 60 Hz. This shows that performance of PI controller to control Z-source inverter with dc voltage source is reliable and effective.

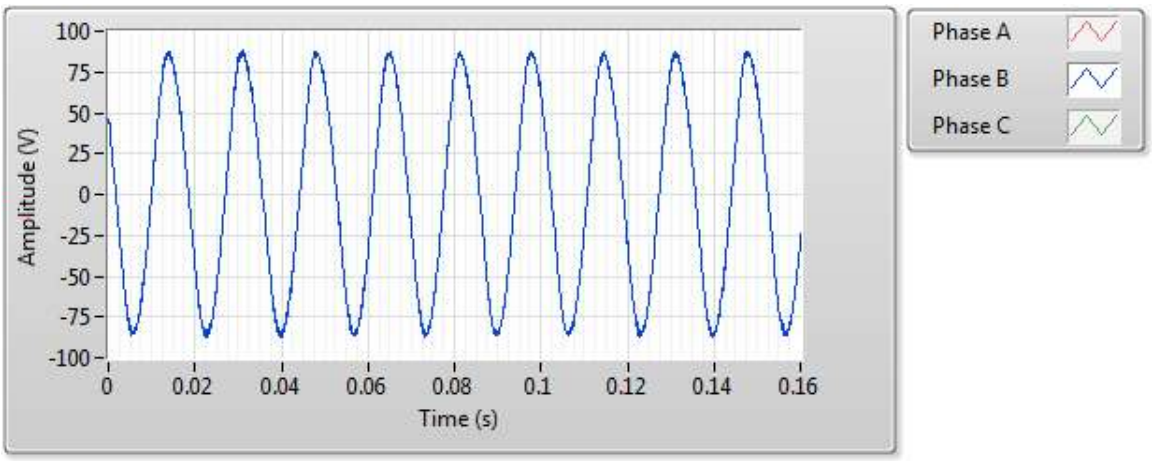

Figure 6.17 Output voltage on phase B of LC filter to load

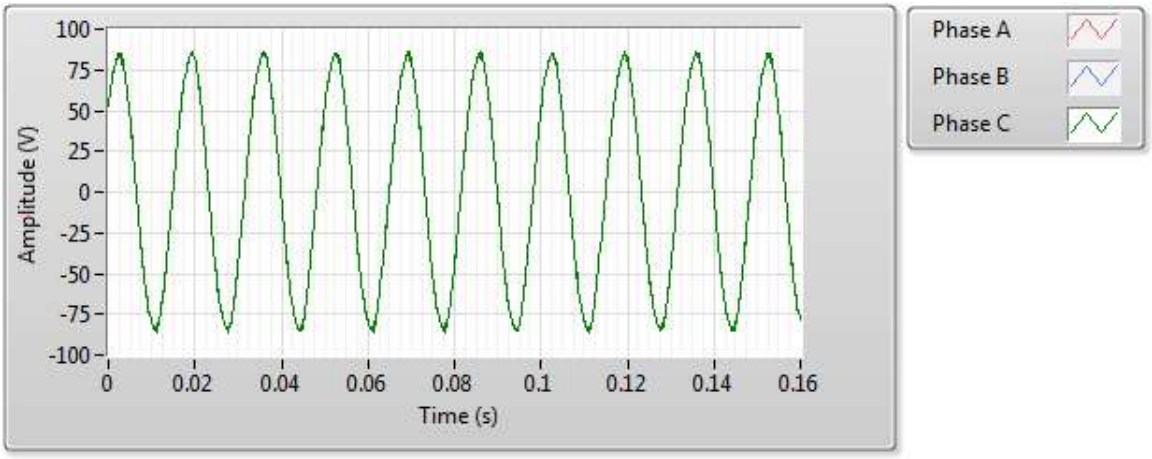

Figure 6.18 Output voltage on phase C of LC filter to load

6.2.2 Zsource with PV MPPT Test

Prototype of Z-source inverter was interfaced with Chroma-Programmable PV Simulator in stand-alone mode with controller running in dSPACE 1103 interfaced with simulink environment. Output of Z-source inverter was fed to resistive load of 500 watt through an LC filter described in previous sections. The simulation results from Dynamic MPPT

testing of Chroma-PV Simulator are shown in Figure 6.19 – Figure 6.25. Maximum voltage of PV module was set at 175 volts and maximum current was set at 3.4 A which corresponds to maximum power point of 595 watts. The carrier frequency was set at 10000 Hz. The Pv model used was Sandia with Trise = 800, Tfall = 800, Vmppt = 175 Volts, Pmppt = 595 watt and Fill factor of 0.68 at STC.

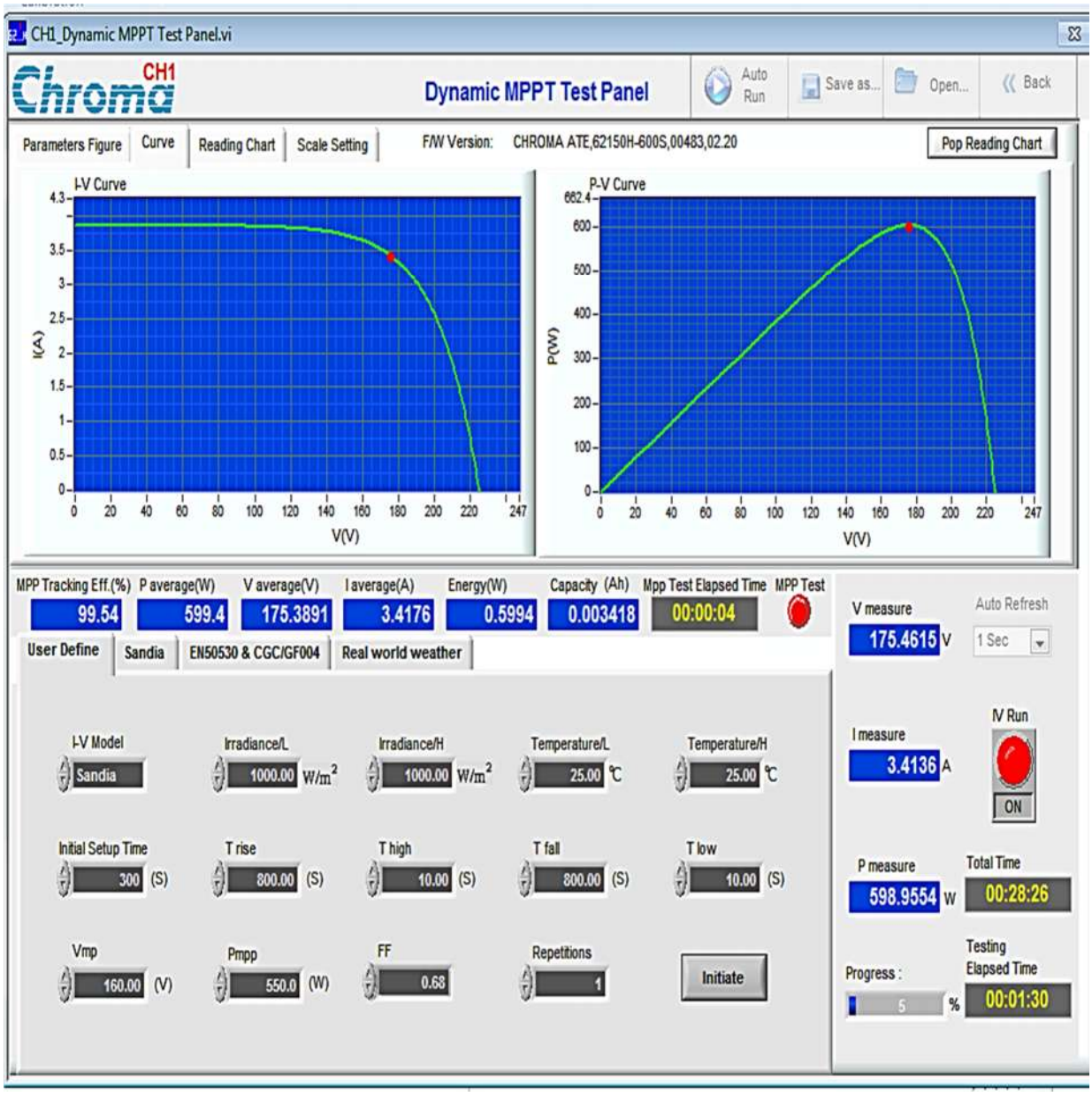

Figure 6.19 MPPT Test of PV-Simulator

The efficiency of MPPT test was 99.54% and 600 watt of power was successfully delivered to the load. Output voltages and current waveforms obtained through control desk are shown in Figure 6.21. Output voltages and current are sinusoidal with a frequency of 60 Hz which shows the accurate filtering action of low pass LC filter.

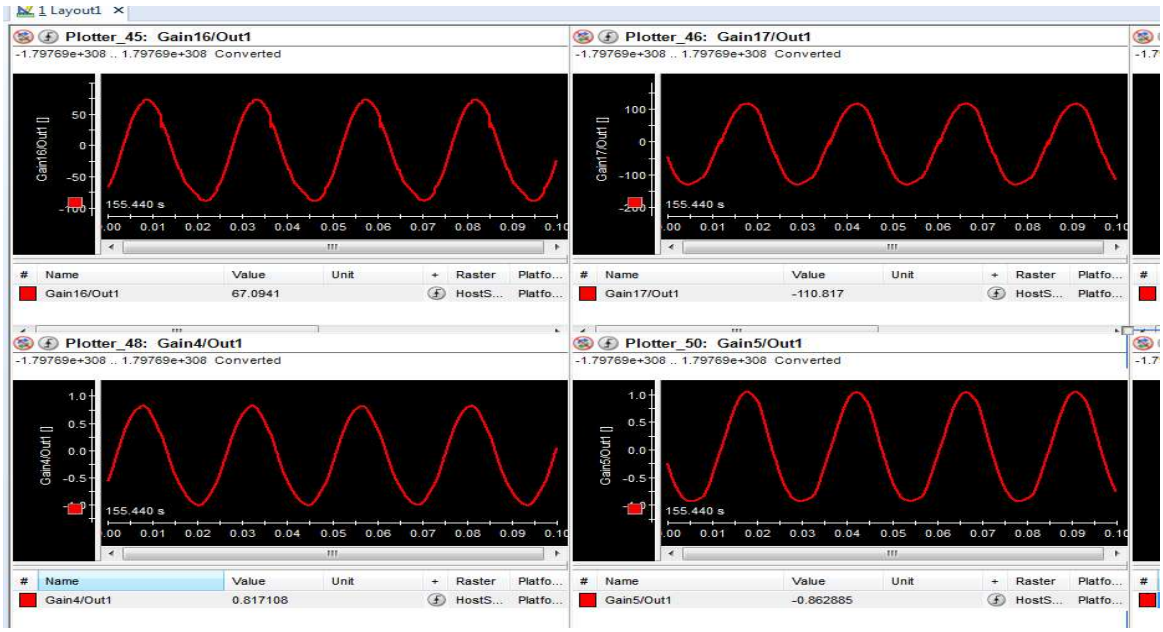

Figure 6.20 Output Voltage and current

The Pulses waveforms obtained through Control Desk software are shown in Figure 6.21. These pulses are obtained from dSPACE1103 and amplified to 15V and then fed to Z-source inverter for proper switching. The current level of the pulses was amplified by the internal current amplifier in inverter module to the required switching level.

Figure 6.21 Firing PULSES at Control Desk

The Control Desk shows the values of PV voltage to be 172.3 V and PV current to be 4.81 A at maximum power point sampled through voltage and current transducers and sent to dSPACE1103 for control action as shown in Figure 6.22.

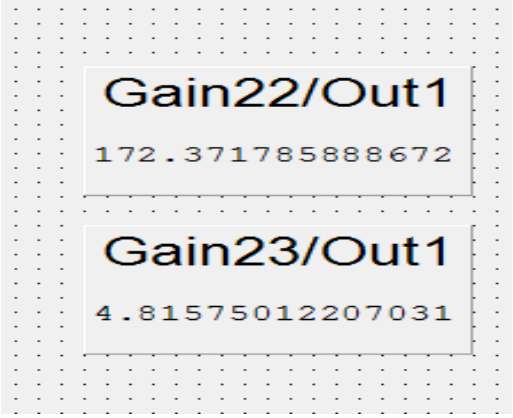

Figure 6.22 Measured Vpv and Ipv by Control Desk

6.2.3 Zsource with PV Partial Shadow Test

A partial shadow test was done with PV-Simulator connected to Z-source inverter prototype in a stand-alone mode with controller running in dSPACE 1103 interfaced with

Simulink environment. The shadow was simulated by a moving cloud over the PV module. The maximum power point tracking of the PV module before, during and after the passage of cloud over the PV module is shown in Figure 6.23 – Figure 6.25.

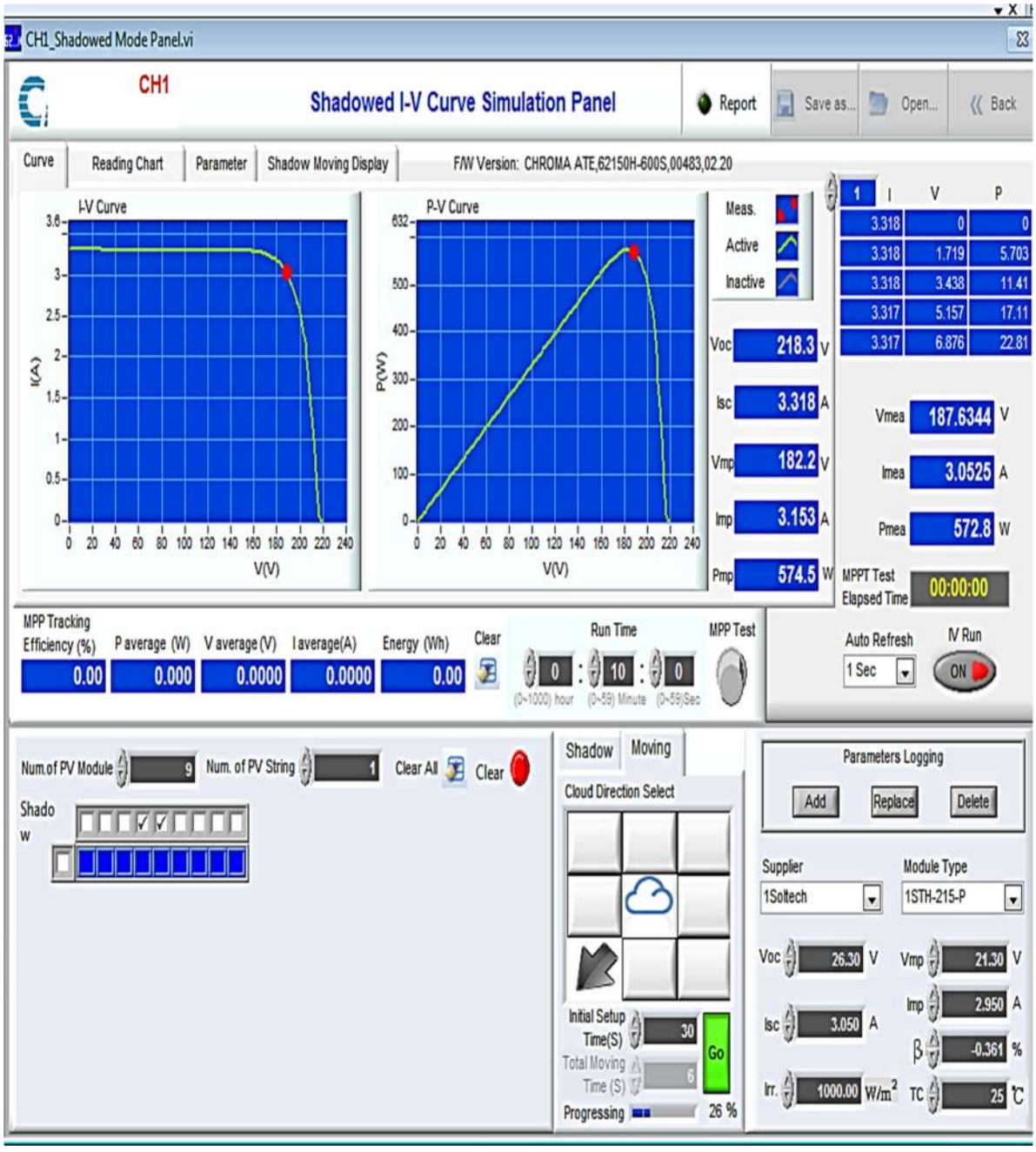

Figure 6.23 MPPT tracking before Passage of shadow

In Figure 6.23, it shown that the cloud will pass over the PV module as shown by the cloud arrow direction. At 26% of simulation before the passage of cloud over the PV modules, the results of MPPT is shown in Figure 6.23. The cloud will pass over module number 4 and 5 as indicated by the tick signs in Figure 6.23. After 85%, the cloud will pass over these two modules and MPPT results are shown during the shadow caused by clouds in Figure 6.24. The MPPT efficiency by PI controller during the shadowing is 98.7%. After 95% of simulation, the cloud have passed and the PV modules are exposed to full sunlight again and MPPT results after the passage of clouds are shown in Figure 6.25. During the shadowing the irradiation was reduced to 600 w/m2 from 1000 w/m2 during normal conditions.

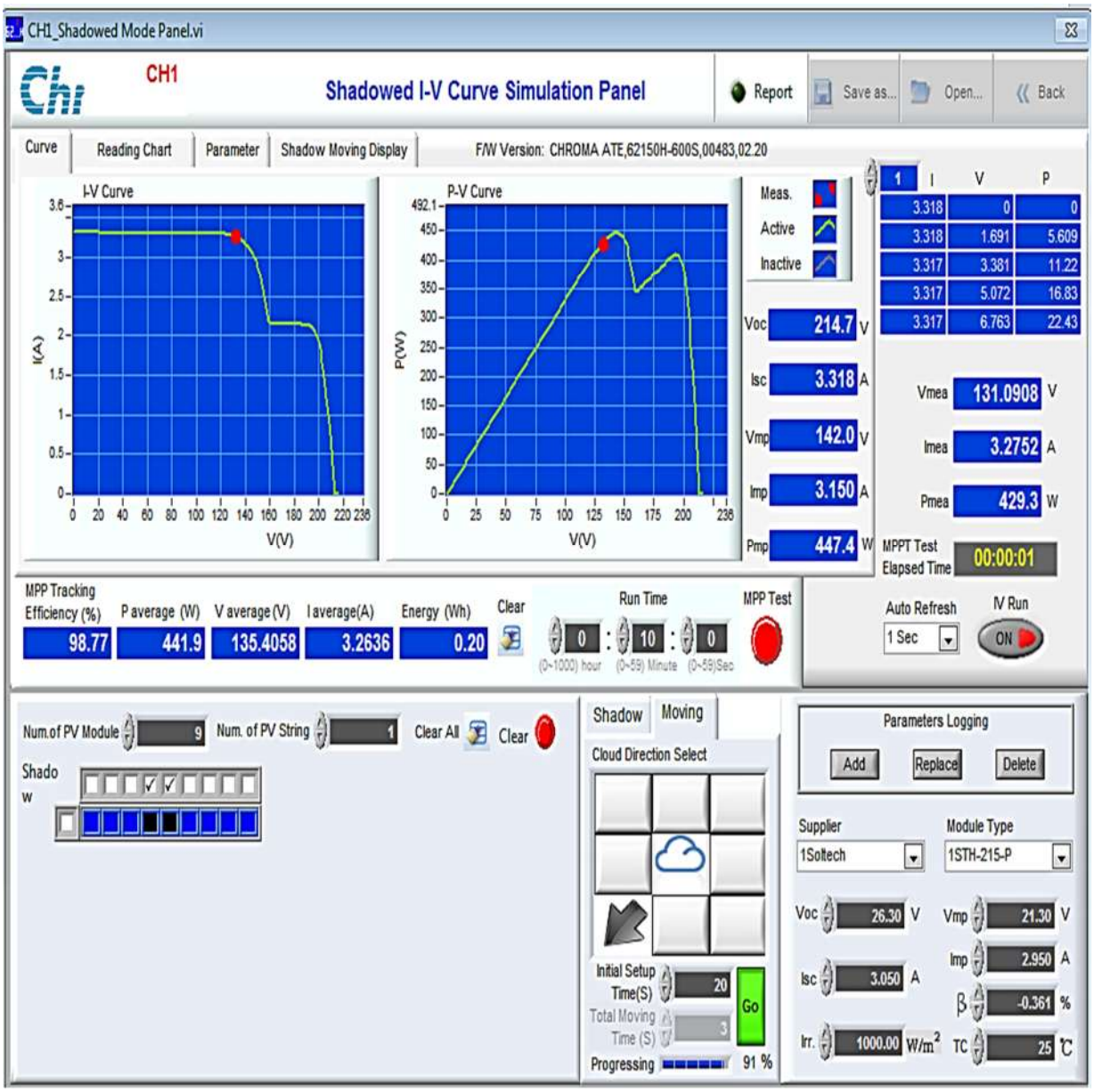

Figure 6.24 MPPT during Shadow

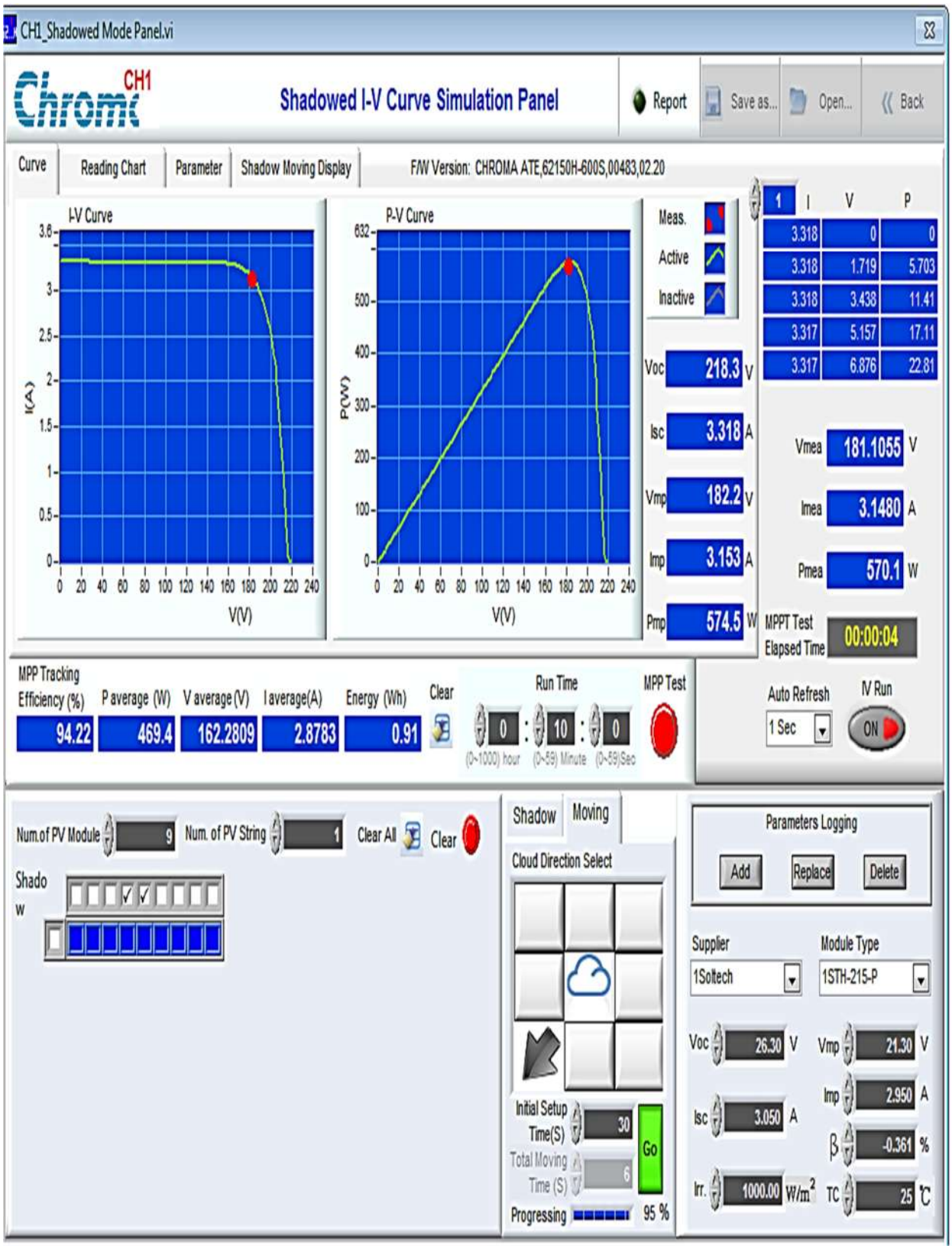

Figure 6.25 MPPT after Passage of Shadow

The hardware prototype of Z-source inverter, amplifiers, inductors and dSPACE1103 controller is shown in Figure 6.26. The batteries are used to supply dc voltages for different equipment in the prototype.

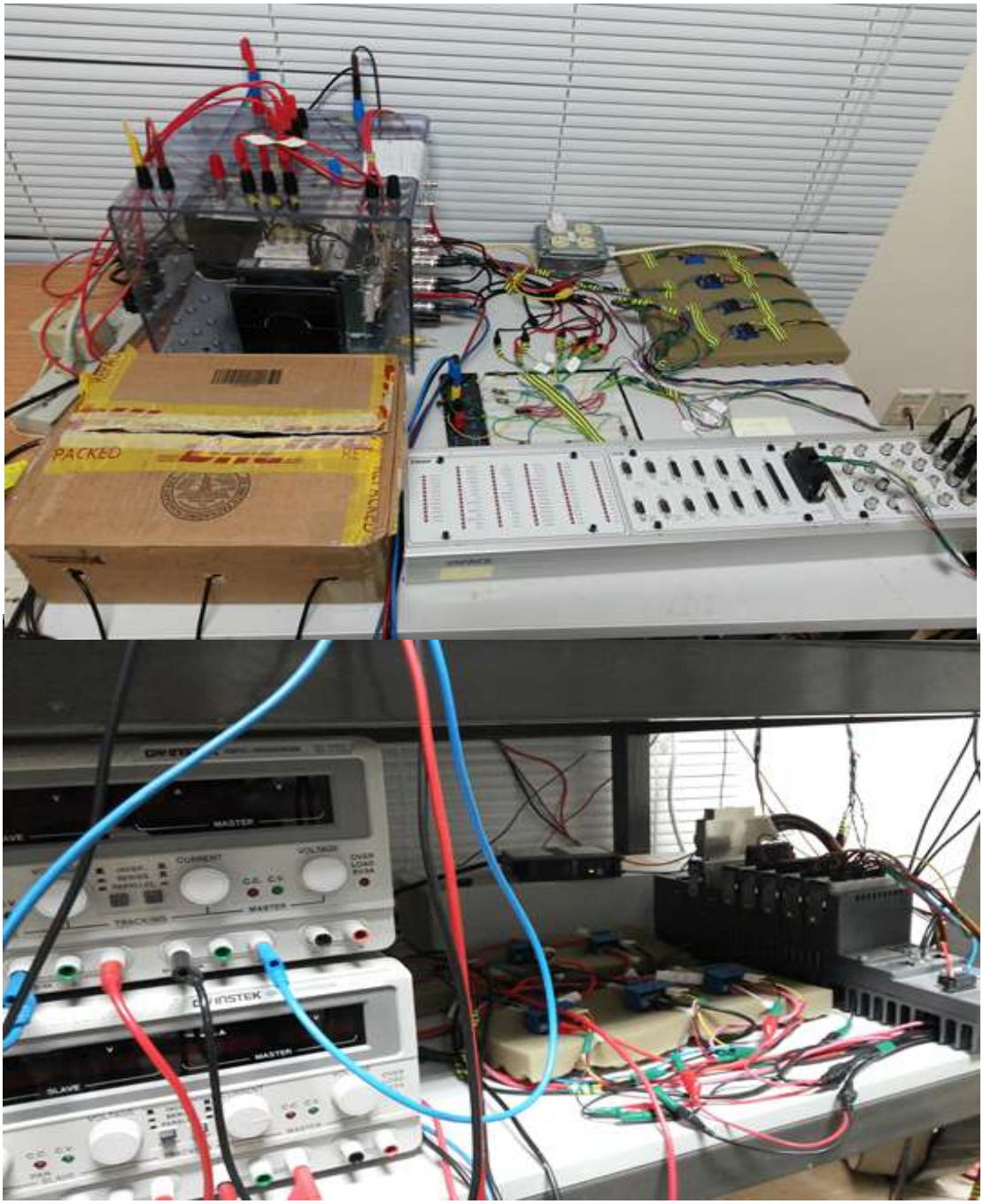

Figure 6.26 Hardware detail of Prototype

6.3 Discussion

In this chapter, the grid-connected PV system with Z-source was successfully implemented in real-time environment and its performance was evaluated which shows the feasibility and robustness of artificial intelligence based ANFIS controllers. A laboratory prototype of Z-source inverter was also built and Pi controller was used in dSPACE 1103 to evaluate the performance of MPPT tracking of Chroma-PV Simulator and partial shadow test case was also carried out. Z-source theory can also be extended to complex grid-connected environment in prototype. Z-source inverters can be used as multi-level inverters in power conversion systems with CMI and ESB and its further performance can be evaluated. This study showed the potential of Z-source inverters to be future technology in power conversion systems of all types. Successful implementation of PI and ANFIS controllers in real-time environment and prototype has taken the research to another level and have helped in evaluating and validating the performance of these converters and controllers.

CHAPTER 7

CONCLUSION AND FUTURE WORK

7.1 Conclusions

In this research work, Z-source inverter has been used with PV to enhance the performance of power conversion systems. Conventional converters have drawbacks as they are two stage converter increasing the cost and component count. Also conventional converters have restrictions on switching states and EMI can cause short-circuit of gates resulting in damage of device. Conventional converters low efficiency and many other limitations. Z-source inverter has been proposed and its performance has been evaluated with different PWM controllers. Also, different feedback controllers like PI controllers with alpha-beta conversion and dq-conversion were implemented and their performance has been evaluated. Artificial intelligence based controllers like Adaptive neuro-fuzzy controllers have been proposed for robust, reliable, and fast current, voltage and power feedback control in power conversion systems.

- Different PWM control methods like Simple boost control, Maximum boost control and constant maximum boost control techniques have been employed and their performance have been evaluated for Z-source converters which paves the

way for future formulation and research of more efficient space-vector PWM techniques for complex power conversion systems.

- The performance of Maximum constant boost controller was higher in terms of harmonic contents, boost factor and voltage gain than other two PWM techniques. These PWM techniques use 5 control signals and a carrier signal to generate switching signals for IGBTs. Out of these 5 signals, three of these signals were generated by feedback controller and 2 by MPPT tracking algorithm. The shoot-through duty ratio was used in these controllers to control the shoot-through of dc-link voltage. Implementation of these techniques will help in developing of new techniques.
- These PWM techniques will help researchers to propose and formulate new PWM techniques and these 3 techniques can be used with different feedback controllers to enhance the performance of power conversion system, thus adjusting the output voltage, reducing harmonic contents, providing more robust, effective and desired results in multi-level inner connected systems with CMI and ESB.

- Different feedback controllers for dc reference tracking, current control, voltage control and power control have been proposed for PV connected Z-source inverter in stand-alone and grid-connected modes. DQ controllers for stand-alone PV system under STC of 25^0 C and 1000 w/m^2 with Z-source inverter were designed and performance was evaluated.
- PI based feedback controllers were designed for grid-connected PV systems with Z-source inverters in Matlab/Simulink environment. The performance of the

controller was evaluated under varying environmental conditions of temperature and irradiations of PV module.

- New ANFIS-based feedback controllers were proposed in this research work. Three ANFIS controllers were used; one for dc reference tracking and two for reference voltage signal generators to control PWM and generate switching signals for IGBTs.
- The proposed ANFIS controller was implemented in Simulink environment and its performance was compared to PI controller and it was found that ANFIS controllers are more robust, fast and reliable under changing conditions to for dc reference tracking, MPPT tracking and power control. The ANFIS controller was also implemented in real time environment of RTDS and dSPACE 1103 and its performance was evaluated in real time environment.
- This proposed controller is very efficient, reliable, fast and is suitable for use in complex power conversion systems and in multi-level cascaded inverter systems.
- A laboratory prototype of Z-source inverter was built and its performance with dc input source and PV-Simulator was evaluated using PI controller in dSPACE 1103 interfaced with Simulink. Different tests were carried out like MPPT test and partial shadow test.
- The PI controller with the laboratory prototype was efficiently tracking Maximum power point under various conditions.

7.2 Future Work

The following future works are recommended.

1. The developed PWM techniques can be modified to present and formulate new PWM algorithms for multi-level cascaded grid-connected converter systems. Combination of these PWM techniques can also be used. New vector based PWM algorithms with more states and more switching patterns can also be presented.
2. New MPPT algorithm based on neural networks, sliding mode and MPC can be used in combination with these PWM techniques.
3. ANFIS Controllers can be extended to common-point coupled Z-source inverters.
4. ANFIS Controllers can be extended to Multi-level Z-source inverter in transformer-less grid-connected mode.
5. ANFIS Controllers can be extended for CMI and ESB connected modes of PV systems and wind systems.
6. ANFIS Controllers can be extended to simultaneously control various power conversion systems and distributed generations.
7. Developed prototype can be used to connect power conversion energy systems to utility grid and evaluate the performance of changing environmental conditions.
8. Wind and PV simulator both can be interfaced with Z-source laboratory prototype and a robust controller based on artificial intelligence can be proposed for future research purposes.

References

[1] "International Energy Outlook 2013 - Energy Information Administration." [Online]. Available: http://www.eia.gov/forecasts/ieo/. [Accessed: 20-May-2014].

[2] "ICER RES and DG Report_FINAL - ICER RES and DG Report_FINAL.pdf." [Online]. Available:http://www.naruc.org/international/Documents/ICER RES and DG Report_FINAL.pdf. [Accessed: 20-May-2014].

[3] "Global Market Outlook For Photovoltaics Until 2016,"(EPIA) Industry Association [Online].Available:http://www.epia.org/fileadmin/user_upload/Publications/Global Market-Outlook-2016.pdf. [Accessed: 20-May-2014].

[4] K. Ishaque, Z. Salam, and H. Taheri, "Modeling and simulation of photovoltaic (PV) system during partial shading based on a two-diode model," Simul. Model. Pract. Theory, vol. 19, no. 7, pp. 1613–1626, Aug. 2011.

[5] A. N. Celik and N. Acikgoz, "Modelling and experimental verification of the operating current of mono-crystalline photovoltaic modules using four- and five-parameter models," Appl. Energy, vol. 84, no. 1, pp. 1–15, Jan. 2007.

[6] T. U. Townsend, "Method for Estimating the Long-Term Performance of Direct-Coupled Photovoltaic Systems," MS Thesis, University Of Wisconsin, madison, 1989.

[7] M. P. Aparicio and J. Pelegrí-sebastiá, “Modeling of Photovoltaic Cell Using Free Software Application for Training and Design Circuit in Photovoltaic Solar Energy.”

Available:http://www.intechopen.com/books/new-developments-in-renewable energy/modeling-of-photovoltaic-cell-using-free-software-application-for-training-and-design-circuit-in-pho

[8] A. Chatterjee, A. Keyhani, and D. Kapoor, “Identification of Photovoltaic Source Models,” IEEE Trans. Energy Convers., vol. 26, no. 3, pp. 883–889, Sep. 2011.

[9] J. A. Gow and C. D. Manning, “Development of a photovoltaic array model for use in power-electronics simulation studies,” IEE Proc. - Electr. Power Appl., vol. 146, no. 2, p. 193, 1999.

[10] Y. Hishikawa, Y. Imura, and T. Oshiro, “Irradiance-dependence and translation of the I-V characteristics of crystalline silicon solar cells,” in Conference Record of the Twenty-Eighth IEEE Photovoltaic Specialists Conference - 2000 (Cat. No.00CH37036), pp. 1464–1467, 2000,.

[11] “Sand2004-3535 - 043535.pdf.” [Online]. Available: http://prod.sandia.gov/techlib/access-control.cgi/2004/043535.pdf. [Accessed: 20-May-2014].

[12] C. Carrero, D. Ramírez, J. Rodríguez, and C. A. Platero, "Accurate and fast convergence method for parameter estimation of PV generators based on three main points of the I–V curve," Renew. Energy, vol. 36, no. 11, pp. 2972–2977, Nov. 2011.

[13] B. Marion, S. Rummel, and A. Anderberg, "Current-voltage curve translation by bilinear interpolation," Prog. Photovoltaics Res. Appl., vol. 12, no. 8, pp. 593–607, Dec. 2004.

[14] "SAND-2004_PV-Performance-Array-Model.pdf."[Online].Available: http://energy.sandia.gov/wp/wp-content/gallery/uploads/SAND-2004_PV-Performance-Array-Model.pdf. [Accessed: 20-May-2014].

[15] R. Chenni, M. Makhlouf, T. Kerbache, and A. Bouzid, "A detailed modeling method for photovoltaic cells," Energy, vol. 32, no. 9, pp. 1724–1730, Sep. 2007.

[16] K. Ishaque and Z. Salam, "An improved modeling method to determine the model parameters of photovoltaic (PV) modules using differential evolution (DE)," Sol. Energy, vol. 85, no. 9, pp. 2349–2359, Sep. 2011.

[17] M. Zagrouba, A. Sellami, M. Bouaïcha, and M. Ksouri, "Identification of PV solar cells and modules parameters using the genetic algorithms: Application to maximum power extraction," Sol. Energy, vol. 84, no. 5, pp. 860–866, May 2010.

[18] C. S. Chin, P. Neelakantan, S. S. Yang, B. L. Chua, K. Tze, and K. Teo, “Effect of Partially Shaded Conditions on Photovoltaic Array ’ s Maximum Power Point Tracking,” IJSST, vol. 12, no. 3, pp. 52–59, 2012.

[19] K. Ishaque, Z. Salam, and H. Taheri, “Modeling and simulation of photovoltaic (PV) system during partial shading based on a two-diode model,” Simul. Model. Pract. Theory, vol. 19, no. 7, pp. 1613–1626, Aug. 2011.

[20] Lijun Gao; Dougal, R.A; Liu, Shengyi; Iotova, AP., "Parallel-Connected Solar PV System to Address Partial and Rapidly Fluctuating Shadow Conditions," Industrial Electronics, IEEE Transactions on , vol.56, no.5, pp.1548,1556, May 2009

[21] Z. Salam, K. Ishaque, and H. Taheri, “An improved two-diode photovoltaic (PV) model for PV system,” in 2010 Joint International Conference on Power Electronics, Drives and Energy Systems & Power India, 2010, pp. 1–5,2010.

[22] F. Z. Peng, “Z-source inverter,” Conf. Rec. 2002 IEEE Ind. Appl. Conf. 37th IAS Annu. Meet. (Cat. No.02CH37344), vol. 2, pp. 775–781, 2002.

[23] Y. Li, J. Anderson, F. Z. Peng, and D. Liu, “Quasi-Z-Source Inverter for Photovoltaic Power Generation Systems,” 2009 Twenty-Fourth Annu. IEEE Appl. Power Electron. Conf. Expo., pp. 918–924, Feb. 2009.

[24] B. Ge, H. Abu-Rub, F. Z. Peng, Q. Lei, A. T. de Almeida, F. J. T. E. Ferreira, D. Sun, and Y. Liu, “An Energy-Stored Quasi-Z-Source Inverter for Application to

Photovoltaic Power System," IEEE Trans. Ind. Electron., vol. 60, no. 10, pp. 4468–4481, Oct. 2013.

[25] Abbass, H.A; Sarker, R.; Newton, C., "PDE: a Pareto-frontier differential evolution approach for multi-objective optimization problems," Evolutionary Computation, 2001. Proceedings of the 2001 Congress on, vol.2, no., pp.971,978 vol. 2, 2001

[26] Mei Shan Ngan; Chee Wei Tan, "A study of maximum power point tracking algorithms for stand-alone Photovoltaic Systems," Applied Power Electronics Colloquium (IAPEC), 2011 IEEE , vol., no., pp.22,27, 18-19 April 2011

[27] V. R and S. Ravivarman, "Z Source Inverter for Photovoltaic System with Fuzzy Logic Controller," Int. J. Power Electron. Drive Syst., vol. 2, no. 4, pp. 371–379, Dec. 2012.

[28] Abu-Rub, H.; Iqbal, A; Moin Ahmed, S.; Peng, F.Z.; Yuan Li; Ge Baoming, "Quasi-Z-Source Inverter-Based Photovoltaic Generation System With Maximum Power Tracking Control Using ANFIS,"Sustainable Energy, IEEE Transactions on , vol.4, no.1, pp.11,20, Jan. 2013

[29] Po Xu, Xing Zhang, Chong-wei Zhang, Ren-xian Cao, and Liuchen Chang, "Study of Z-Source Inverter for Grid-Connected PV Systems," in 37th IEEE Power Electronics Specialists Conference, pp. 1–5, 2006,.

[30] B. Sun, J. Mei, J. Zheng, and K. Deng, “Grid-connected photovoltaic system based on switched-inductor quasi-Z-source inverter and its low voltage ride-through control strategy,” J. Renew. Sustain. Energy, vol. 5, no. 3, p. 033120, 2013.

[31] S. Thangaprakash, “Unified MPPT Control Strategy for Z-Source Inverter Based Photovoltaic Power Conversion Systems,” J. Power Electron., vol. 12, no. 1, pp. 172–180, Jan. 2012.

[32] B. Sun, J. Mei, J. Zheng, and K. Deng, “Grid-connected photovoltaic system based on switched-inductor quasi-Z-source inverter and its low voltage ride-through control strategy,” J. Renew. Sustain. Energy, vol. 5, no. 3, p. 033120, 2013.

[33] Y. Zhou, W. Huang, P. Zhao, and J. Zhao, “A Transformerless Grid-Connected Photovoltaic System Based on the Coupled Inductor Single-Stage Boost Three-Phase Inverter,” IEEE Trans. Power Electron., vol. 29, no. 3, pp. 1041–1046, Mar. 2014.

[34] E. Beser, B. Arifoglu, S. Camur, and E. K. Beser, “A grid-connected photovoltaic power conversion system with single-phase multilevel inverter,” Sol. Energy, vol. 84, no. 12, pp. 2056–2067, Dec. 2010.

[35] F. Z. Peng, “Z-source inverter,” IEEE Trans. Ind. Applicat.,vol. 39, no. 2, pp. 504–510, 2003.

[36] Y. Li, S. Jiang, J. Cintron-Rivera, and F. Peng, "Modeling and control of quasi-Z-source inverter for distributed generation applications,"IEEE Trans. Ind. Electron., vol. 60, no. 4, pp. 1532–1541, Apr. 2013.

[37] C. J. Gajanayake, D. M. Vilathgamuwa, and P. C.Loh, "Development of a comprehensive model and a multiloop controller for Z-source inverter DO systems," IEEE Trans. Ind. Electron., vol. 54, pp. 2352–2359, Aug. 2007.

[38] Q.-V. Tran, T.-W. Chun, H.-G. Kim, and E.-C.Nho, "Minimization of voltage stress across switching devices in the Z-source inverter by capacitor voltage control," J. Power Electron., vol. 9, no. 3, pp. 335–342, May 2009.

[39] X. Ding, Z. Qian, S. Yang, B. Cui, and F. Z. Peng, "A direct DC-link boost voltage PID-like fuzzy control strategy in Z-source inverter," in Proc. IEEE Power Electronics Specialists Conf., pp. 405–411, 2008.

[40] Y. Ta ng, J. Wei, and S. Xie, "A new direct peak dc-link voltage control strategy of Z-source inverters," in Proc. 25th Annu. IEEE Applied Power Electronics Conf. Exposition (APEC), pp. 867–872, Feb.21–25, 2010,.

[41] O. Ellabban, J. VanMierlo, and P. Lataire, "A DSP-based dual-loop peak DC-link voltage control strategy of the Z-source inverter,"IEEE Trans. Power Electron., vol.27, no. 9, pp. 4088–4097,Sept. 2012.

[42] A. H. Rajaei, S. Kaboli, and A. Emadi, "Slidingmode control of Z-source inverter," in Proc. IEEE 34th Annu. Conf. Industry Electronics, pp. 947–952 ,Nov.10–13, 2008,.

[43] H. Rostamiand D. A. Khaburi, "Neural networks controlling for both the DC boost and AC output voltage of Z-source inverter," in Proc. 1st Power Electronics Drive System Technology Conf., pp. 135–140, Feb.17–18, 2010,.

[44] W. Mo, P. C. Loh, and F. Blaabjerg, "Model predictive control for Z-source power converter," in Proc. 8th Int. Conf. Power Electronics, pp. 3022–3028, 30 May–3 June, 2011.

[45] M. Mosa, H. Abu-Rub, and J. Rodríguez, "High performance predictive control applied to three phase grid connected quasi-Z-source inverter," in Proc. 39th Annu. Conf. IEEE Industrial Electronics Society (IECON 2013), , pp. 5812–5817, Nov.10–13,2013.

[46] S. Rajakarunaand L. Jayawickrama, "Steadystate analysis and designing impedance network of Z-source inverters," IEEE Trans. Ind. Electron., vol. 57, no. 7, pp. 2483–2491, July 2010.

[47] J. B. Liu, J. G. Hu, and L. Y. Xu, "Dynamic modeling and analysis of Z-source converter—Derivation of AC small signal model and designoriented analysis," IEEE Trans. Power Electron., vol. 22, no. 5, pp. 1786–1796,Sept. 2007.

[48] F. Guo, L. X. Fu, C. H. Lin, C. Li, W. Choi, and J.Wang, "Development of an 85-kW bidirectional quasi-Z-source inverter with DC-link feed-forward compensation for electric vehicle applications," IEEE Trans. Power Electron., vol. 28, pp. 5477–5488, Dec. 2013.

[49] F. Z. Peng, M. Shen, and K. Holland, "Application of Z-source inverter for traction drive of fuel cell—battery hybrid electric vehicles,"IEEE Trans. Power Electron., vol.22, no. 3, pp. 1054–1061, May 2007.

[50] P. Liuand H. P. Liu, "Permanent-magnet synchronous motor drive system for electric vehicles using bidirectional Z-source inverter," Electr. Syst. Transp., IET, vol.2, no. 4, pp. 178–185, Dec. 2012.

[51] Y. Liu, B. Ge, F. Z. Peng, A. R. Haitham, A. T.de Almeida, and F. J. T. E. Ferreira, "QuasiZ-source inverter based PMSG wind power generation system," in Proc. 2011 IEEE Energy Conversion Congress and Exposition (ECCE), pp. 291–297, Sept.17–22, 2011.

[52] U. Supattiand F. Z. Peng, "Z-source inverter with grid connected for wind power system," in Proc. IEEE Energy Conversion Congress Exposition (ECCE 2009),Sept.20–24, pp. 398–403,2009.

[53] S. M. Dehghan, M. Mohamadian, and A. Y.Varjani, "A new variable-speed wind energy conversion system using permanent-magnet synchronous generator and Z-source inverter," IEEE Trans. Energy Convers., vol. 24, no. 3, pp. 714–724,Sept. 2009.

[54] Y. Huang, M. Shen, F. Z. Peng, and J. Wang, "Z-source inverter for residential photovoltaic systems," IEEE Trans. Power Electron., vol. 21, no. 6, pp. 1776–1782, Nov. 2006.

[55] Y. Li, J. Anderson, F. Z. Peng, and D. Liu, "Quasi-Z-source inverter for photovoltaic power generation systems," in Proc. 24th Annu. IEEE Applied Power Electronics Conf. Exposition (APEC), pp. 918–924, Feb.15–19, 2009.

[56] M. Hanif, M. Basu, and K. Gaughan, "Understanding the operation of a Z-source inverter for photovoltaic application with a design example," IET Power Electron., vol. 4, no. 3, pp. 278–287, Mar. 2011.

[57] B. Ge, "Single-stage buck/boost energy stored photovoltaic grid-tie power generation system," China patent CN101917017A, Dec. 2010.44 IEEE IndustrIal ElEctronIcs magazInE , December 2014

[58] D. Sun, B. M. Ge, D. Bi, and F. Z. Peng, "Analysis and control of quasi-Z source inverter with battery for grid-connected PV system," Int. J. Electr. Power Energy Syst., vol. 46, pp. 234–240, Mar.2013.

[59] Y. Liu, B. Ge, H Abu-Rub, and F. Z. Peng, "Control system design of battery-assisted quasiZ-source-inverter for grid-tie photovoltaic power generation," IEEE Trans. Sustain. Energy, vol. 4, no. 4, pp. 994–1001, Oct. 2013.

[60] H. Abu-Rub, A. Iqbal, Sk. Moin Ahmed, F. Z.Peng, Y. Li, and G. Baoming, "Quasi-Z-source inverter-based photovoltaic generation system with maximum

power tracking control using ANFIS,"IEEE Trans. Sustain. Energy, vol. 4, no. 1, pp. 11–20, Jan. 2013.

[61] J. Liu, S. Jiang, D. Cao, and F. Z. Peng, "A digital current control of quasi-Z-source inverter with battery," IEEE Trans. Ind. Informat., vol. 9, no. 2, pp. 928–937, May 2013.

[62] B. Ge, H. Abu-Rub, F. Peng, Q. Lei, A.de Almeida, F. Ferreira, D. Sun, and Y. Liu, "An energy stored quasi-Z-source inverter for application to photovoltaic power system," IEEE Trans. Ind. Electron., vol. 60, no. 10, pp. 4468–4481, Oct. 2013.

[63] B. Ge, F. Z. Peng, H. Abu-Rub, F. J. T. E. Ferreira, and A. T. de Almeida, "Novel energy stored single-stage photovoltaic power system with constant DC-link peak voltage," IEEE Trans. Sustain. Energy, vol. 5, no. 1, pp. 28–36, Jan.2014.

[64] B. Ge, Q. Lei, W. Qian, and F. Z. Peng, "A family of Z-source matrix converters," IEEE Trans. Ind. Electron., vol. 59, no. 1, pp. 35–46, Jan. 2012.

[65] M.-K. Nguyen, Y.-G. Jung, Y.-c. Lim, and Y.-M.Kim, "A single-phase Z-source buck-boost matrix converter," IEEE Trans. Power Electron., vol. 25, no. 2, pp. 453–462, Feb. 2010.

[66] S. Liu, B. Ge, H. Abu-Rub, F. Z. Peng, and Y.Liu, "Quasi-Z-source matrix converter based induction motor drives," in Proc. 38th Annu. Conf. IEEE Industrial Electronics Society (IECON 2012), Montreal, Canada, Oct.25–28, pp. 5285–5289.

[67] P. C. Loh, F. Gao, F. Blaabjerg, S. Y. C. Feng, and K. N. J. Soon, “Pulsewidth-modulated Z-source neutralpoint-clamped inverter,”IEEE Trans. Ind. Applicat., vol.43, no. 5, pp. 1295–1308,Sept.–Oct. 2007.

[68] P. C. Loh, S. W. Lim, F. Gao, and F. Blaabjerg, “Three-level Z-source inverters using a single LC impedance network,” IEEE Trans. Power Electron., vol. 22, no. 2, pp. 706–711, Mar. 2007.

[69] S. Tennerand W. Hofmann, “A comparison of Z-Source three-level NPC inverter versus Z-Source two-level inverter,” in Proc. Emobility - Electrical Power Train, Nov.8–9, 2010, pp. 1–7.

[70] L. P. Chiang, F. Blaabjerg, and W. C. Pang, “Comparative evaluation of pulsewidth modulation strategies for Z-source neutral-point-clamped inverter,”IEEE Trans. Power Electron., vol. 22, no. 3, pp. 1005–1013, 2007.

[71] L. Liu, H. Li, Y. Zhao, X. He, and Z. J. Shen, “1 MHz cascaded Z-source inverters for scalable grid-interactive photovoltaic (PV) applications using GaN device,” in Proc. 2011 IEEE Energy Conversion Congress and Exposition (ECCE),Sept.17–22, pp. 2738–2745.

[72] Y. Zhou, L. Liu, and H. Li, “A high-performance photovoltaic module-integrated converter (MIC) based on cascaded quasi-z-source inverters (qZSI) using eGaN FETs,”IEEE Trans. Power Electron., vol. 28, no. 6, pp. 2727–2738, June 2013.

[73] D. Sun, B. Ge, F. Z. Peng, A. Haitham, D. Bi, and Y.liu, "A new grid-connected PV system based on cascaded H-bridge quasi-z source inverter," in Proc. 2012 IEEE Int. Symp. Industrial Electronics (2012 ISIE), May28–31, pp. 951–956.

[74] B. Ge, "Energy stored cascade multilevel photovoltaic grid-tie power generation system," China patent CN101917016A, Dec. 2010.

[75] Y. Liu, B. Ge, H. Abu-Rub, and F. Z. Peng, "A modular multilevel space vector modulation for photovoltaic quasi-Z-source cascade multilevel inverters," in Proc. 28th Annu. IEEE Applied Power Electronics Conf. Exposition (APEC), Mar.17–21, 2013, pp. 714–718.

[76] Y. Liu, B. Ge, H. Abu-Rub, and F. Z. Peng, "An effective control method for quasi-Z-source cascade multilevel inverter based grid-tie single-phase photovoltaic power system," IEEE Trans. Ind. Informat., vol. 10, no. 1, pp. 399–407, Feb. 2014.

[77] Y. Xue, B. Ge, and F. Z. Peng, "Reliability, efficiency, and cost comparisons of MW scale photovoltaic inverters," in Proc. 2012 IEEE Energy Conversion Congress and Exposition (ECCE),Sept.15–20, pp. 1627–1634.

[78] Y. Shuitao, F. Z. Peng, L. Qin, R. Inoshita, and Q.Zhaoming, "Current-fed quasi-Z-source inverter with voltage buck-boost and regeneration capability," IEEE Trans. Ind. Applicat., vol. 47, no. 2, pp. 882–892, 2011.

[79] Q. Lei, D. Cao, and F. Z. Peng, "Novel loss and harmonic minimized vector modulation for a current-fed quasi-Z-source inverter in HEV motor drive application," IEEE Trans. Power Electron., vol. 29, no. 3, pp. 1344–1357, Mar. 2014.

[80] L. Poh Chiang, D. M. Vilathgamuwa, C. J. Gajanayake, W. Li Tya n, and A. C. Ping, "Z-source current-type inverters: digital modulation and logic implementation,"IEEE Trans. Power Electron., vol. 22, no. 1, pp. 169–177, 2007.

[81] D. Caoand F. Z. Peng, "A family of Z-source and quasi-Z-source DC-DC converters," in Proc.2009 IEEE Applied Power Electronics Conf. Exposition (APEC), vols. 1–4, pp. 1097–1101.

[82] R.Strzeleckiand D. Vinnikov, "Models of the qZ-Converters," Przeglad Elektrotechniczny, vol. 86, no. 6, pp. 80–84, June 2010.

[83] D.Vinnikovand I. Roasto, "Quasi-Z-sourcebased isolated DC/DC converters for distributed power generation," IEEE Trans. Ind. Electron., vol. 58, no. 1, pp. 192–201, Jan. 2011.

[84] D. Vinnikov, I. Roasto, R. Strzelecki, and M. Adamowicz, "Step-up DC/DC converters with cascaded quasi-Z-source network," IEEE Trans. Ind. Electron., vol. 59, no. 10, pp. 3727–3736, Oct. 2012.

[85] D. Vinnikov, J. Zakis, O. Husev, and R. Strzelecki, “New high-gain step-up DC/DC converter with high-frequency isolation,” in Proc. 27th Annu. IEEE Applied Power Electronics Conf. Exposition (APEC), Mar. 2012, pp. 1204–1209.

[86] O. Husev, A. Blinov, D. Vinnikov, and A. Chub, “Steady-state analysis of qZS-derived push-pull DC/DC converter with wide input voltage regulation range,” in Proc. 8th Int. Conf. Compatibility and Power Electronics (CPE), June5–7, 2013, pp. 320–325.

[87] E. Romero-Cadaval, G. Spagnuolo, L. Garcia Franquelo, C. A. Ramos-Paja, T. Suntio, and W. M.Xiao, “Grid-connected photovoltaic generation plants: Components and operation,” IEEE Ind. Electron. Mag., vol. 7, no. 3, pp. 6–20,Sept. 2013.

[88] M. Begovic, “Renewable energy technologies: The future of photovoltaics,” in Proc. 2012 IEEE PES Innovative Smart Grid Technologies (ISGT), Jan.16–20, pp. 1–1.

[89] R. Singh, G. F. Alapatt, and A. Lakhtakia, “Making solar cells a reality in every home: opportunities and challenges for photovoltaic device design,” IEEE J. Electron Devices Soc., vol. 1, no. 6, pp. 129–144, June 2013.

[90] J. M. Carrasco, L. G. Franquelo, J. T.Bialasiewicz, E. Galvan, R. C. P. Guisado, M. A. M. Prats, J. I. Leon, and N. Moreno-Alfonso, “Power-electronic systems for the grid integration of renewable energy sources: A survey,” IEEE Trans. Ind. Electron., vol. 53, no. 4, pp. 1002–1016, June 2006.

[91] S. B. Kjaer, J. K. Pedersen, and F. Blaabjerg, "A review of single-phase grid-connected inverters for photovoltaic modules," IEEE Trans. Ind. Applicat., vol. 41, no.5, pp. 1292–1306,Sept.2005.

[92] X. Li, D. Hui, and X. Lai, "Battery energy storage station (BESS)-based smoothing control of photovoltaic (PV) and wind power generation fluctuations," IEEE Trans. Sustain. Energy, vol. 4, no. 2, pp. 464–473, Apr. 2013.

[93] H. Beltran, E. Bilbao, E. Belenguer, I. EtxeberriaOtadui, and P. Rodriguez, "Evaluation of storage energy requirements for constant production in PV power plants," IEEE Trans. Ind. Electron., vol. 60, no. 3, pp. 1225–1234, Mar. 2013.

[94] S. Daher, J. Schmid, and F. Antunes, "Multilevel inverter topologies for stand-alone PV systems," IEEE Trans. Ind. Electron., vol. 55, no. 7, pp. 2703–2712, July 2008.

[95] S. Kouro, C. Fuentes, M. Perez, and J. Rodriguez, "Single DC-link cascaded H-bridge multilevel multistring photovoltaic energy conversion system with inherent balanced operation," in Proc. 38th Annu. Conf. IEEE Industrial Electronics Society (IECON 2012), Oct.25–28, pp. 4998–5005.

[96] S. Rivera, S. Kouro, B. Wu, J. I. Leon, J. Rodriguez, and L. G. Franquelo, "Cascaded H-bridge multilevel converter multistring topology for large scale photovoltaic systems," in Proc. 2011 IEEE Int. Symp. Industrial Electronics (ISIE), June27–30, pp. 1837–1844.

[97] J. Holtz, M. Holtgen, and J. O. Krah, "A space vector modulator for the high-switching frequency control of three-level SiC inverters," IEEE Trans. Power Electron., vol. 29, no. 5, pp. 2618–2626, May 2014.

[98] C. N.-M. Ho, H. Breuninger, S. Pettersson, G.Escobar, and F. Canales, "A comparative performance study of an interleaved boost converter using commercial Si and SiC diodes for PV applications," IEEE Trans. Power Electron., vol. 28, no. 1, pp. 289–299, Jan. 2013.

[99] B. Sahan, S. V. Araújo, T. Kirstein, L. Menezes, and P. Zacharias, "Photovoltaic converter topologies suitable for SiC-JFETs," in Proc. PCIM Europe Conf., 2009, pp. 431–437.

[100] J. Millan, P. Godignon, X. Perpinya, A. PerezTomas, and J. Rebollo, "A survey of wide band gap power semiconductor devices," IEEE Trans. Power Electron., vol. 29, no. 5, pp. 2155–2163, May 2014.

[101] M. A. Briere, "GaN based power conversion: A new era in power electronics," in Proc. PCIM Eur., Nuremberg, Germany, 2009, pp.317–322.

[102] T. Kerekes, E. Koutroulis, D. Séra, R. Teodorescu, and M. Katsanevakis, "An optimization method for designing large PV plants,"IEEE J. Photovolt., vol. 3, no. 2, pp. 814–822, Apr. 2013.

[103] W. Liand X. He, “Review of non-isolated highstep-up dc/dc converters in photovoltaic gridconnected applications,” IEEE Trans. Ind. Electron., vol. 58, no. 4, pp. 1239–1250, Apr. 2011.

[104] S. Vighetti, J. P. Ferrieux, and Y. Lembeye, “Optimization and design of a cascaded dc/dc converter devoted to grid-connected photovoltaic systems,” IEEE Trans. Power Electron., vol. 27,no. 4, pp. 2018–2027, Apr. 2012.

[105] M. A Eltawiland Z. Zhao, “Grid-connected PV power system: Technical and potential problems-A review,” Renew. Sustain. Energy Rev., vol. 14, no. 1, pp. 112–129, Jan. 2010.

[106] S. Afari, A. Castellazzi, and P. Wheeler, “Experimental and analytical performance evaluation of SiC power devices in the matrix converter,” IEEE Trans. Power Electron., vol. 29, no. 5, pp. 2584–2596, May 2014.

[107] L. Empringham, L. de Lillo, and M. Schulz, “Design challenges in the use of silicon carbide JFETs in matrix converter applications,” IEEE Trans. Power Electron., vol.29, no. 5, pp. 2563–2573, May 2014.

[108] J. Jordan, V. Esteve, E. Sanchis-Kilders, E. J.Dede, E. Maset, J. B. Ejea, and A. Ferreres, “A comparative performance study of a 1200 V Si and SiC MOSFET intrinsic diode on an induction heating inverter,” IEEE Trans. Power Electron., vol. 29, no. 5, pp. 2550–2562, May 2014.

[109] R. Kuffel, J. Giesbrecht, T. Maguire, R. P. Wierckx, and P. McLaren, "RTDS-a fully digital power system simulator operating in real time," in *IEEE WESCANEX 95. Communications, Power, and Computing. Conference Proceedings*, 1995, vol. 2, pp. 300–305.

[110] W. Ren, M. Steurer, and T. L. Baldwin, "An effective method for evaluating the accuracy of Power Hardware-in-the-Loop simulations," in *2008 IEEE/IAS Industrial and Commercial Power Systems Technical Conference*, 2008, pp. 1–6.

[111] X. Yang, X. Zha, and S. Li, "Study on Hardware-in-the-Loop of Active Power Filer Based on RTDS," in *2010 International Conference on Electrical and Control Engineering*, 2010, pp. 4295–4298.

[112] M. Dargahi, A. Ghosh, G. Ledwich, and F. Zare, "Studies in power hardware in the loop (PHIL) simulation using real-time digital simulator (RTDS)," in *2012 IEEE International Conference on Power Electronics, Drives and Energy Systems (PEDES)*, 2012, pp. 1–6.

[113] Anderson, J.; Peng, F., "Four quasi-Z-Source inverters," in *Power Electronics Specialists Conference, 2008. PESC 2008. IEEE* , vol., no., pp.2743-2749, 15-19 June 2008

[114] Montoya, D.G.; Paja, C.A.R.; Petrone, G., "Design method of the perturb and observe controller parameters for photovoltaic applications,"

in *Circuits and Systems (CWCAS), 2012 IEEE 4th Colombian Workshop on* , vol., no., pp.1-6, 1-2 Nov. 2012.

[115] Jong-Hyoung Park; Heung-Geun Kim; Eui-Cheol Nho; Tae-Won Chun; Choi, J., "Grid-connected PV System Using a Quasi-Z-source Inverter," in *Applied Power Electronics Conference and Exposition, 2009. APEC 2009. Twenty-Fourth Annual IEEE* , vol., no., pp.925-929, 15-19 Feb. 2009

APPENDIX A

EXPERIMENTAL SETUP FOR Z-SOURCE INVERTER

A.1 Programmable AC Source

Programmable AC source provides powerful functions to simulate the standard power quality disturbances. In this work, Chroma 61511 is used as a grid source for the distribution system as shown in Figure A.1. It can provides upto 300 Vac output voltage and 12 KVA power ratings. It is capable to generate the first forty harmonics and inter-harmonics ranging from 0.01 Hz to 2400 Hz.

Figure A.1: Chroma AC source

A.2 Programmable PV Simulator

Programmable PV Simulator is multi-function Chroma device that can simulate a dc source of voltage range 0-2500V and current up to 25 A as shown in Figure A.2. It can also simulate a PV module with different parameters can be set according to international standards. Maximum power point tracking and shadow testing options are also available. The PV Simulator can be controlled through a soft panel and different parameters like temperature, irradiation, rise time, fall time, fill factor, open circuit voltage and short-circuit current can be adjusted.

Figure A.2 Programmable PV Simulator

A.3 dSPACE Controller

dSPACE is an industrial controller mainly used for the application development and prototyping. In this study, DS-1103 is used for the real time controller implementation of

SAPF as shown in A.3. It has two major parts expansion box and connection panel. The connection panel consists of 50 bit analog and digital I/O channels including 20 analog to digital input channel (ADCH) and 8 digital to analog output channels (DACH). dSPACE can be easily programmed with the Matlab/Simulink with the aid of real time interface (RTI) blocksets. All I/O's can be configured for real time applications using RTI. dSPACE uses control Desk as a software for the real time monitoring, measurement and control actions. DS-814 interface card is used in the expansion box while DS-817 card in the workstation for real time monitoring and control of the system.

The instantaneous power PQ and synchronous reference current DQ controllers are designed in Matlab/Simulink environment with the aid of RTI and RTW tools provided by the dSPACE. The dSPACE DS-1103 controller has two major parts expansion box and connection panel. The connection panel contains 20 analog to digital input channel (ADCH) and 8 digital to analog output channels (DACH).

The three-phase source voltage and DC bus voltage waveforms are fed to the dSPACE controller using DACH 1-4 obtained from the voltage transducers. The real time current waveforms consisting of three phase load current and three phase SAPF current are input to the dSPACE controller using DACH 5-7 and DACH 9-11 respectively. The instantaneous power PQ and synchronous reference current DQ controllers are implemented using 50 μsec sampling time. The gate pulses are obtained from the dSPACE using high speed digital DS1103BIT_OUT block of master PCC.

Figure A.3 dSPACE DS-1103

A.4 Real Time Inverter/Rectifier Module

SEMITEACH – IGBT inverter and rectifier are used for real time SAPF implementation. It has three major functions including single and three phase inverter, buck or boost converter and brake chopper as shown in A.4. An isolated uncontrolled rectifier is also a part of this embedded system. A pair of 2200μF DC capacitor is also installed for energy storage purpose. The rectifier input is 230/ 400V while the output of may vary up to 600V DC. The input output range of inverter can also varied up to 400V AC and 600V DC with 30A as a maximum current.

In this study, the voltage source inverter and three phase inverter are used. The voltage source inverter is used to inject the nonlinear harmonic current required by the load

attached to the DC side of the diode rectifier. The gate pulses are provided to the inverter generated by the dSPACE controller using amplifier. A DC voltage source of 15 volts is applied to drive the gate driven circuit of the inverter. The DC bus capacitor are used to store the energy and provide the required nonlinear current while maintaining the certain reference value.

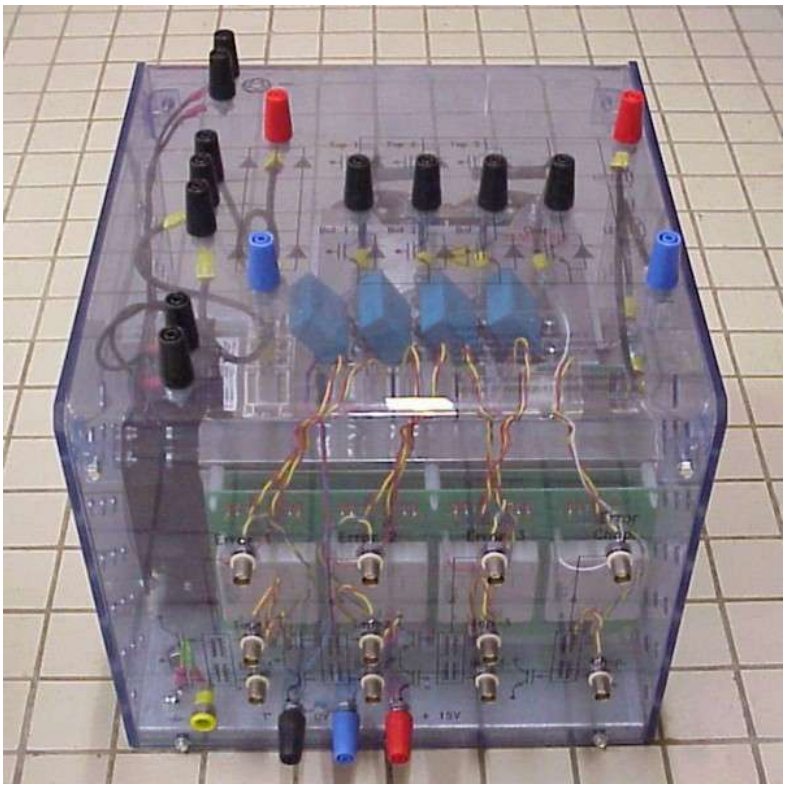

Figure A.4 Real Time Inverter and Rectifier Module

A.5 Mixed Domain Oscilloscope

Tektronix 4104B-3 mix domain oscilloscope is used to record the experimental results as shown in Figure A.5. It is capable of analyzing signals both in frequency and time

domain. It can be used a spectrum analyzer. It has four channels that can be used for the measurement of voltage and current signals.

The voltage probe Tektronix TPP-1000 is a 1GHz bandwidth probe used for the measurement of voltage signals up to 300 volts. It offers 10X and 2X attenuation factors. Tektronix TCP0030A probe is utilized for the measurement of source, load and SAPF current signals. This probe provides the selectable measurement of 5A and 30A with the bandwidth greater than 120 MHz.

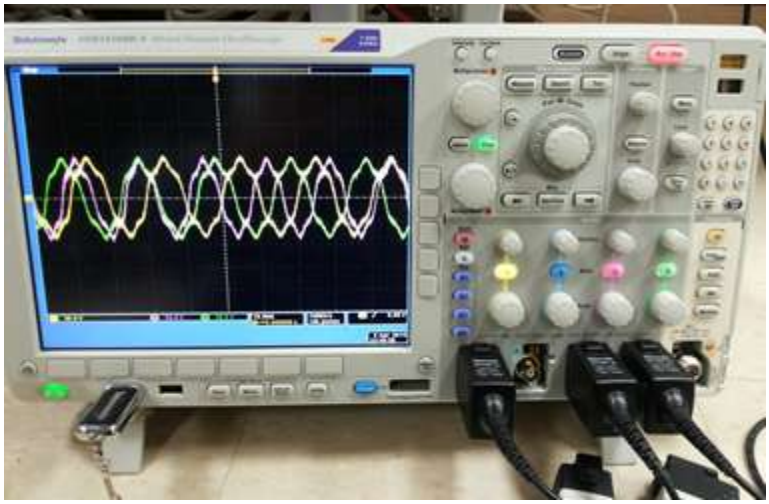

Figure A.5 Mix Domain Tektronix Oscilloscope

A.6 Voltage and Current Transducers

Voltage and current transducers are utilized to reduce the voltage and current signals of distribution system, which can be fed to the controller for a possible control action. The dSPACE controller, used in this work has input output range up to ±10V while the actual voltage and current ratings are much higher. So, voltage and current transducers are used to make the input voltage and current signals compatible with the controller I/O range.

(a)Voltage Transducer

LEM LV 25P/SP5 sensor is used as a voltage transducer for the real time measurement of voltage signal. It is a closed loop sensor, which can measure DC, AC and pulsed voltage signals from 10 to 1500 V using the Hall effect as shown in Figure A.6. A user specified input resistor is used to induce a current in the secondary side of the transducer, where a measurement resistor can be used to obtain the output voltage from the induced current. In this work, input resistor of 47 kΩ is used for the three-phase voltage measurement while 94 kΩ is used for the DC bus side with a 500Ω as a measurement resistor.

Figure A.6 Voltage Transducers LEM LV 25P/SP5

Voltage transducers are used to reduce the level of the voltage signals, which can be fed to the controller for a possible control action. The dSPACE controller, used in this work has input output range up to ±10V while the actual voltage ratings are much higher. So, voltage and transducers are used to make the input voltage waveform compatible with the permissible controller I/O range.

LEM LV 25P/SP5 sensor is used as a voltage transducer for the real time measurement of voltage signal. It can measure DC, AC and pulsed voltage signals from 10 to 1500 V using the Hall effect. The basic block diagram of the voltage transducer is shown in the Figure A.7. The terminal *HT+* and *HT-* represents the signal phase connection terminals of supply voltage. The user specified resistor *R* is used as an input resistors to limit the input current less than 10mA at the primary side. The current conversion ratio of the LV 25-P/SP5 is 2500 : 1000. The resistor R_M is used as a measurement resistor. The value of R_M should be carefully selected so that the output voltage will remain the range less than ± 10V. The voltage terminal $\pm V_c$ represents the terminal of the supplied DC voltage of ±15V. An example is illustrated below to explain the functionality of voltage transducer.

Suppose V_s = 230 V

Input Resistor = R = 47000 Ω

Measurement Resistor = 500 Ω

$$\text{Primary Currnet} = I_p = \frac{V_s}{R} = \frac{230V}{47,000} = 4.8936\,mA$$

$$I_s = 2.5\ x\ I_p = 12.2340\ mA$$

$$\begin{aligned} \text{Output Voltage} = V_M &= I_s\, x\, R_M \\ &= 12.2340\ x\ 0.5 \\ &= 6.11 Volts \end{aligned}$$

It can be seen that for a supply voltage of 230 volts the transducer output voltage is 6.11 volts which is far less than 10 Volts. So, the transducer output can be fed to the dSPACE controller.

In this work, input resistor of 47 kΩ is used for the three-phase voltage measurement while 94 kΩ is used for the DC bus side with a 500Ω as a measurement resistor.

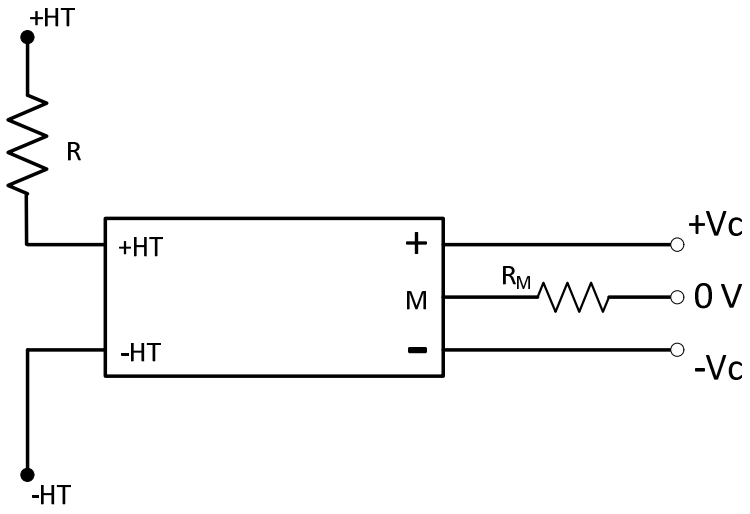

Figure A.7 Circuit Diagram of Voltage Transducer

(b)Current Transducer

HAS 50-s sensor is used as a current transducer for the real time measurement of source load and active power filter current. It is a closed loop sensor, which can measure DC, AC and pulsed current signals up to 50A using the Hall effect as shown in A.7. The output of this sensor is an AC voltage signal which can be easily used in any industrial controller like dSPACE.

Figure A.8 Current Transducers HAS 50-s

Current transducers are utilized to transform the high rated current signals into the low valued voltage signals in the distribution system, which can be fed to the controller for a possible control action.

HAS 50-s sensor is used as a current transducer for the real time measurement of source load and active power filter current. It is a closed loop sensor, which can measure DC, AC and pulsed current signals up to 50A using the Hall Effect. A single phase wire is passed through the sensor to induce the current in sensors coil. The output of this sensor is an AC voltage signal which can be easily used in any industrial controller like dSPACE. The basic block diagram of the current transducer is shown in the Figure A.9, where I_p represents the directions of current. The voltage terminal $\pm V_c$ represents the terminal of the supplied DC voltage of ±15V. The resistor R_M is used as a measurement resistor. The value of R_M should be carefully selected so that the output voltage will remain the range less than ± 10V.

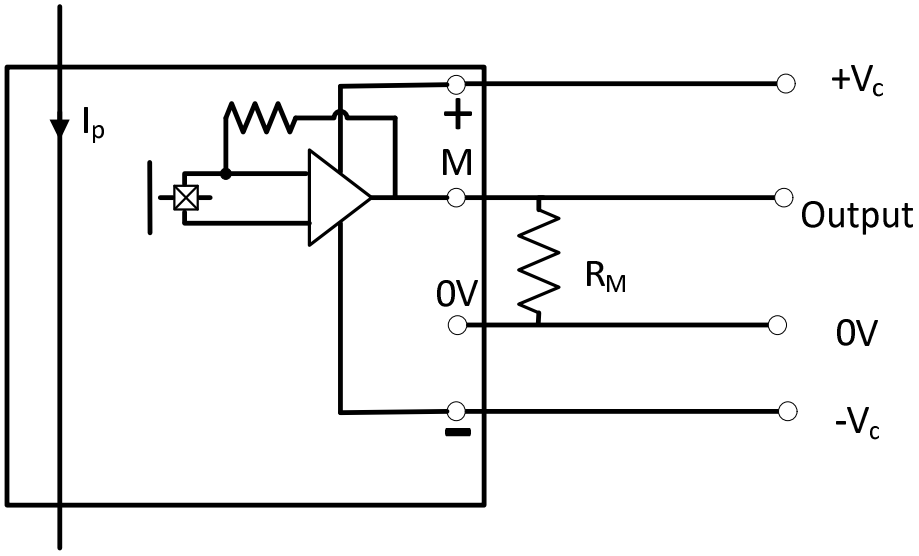

Figure A.9 Circuit Diagram of Current Transducer

A.7 AMPLIFIER DESIGN

The digital output of the dSPACE controller is in the range of ±10V, while the gate pulses input required by the real time inverters are ±15V. Therefore, a double gain amplifier is designed using the hex inverter TTL logic integrated circuit SN7416. The schematic diagram of the hex inverter circuit is shown in Figure A.10. This TTL hex inverter has a minimum breakdown voltage of 15 volts. A 15 volts DC supply is provided at the Vcc terminal. The output level can be adjusted using pull up resistors. This TTL hex inverter can sink maximum current up to 30mA.

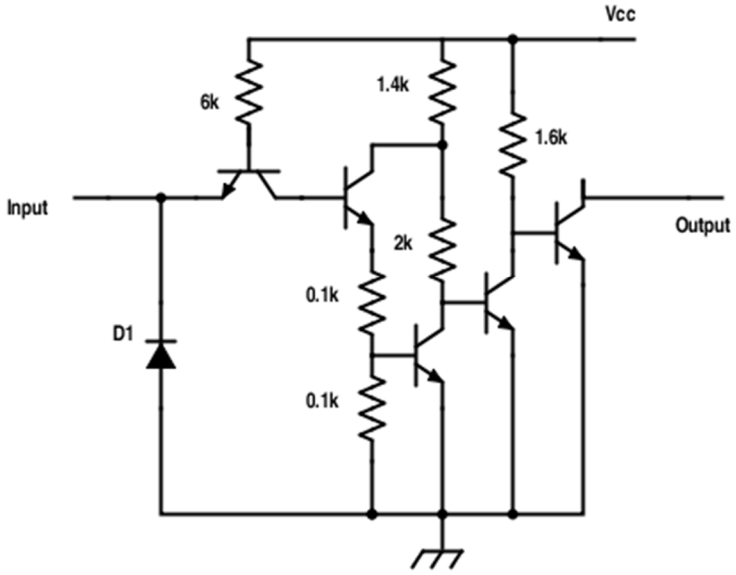

Figure A.10 Schematic Diagram of SN7416 TTL hex Inverter

APPENDIX B

HARDWARE IN THE LOOP REAL TIME DIGITAL SIMULATOR (RTDS) AN OVERVIEW

B.1 Real Time Digital Simulator (RTDS)

In power systems, a power hardware in loop (PHIL) systems represents the power systems interfaced with a piece of hardware. PHIL simulations plays a vital role in the design and testing of power system problems [109]–[111].

RTDS is one the most advance simulator that solves the complex power systems in near real time. RTDS consists of the specialized dedicated hardware and software that specifically designed to efficiently solve the electromagnetic transients as shown in Figure . RTDS is capable of solving a wide range of power system application with the aid of wide variety of built in power system components and friendly graphical user interface [112], [113].

Figure B.1 Real Time Digital Simulator (RTDS)

B.2 RSCAD Software

RSCAD is the graphical user interface used to design, run, operate and troubleshoot the power system. RSCAD mainly consist of two parts namely DRAFT and RUNTIME. The Draft file is used to create the power system circuit by copying and pasting the individual power system components from the user library as shown in Figure B.2. A number of power system components are available in the library that are designed and refined over the time. After the power system network has been constructed, the draft file is compiled to create the simulation code required by the simulator.

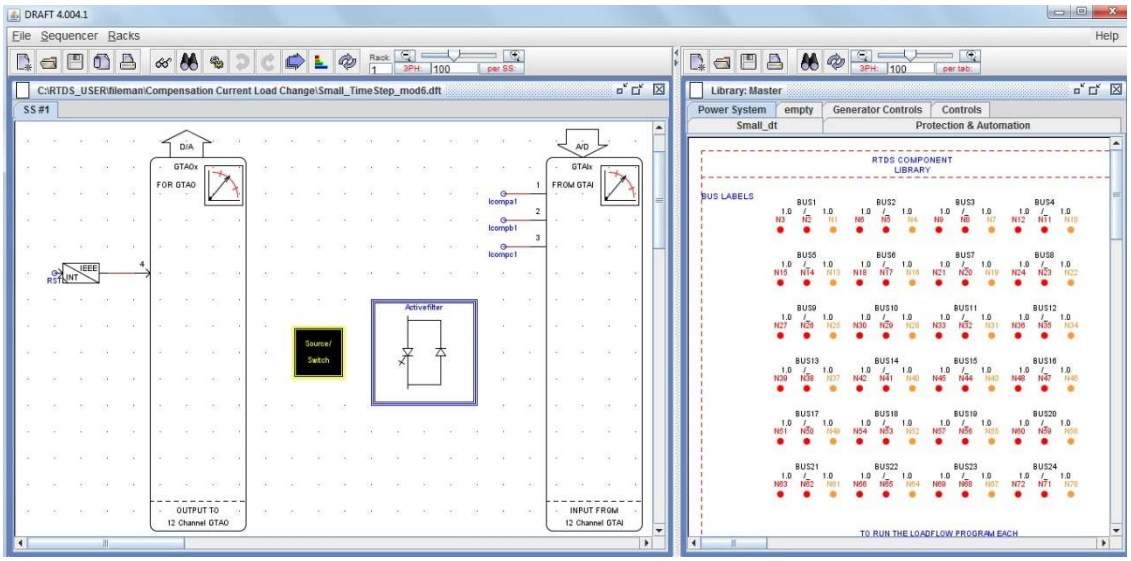

Figure B.2 RSCAD Draft File

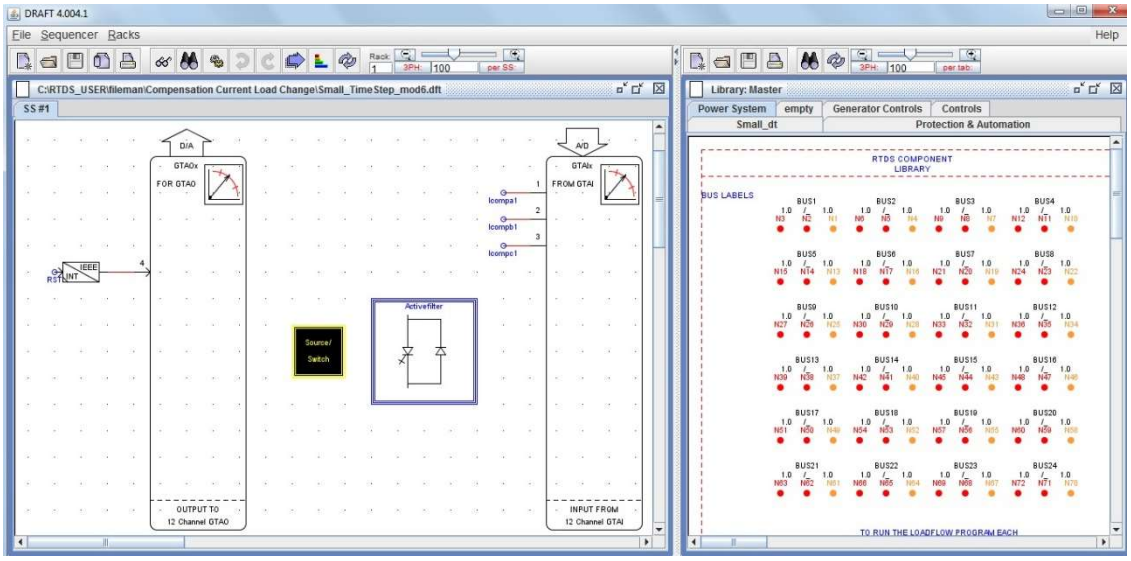

Figure B.3 RSCAD Run Time File

After the successful compilation of the draft file, the simulation code can be downloaded to the simulator using the run time file. Run time files can be used to observe, record and control the real time simulation using controls and graph indicators as shown in Figure B.3. Power system parameters like voltage, current frequency, power etc. can be

examined using plots and other indicators. The transient behavior of the system can be easily observed and recorded.

B.3 Hardware Components

The RTDS simulator hardware is based on the modular architecture. It can be easily extendable by adding modules or racks to accommodate the larger models power system. Each rack contains three different cards for communication and processing such as:

- Inter-Rack Communication card (IRC)
- Giga Transceiver Workstation Interface Card (GTWIF)
- Giga Processor Card (GPC)

The GTWIF card is responsible for the synchronization between the racks. It also communicate with the RSCAD to start and stop the simulation. GPC is used to solve the power/control systems components equations. Every GPC card contains two IBM 1GHz processor each can solve 66 power system nodes. GPC card also govern the connection to the gigabit transceiver analog input/output card (GTIO). The GTAI/O input/output cards are used to interface the RTDS with external devices as shown in Figure B.4. Each GTAI/O contains 12 input/output channel available for the external connection, while the gigabit transceiver digital input/output (GTDI/O) cards contains 64 digital input/output channels.

a) PB5

b) GTWIF

c) GTAO

d) GTAI

e) GTDI

Figure B.4 RTDS Processors and I/O Cards

PUBLICATIONS:

(1) Renewable based distributed generation in Uganda: Resource potential and status of Exploitation [**Published in Renewable and Sustainable Energy Reviews, Elsevier Journal, impact factor: 5.9**]

(2) Optimal Hybrid Renewable-Based Distributed Generation System with Feed-in Tariffs and Ranking Technique" 2014 IEEE 8th International Power Engineering and Optimization Conference [**Published**].

(3) Improved Stability index by optimal Placement of wind farms using Differential Evolution, ISAP 2015 Conference, PORTUGAL [**Accepted**].

(4) Performance Analysis of Parabolic Trough Collectors for Pakistan Using Mathematical and Computational Models. [**Accepted in 2016 Clemson University Power Systems Conference, USA**].

(5) A Novel ANFIS-Based Power Controller for Grid-Connected PV System [**IEEE Transaction paper submitted**]

(6) Implementation of various PWM Techniques for novel ANFIS Control for Grid connected PV system.**[Transaction Paper]**

(7) Prototype Implementation of Z-source Inverter with PI Controller and PV Simulator **[Transaction Paper]**

(8) Implementation of Active Power Filter for Three Phase Grid Connected System. (Submitted)

Vitae

Name: Muhammad Usman Mukhtiar

Date of Birth: 04th June, 1989

Address: Village Shakardara, District Kohat, Pakistan

Contact Number: 00923329780301

Email: Usman.Mukhtiar@hotmail.co.uk

Education:

BSc Electrical Engineering: UET Peshawar, 2011, Pakistan

MSc Electrical Engineering: KFUPM, KSA , 2015

Research Experience:

Energy System Research Group for 3 years in KFUPM.